Glioblastoma cell behaviour: a study of chemically-induced cellular connectivity and 3D modelling of cellular migration

Bárbara Luísa da Silva

Submitted in accordance with the requirements for the degree of

Doctor of Philosophy

The University of Leeds

School of Medicine

Faculty of Medicine and Health

June 2018

The candidate confirms that the work submitted is her own and that appropriate credit has been given where reference has been made to the work of others.

Acknowledgments

Firstly, I would like to express my sincere gratitude to BTRS and, in particular, to Ian Meek and his family. It was due to their courage and strength after a dire diagnosis that the Ian Meek studentship was made possible; and the work I present in this thesis would not have been accomplished without it. I hope my contribution to the tackling of this terrible disease honours Ian Meek's efforts and legacy.

For his support during my PhD, as well as building an environment that encouraged creative freedom, and allowed me to "play around" with science, I am most grateful to my supervisor, Dr. Heiko Wurdak. His enthusiasm and dedication to research were contagious; and his guidance key in my PhD and now beyond. I would also like to thank my co-supervisors Prof Graham Cook, who provided me with invaluable support, words of encouragement and, above all, motivation; and Prof Susan Short for her much appreciated feedback.

For all their help throughout the years, I would like to thank all past and present members of the Wurdak group. I would like to give a special thanks to Dr. Euan Polson and Dr^2. Ryan Mathews for all their help, scientific expertise, invaluable input and friendship. I am very grateful to Dr. Alastair Droop for computation analysis of gene expression data and network analysis.

Furthermore, I thank everyone on Level 5 for all the help, support, laughs and just simply putting up with me (ask Celso, it is not easy). I would like to thank Gina for all the cookies (I believe the sugar helped fuel my brain) and Aarren for keeping me company and filling me in on all the gos after hours. Most importantly, my sincere thanks go to them, as well as Chiara Galloni, Jenny Williams, Nora Rippaus and

Verena Kuchler for keeping me sane during these years. Your continuous support and friendship made me feel at home. You are the best friends I could have.

Lastly, but by no means least, I am extremely grateful to my family. To my parents and siblings, who, without even understanding why I am still "studying" at the age of 30, continue to offer the support and words of encouragement that help keep me moving forward. I am here thanks to you – not only your encouragement, but also your hard work to enable us to reach for the stars. But, most importantly, I am extremely grateful and lucky to have had Celso by my side during this whole experience. You have been with me through thick and thin and I am sure that without you I would not have been able to finish this. I am forever grateful for everything you have done. These are the most important people in my world and I dedicate my thesis to them.

Abstract

Glioblastoma multiforme (GBM) is the most common and deadliest brain cancer in adults. Despite considerable efforts at both bench and bedside, the average survival for GBM patients is only 14-15 months. This dismal prognosis stems from challenges in treatment and a malignant tumour biology. A key need in addressing GBM is to better understand and therapeutically target GBM cell invasion into the surrounding healthy brain tissue.

Cytoskeletal remodelling and dynamics, mediated by ROCK effector proteins, play an important role in the ability of GBM cells to migrate. ROCK inhibition is being considered as potential cancer therapy; however, there is insufficient data examining a chemical pan-ROCK inhibition effect in the cellular context of GBM. I address this gap in the context of undifferentiated patient-derived brain tumour stem cell (BTSC) models. My results show that chemical ROCK pathway inhibition with several different compounds led to a reversible neurite-like outgrowth phenotype across three different patient-derived cell models. This phenotype was accompanied by a decrease in BTSCs motility, which enabled the cells to form an interactive multicellular network. Interestingly, ROCK inhibition did not alter the self-renewal ability or proliferation capacity of BTSCs.

To further investigate this diffusive nature of GBM cells, I developed an *in vitro* 3D model that allows the study of GBM infiltration in real-time. My work demonstrates the ability of GBM spheres to spontaneously fuse with, and infiltrate, neural-like early-

stage cerebral organoids (eCOs) with the use of stem cell culture-based organoid methodology. In addition, this 'hybrid' GBM tumour organoid possessed an invasive tumour compartment, which was specific to GBM cells. Thus, this self-assembly GBM tumour organoid may be used to identify anti-GBM invasion treatment approaches.

Table of Contents

List of Figures

List of Tables

List of Abbreviations

A	Antimycin A
AIF1L	Allograft Inflammatory Factor 1-like
AKT	Protein Kinase B
ARGHAP	Rho GTPase Activating Protein
bFGF	Human basic Fibroblast Growth Factor
BMP	Bone Morphogenic proteins
BTSC	Brain Tumour Stem Cells
CBX	Carbenoxolone
CDK1	Cyclin Dependent Kinase 1
CDKNA2A	Cyclin Dependent Kinase Inhibitor 2A
CNS	Central Nervous System
CRISPR	Clustered Regularly Interspaced Short Palindromic Repeats
CT	Computed Tomography
Cx	Connexins
DCX	Doublecortin
DMEM	Dulbecco's Modified Eagle Medium
DMSO	Dimethylsulfoxide
DAPI	4',6-diamidino-2-phenylindole
EB	Embryoid Body
ECM	Extracellular Matrix
eCOs	Early-stage Cerebral Organoid
EDTA	Ethylenediaminetetraacetic Acid

EGF	Endothelial Growth Factor
EGFR	Epidermal Growth Factor Receptor
EGFRvIII	Epidermal Growth Factor Receptor variant III
EMT	Epithelial-to-Mesenchymal Transition
FBS	Fetal Bovine Serum
FCCP	Carbonyl cyanide-4 phenylhydrazone
Fn14	Fibroblast Growth Factor inducible 14
GBM	Glioblastoma Multiforme
GFAP	Glial Fibrillary Acidic Protein
GFP	Green Fluorescent Protein
GMEM	Glasgow Minimum Essential Medium
HBS	Human Embryonic Kidney
HEK	HEPES buffered saline
HSV-tk	Herpes Simplex Virus-Thymidine Kinase
IC50	Inhibitory Concentration 50
IDH	Isocitrate Dehydrogenase
IL-2	Interleukin-2
iPSCs	Induced Pluripotent Stem Cells
KSR	Knockout Serum Replacement
LED	Light-emitting Diode
LIF	Leukaemia Inhibitory Factor
LIM K	LIM kinase
MACF1	Microtubule-actin Crosslinking Factor 1
MAP-2	Microtubule-associated Protein-2
MEF	Mouse Embryonic Fibroblasts
MEM-NEAA	Minimum Essential Medium-Non-Essential Amino Acids
mESC	Mouse Embryonic Stem Cells
MET	Met Proto-oncogene

MGMT	O-6 methylguanine-DNA methyltransferase
MLC	Myosin Light Chain
MMP	Matrix Metalloproteinase
MN	Membrane Microtubes
MRI	Magnetic Resonance Imaging
NEK2	NIMA-Related Kinase 2
NESTIN	Neuroectodermal Stem Cell Marker
Neuro D1	Neurogenic Differentiation 1
NLM	Neurite-like Microtubes
NMII	Nonmuscle Myosin II
NOS	Not Otherwise Specified
NOTCH2	Neurogenic Locus Notch Homolog Protein 2
NOTCH3	Neurogenic Locus Notch Homolog Protein 3
NP	Neuro Progenitor
NSC	Neural Stem Cells
NTRK2	Neurotrophic Receptor Tyrosine Kinase 2
NUF2	NDC80 Kinetochore Complex Component
O	Oligomycin
OCR	Oxygen Consumption Rate
PAK	P21-Activated kinase
PBS	Phosphate Buffered Saline
PD-1	Programmed Cell Death 1
PD-1L	Programmed Cell Death Ligand 1
PDGFRA	Platelet-derived Growth Factor Receptor α
PET	Positron Emission Tomography
PFA	Paraformaldehyde
PI3K	Polo Kinase Like 3
PLK3	Phosphoinositide 3-Kinase

PTEN	Phosphate and Tensin Homologue
R	Rotenone
RAS	Rat Sarcoma
rhEGF	Epidermal Growth Factor
ROCK	Rho-associated Protein Kinases
RT	Room Temperature
RTK	Receptor Tyrosine Kinase
SOX2	Sex Determining Region Y-box 2
TM	Tumour Microtubes
TMZ	Temozolomide
TP53	Tumour Protein 53
TuJ1	Neuronal Class III β-Tubulin
ULA	Ultra-low Attachment
VEGF	Vascular Endothelial Growth Factor
WHO	World Health Organization
YKL-40	Chitinase-3-Like Protein

1. Introduction

This thesis describes work undertaken to address gaps in the understanding of migration and invasion of Glioblastoma Multiforme (GBM) using two complementary approaches: the study of cytoskeleton modulation mediated by Rho-associated protein kinases (ROCK) signalling pathway inhibition and its effect on GBM behaviour, and the creation of a 3D model to study real-time invasion. In this introductory chapter, I will establish the rationale underlying the aims of this work.

I start by characterising the pathology of GBM, explaining how it is categorised, and argue that the poor current outcomes make it a pressing unmet clinical need (1.1). I then briefly outline how GBM is being treated at present and the range of (targeted) therapies being developed. I briefly address how new treatments, while initially promising, have often failed in later phases of clinical trials (1.2). I then move on to describe key features of the biology of GBM – a likely hurdle in the development of successful therapies. I do so in three main sections. Firstly, I describe the (inter and intra tumoural) heterogeneity of GMB, which is a main cause of differential treatment response amongst patients (1.3); I then address brain tumour stem cells and their role in treatment resistance and tumour recurrence (1.4). In the third section I explore the question of migration in brain tumours (1.5). While all three sections are relevant for this work, the focus of my PhD is on the broad issue of GBM cell migration. Thus, in section 1.5 I examine the role of cytoskeletal mechanisms in this process in some detail, with particular focus on the RhoGTPase effector protein ROCK. I also reflect on how migration in brain tumours has been studied; and the appropriateness / possibilities

opened up by the use of organoid models for studying migration in a final section (1.6). Lastly, I outline the aims and objectives of the work developed under this PhD.

1.1. Glioblastoma multiforme

The majority of primary brain tumours are thought to originate from cells of the glial lineage. These tumours are categorised collectively as gliomas, and together account for nearly 80% of all malignant brain tumours (1-3). Gliomas can be (and have historically been) classified according to their presumed cell of origin/predominant cell type (morphological features) as astrocytomas, oligodendrogliomas, oligoastrocytomas and ependymomas. However, the current international standard for the diagnosis of gliomas is the more sophisticated World Health Organization (WHO) grading system (Table 1) (4). Under this system, tumours are grouped based on their pathological features, their proliferation rate and potential to spread into healthy neighbour tissue. The WHO classification of central nervous system (CNS) tumours distinguishes four classes of gliomas, grades I-IV; grades I and II are classified as low-grade gliomas and grades III and IV are defined as high-grade gliomas.

There is one prominent glioma classified as WHO grade IV, and that is Glioblastoma Multiforme. GBM is the most common primary brain tumour in adults, (5) with a yearly global incidence for newly diagnosed cases of 3-5 per 100,000 people (6, 7). In England, for example, incidence in the period 2007-2011 has been found to be closer to the upper bound, with approximately 2,100 new cases being diagnosed on average each year (8). With a rapid clinical onset, the symptoms presented by patients are highly variable and depend on the tumour location and size as well as the anatomic brain structures involved (9). The initial clinical presentation may include focal neurologic deficits (aphasia, paresthesia and visual disturbances); symptoms resulting from increased intracranial pressure (headaches, nausea and vomiting); changes in mood and personality and also seizures (4, 9). Diagnosis of the disease results from

imaging studies of the brain which include computed tomography (CT), positron emission tomography (PET) and magnetic resonance imaging (MRI) (4, 10).

Oligodendrogliomas	
Grade II	Oligodendroglioma
Grade III	Anaplastic oligodendroglioma
Astrocytomas	
Grade II	Diffuse astrocytoma
Grade III	Anaplastic astrocytoma
Grade IV	Diffuse midline glioma
Grade IV	Glioblastoma Multiforme
Other Astrocytic Tumours	
Grade I	Pilocytic astrocytoma
Grade I	Subependymal giant cell astrocytoma
Grade II	Pleomorphic xanthoastrocytoma
Grade III	Anaplastic pleomorphic xanthoastrocytoma
Mixed Gliomas	
Grade II	Oligoastrocytoma
Grade III	Anaplastic oligoastrocytoma
Ependymal Tumours	
Grade I	Subependymoma
Grade I	Myxopapillary ependymoma
Grade II	Ependymoma
Grade III	Anaplastic ependymoma
Other Gliomas	
Grade I	Angiocentric glioma
Grade II	Choroid glioma of the third ventricle
Not graded	Astroblastoma

Table 1.1- The 2016 WHO classification and grading of the distinct glioma tumours (adapted from (26)).

While a common brain tumour, from the standpoint of (general) cancer epidemiology, GBM is rare, accounting for only 2.5% of cancer diagnoses. However, it is the third foremost cause of death from cancer, due to its extremely poor prognosis (11, 12). Unfortunately, regardless of multimodal therapy efforts, 70% of GBM patients

will suffer disease progression and die of the disease within a year (13). Indeed, and despite the diversity of modern therapies against GBM, these tumours are amongst the most devastating cancers leaving patients with a median survival of approximately 14 to 15 months from the moment of diagnosis (14, 15), and less than 5% surviving five years (16).

The poor prognosis for GBM patients stems from the infiltrative character of the disease and its complex and heterogeneous biology (17). Given GBM's highly diffuse and invasive growth pattern, the malignant cells have the tendency to disseminate along the white matter tracts and frequently cross the corpus callosum, thus rendering complete surgical resection of the tumour impossible (18). As a result, tumour recurrence takes place in almost 80% of cases (and usually appears within 2-3 cm of the margin of the primary lesion) (11, 19). Furthermore, it has been proposed that the main cause for tumour progression lies in the presence of a highly heterogeneous population of cells; and that beyond a highly heterogeneous subpopulation of differentiated cancerous cells there is also a subpopulation of stem-like cells which are highly malignant (20). These cells which possess molecularly different phenotypes are the likely cause for individual sensitivities and resistances of GBM patients to treatment (21). Hence, the extensive inter-patient cellular and genetic heterogeneity in GBM coupled with the intra-tumoural heterogeneity may contribute to therapeutic failure (22-25).

This recent foregrounding of heterogeneity in GBM has also been reflected in a revision of the WHO classification of the tumours (26). Traditionally, GBM diagnosis has relied on histological features – mainly pseudopalisading necrosis, increased cellularity, pleomorphism, vascular endothelial proliferation and high KI 67 labelling index (16). However, the WHO grading system was revised in 2016 with one of the key aims being the better defining of tumour entities within CNS tumours. GBM classification no longer relies solely on pathological/histological features, but it now also incorporates molecular parameters (Table 2) (4). Glioblastomas are now to be

classified into one of the following three diagnoses: 1) Isocitrate dehydrogenase (IDH)-wildtype (>90%, primary glioblastoma), which corresponds frequently with the clinical definition of primary, or de novo, GBM which arises without a known precursor and prevails in patients over 55 years of age (1, 27, 28); 2) IDH-mutant (about 10% of the cases), which corresponds to the clinical definition of secondary GBM, and progresses slowly from a pre-existing lower grade diffuse tumour and normally arises in younger patients (1, 27, 28); and 3) NOS (not otherwise specified), which corresponds to tumours in which the IDH testing cannot be performed (4).

Glioblastoma, IDH wildtype
- Giant cell glioblastoma
- Gliosarcoma
- Epithelioid glioblastoma
Glioblastoma, IDH mutant
Glioblastoma, NOS

Table 1.2- Glioblastoma classification according to the WHO classification of CNS tumours (adapated from (26)).

1.2. Current treatment

Despite clinical and technological advances in neuroimaging, neurosurgery and radiation therapy, the overall survival rate of patients with GBM has changed very little (18). The standard of care for GBM patients has remained consistent for the last 30 years and continues to consist of maximal safe surgical resection of the tumour mass, followed by radiation therapy and concomitant chemotherapy (29-31). The infiltrative nature of these tumours renders complete surgical removal of these tumours impossible, and GBM is thus a surgically incurable neoplasm (15, 32). Nevertheless, tumour resection still provides considerable benefit, namely by reducing the number of cancer cells that need to be treated; the procedure also frequently removes the

hypoxic core of the tumour which is resistant to radiation and normally inaccessible to chemotherapy (16). In addition, studies have supported the importance of aggressive total resection, which resulted in better outcomes and a longer overall survival for the patients with greater extent of resection (30, 31, 33, 34). In order to increase maximal surgical resection, it is necessary to distinguish viable tumour from healthy adjacent brain during surgery. The development of fluorescence-guided surgery using 5-aminolevulinic acid has helped increase the thoroughness of resection (35, 36), though complete resection remains out of reach.

Following optimal surgical resection, standard fractionated radiation remains the most effective therapy for patients with GBM. Randomized studies have shown that 50 to 60 Gy radiation after surgery significantly increased the average survival of patients from 14 to 36 weeks (37-42) (though higher doses resulted in increased radiation injury to normal brain without any additional survival benefits (43-46)). In addition to radiotherapy treatment, GBM patients also receive the chemotherapeutic agent temozolomide (TMZ), which is a DNA alkylating agent (47); similarly to radiotherapy, this intervention elicits therapeutic effects by triggering apoptosis through the induction of DNA damage and cytotoxicity (48). The clinical benefit of the addition of TMZ therapy has been shown in a large phase 3 clinical trial. The administration of radiation therapy with concomitant TMZ chemotherapy, followed by an adjuvant TMZ chemotherapy, enabled an increase in survival when compared to radiotherapy alone; it increased the median overall survival to 14.6, from a 12.1 months baseline with radiotherapy alone, and also increased the 2 year survival more than two fold (from 10.4 to 26.1%) (49). However, this still constitutes a poor prognosis.

1.2.1. Developing targeted therapies

Despite the aggressive standard treatment regime of surgical resection and radio- and chemotherapy, the poor patient prognosis highlights the need for agents that target GBM; and, in particular, specific cell populations in GBM tumour responsible

for tumour recurrence. Extensive research into potential new avenues for treatment has led to the discovery of therapeutic agents that directly target GBM cells or modulate the tumour microenvironment. Elucidating the molecular signalling pathways activated in GBM – such as those involved in tumour growth, apoptosis, invasion/migration and angiogenesis – yields knowledge of specific molecular abnormalities of a particular tumour; abnormalities which may potentially be usefully targeted to better direct therapies. In this section, I will briefly address three such novel strategies (and their shortcomings) – gene therapy, immunotherapy and molecularly targeted therapies.

Over the last 2-3 decades, efforts to develop more effective gene therapy treatment for GBM has resulted in the development of several new and promising approaches (5, 50). With regards to GBM treatment, the most used gene therapy strategy involves the delivery of tumour-suppressor genes, suicide genes, genetic immunotherapy and oncolytic virus (50). Still, despite encouraging preclinical animal model data and results from phase I clinical trials demonstrating that these treatments possess promising safety profiles, this strategy has failed to show significant therapeutic efficacy in phase III clinical trials (5).

One of the largest phase III randomised clinical trials for the use of gene therapy for GBM treatment involved the delivery of herpes simplex virus thymidine kinase (HSV-tk) gene using retroviral packing cells. However, the addition of gene therapy to standard care yielded no significant therapeutic benefit, with the 12-month survival rates for control groups being 50% versus 55% in the treatment group (51). A later trial conducted by Colombo, where retroviral vector producing cells were used to deliver interleukin-2 (IL-2)/HSV-tk illustrated a common pitfall of GBM treatment (53). Of a total of 12 patients that received the therapy, 2 of them showed partial response to the therapy, 4 showed minor response, 4 showed stable disease and 2 had disease progression. These results highlight the heterogeneous response GBM tumour has to treatment and the difficulty of treating the disease as a whole (52).

A second type of targeted therapy is based on GBM treatment through immunotherapy strategies. A prominent recent strategy has shown that targeting the immune checkpoints programmed cell death 1 (PD-1) and programmed cell death ligand 1 (PD-L1) resulted in dramatic results in a pre-clinical model (53). Furthermore, preliminary data from the ongoing phase II clinical trial shows that 5 patients out of the 31 patients enlisted in the cohort analysed remain progression free after 1 year (54). Other attempts to treat GBM by targeting the patient's immune system are being accomplished by activating the immune system to eliminate the tumour. This can be achieved by presenting tumour lysate to the patient's own dendritic cells and then reintroducing the cells into the patients (DC vaccination). The most advanced DC vaccine in clinical trials –DCVax-L (NCT00045968) – is showing encouraging results with 33% of the patients surviving for at least 48 months and 27% of the patients reaching the 72 months mark (55). A first analysis after trial completion confirmed the elongation of the survival tail, as well as a significant extension of the median overall survival for patients with O-6 methylguanine-DNA methyltransferase (MGMT) methylation (56). As such, the therapy appears to yield an impressive extension of survival, but only to some populations.

Molecularly targeted strategies have gradually come to the fore over the course of this century. Due to the highly vascularized nature of tumours in GBM, one of the first molecularly targeted strategies was based on the use of angiogenesis inhibitors (57, 58). Following an initial promising single arm clinical study (59), a humanised monoclonal antibody – bevacizumab – was used to prevent neovascularisation by blocking vascular endothelial growth factor (VEGF) signalling. Unfortunately, clinical trials showed that, after the initial promise, bevacizumab in combination with standard therapy did not result in a clear survival benefit versus standard treatment alone (57). Another high-profile strategy was the targeting of epidermal growth factor receptor (EGFR). EGFR is a popular target for (oncological) drug development (60), and since changes to EGFR can be found in more than 50% of GBM it was deemed a potentially promising target.

A further intervention targeting this pathway was the development of a conjugate peptide vaccine, rindopepimut, which targets epidermal growth factor receptor variant III (EGFRvIII) specifically. This approach was predicated on the fact that 50% to 60% of EGFR mutants present the mutation EGFRvIII. Preliminary studies appeared promising (61), which led to the design of a successful phase II clinical trial (62) and a further push into phase III. Regrettably, however, the randomized study uncovered there was no survival benefit to this compound, with the median overall survival comparing even unfavourably to the control arm (20.4 vs 21.1 months) (63).

The up and downs of recent clinical trials results highlight the heterogeneity and complex pathogenesis of glioblastoma tumours and the unlikely event of there being a single-agent for GBM treatment. That is largely due to three key features of GBM: its heterogeneity, the presence of brain tumour stem cells (BTSCs) and the highly invasive nature of the malignancy. I will now briefly address the issues of heterogeneity and BTSCs in the two following sections, and finish by exploring the main focus of this thesis – migration.

1.3. Heterogeneity in GBM

An important hallmark of GBM tumours is their level of heterogeneity, as is indicated by the term multiforme. Tumour heterogeneity results from the presence of distinct cellular populations or clones within a tumour that contain different biologic, genetic or expression profiles (64). A recent study by Soeda et al. (65)showed that the sensitivities of subclones within the same population to treatment differed amongst these cells, denoting that other factors such as heterogeneity are a cause of treatment resistance. Thus, the presence of clones which are resistant to treatments are a cause of treatment failure and tumour relapse (66).

1.3.1. GBM subtypes

Recent studies focusing on the mutational landscape, heterogeneity and lineage of each tumour, allied with the large-scale sequencing of the glioblastoma genome, have revealed genomic abnormalities and gene expression profiles linked with GBM tumorigenesis (67-69). Initial results arising from these studies demonstrated that at least two distinct molecular pathways lead to the development of GBM and this would allow the subtyping of the disease into primary and secondary glioblastoma (70, 71). Even though primary and secondary glioblastoma are histologically indistinguishable, these subtypes constitute different disease entities that affect patients in different age groups; that progress through distinct genetic pathways; and that present different expression profiles for RNA and proteins (70). Frequent genetic alterations associated with primary GBM are the overexpression of EGFR, mutations in phosphate and tensin homologue (PTEN) and loss of chromosome 10q. On the other hand, secondary GBM commonly have mutations in isocitrate dehydrogenase 1 (IDH1), tumour protein 53 (TP53) and loss of chromosome 19q (5, 72, 73).

In addition, further analysis of the data from the Cancer Genome Atlas network by Verhaak et al. (74) resulted in a robust gene expression-based molecular subtype classification of GBM. Using integrated multidimensional genomic data to establish patterns of mutations, DNA copy number and transcriptional signatures, four distinct subtypes were identified: Classical, Proneural, Mesenchymal and Neural (74).

Classical subtype. The GBM classical subtype presents with mutated EGFR, which leads to the high expression of EGFR, and lacks the mutation in TP53 and the deletion of cyclin dependent kinase inhibitor 2A (CDKNA2A), resulting in the inactivation of the retinoblastoma associated pathway. It is characterized by the amplification of chromosome 7 and deletion of chromosome 10. Transcriptional changes associated with classical subtype include high expression of neural precursor

and stem cell marker nestin as well as neurogenic locus notch homolog protein 3 (NOTCH3), smoothened, frizzled class receptor and growth arrest specific gene 1.

Proneural subtype. Main features of the proneural subtype are the alterations in the platelet-derived growth factor receptor α (PDGFRA) and point mutations in IDH1. Mutations in PDGFRA lead to the activation of phosphoinositide 3-kinase (PI3K) and rat sarcoma (RAS) pathway and, interestingly, the presence of PDGFRA abnormalities is related to the absence of IDH1 mutations. The majority of TP53 mutations and loss of heterozygosity were found in this subtype. Furthermore, this subtype presented with high expression of oligodendrocytic developmental genes.

Mesenchymal subtype. The mesenechymal subtype has mutations not only in NF, which in turn activates the PI3K/protein kinase B (Akt) pathway, but also in PTEN, which activates the RAS pathway (74). This subtype also displayed the expression of chitinase-3-like protein (YKL-40) and met proto-oncogene (MET), which is suggestive of an epithelial-to-mesenchymal transition (74, 75).

Neural subtype. Even though no genetic signature has been attributed to the neural subtype, it is associated with transcriptional expression of neuron markers, such as neurofilament, light polypeptide, synaptotagmin 1, gamma-aminobutryc acid A receptor α 1, or solute carrier family 12 member 5 (74).

The stratification of GBM into molecular subgroups is proposed to be linked to different patterns of disease progression and survival outcomes. For example, the overall survival of treated patients varies with the subtype, with classical or mesenchymal subtypes surviving longer than the proneural subtype. Thus, the discovery of these subtypes in GBM may be of clinical relevance in suggesting different therapeutic approaches that each subtype may require (69), and might accelerate our understanding of the disease.

1.3.2. Inter and intra-tumour heterogeneity

Tumour heterogeneity can result from mutational and transcriptional variability amongst tumours as well as different genetic, epigenetic, functional and phenotypic properties of cellular subsets and even single cells within a tumour (76). Inter-tumoural heterogeneity has been described in GBM for matrix metalloproteinase-2 (MMP-2), integrins and MGMT (77-79).

The implications of inter-tumoural heterogeneity regarding therapeutic treatment is clear for the case of patients with MGMT hypermethylation. The recognition of MGMT hypermethylation as a valid prognostic and predictive marker in patients undergoing chemotherapy with alkylating agents is the perfect example of the successful implementation of personalized therapy based on the individual's genomic landscape (80, 81). MGMT is a repair protein that specifically removes promutagenic alkyl groups from O6-methyguanine (82). The promoter methylation of the gene encoding for MGMT leads to the loss or reduction of MGMT activity, which ultimately causes the increase of double strand breaks and induces apoptosis and cell death (82). The methylation status of the MGMT promoter is associated with increased efficacy of current standard of care (concomitant and adjuvant radiotherapy with TMZ), with the median survival of patients with methylated MGMT promoter of 21.7 months versus 12.7 months in non-methylated patients (83, 84). In addition, studies have shown that profiling-based subtypes have clinical relevance when it comes to therapeutic strategies directed at MGMT methylated tumours (74). In both classical and mesenchymal subtypes, MGMT methylated tumours respond better to aggressive treatment when compared to the non-MGMT methylated tumours. In the neural and proneural subtypes there was no difference in the response to aggressive treatment when these were stratified based on their MGMT status (74). In addition to the heterogeneous expression of MGMT amongst distinct tumours, there is also intra-tumoural heterogeneity regarding MGMT promoter methylation, with the tumour

possessing distinct areas with positive MGMT expression surrounded by negative cells (85, 86).

Similarly, several studies have described a heterogeneous inter and intra-tumoural pattern of receptor tyrosine kinase (RTK) amplifications in GBM (87, 88). From the most commonly amplified RTK in GBM (EGFR, PDGFRA and MET) studies revealed that amplifications of these occurred in a heterogeneous fashion amongst tumours; with the majority of tumours possessing amplification to either one or two RTK (87, 89, 90). This discovery may explain why small-molecule inhibitors used in GBM clinical trials show little or no improvement in overall survival of the patient. The targeting of a single RTK is not effective because the cells can switch to another RTK (RTK-switching), thus maintaining the activation of the downstream pathway and driving tumour growth (89). Furthermore, amplification of these three RTKs have also been detected in small subsets of cells in separate regions or dispersed throughout the tumour (89).

A recent study by Patel et al. (25) highlighted the intratumoural heterogeneity in primary glioblastoma using single-cell RNA-seq. Cellular variability within each tumour was demonstrated by the differential expression and splicing patterns in signalling molecules pertinent to GBM, as for example EGFR, fibroblast growth factor 1 and its receptor, and neurogenic locus notch homolog protein 2 (NOTCH2). Interestingly, an attempt to cluster the single cells into the four glioblastoma subtypes described above resulted in the single cells from a unique tumour corresponding to different glioblastoma subtypes (25). This cell-to-cell variability highlights the fact that analysis of the tumour bulk detects the dominant subtype and does not truly represent the diversity of subtypes within a tumour.

Heterogeneity exists in every GBM and it has been shown that increased intratumoural heterogeneity is associated with decreased survival (25, 91). Hence, the understanding of tumour heterogeneity is crucial for the treatment of the disease. As mentioned above, the use of single-agent targeted therapies has been disappointing,

and this is because GBM rely on multiple redundant signalling pathways. Consequently, an effective GBM therapy must result from combined therapies and personalized medicine which is based on the mutational landscape and heterogeneity of each tumour.

1.4. Brain tumour stem cells (BTSCs)

In addition to the heterogenous nature of GBM cells, it has been demonstrated that this disease has an apparent stem cell foundation – here termed brain tumour stem cells (BTSCs) (20). The important role that brain tumour stem cells play in the heterogeneity of GBM requires an extensive understanding of the nature of these cells. Traditionally, genetic analyses of brain tumours were carried out on the bulk tumour mass. However, these studies were unable to explain why brain tumours that have similar morphology and phenotype can also have different prognosis and response to therapy (92). While this difference can reasonably be attributed to tumour heterogeneity, studies have also linked this to a small population of tumours cells with self-renewing capacity (93). Studies in other cancers, such as leukaemia and breast cancer proved the existence of a population of rare cells that had considerable proliferative and self-renewal potential and was also able to drive tumour growth and formation (94, 95).

While established for other cancers, the cell(s) that gives rise to the brain tumour stem cell subpopulation is still contested (96). Identification of the cell of origin for GBM would contribute to a wider knowledge regarding the initiation and propagation of the tumour as well as its biology. Although the exact mechanisms by which BTSCS arise remains unknown, diverse evidence demonstrated that this subpopulation may originate from either the de-differentiation of differentiated cells or from neural stem cells or progenitor stem cells (97, 98). These cells then have the capacity to give rise to the tumour's cellular hierarchy via differentiation and thanks to their self-renewing

abilities (97). Albeit the mainstream consensus is that BTSCs originate from stem cells (neural or progenitor), studies have shown that somatic cells can dedifferentiate and acquire pluripotency and the ability to self-renew. For example, Friedmann-Morvinski et al.(99) demonstrated, in mice, that a diversity of cells in the brain, comprising terminally differentiated neurons and cortical astrocytes, had the ability to originate GBM (99).

Conversely, it is conceivable that the cell of origin can be derived from the transformation of either a neural or of a progenitor stem cell (98). Whilst the former cells are pluripotent and can give rise to all cell types in the body, the latter cells are multipotent and restricted to cells in a particular lineage (100). Despite the initial uncertainty of whether adult brains possessed an active neural stem cell (NSC) niche, studies have now identified multipotent NSC in the subventricular zone of the adult human brain (101, 102). Thus fuelling the theory that these cells might act as the cell of origin for GBM. Genomic analysis presented by Verhaak *et al.* (74) and Galli et al. (103) showed that there was an evident relationship between GBM classes and cellular lineages. Therefore, suggesting that a common cell of origin, such as the neural stem cell, exists for the disease and that each subtype merely results from diverse differentiation pathways.

Moreover, a recent study by Lee et al. (104) showed that NSC niches in the subventricular zone of the human brain, can harbour neural stem cells that possess low-level driver mutations which are typically associated with GBM (104). Hence, this study shows for the first time a direct genetic link between human NSC and GBM (104). Nevertheless, it also remains unclear whether GBM is the result of unique cell of origin or if the BTSCs result from a combination of several cells with the ability of self-renewal and give rise to differentiated progeny. This latter hypothesis could potentially explain the inter and intra tumour heterogeneity seen in GBM.

Regardless of the proposed origin, BTSCs are now described as undifferentiated tumour cells that are characterized by their capacity to self-renew (maintaining

tumour growth indefinitely); their ability to give rise to more differentiated cell progeny of neuronal, astroglial and oligodendriglial phenotypes (constituting the bulk of the tumour) and their capacity to initiate tumour growth *in vivo* (75). In addition, BTSCS diverge from differentiated tumour cells with regards to gene expression and biological behaviour, like proliferation and resistance to conventional therapeutic interventions (105-107). Their self-renewal capacity is reminiscent of self-renewal mechanisms of neural stem cells; hence, they share various features with NSCs including NSCs surface markers – e.g., neuroectodermal stem cell marker (NESTIN), sex determining region Y-box 2 (SOX2), CD133, and CD44 (20, 108). Furthermore, Lan et al.(109) also confirmed the existence of BTSCs and their ability to form a tumour *in vivo* with a serial xenotransplantation of barcoded GBM cells. Following serial passaging of the GBM cells, a subset of clonal cells only became apparent after the second passage, which demonstrates that the initial population contained a fraction of cells with self-renewing capacity (109).

However, targeting this subpopulation of BTSCs continues to pose a serious hurdle, given that their resistance to standard cytotoxic therapies. They exhibit resistance to both radiotherapy and chemotherapy, possibly due to the activation of DNA repair mechanisms, in the former case, and the existence of efflux drug transporters (ATP mediated cassette transporters), in the latter (106, 110, 111). Thus, it comes as no surprise that these relatively quiescent chemo- and radio- resistant stem cells are the fundamental driving force not only in maintaining long-term tumour propagation, but also in tumour recurrence (112, 113).

A promising therapeutic avenue that specifically targets BTSCs resulted from *in vitro* studies in which BTSCs were forced to differentiate with the use of small chemical compounds, such as bone morphogenetic proteins (BMP), retinoic acid, 2-hyroxyoleic acid, serum and curcumin (114-118). Piccirillo et al. demonstrated that there was a significant decrease in tumourigenicity following differentiation (118). In addition, continuous propagation of BTSCs in the presence of serum forces the cells towards a

differentiated state resulting in alterations of the molecular and phenotypic characteristics of the cells (119). Thus, the combination of differentiation therapy and current available therapies could provide an encouraging treatment for reducing GBM recurrence and ameliorating patient survival.

1.4.1. Isolation and culturing of BTSCs

The initial discovery of brain tumour stem cells in GBM was based on the surface expression levels of neural stem cell markers. Singh et al. (20) reported the existence of tumour cells which possesses stem-like features in phenotypically distinct human brain tumours. In this study, they demonstrated that the enrichment of these stem-like cells was possibly based on the isolation, from patient tumours, of a CD133-positive population. This subpopulation of CD133 positive cells, also termed BTSCs, possessed the capacity to proliferate, self-renew and differentiate. Furthermore, only the CD133 positive population was able to grow a xenograft tumour in mouse models, which displayed histopathological resemblance to the patient tumour (20). Nevertheless, other studies have demonstrated that CD133 negative cells also have tumorigenic potential (120-122). Additionally, recent studies have further identified other stem cell markers related to BTSCs, i.e. CD15 and CD44 (107, 123). However, the notion of using surface markers as a universal marker for BTSCs is contested, with studies showing that the process of tumour cell isolation can result in the reorganization of cell surface markers, thus, leading to the loss of these stem cell markers over time (124).

Other methods of BTSC enrichment have been proposed. In particular, Lee et al. (119) showed that tumour cells cultured, either as adherent cells or as neurospheres, in media containing human basic fibroblast growth factor (bFGF) and epidermal growth factor (rhEGF) allowed the maintenance of their stem-cell like phenotype when compared to serum-cultured cells. Furthermore, they showed that these BTSCs closely resembled the genotype, gene expression profile and *in vivo* biology of their

parental tumour. Notably, these cell once xenografted also mimicked the invasive nature of GBM.

The *in vitro* expansion of BTSCs as a stable stem-like cell line has been successfully used in chemical and genetic screens and has proven to be a disease-relevant experimental model (125, 126). The ability of long-term culturing of BTSCs as an adherent monolayer constitutes also an ideal model to research the underlying mechanisms behind this malignant and invasive disease (125, 126).

1.5. GBM invasion

In GBM, one of the major contributor to tumour recurrence is the diffusive invasion of single tumour cells into neighbouring brain tissues (127). Invasion defies even radical surgical approaches, as in the case of hemispherectomies, where the removal of the entire brain hemisphere affected by the tumour was unable to stop tumour recurrence, for tumour cells had crossed over to the other hemisphere (128). Even nowadays, in the era of modern surgical techniques, this diffusive nature enables tumours to escape maximal tolerable surgical resection and in 95% of the cases, the tumour will recur within 2 to 3 centimetres from the original tumour borders (129, 130). Whilst invasion implies that cancer cells actively move within the tissue, this process is only possible due to the cells intrinsic ability to migrate. Brain cells are inherently motile and migration plays a fundamental role in normal brain development (131). In the brain, the tightly regulated process of neural progenitor cell / neuroblast migration allows the correct spatial positioning of the cells and enables them to interact appropriately (131). However, these same routes of migration that immature neurons use during embryonic development, or adult stem cells use in the mature brain, can also be exploited by brain tumour cells once motility becomes dysregulated (132-134).

Despite all the important progress in understanding the genetic modifications that characterize glioblastoma and the impact this research has on the treatment of the disease, one feature is conserved amongst the subtypes. This aggressive invasiveness that is, in a way, characteristic to GBM cells (24). In fact, a recent fate mapping study of human glioblastoma cells by Lan et al. (109) demonstrated that self-renewal and invasion capacity were coincident characteristics of the same labelled clone, indicating that GBM stem-like clones are uniformly invasive.

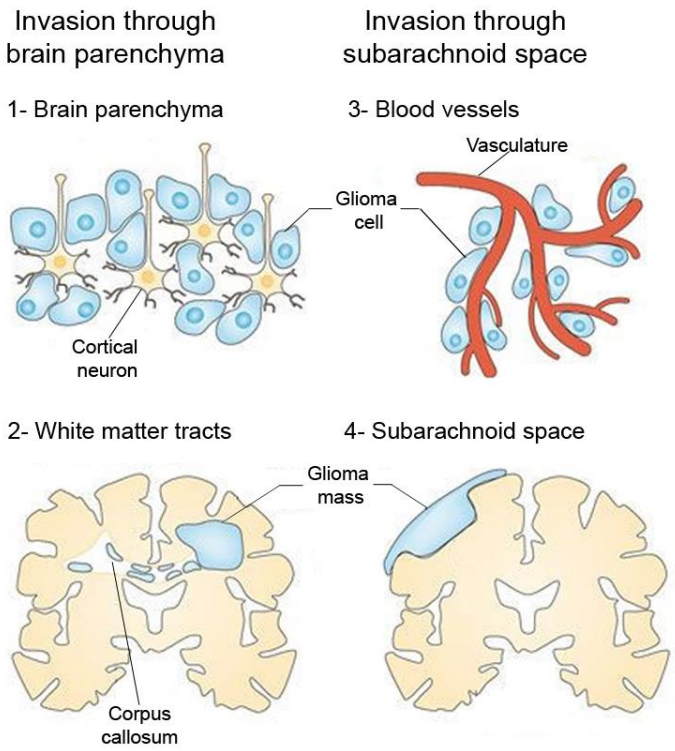

Figure.1.1 Pathways of glioblastoma cell invasion. GBM cells are able to migrate into the brain by: (1) moving through the interstitial spaces of the parenchyma; (2) along white matter tracts; (3) by using pre-existing blood vessels and (4) through the subarachnoid space (adapted from [127]).

Normally, malignant cancers spread through two distinct manners. The first route includes the invasion to another organ leading to metastasis; whilst the second involves intra-organ invasion (132). In contrast to other invasive cancers, the occurrence of metastases in glioblastoma is extremely rare; with only a small proportion (up to 2%)

metastasising outside the brain (135-137). Even though the exact reason for the lack of metastasis is unknown, it is hypothesised that the rapid progression of the disease does not allow time for metastasis to establish outside the brain and become apparent (132). Furthermore, it is also possible that other organs do not possess the appropriate microenvironment to support GBM growth (132). On the other hand, GBM cells are extremely proficient at intra-organ invasion, migrating through the extracellular spaces of the brain parenchyma (132).

1.5.1. Pathways of invasion

GBM achieves an extensively invasive phenotype via actively traveling using existing brain structures (138). It is possible to divide these invasion pathways into two types of extracellular spaces: invasion using perivascular spaces and invasion through brain parenchyma (Figure 1.1) (138). In the first category, cells rely on the use of pre-existing blood vessels or on the subarachnoid space to invade the brain (139). The migration along blood vessels is an important pathway for GBM invasion. The vasculature provides the cells with a generous supply of oxygen and essential nutrients. Montana et al. (140) have demonstrated that when glioma cells are injected into the brain, the majority of these cells (85%) move in order to be in contact with a blood vessel. In the second category, cells migrate across the whole of the brain parenchyma; through both neurons and glial cells and also along white matter fibre tracts (139). Migration through the parenchyma involves the movement of cells through narrow and tight extracellular spaces, which poses greater resistance than the perivascular movement (139). Importantly, invasion using white tract matter accounts for the migration of BTSCs to the other hemisphere of the brain (139).

The ability of GBM cells to move through these tight spaces is a result of a sequence of coordinated biological changes (134). This biological process starts with the cells becoming morphologically polarized; developing a leading edge; anchoring to the extracellular matrix (ECM) and finally detaching the trailing end (134, 141). For

the cells to travel through these extracellular spaces, they need to be capable of altering their shape and morphology (134, 141-143).

1.5.2. Modes of invasion

Typically, single cells that migrate through the ECM can be divided into two distinct modes of invasion: mesenchymal mode or amoeboid (142, 143). For GBM cells, the main form of single cell invasion is a result of mesenchymal movement (144, 145). In this form of movement, cells are presented with polarized cytoskeletal extensions at the leading edge and integrin-mediated adhesion dynamics. This form of movement is a result of the combined effect of processes mediated by Rac and Cdc42; and the antagonistic effect of Rho-mediated adhesion strengthening and cell contractility (146). Such cytoskeletal reorganization and adhesion dynamics result in morphological changes in the cells. These become elongated and spindle-shaped (147, 148). In this form of migration, the leading edge indicates the direction of the migration (149). Contrary to the amoeboid mode, mesenchymal movement is dependent of the proteolytic degradation of the ECM (150). The proteolytic degradation of the ECM is achieved by the production a large number of secreted proteases. In GBM, the distinct proteases secreted include matrix-metalloproteinases 2,9 and 14 (MMPs – 2, -9, -14) (151), the serine proteases uPA and cell surface proteases (132).

However, Koh et al. (152) recently demonstrated that GBM cells were able alter their invasion route and transition from a mesenchymal mode of invasion to an amoeboid mode, depending on the microenvironment. Amoeboid cells have the tendency to migrate in the absence of proteolytic ECM degradation and squeeze through extracellular gaps (142, 153). Merely blocking the proteolytic degradation of the ECM was enough to cause the switch in invasion mode to amoeboid (152). In this form of migration, cells present with a rounded morphology and migrate with low adhesion force or high actomyosin-mediated contractility (142, 143). Generally, this

form of movement can be dependent on Rac signalling or be controlled by the small GTPase RhoA (146). In the first instance, engaged adaptor proteins lead to focalized actin assembly, in the form of pseudopodia, lamellipodia and filopodia. In this movement the adhesion sites are poorly defined and generate weak adhesion forces (154). In the second instance, Rho-dependent blebbing mediates the movement by producing either blebs or protrusions at the leading edge, thus lacking adhesion sites (155, 156). As a result of the diffusely organized protrusions and blebbing-dependent movement, these rounded cells move in a random manner (154-156).

Regardless of the specific mode of invasion that the GBM cells use to invade the brain, this movement is dependent on cytoskeleton dynamics. Thus, the investigation of the mechanisms that cause cell migration in GBM has the potential to lead to the development of promising treatment avenues that can tackle this GBM hallmark.

1.5.3. Cytoskeleton dynamics in migration

The human cytoskeleton is a complex framework composed of actin, tubulin and intermediate filament proteins (141). These distinct classes of proteins cluster non-covalently into filamentous polymers, which not only support the integrity of the cell, but also furnishes the cells with the molecular motors necessary for movement (157). In order to respond to migratory and chemotactic stimuli, the rapid remodelling of the cytoskeleton provides the cells with the necessary motive and tractor forces to drive motility (158, 159). The process of cellular migration is initiated by the polarization and extension of cellular protrusions toward the direction of movement (157). These extensions, which are typically driven by actin polymerization, can either be broad lamellipodia or spike-shaped filopodia (157, 159). The stabilization of these adhesion sites is possible thanks to the anchoring to the ECM or to other nearby cells, a process which is associated with the actin cytoskeleton (141). These adhesion points function as gripping points, allowing the cells to move forward, while concurrently disassembling the cytoskeleton at the rear (157, 159). While this migration process is

shared between distinct cell types, the cells exact migratory behaviour is dependent on the underlying microenvironment; cancer cells are thus able to alter their mode of migration in response to their microenvironment (158).

1.5.4. Actin cytoskeleton and regulators in cancer invasion / migration

The aberrant control of the cells inherent migratory ability causes the invasive cancer cells to invade nearby tissue and vasculature (160). Cancer migration is a complex and multifaceted process, which naturally involves the dynamic spatial and temporal reorganization of the actin cytoskeleton (160). In the literature, studies demonstrate the upregulation of molecules that link migratory signals to the actin cytoskeleton in invasive cancer cells (161-164). For example, it has been shown that the production of endothelial growth factor (EGF), an important chemotactic in breast cancer, is directly correlated with the formation of lamellipodia (162). In this study, gene expression analyses showed that proteins involved in the upstream signals that induce actin polymerization (Wiskott-Aldrich syndrome family protein-Arp2/3) were upregulated following the activation of the EGF signalling pathway (162). The formation of lamellipodia, which is initiated by the local polymerization of actin, led to increased invasion and intravasation in breast cancer cells (162).

In the case of GBM, studies have shown that cortactin, which is a ubiquitously expressed protein that binds to actin, plays a fundamental part in the dynamic actin cytoskeleton regulation. Wang et al.(163) uncovered that cortactin promotes migration and invasion of the U251 glioblastoma cell line via regulation of lamellipodia formation. They further reported that inhibition of cortactin expression resulted in the reduction of lamellipodia. Conversely, Zhang et al. (164) demonstrated that metastasis suppressor 1 reduced cell migration in the U-87 glioblastoma cell line by inhibiting the expression of cortactin. From a different standpoint, it has been demonstrated in GBM that hypoxic environments are also able to coordinate changes

in cytoskeleton dynamic, thus increasing cellular migration (165-167). In addition, cytoskeleton modulators like Rho GTPases and βIII-tubulin also play a crucial role in the invasive phenotype of GBM cells (168, 169). Even though these are just a few examples, they paint a clear picture regarding the important role the actin cytoskeleton and its molecular regulators play in invasion/migration; both across a number distinct cancer types and specifically in GBM.

1.5.5. Rho GTPases as cytoskeletal regulators in cancer

Rho GTPases are signalling G proteins, best known for their role in actin and microtubule cytoskeleton organization. However, they have also been implicated in cellular motility, proliferation, survival and differentiation (170-172). They are part of a distinct family within the Ras protein superfamily and act as molecular switches in signalling pathways. The Rho family comprises 20 members, counting Rho, Rac and Cdc42 amongst them (170, 173). It is through the action of these downstream effector proteins that the Rho family can control the cytoskeleton (170, 172, 173). Rho GTPases have oncogenic activity which has been linked to pathological processes including cell migration and invasion (172, 174, 175).

Studies performed on p21-activated kinase (PAK), which is a protein kinase downstream of Rac and Cdc42, showed that this protein plays an important role in actin dynamics and adhesion (176). Adam et al. (177) illustrated that the inhibition of PAK activity abrogated the invasive behaviour of the breast cancer cells, MDA-MB435, into a gel matrix substrate. This study further showed that the abrogation was a result of PAK downstream pathways that lead to the reorganization of cytoskeletal components. Another study, by Eitaki et al.(178), reported that microtubules played a fundamental role in the regulation of the mode of invasion on the gastric adenosarcoma cells MKN45. This study showed that treatment of the MKN45 cells led to the increase of motility and invasion through the activation of the RhoA/ROCK/MLC pathway (178).

In GBM, it has also been shown that the aberrant regulation of Rho GTPase has an effect on tumour invasion and progression (reviewed in (168)). For example, it has been described that levels of Rac1 protein positively correlate with tumour grade in (179, 180). In fact, Tran et al.(180), showed that activation of Rac1 encouraged the invasive behaviour in the glioblastoma cell line, U87. Furthermore, in this study they demonstrated that the invasive behaviour induced by overexpression of fibroblast growth factor-inducible 14 (Fn14) was inhibited by depletion of Rac1 (downstream of Fn14) using RNAi. Rac1 also has an overlap of activators and effectors with Cdc42(181), although it has been shown that the latter can regulate migration in a Rac1-independent manner (182, 183). Bigarella et al.(184) described that the depletion of the upstream effector of Cdc42 (Rho GTPase activating protein (ARHGAP21)) resulted in changes in cell morphology, MMP-2 production and rate of cell migration. However, much of the work done to study the effect Rho GTPase has on GBM migration has focused on the activity of RhoA, and specifically on the role of its effector protein Rho-associated coiled coil kinases (ROCK1 and 2) (168, 180, 185-187). It is to that effector protein that I now turn my focus.

1.5.6. ROCK and cancer

The Rho-associated protein kinases (of which there are two, ROCK1 and ROCK2, referred to collectively as ROCK) are major downstream effector of the Rho GTPase family of proteins (188). Research over the last few decades has shown that ROCK plays a central role in the regulation of actin cytoskeleton remodelling and dynamics, with its main function being to promote contractile force generation (189, 190). Through its kinase domain, active ROCK exerts its effect on the cytoskeleton by phosphorylating and activating downstream targets, i.e. myosin light chain (MLC), Map tau and Lim kinases (191). The phosphorylation of MLC activates this protein and its ability to inhibit the dephosphorylation of myosin phosphatase target 1 subunit. This impacts actin reorganization and stress fibre formation (191). Additionally,

ROCK kinase also plays an important part in distal cellular processes, such as cellular proliferation and differentiation, apoptosis, or oncogenic transformation (192-194). It is also assumed that ROCK phosphorylation of MLC further impacts cell invasion and migration by altering the conformation of the cytoskeleton (195, 196).

It has been described that the two isoforms of ROCK have slightly different patterns of expression, depending on the tissue (194). Whilst the expression of messenger RNAs for both ROCK 1 and 2 are ubiquitous in the majority of cell types, ROCK 1 transcripts are mostly expressed in the haematopoietic system and digestive organs, while ROCK 2 transcripts are heavily expressed in the brain and muscles (194, 197). Despite the differences in expression, similar roles in cytoskeleton organization, migration and cellular morphology have been shown for these isoforms (198, 199).

Recent studies have shown that amplification of ROCK signalling enhances cell migration, invasion, proliferation and metastasis (200-202). Indeed, ROCK levels were found to be highly expressed in several cancers, like prostate, bladder, gastric and lung cancers and glioma (198, 201-205). In glioma, the high expression was correlated not only with the tumour's ability to invade, but also with its malignancy (185, 198).

Itoh et al.(206), showed that the inhibition of ROCK in hepatoma cells (MM1) hindered the ability of the cells to form tumour in an animal model, thus reducing their metastatic potential. Furthermore, Murata et al.(207) demonstrated that ROCK inhibition prevented the hepatic carcinoma cells from dissemination by reverting the cells into a less aggressive form of growth in the liver. Likewise, other studies have also demonstrated that suppression of ROCK could prevent the invasion and metastasis of gastric and also prostate cancer cells (208, 209).

In GBM the inhibition of ROCK in the GBM line, U87, resulted in the reduction of cell migration and proliferation (210). Similar results were observed by Zohrabian et al. (211) in the glioblastoma cell line, Ln18. In addition, Wan et al. (212) showed that the downregulation of ROCK by miR-145 could inhibit the invasive phenotype of U87 cells. Moreover, loss-of-function and chemical inhibition studies have implicated

ROCK signalling in cell fate decisions and malignant cellular behaviour, although the underlying mechanisms are not well understood (203). In sum, these studies illustrate the importance cytoskeleton modulation has on cancer cell behaviour, migration, proliferation and metastasis. Thus, it is conceivable that disrupting ROCK signalling could represent a promising pharmaceutical approach for tackling GBM migration.

1.5.7. Y-27632 in the study of GBM migration

Several small molecules inhibitors have been used to inhibit the ROCK signalling pathway (H1152, GSK269962A, GSK-429286, etc.), but amongst them the inhibitor Y-27632 has been the most widely used and studied (213). The pan-ROCK inhibitor Y-27632 has been previously used to investigate the involvement of ROCK in many physiological and pathophysiological processes, including GBM progression (203, 205, 212). Nevertheless, there have been several conflicting reports of the effect ROCK pathways inhibitors might have on distinct cell types. Mixed outcomes for the inhibition of ROCK signalling pathway has been described for distinct cell types. Routhier et al. (214) demonstrated that the chemical inhibition of ROCK blocks tumour melanoma growth and invasion. However, when added to human stem cells, Watanabe et al. (215) showed that Y-27632 led to an increase of survival and proliferation of the cells.

Reports are similarly inconsistent in the context of GBM. ROCK inhibition has been linked to the suppression of cell migration and the reduction of cell proliferation in a GBM cell line (211). These results were contradicted by Tilson et al. (216), who demonstrated that the inhibition of the ROCK pathway using Y-27632 increased the proliferation of GBM BTSCs; and by Salhia et al. (187), who showed that chemical ROCK inhibition increased the migration and invasion of astrocytoma cells by 2-fold. Overall, the dissonant evidence on ROCK inhibitors dose response relationships and cell type-specific effects suggests the need for further work towards clarifying potential beneficial pharmacological applications for ROCK inhibitors.

In addition, with the current use of the ROCK inhibitor (Fausidil) in the clinic in Japan, and the first-in-human clinical trials of another ROCK I and II inhibitor (AT13148 [ClinicalTrials.gov Identifier NCT01585701]), taking place in patients with advanced solid tumours, there has been a pivot towards reconsidering the use of ROCK inhibitors for cancer treatment. However, Rath and Olson (217) make the compelling argument that, despite the initial promise of using ROCK inhibitors in a clinical setting, additional pre-clinical research is required to successfully translate knowledge of ROCK signalling inhibition into a clinical setting. Thus, there is a gap in knowledge regarding the effect pan chemical ROCK inhibition has on GBM cells which needs to be addressed before these small molecules inhibitors become integrated into the clinic.

1.6. Studying GBM migration

The ability to study cellular migration and invasion is crucial for understanding the molecular mechanisms involved in this dynamic process. The development of several 2D and 3D *in vitro* and *in vivo* techniques has been instrumental in enabling the study of this process (218, 219). Generally, 2D *in vitro* techniques are the most commonly used because they are also fast and quantitative methods (161). Among these, the most frequently used are the scratch/ring assay, transwell/(modified)boyden assay and the tracking of cellular movement on a 2D substrate (161). While all these techniques have the advantage of being cheap and simple, there are also firm caveats to their use (218). In the scratch/ring assay, the cells move in a defined direction, making the visualization of the movement easy (161). Unfortunately, the analysis of these results can be less than straightforward; the cellular adhesions can interfere with cell motility and it is difficult to discern cellular proliferation from cellular migration (218). For the transwell assay, the ability to use different ECM components and analyse movement in response to a chemo-attractant gradient is a clear advantage but, on the other hand, high resolution imaging is very difficult to accomplish (218). Finally, tracking

movement on a 2D substrate has the advantages of being easy to modify (distinct components can be used as substrates) and the conditions easy to manipulate (media can be easily changed to study effect of different components) (161). However, the analysis of the cellular movement can prove to be quite difficult, given that cells move in a random pattern and cellular confluency also hinders the tracking of the cells (161). Despite all the potential advantages of using *in vitro* assays, the study of migration in an *in vitro* context has a common and obvious disadvantage – the cells are in an artificial environment (161, 218, 219).

As noted in section 1.5, for GBM cells to invade healthy tissue, the cells need to be able to move through tight and tortuous spaces and degrade the ECM. These important characteristics that lead to GBM's invasive behaviour are not fully captured in a 2D context. In addition, there is increasing evidence that suggests that the migratory behaviour of cells in an *in vitro* context can differ from the cells *in vivo* behaviour (220, 221). Thus, assays that simulate this 3D environment are also needed for the study of migration.

The use of 3D *in vitro* collagen/ECM invasion assay for the study of migration has been growing in popularity (152, 222, 223). In this approach, cells are seeded onto a reconstituted 3D matrix, which is normally composed of collagen or a mixture of ECM-like components, and cells are observed actively migrating into this matrix. In this technique, the use of a 3D matrix which can contain components of the ECM that closely recapitulates the degradation of the ECM observed *in vivo* (161, 219). Still, this model does not mimic the complete tumour microenvironment. Tumour cells in the brain do not interact only with the ECM, but also with brain cells, neurons and glial cells (219, 224). More importantly, it has been shown that the interaction of tumour cells with the microenvironment also impacts the ability of the tumour cells to migrate and invade (219, 224).

In order to address this problem, some cell migration studies focused on the use of animal models or of brain slices. The use of intravital imaging to study labelled

tumour cells in mouse models has provided great insight into cell migration in vivo and in real-time (225). Even though this approach has the correct tumour environment (albeit not human), given that it has stromal cells and ECM, it is a costly and labour-intensive technique which is not easily accessible (225). In addition, 3D context has also been obtained using ex vivo human organotypic brain slice cultures (226-229). Even though these ex vivo brain slices are amenable to the real-time study of GBM migration, the life time of these specimens is reduced (maximum life span is 14 days) and it is difficult to obtain these slices from the clinic (226, 229). Hence, as suggested by the emergence of the approaches described, there is a gap in model development and there is still a need for a 3D human model that allows for the real-time study of tumour invasion into healthy brain tissue.

1.6.1. Cerebral organoid model as a potential platform for GBM migration studies

Although, these studies provide insights into the mechanisms behind the invasive phenotype of GBM cells, none completely recap the precise brain microenvironment or recapitulate the heterogeneity and complexity of the brain. Fortunately, the recent boom in organoid methodology provides the ideal platform to model disease invasion in an *in vitro* 3D model (226, 230-234).

The development of organoids has been one of the most stimulating advancement in stem cell research (235). Organoids constitute miniaturized and simplified versions of organs; in contemporary use, they are further "defined as a 3D structure grown from stem cells and consisting of organ-specific cell types that self-organizes through cell sorting and spatially restricted lineage commitment" (236), similarly to the process *in vivo*. Organoids have already been generated for various organs (among them intestine, retina, liver, kidney, prostate and brain) and provide an exclusive alternative to replicate normal human organ development or to model diseases in a system comparable to *in vivo* development (226, 230-234, 237). Following the initial creation

of cerebral organoids, there have been several reports which build upon the original idea and developed new models to recapitulate brain development and distinct brain regions (238-241).

Studies focusing on brain disease modelling using organoids have led to the development of models capable of mimicking microcephaly, autism, cancer and modelling Zika virus exposure (232, 233, 242-246). The use of cerebral organoids to model GBM initiation, progression and heterogeneity has already been published. Ogawa et al. (247) showed that the GBM organoid was able to model the influence of microenvironmental hypoxic gradients on GBM biology; and they also saw that the organoid was representative of the heterogeneity found in patient tumours. Hubert et al. (248) made use of clustered regularly interspaced short palindromic repeats (CRISPR)/Cas9 technology to model tumour initiation in cerebral organoids; and further studied tumour progression using time-lapse microscopy (248). However, these models focus on the progression of GBM, rather than on its invasive and migratory phenotype. Still, they demonstrate the possibility of using cerebral organoids to study GBM features and highlight the enormous potential this system has to be developed into a model that allows the real-time study of GBM migration and invasion.

1.7. Aims and objectives

Glioblastoma multiforme (GBM) is the most frequent and aggressive malignant primary brain tumours in adults. One of the major challenges in the treatment of GBM stems from the highly invasive nature of glioblastoma cells, which migrate/infiltrate into the healthy brain tissue. This phenomenon complicates the complete surgical removal of the tumour and ultimately enables tumour recurrence. The complex process of tumour migration/infiltration involves the dynamic reorganization of the actin cytoskeleton, which allows the cells to migrate through the brain's extremely

limited extracellular spaces. The underlying molecular mechanisms of this dynamic process are still insufficiently understood. Thus, in my thesis I sought to: 1) investigate the effect the inhibition of ROCK, which is a major mediator of cytoskeleton remodelling, has on the phenotype, migration and proliferation of undifferentiated GBM cells; and 2) to develop a 3D hybrid tumour-cerebral organoid model to study GBM tissue infiltration in real-time.

The first aim of my thesis was to examine the effect chemical inhibition of ROCK signalling pathway has on undifferentiated human-derived glioblastoma cells by using the small molecule inhibitor Y-27632. ROCK pathways inhibitors have been described as potential components of cancer therapy. However, the lack of consistent tumour-type specific data regarding the effects pharmacological ROCK inhibition has on brain cancer highlights the need for studies to address this gap in knowledge before these inhibitors are used in a clinical setting. To this end, I examined the effect chemical inhibition of the ROCK signalling pathway utilizing human-derived glioblastoma cells. These cells have been successfully used to mimic GBM heterogeneity and to study phenotypic changes in patient-derived glioblastoma cells. To further understand the effect ROCK signalling pathway has on GBM morphology, I also tested the effect distinct chemical inhibitors which targeted ROCK and downstream effectors of the Rho pathway had on GBM morphology. Moreover, given that previous studies have associated the use of Y-27632 with a differentiation phenotype I also investigated the potential of using this compound to differentiate GBM stem cells.

Synergistically, in a second line of investigation, my objective was to study GBM tissue infiltration in real-time. The invasive nature of GBM cells results in the diffuse infiltration of these cells into surrounding tissues. GBM cells are able to migrate within the brain parenchyma and are challenged by the reduced extracellular space between brain cells. For this reason, the examination of GBM cell migration could strongly benefits from 3D *ex vivo* modelling. To this end, I developed a 3D hybrid tumour-cerebral organoid model to study the GBM migration into a brain-like structure. The

utilization of recent organoid methodology required the testing of several experimental approaches. These were developed sequentially, in the search for a viable approach, starting with the development of hybrid tumour organoids containing single GFP-BTSCs; followed by the use of BTSC-spheres to improve tumour compartment localization within the hybrid tumour organoid; then dissociated early-stage organoid with BTSC spheroids; and lastly the development of a self-assembly tumour-organoid model.

2. Material and methods

2.1. Cell culture

2.1.1. Brain tumour stem cells

BTSCs lines were obtained from surgically resected tumour tissues following patient consent under the governance of the ethically approved Leeds multi-disciplinary tissue bank. Processed sample-derived cells were cultured as monolayers in Neurobasal medium (Gibco; 21103-049) supplemented with B-27 (0.5x; Invitrogen; 17504-044), N-2 (0.5x; Invitrogen; 17502-048), recombinant human basic fibroblast growth factor (bFGF; 40 ng/mL; Gibco; PHG0024) and epidermal growth factor (rhEGF; 40 ng/mL; R&D systems; 236-EG). Cells were maintained in a humified incubator with 5% CO2 at 37 ^{o}C on poly-L-ornithine (5μg/mL; Sigma; P3655) and laminin (5 μg/mL; Invitrogen; 23017-015) coated cell culture flasks/plates.

2.1.2. Human neuro progenitor cells

Human neuro progenitor cells were derived from non-tumour brain surgical tissues obtained from epilepsy surgery at Stanford University Medical Centre. Cells were cultured in Dulbecco's modified eagle medium (DMEM)/F-12 medium (Gibco; 2133-020) supplemented with 0.5x B-27, 0.5x N-2, bFGF (40 ng/mL), rhEGF (40 ng/mL), 1x GlutaMAX (Gibco; 35050-038) and 5% (v/v) foetal bovine serum (FBS) at 37 ^{o}C with 5% CO_2.

2.1.3. ROCK pathway inhibitor and washout treatments

For neurite outgrowth phenotype, cells were seeded at densities of 25,000 cells per cm^2 (using a 24-well plate) and allowed to adhere overnight. For the outgrowth assays the ROCK pathway inhibitors Y-27632, H1125, Blebbistatin as well as the LIM kinase inhibitor were added for 24 hours.

Y-27632 (Sigma; Y0503) was prepared by adding water to obtain a final stock concentration of 5mM. Y-27632 was added at the final concentration of 20 μM. H1152 (Tocris; 2414) was prepared by adding dimethylsulfoxide (DMSO) to obtain a final stock concentration of 10 mM. Neurite-outgrowth assay was carried out using the concentration of 10 μM. GSK 269962 (Tocris; 4009) was dissolved in DMSO to obtain a final concentration of 50 mM. Neurite-outgrowth assay was carried out using the concentration of 5 μM. Blebbistatin (Tocris; 1853) was prepared by adding DMSO in order to obtain a stock solution with the concentration of 25mM. Outgrowth assay was accomplished by using the final concentration of 2.5 μM. LIM kinase III was kindly provided by Dr Georgia Mavria at the concentration of 25mM (249). Neurite-outgrowth assay was carried out by using the concentration of 5 μM.

Vehicle control condition cells were treated with either DMSO or water. DMSO was utilised as a vehicle during assays that included H1152, GSK 269962, Blebbistatin or LIM kinase, whilst water was used as vehicle in experiments that only included Y-27632.

For washout conditions, cells were treated with the small molecule inhibitors for 24 hours, after which the media was removed and cells washed with phosphate buffered solution (PBS, Sigma, P3744). Fresh media lacking the inhibitor was added and cells were assessed 8 hours following removal of the compound. All neurite-outgrowth assays were carried out for 24 hours after addition of the small molecule inhibitor. Reversibility assays were carried out for either 3 or 5 days after addition of the inhibitor and media was changed on day 2 and 4 of the experiment.

2.1.4. Mouse stem cells

Mouse R1 (ATTC; SCRC-1011) embryonic stem cells (mESC) were cultured in mitomycin-C inactivated mouse embryonic fibroblasts (MEF) feeder layer. To produce the feeder layer, MEF (ATTC; SCRC-1040.1) cells were grown to 80-90% confluence and treated with mitomycin-C, which binds to the DNA of the cells halting their proliferation whilst allowing the production of growth factors necessary for the growth of stem cells. R1 cells were cultured in ESC media consisting of DMEM high glucose (Gibco; D5671) supplemented with 10% (v/v) knockout serum replacement (KSR; Invitrogen; 10828028), 0.1 mM minimum essential medium-non-essential amino acids solution (MEM-NEAA; Invitrogen; 11140050), 2mM glutamine (Invitrogen; 25030081), 1 mM sodium pyruvate (Invitrogen; 11360070), 0.1 mM β-mercaptoethanol (Sigma) and leukaemia inhibitory factor (LIF, 1000U/mL, Millipore; ESG1107) at 37 ^{o}C with 5% CO_2. In order to preserve the undifferentiated state of the R1 cells which is crucial for organoid development, the media was changed daily and cells were split every 2-3 days or when ESC colonies were confluent and in close contact.

2.2. 3D mouse model establishment

2.2.1. Experimental approach 1

Cerebral organoids were developed using R1 mESCs and GFP-GBM1 BTSCs following an adaptation from Lancaster et al. (250). Mouse embryonic stem cells were cultured as described and trypsinised when the cells reached appropriate confluency (70-80%). The separation of MEF cells from the mESC was accomplished by differential adherence of MEF cells to gelatinised plates. MEFs cells adhere to gelatinised plasticware after 30 minute incubation, unlike mESC, which need longer to adhere.

In total, 2,000 single cell mESC and either 1, 5 or 50 GFP-GBM1 BTSCs were plated in each well of an ultra-low attachment (ULA) 96-well plate. They were cultured in differentiation media consisting of Glasgow minimum essential medium (GMEM, Gibco) supplemented with 10% (vol/vol) KSR, 2 mM glutamine, 1 mM sodium pyruvate, 0.1 mM MEM-NEAA, 0.1 mM β-mercaptoethanol and 10 μM SB431542 (Sigma). Cells were maintained in the media for 4 days, providing suitable conditions for embryoid body formation.

After 4 days, the embryoid bodies were transferred to ultra-low binding 24 well plates and cultured in neural induction media consisting of DMEM/F12, N2 supplement (1:100), 1x Glutamax, 1x MEM-NEAA and 1 μg/mL heparin (Sigma). The neural induction media allowed the embryoid bodies to initiate the formation of neuroepithelial tissue.

On day 6, the tissues were transferred to Matrigel (BD Bioscience), which was prepared by placing ice cold Matrigel droplets on a section of parafilm and inserting the tissue into the droplet. These droplets solidified at 37°C and subsequently they were removed from the parafilm and grown in differentiation media. Differentiation media consisted of a mixture of Neurobasal and DMEM/F12 media (1:1) supplemented with N2 supplement (1:200), B27 supplement without vitamin A (1:100, Invitrogen), 3.5 μL/L of β-mercaptoethanol, 1:4,000 Insulin, Glutamax (1:100) and MEM-NEEA (1:200). The Matrigel provided a scaffold that was used by the cells as a means to grow and project into the gel.

On day 9, after 3 days of stationary growth, the droplets were transferred to spinner flasks containing the same media mentioned above, with the exception of the B27 containing vitamin A. The droplets stayed in the spinner flasks for at least 3 weeks, allowing the cerebral organoids to differentiate and grow.

2.2.2. Experimental approach 2

To facilitate placement and visualization of the GFP GBM1-BTSCs, 500 of these cells were seeded into a 96 ULA to create GFP-BTSC spheroids 24 hours prior to addition to the initial 2000 R1 mESCs necessary to initiate embryoid body formation. Further development of the cerebral organoid continued as described in Section 2.2.1.

2.2.3. Experimental approach 3

Mouse early-stage cerebral organoids (eCOs) were developed using R1 mESCs as described in Lancaster et al. (250) with minor modifications starting from differentiation day 6. In contrast to the Lancaster et al. protocol, organoids were not cultured in Matrigel droplets, but instead continued to grow in the ULA 24-well plate; neural induction medium was still replaced with differentiation media (without vitamin A) as described in 2.2.1. On day 9 the neural induction medium was removed and replaced with differentiation media in which the B27 without vitamin A was replaced with B27 with vitamin A. After four days, at day 12, the eCOs were mechanically dissociated. Each dissociated eCO was transferred to a ULA 96-well plate containing a pre-made spheroid which consisted of 500 GFP-GBM1 BTSCs. Re-assembling organoid and spheroid were maintained in differentiation media containing vitamin A.

2.2.4. Experimental approach 4

eCOs were developed as described in 2.2.3 and transferred to ULA 96-well plates containing either BTSCs or NP spheres (resulting from the aggregation of 500 GFP cells of either GBM1 BTSCS or NP1 cells which were generated 24-hours prior). eCO/BTSC and eCO/NP were correspondingly cultured in either GBM or NP media for 48 hours. Afterwards, differentiation medium containing vitamin A was added in a 1:1 proportion.

2.3. Live cell imaging

Cells were plated in 6-well tissue culture plates and allowed to adhere. Cells were treated with 25 μM of Y-27632 or 0.1% (v/v) DMSO and the plates transferred to an IncuCyte ZOOM® live cell imaging system (Essen Bioscience). Washout treatments were performed on day 2 and the media containing Y-27632 was removed and replaced with fresh media lacking Y-27632. Phase contrast images were acquired for all conditions every hour over a period of 3 days (using a 10x objective). Real time movies were compiled using the IncuCyte ZOOM® software package.

2.4. Immunocytofluorescence

Cells grown as adherent monolayers were washed with PBS prior to being fixed with 4% paraformaldehyde (PFA, Sigma, P6148) at room temperature (RT) for 10 minutes. Cells were permeabilised with PBS containing 0.2% (v/v) Triton X-100 (Sigma, X100; T8787) for 10 mins at RT. Cells were then washed with PBS (3x) and blocked in staining buffer (0.03% (v/v) Triton X-100 + 10% FBS in PBS) for 1 hour at RT, thus reducing unspecific binding to the primary antibody.

Next, the cells were incubated at 4°C overnight with the following primary antibodies diluted in staining buffer: anti-neuronal class III β-tubulin (TUJ-1, 1:500, Covance; 801213), anti-microtubule-associated protein 2 (MAP-2, 1:1000, Abcam; ab5392), anti-KI 67 (1:200; Abcam; ab16667) and anti-phospo-H_2AX (γH_2AX; 1:800; Merck; JBW301). Following primary antibody incubation cells were washed 3 times with PBS (5 minute incubation periods) and subsequently incubated with secondary antibody in staining buffer for 1 hour at RT. Secondary antibodies used were AlexaFluor488 (Molecular Probes; A11029; 1:200), Cy3 (Jackson ImmunoResearch; 711-165-152; 1:400) conjugated or AlexaFluor647 (Molecular Probes; A20186; 1:200). After secondary incubation, cells were washed three times with PBS (5 minutes each)

and nuclei were stained during the first PBS wash with 4',6-diamidino-2-phenylindole (DAPI;1 μg/ml; Sigma) in PBS for 5 minutes at RT. Image acquisition was achieved using an EVOS digital inverted fluorescence microscope (Life Technologies) or a Nikon A1R confocal microscope.

2.5. Immunohistochemistry of the cerebral organoids

2.5.1. Paraffin embedded organoids

Organoids were removed from the spinner bioreactor 3-4 weeks after incubation and fixed in 4% PFA at 4°C overnight. Following the incubation, the tissues were washed 3 times in PBS for 10 minutes and then subjected to a dehydration process. This consisted of incubating the tissues in progressively more concentrated ethanol solutions (30%; 50%; 70%), each step taking 10 minutes. After the dehydration process, the cerebral organoids were embedded in paraffin. For immunostaining, the paraffin blocks were sectioned into 5 μm using a microtome. Prior to immunohistochemistry the sections were deparaffinised, rehydrated and subjected to heat mediated antigen retrieval, which is necessary to expose the antigenic sites and allow antibody binding. Sections were then blocked in staining solution for 1 hour and subsequently incubated with the following primary antibodies: SOX2 (1:100, Abcam) and VIMENTIN (1:100, Abcam). For sections stained with VIMENTIN the secondary antibody used was Anti human FITC; sections stained with SOX2 were detected using DAB substrate kit (Abcam). Sections were then visualised using an EVOS digital inverted fluorescence microscope.

2.5.2. OCT embedded organoids

The organoids were fixed with 4% (w/v) PFA for 15 minutes at 4 °C. Following three PBS washes, the organoids were re-suspended in 30% (w/v) sucrose solution and

left in 4 °C until the organoids sunk. After that period, organoids were embedded in OCT (VWR; 361603E) in cryo-moulds and sectioned on a cryostat (20 μm thickness).

For immunohistochemistry, the sections were equilibrated in PBS for 10 mins, allowing the removal of OCT from the slides. They were subsequently permeabilised for 10 minutes with PBS containing 0.2% (v/v) Triton X-100, and then incubated with PBS blocking/staining solution containing 0.03% (v/v) Triton X-100 and 10% (v/v) FBS at RT for 1 hour. Next, the following primary antibodies were incubated overnight at 4°C: anti-TuJ1 (1:1000; Cambridge Bioscience; 801202), anti-GFAP (1:200; DAKO; Z0334), anti-KI67 (1:200; Abcam; Ab16667), anti-SOX2 (1:150; Cell signalling; 35795), anti-Vimentin (1:200; DAKO; M0725), Anti-DCX (1:300; Santa Cruz Antibodies; sc-8066) and anti-Nestin (1:200; Millipore; MAB5326). The following day the organoids were washed three times with PBS and incubated, in the dark, with the following secondary antibodies for 1 hour at RT: Alexa-fluor-488 goat anti-mouse (1:200; Molecular Probes; A11029) and Alexa-fluor-Cy3 (1:400; Jackson ImmunoResearch; 711-165-152). Nuclei were stained with DAPI (1μg/mL; Sigma; D9542) during the first PBS wash for 10 minutes, which was followed by two more PBS washes. The slides were mounted and imaging was carried out using an EVOS digital inverted fluorescence microscope (Life Technologies) and a Nikon A1R confocal microscope. For the Nikon A1R confocal microscope, the imaging package used was the NIS-Elements C advanced software platform. Multidimensional imaging acquisition was performed (Z-stack) and images shown represent the maximum intensity projections of the images captured.

2.6. Illumina gene expression analysis

GBM1 cells were cultured under adherent conditions and RNA was isolated 24 hours after treatment with DMSO (0.01%) or 20 μM Y-27632 using RNeasy Mini kits following the manufacturer's instructions for purification of total animal RNA

(Qiagen; 74106). The integrity and concentration of RNA were determined using the Agilent 2100 Bioanalyzer. Gene expression data was obtained using the Illumina Human GeneChip v4. Analysis of raw data was performed by Alastair Droop (University of Leeds). Raw data were pre-processed using the beadarray package in Bioconductor within the R numerical analysis software using quantile normalization (251-254). Probes with missing values in all samples were excluded (detection $p > 0.05$). Differential analysis between sample groups was performed in R using the LIMMA package (255). Multiple testing correction was performed using False discovery rate.

2.7. BMP4 differentiation treatment.

For BMP4 induced differentiation, cells were seeded into a 24-well plate at the density of 15,000 cells per cm^2 and allowed to adhere overnight. Cells were treated with recombinant human BMP4 at 100 ng/ml and 10% FBS in order to induce BTSCs differentiation. Two distinct experimental approaches were performed. The first approach involved treating BTSCs with BMP4 and FBS for 3 days followed by the addition of 20 μM of Y-27632 and on the fifth day cells were fixed with 4% PFA. On the second approach cells were treated simultaneously with the BMP4/FBS differentiation mixture and Y-27632 (20 μM) for 5 days, after which cells were fixed with 4% PFA.

2.8. Calcium signalling

GBM1 cells were treated with vehicle (water) and 20μM Y-27632 for 24 hours. The following day Fluor 3AM (ThermoFisher; F23915) was added to the cells and incubated for 30 minutes in the dark at RT. The cells were then washed with PBS and kept in the dark for another 30 minutes, in order to allow the de-esterification process to occur. Live cell imaging was done using the Zeiss LSM780 on a Zeiss Observer Z1

equipped with a Coherent Chameleon laser. Laser injury was performed using 100% of the Coherent Chameleon laser at 800nm. Images were taken every 1.95 sec.

2.9. Mitochondria and Lysosome staining

GBM1 cells were treated with vehicle (water) or 20μM of Y-27632 for 24 hours. The next day the lysosomes were stained using LysoTracker® (Thermo Fisher Scientific; L7528) while the mitochondria were stained using MitoTracker® (Thermo Fisher Scientific; M7512). LysoTracker® (50 nM final concentration) was incubated with the cells for 2 hours, while MitoTracker® (25 nM final concentration) was incubated for 1 hour. The cells were then fixed with 4% PFA for 10 minutes. Images were obtained using the A1R confocal microscope. For live cell imaging, images were taken every 30 seconds, for a total of 20 minutes, using the Zeiss LSM780 on a Zeiss Observer Z1 microscope.

2.10. Lucifer yellow dye loading via scratch assay

GBM1 cells were treated with vehicle (water) or 20 μM of Y-27632 for 24 hours. The next day cells were rinsed with PBS before the addition of 0.05% lucifer yellow (Thermo Fisher Scientific; L1177). A scratch wound was inflicted on the cell monolayer using a pipette tip and the dye was left on the cells for 2 mins, to allow its uptake. The dye was then rinsed with PBS and incubated with media for 8 minutes. After that period images were taken immediately on the A1R confocal microscope. The imaging package used was the NIS-Elements C advanced software platform. Multidimensional imaging acquisition was performed (Z-stack) and images shown represent the maximum intensity projections of the images captured.

2.11. Cell viability

Cells were seeded at densities of 15,000 cells/well (3 day irradiation treatment) or 10,000 cell/well (5 day irradiation treatment) in white 96-well plates (Greiner bio-one; 655083) and allowed to adhere overnight. The following day cells were treated with vehicle control (water) or with 20 μM Y-27632 for 24-hours. Cells were irradiated the next day with increasing doses (0, 2, 8, 20 Gy). For the Y-27632 washout conditions, media containing Y-27632 was removed and replaced with fresh media without the inhibitor 8 hours before radiation. Cell viability was measured using CellTiter-Glo® assay (Promega; G7572) 3 and 5 days after radiation. Following equilibration of reagents and cells to RT, 100 μL of CellTiter-Glo® was added to each well and then incubated for 10 minutes in the dark. Measurement of the luminescence signal was achieved using the Mithras LB 940 plate reader.

2.12. Lentiviral transduction

Lentivirus stocks for GFP labelling of cells was produced using human embryonic kidney (HEK) 293 cells. HEK293 cells were seeded into 10-cm plates coated with poly-L-lysine coated at a density of $2x10^6$. The next day, a transfection mixture of 0.1x TE (10 mM Tris, pH 8.0, 1 mM ethylenediaminetetraacetic acid [EDTA]) containing Gag-pol plasmid, VSV-G plasmid, pRSV-Rev plasmid and the pFUGW plasmid in a total volume of 450 μL per plate was prepared. While being vortexed, 500 μL of HEPES buffered saline (HBS) (100 mM HEPES, 281 mM NaCl, 1.5 mM Na2HPO4) was added to the solution. This final solution was added to HEK293 cells drop-wise. The following day, the medium was removed and fresh medium was added to the cells. The virus was collected at 24 and again at 48 hours. To produce the first batch of virus, media was collected and filtered using a 0.45μm filter. Fresh media was added for the second batch. Media from the second batch was collected and filtered and all virus was stored

at -80°C. For GFP labelling, viral particles were added to GBM1 and NP cells at an MOI of 3.07. The medium was replaced the following day and cells were used within 2 weeks of transduction.

2.13. Clonal assay growth

Cells were seeded at a density of 150 cells/well in a 24-well plate and allowed to adhere for 24 hours. The next day, the single cells in each well were counted and triplicate wells were treated with vehicle (water) or 20 μM of Y-27632. For washout condition, the cells were treated for 24 hours with Y-27632, followed by the removal of the compound and media and concomitant replacement with fresh media. Clonal colonies which consisted of over 4 cells were counted 7 days later and the percentage of cells that were able to establish colonies was assessed.

2.14. Radiation treatment

Cells were treated with vehicle (water) or with 20μM of Y-27632 for 24 hours. The following day cells were irradiated with 0 Gy, 2 Gy, 8 Gy and 20 Gy. For the washout condition, media containing compound was removed after 24 hours and cells were washed with PBS. Fresh media was added and cells were irradiated with the same doses above mentioned 8 hours after washout.

2.15. Metabolic Assay

Measurement of mitochondrial function following radiotherapy was performed using the Seahorse XF extracellular flux analyser (Agilent). Cells were treated with vehicle (water) or 20μM Y-27632 for 24 hours. The following day the cells were either non-irradiated or received 20 Gy radiation. Five days after radiation treatment cells were trypsinised and seeded into the provided microplates at a density of 30,000 cells per

well and allowed to adhere overnight. Before analysis, the medium was replaced with XF base media (Seahorse Bioscience; 102353-100) and transferred to a 37°C non-CO2 humidified incubator. For the "Mito stress test", XF base media was supplemented with glucose (25 mM; Sigma; G8769), sodium pyruvate (0.5 mM; Sigma; S8636) and L-glutamine (2 mM; Gibco; 35050-061). The final culture media was adjusted to pH 7.4 and filtered using a 0.2 μM filter. Oligomycin (O, 1 μM), Carbonyl cyanide-4 (trifluoromethoxy) phenylhydrazone (FCCP, 0.5 μM), antimycin and rotenone (A, R, 0.5 μM) were injected according to the "Mito Stress Test" (Seahorse Bioscience; 101848-400) protocol.

2.16. Image analysis

2.16.1. Neurite outgrowth

Data analysis of neurite outgrowth was performed using a NeuriteTracer plugin for ImageJ (Fiji). This plugin allows the quantification of neurite outgrowth. It was first necessary to transform the image into an 8 bit greyscale image. Next it was necessary to choose the thresholds, which corresponds to the covering of the neurites in every image with the programs' marker. The program analysed the size of the neurite outgrowths and returned an output which corresponds to the total of neurite outgrowth per image. Finally, it was necessary to divide this value by the number of DAPI positive cells to obtain the average of neurite outgrowth per cell; this is represented as: Outgrowth per Cell (μm ± SD).

2.16.2. Measurement of proliferation rate

Live cell imaging was performed using GBM cells treated with Y-27632 or vehicle (water) and observed using the IncuCyte ZOOM® live cell imaging system (Essen Bioscience). Phase contrast images were acquired for all conditions every hour over

the indicated periods using a 10X objective. Real time movies and confluency/growth curves data was obtained using the IncuCyte ZOOM® software package.

2.16.3. Cell tracking

Cell treated with vehicle (water) or 20 μM of Y-27632 for 24 hours were then monitored using the IncuCyte ZOOM® system. Images were taken every 30 minutes and cellular tracking was performed on the obtained movies and setting the nuclei as the point of movement. Cells were tracked using ImageJ analysis software (http://rsb.info.nih.gov/ij).

2.16.4. Definition of regions of interest

Region of interest (ROIs for the cytoplasmic area and for the tumour compartment in eCOs/GBM1 and /NP) were defined by colour thresholding using ImageJ (default setting, colour space: HSB) and the percentage of area was calculated.

2.16.5. Cell behaviour cell map

Cells were treated with vehicle (water), 20 μM Y-27632 for 24 hours or Y-27632 8 hour washout. The next day the cells were subjected to the following radiation doses: 0, 2, 8 and 20 Gy. Live cell imaging of the cells started right after irradiation and was performed using the IncuCyte ZOOM® system. Five cells per experiment were tracked for 3 days; three independent experiments per condition was analysed. A matrix was created by assessing each of the cells against the five following parameters:

1- Does the cell have a neurite outgrowth phenotype?
2- Is the cell part of a network?
3- Does the cell move a lot?
4- Is the cell multinucleated?
5- Does the cell divide?

The first four parameters were created as dichotomous variables – possible outcomes were *yes* and *no*; the fifth also encompassed *cell cycle arrest* and *cell death*. A graphical representation of this matrix was subsequently generated, in the form of a heat map.

2.17. Statistical analysis

In vitro data was analysed by two-sided paired t-test or 2-way ANOVA and expressed as mean ± SD. P values of ≤0.05 were presented as *; P≤0.01 as **; P≤ 0.001 as *** and P values of ≤ 0.0001 were considered highly significant (****). Organoid data is shown as mean ± standard deviation (SD). N represents independent dCO/GBM and dCO/NP specimens and analysed by two-sided unpaired Student's t-test.

3. Effect of pan-ROCK chemical inhibition on GBM cell behaviour

3.1. ROCK pathway inhibition with Y-27632 in undifferentiated GBM1 BTSCs

3.1.1. Y-27632 resulted in a pronounced neurite-like outgrowth phenotype in undifferentiated GBM1 BTSCs

The lack of tumour type-specific data on chemical ROCK inhibition motivated me to address the question as to whether Y-27632 treatment affects GBM cell morphology, motility and/or proliferation in BTSCs derived from human glioblastomas. A wide range of Y-27632 concentrations (from 0.1 μM to over 40 μM) have been reported to lead to effects in different cell types(213, 215, 216, 256, 257). For example, Tilson et al. (216) used a range of Y-27632 concentrations (0.1 μM to 50μM) to study the effect ROCK inhibition has on the expansion of glioblastoma stem-like cells. Based on this report, I decided to initially use a "mid-range" concentration of Y-27632 (25 μM) and carried out time-lapse microscopy of GBM1 BTSCs in the presence and absence of 25 μM Y-27632 for 48 hours. Still-frame images showed that the addition of the inhibitor induced a pronounced cellular phenotype reminiscent of neurite-like outgrowth when compared to vehicle control. Morphological changes indicative of neurite outgrowth were observed 6 hours after Y-27632 addition (Figure 3.1A).

To further characterize the Y-27632-induced neurite-like cell projections, I stained the GBM1 BTSCs for neuron-specific cytoskeletal markers. Neuronal class III β-tubulin (TuJ1) is a structural protein which is a major constituent of the

cytoskeleton. Microtubule-associated protein 2 (MAP-2) is a neuron-specific protein that is involved in the stability of the microtubule network. Consistent with the neurite protrusion morphology, the cell projections stained positive for TuJ1 and MAP-2 (Figure 3.1B). The immunofluorescence images were used to quantify the formation of neurite-like projections using the NeuriteTracer plugin and ImageJ software. Figure 3.1C shows a representative image of how the plugin measures the neurite-like protrusions (red lines correspond to the protrusion length measured by the plugin).

I next sought out to establish the optimal concentration range for the Y-27632-induced neurite outgrowth phenotype in BTSCs, which would result in the strongest phenotype. I used a broad titration of Y-27632 ranging from 0.2 μM to 400 μM and assessed neurite outgrowths at 24 (Figure 3.2A) and 48 (Figure 3.2B) hour time points as compared to vehicle control. Low Y-27632 concentrations (0.2 and 2 μM) were sufficient to increase the average TuJ1 (Figure 3.2A, 0.2 and 2 μM) and MAP-2 (Figure 3.2B, 0.2 and 2 μM) positive protrusion outgrowth per cell by ~2-3 fold, suggesting that the observed effects are ROCK-dependent. Higher Y-27632 concentrations (20 and 100 μM) increased neurite-like protrusions by ~4-fold, which was the maximum increase observed over the vehicle control (Figure 3.2A and 3.2B, concentrations 20 and 100 μM). However, cells that were submitted to higher concentrations of Y-27632 for 48 hours (400 μM) appeared unhealthy suggesting that Y-27632 can be toxic (Figure 3.2B).

To establish the optimal treatment period for eliciting the Y-27632 phenotype, I treated GBM1 BTSCs with 20 μM of Y-27632 and quantified the neurite projections using immunofluorescence images taken over treatment periods ranging from 6 to 72 hours (Figure 3.3A). There was a gradual increase in cellular neurite-like outgrowths, assayed via TuJ1 and MAP-2 staining, reaching the maximum at the 24-hour time-

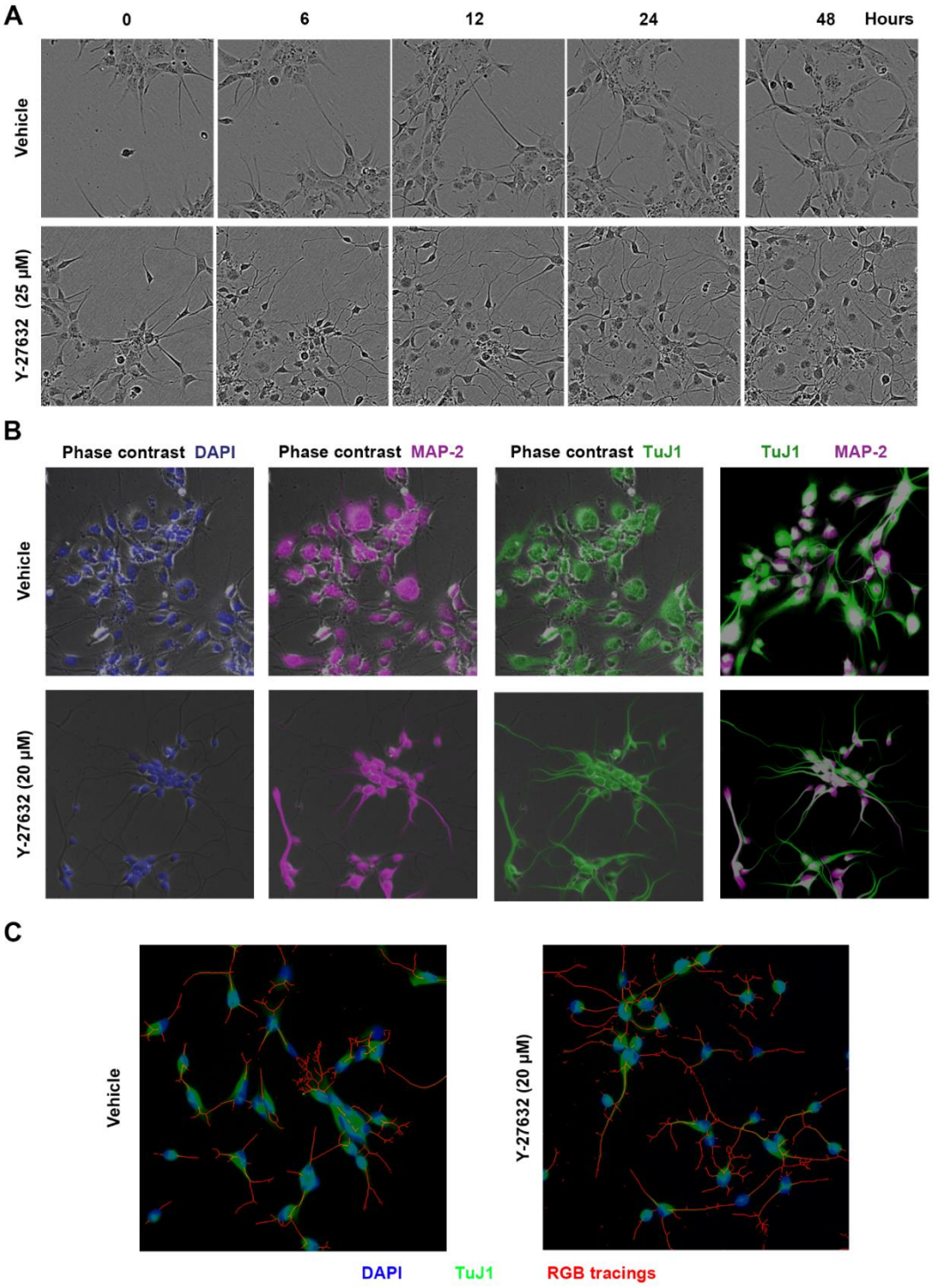

Figure 3.1 Y-27632 induces a pronounced neurite outgrowth-like phenotype in undifferentiated GBM1 BTSCs cells. **A**- Still frames of live cell imaging of GBM1 BTSCs before and after the addition of Y-27632 (25 µM) and vehicle control. The images were taken over a time-lapse microscopy period of 48 hours showing the formation of neurite-like projections in the presence of the ROCK inhibitor. **B**- Representative images of GBM1 BTSCs treated with Y-27632 (20 µM, 24 hours) compared with vehicle control (24 hours) show that chemical ROCK inhibition resulted in neurite-like cell protrusions which are immunopositive for the neuron microtubule-associated protein 2 (MAP-2) and class III β-tubulin (TuJ1). **C**- Neurite-like cell protrusions are measured using the NeuriteTracer ImageJ plugin. Red lines correspond to the cellular protrusion length as measured by the software.

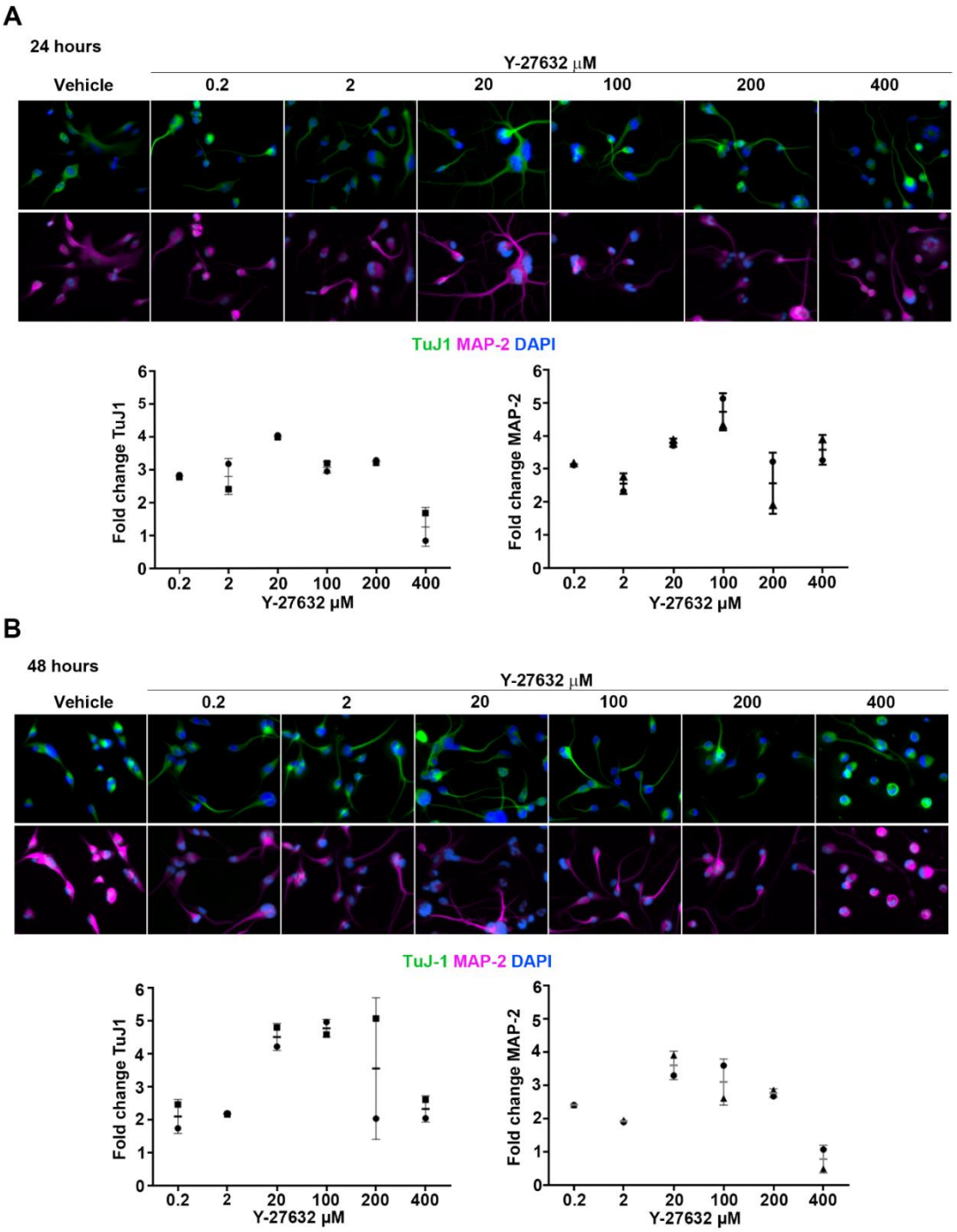

Figure 3.2 ROCK inhibitor-induced formation of neurite-like projections in undifferentiated GBM1 BTSCs is concentration-dependent. **A, B**- GBM1 BTSCs were treated with vehicle control or with a range of concentrations of Y-27632 (0.2μM - 400μM) for 24 hours **(A)** or 48 hours **(B)**. Top, representative images of GBM1 BTSCs treated with different concentration of Y-27632 (as shown) or vehicle control for 24 hours **(A)** or 48 hours **(B)**. Bottom, quantification of the average TuJ1 positive and MAP-2 positive neurite-like outgrowth per cell (μM) in GBM1 BTSCs induced by Y-27632 and vehicle control after 24 **(A)** and 48 **(B)** hour treatments. Fold changes of biological replicates normalized to the control are shown for different Y-27632 concentrations (ranging from 0.2 to 400 μM).

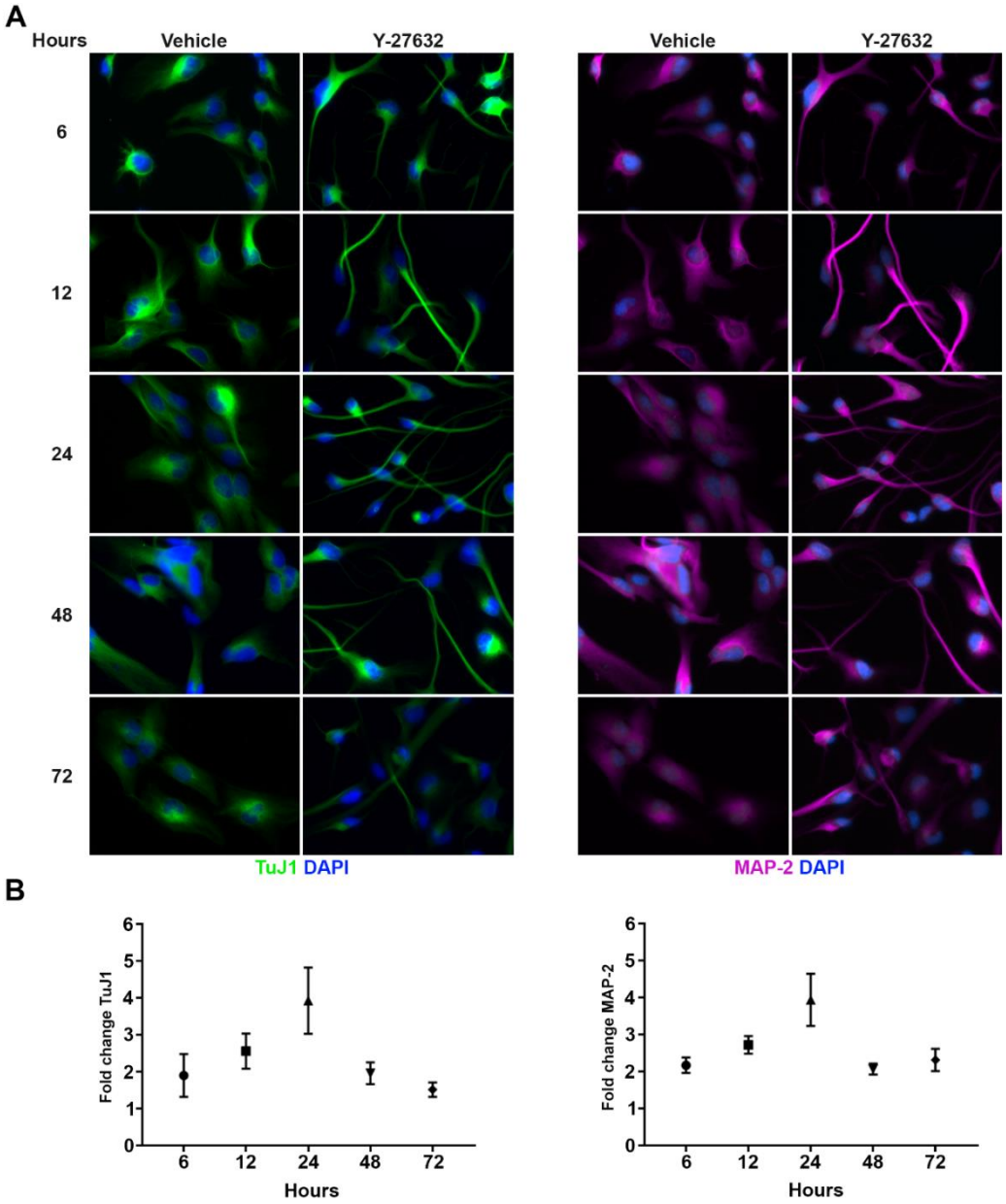

Figure 3.3 ROCK inhibitor-induced formation of neurite-like projections peaks at ~24 hours after treatment in undifferentiated GBM1 BTSCs. **A**- Representative images of GBM1 BTSCs treated with Y-27632 (20 μM) or vehicle control over a time course (as indicated). **B**- Quantification of cellular outgrowth based on immunofluorescence of TuJ1 (left) or Map-2 (right) demonstrates that the chemical induced neurite outgrowth effect of Y-27632 reaches its peak in GBM1 BTSCs after 24 hours and steadily decreases following that time point. Results are shown as fold changes of biological replicates normalized to vehicle control for the different time points.

point (Figure 3.3B). However, at 48 and 72 hours, these neurite-like outgrowths started to decrease to a point that resembles earlier time point measurements (6-hour time point). Furthermore, the immunofluorescence images showed that this concentration did not have a cytotoxic effect over time; the cells appeared healthy and

there was no indication of cell death (Figure 3.3A). In summary, the inhibition of ROCK pathway with Y-27632 leads to a pronounced neurite-like phenotype in GBM1 BTSCS. Moreover, I identified that a 20 μM treatment for 24 hours reproducibly induced the formation of neurite-like protrusions in GBM1 BTSCs.

3.1.2. ROCK pathway inhibition results in neurite-like protrusion in distinct patient-derived GBM BTSCs

An important feature of GBM tumours is their high level of cellular heterogeneity which is a major obstruction to the efficacy of GBM therapeutic approaches. This inter- and intra-tumour heterogeneity is characterised by the presence of highly heterogeneous cell populations of molecularly distinct phenotypes which resist treatment and are responsible for tumour recurrence (20, 25, 74).

It was important to examine whether Y-27632 would induce the same phenotype in a spectrum of clinically-relevant BTSCs subtypes. Therefore, I assessed the effect of chemical ROCK pathway inhibition using a panel of different patient-derived primary and recurrent BTSCs models. Three distinct BTSCs models were used: 1) GBM1 cells, which were derived from a primary tumour and have a mixed proneural/classical subtype, 2) GBM13 cells, which were derived from a primary tumour and display a proneural GBM subtype signature, 3) GBM20 cells that were derived from a recurrent tumour and exhibit a proneural/mesenchymal GBM subtype profile (258). After treatment with 20 μM of Y-27632 for 24 hours GBM1, 13 and 20 all displayed pronounced neurite-like outgrowth compared to the vehicle control (Figure 3.4A, B, C respectively). GBM13 BTSCs showed the most pronounced formation of neurite-like protrusions (≥400 μm) upon Y-276232 treatment (Figure 3.4B). These results demonstrate that Y-27632 elicits neurite-like outgrowth in a heterogeneous spectrum of patient-derived BTSCs model.

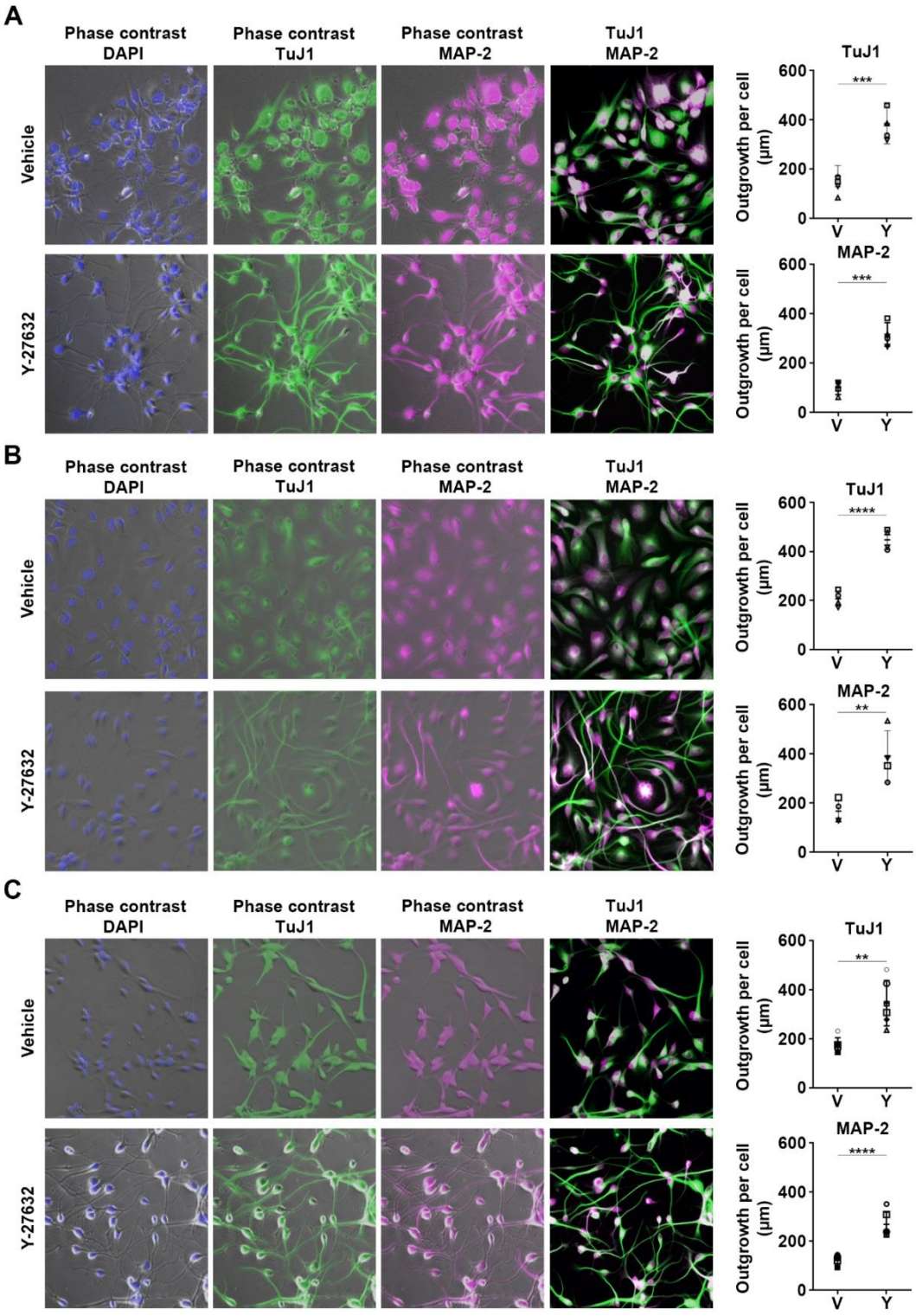

Figure 3.4 Marked neurite-like outgrowth appears upon Y-27632 treatment in three-different human patient-derived BTSCs models. **A, B, C**- Left, representative immunofluorescence images of TuJ1 positive and MAP-2 positive GBM1 (A), GBM13 (B), and GBM20 (C) cells 24 hours after treatment with vehicle control or Y-27632 (20 µM). Right, quantification of the average TuJ1 (top) and MAP-2 (bottom) positive neurite outgrowth per cell (µM) in GBM1, 13, and 20 cells treated with Y-27632 (Y,20 µM, 24 hours) and vehicle control; V, 24 hours). Data are biological triplicates, mean ± SD, **, $p<0.01$; ***, $p<0.001$; ****, $p<0.0001$ Student's t-test).

3.1.3. Neurite-like outgrowths in BTSCs results from the pan inhibition of the ROCK pathway

The ROCK inhibitor Y-27632 has been used extensively to study the effect ROCK pathway inhibition has on cellular processes (217). To exclude the possibility that the observed neurite outgrowth phenotype was a result of Y-27632 off-target effects, I tested whether different inhibitors that targeted ROCK, as well as downstream effectors of the Rho-pathway (H1152, GSK 26992, Blebbistatin and Lim kinase inhibitor 3) can induce a similar neurite outgrowth phenotype in GBM1 BTSCs (Figure 3.5A). For this, BTSCs cells were treated with 10 μM of H1152; 5 μM of GSK 269962, 2.5 μM of Blebbistatin and 10 μM of LIM kinase (LIM K) inhibitor for 24 hours and then stained for TuJ1. As shown in Figure 3.5B and C, the addition of different compounds that inhibited ROCK and downstream effectors in BTSCs seemed to exhibit a similar neurite outgrowth when compared to Y-27632, with the exception of LIM K inhibitor 3. H1152 is an ATP-competitive inhibitor of ROCK as is Y-27632, but it is a more potent inhibitor (inhibitory concentration 50 (IC50) 140nM vs 12nM, (259)). Comparison of the phenotypes shows that there is no significant difference amongst the neurite-like outgrowths observed with each drug treatment but there is a significant difference when these are compared to control (non-treated) cells (Figure 3.5B and C, H1152, H). Additionally, GSK 269962 which is another Rho kinase inhibitor that has a higher IC50 value for ROCK was tested (IC50=1.4 (260)). Notably, GSK 269962 induced neurite-like outgrowth in BTSCs cells at levels that were comparable to Y-27632 (20 μM) treatment (Figure 3.5B and C, GSK 269962, G).

To further investigate the signalling pathway that is associated with this outgrowth phenotype, I inhibited two distinct downstream effectors of ROCK using Blebbistatin (261) and LIMK inhibitor 3 (249). Blebbistatin is a cell-permeable

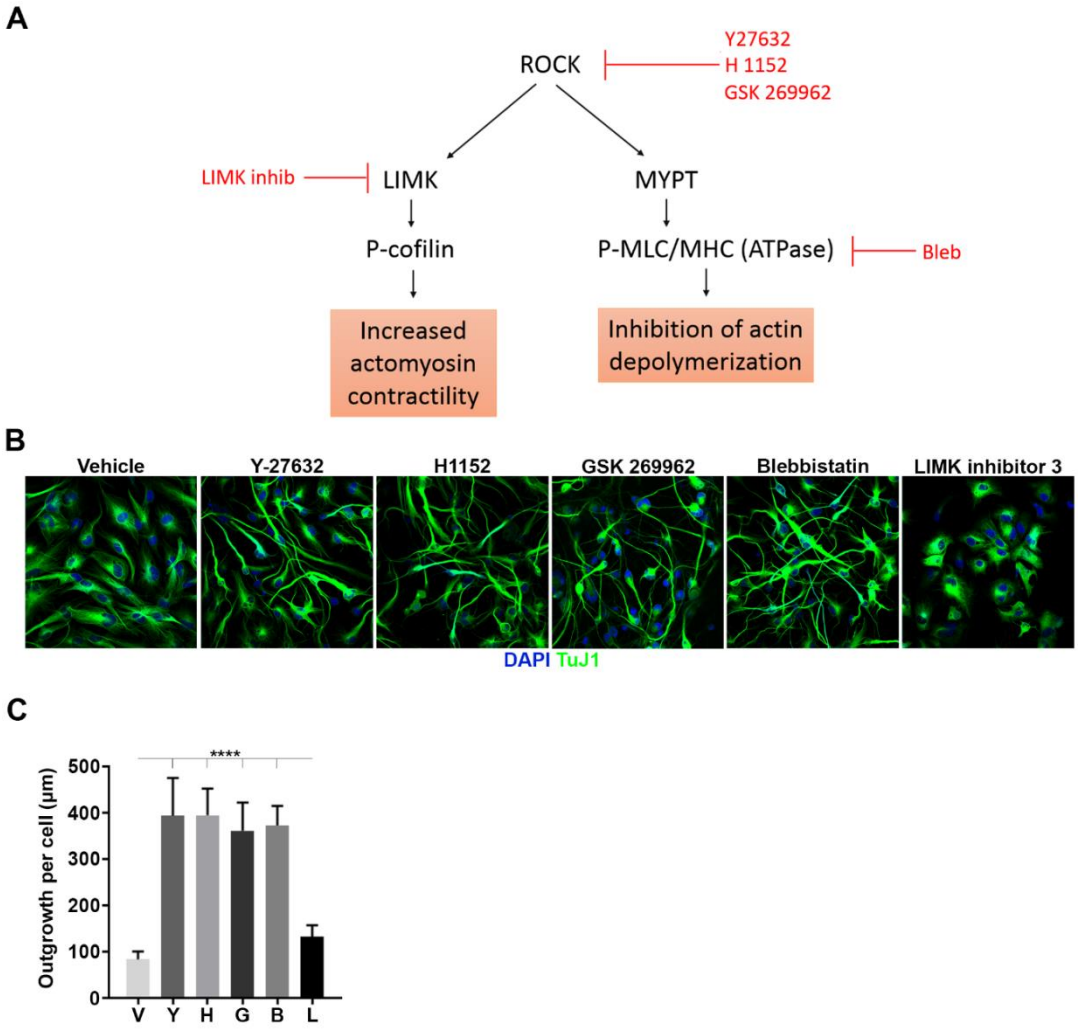

Figure 3.5 Different ROCK and MYPT pathway inhibitors but not LIM kinase inhibitor cause neurite-like outgrowth in GBM1 stem-like cells. **A**- Schematic of the ROCK signalling pathways with an emphasis on the target proteins of the different inhibitors. The effect of the inhibition on the cell morphology is shown (red squares). **B**- Representative images of TUJ1 positive BTSCs treated with vehicle (DMSO, 0,1%, V) and ROCK pathway inhibitors show that H1152, GSK 269962 and Blebbistatin induce neurite-like outgrowth comparable to Y-27632. **C**- Graph illustrates the quantification of TuJ1 positive neurite-like outgrowth in BTSCs following the treatment with Y-27632 (Y, 20 µM), H1152 (H, 10 µM), GSK 269962 (G, 5 µM), Blebbistatin (B, 2.5 µM) and LIM kinase inhibitor 3 (L, 10 µM) for 24 hours compared with the vehicle control. H1152, GSK 269962 and Blebbistatin increase the average length (µM) of neurite-like projections in BTSCs by ~4-fold over vehicle (V, 0.1%), which is comparable to the Y-27632 effect. LIMK inhibitor 3 does not induce neurite-like outgrowth in BTSCs. (Data are biological triplicates, mean ± SD, ****, $p<0.0001$, Student's t-test).

inhibitor of non-muscle myosin II which is a downstream effector protein of the ROCK pathway. In normal conditions ROCK phosphorylates the myosin binding subunit of myosin light chain phosphatase which in turn inhibits the dephosphorylation of myosin light chain, ultimately leading to an increase in myosin

II activity. So, the inhibition of the ROCK pathway will lead to a decrease in myosin II activity and, therefore, the direct inhibition of myosin II when Blebbistatin is used should re-capitulate the phenotype. The comparison of Y-27632 with Blebbistatin showed that there is no significant difference between the two compounds with regards to neurite-outgrowth. Blebbistatin significantly increased the neurite-like outgrowth of BTSCs by ~4 fold (Figure 3.5B and C, Blebbistatin, B).

The LIM kinase inhibitor 3 suppresses the phosphorylation of cofilin. In the active Rho signalling pathway, ROCK phosphorylates LIM K which is then activated to phosphorylate cofilin. Phosphorylation of cofilin then leads to the inhibition of its actin-depolymerizing activity. Therefore, the inhibition of ROCK would lead to a decrease in LIM kinase phosphorylation, hence resulting in an increase of cofilin's actin-depolymerizing activity. In contrast to this expectation, the treatment with 10μM of LIM kinase inhibitor 3 for 24 hours in BTSCs did not result in a neurite-outgrowth phenotype as compared with the aforementioned inhibitors (Figure 3.5B and C, LimK inhibitor 3, L). These results suggest that the neurite-like outgrowth phenotype in BTSCs is mediated through blockade of ROCK-dependent activation of nonmuscle myosin II (NMII) rather than LIM K protein (Figure 3.5B and C).

3.1.4. The neurite outgrowth is a reversible phenotypic modulation

Treatment of BTSCs with Y-27632 leads to a pronounced neurite-like outgrowth phenotype which stains positively for the neuronal makers, TuJ1 and MAP-2 (Figure 3.1). I therefore hypothesised that Y-27632 has the potential to differentiate BTSCs. As differentiation would induce a different gene expression pattern and lead to a decrease in proliferation, I performed microarray gene expression analysis, drug washout experiments and quantified the proliferation capacity of GBM1 BTSCs in the presence and absence of Y-27632 (20 μM).

For the gene expression analysis, GBM1 BTSCs were treated with 20 μM of Y-27632 or vehicle for 24 hours. Total RNA was extracted from the DMSO and the Y-27632 treated BTSCS and the RNA integrity and concentration was assessed. Samples were sent to Cambridge genomics for processing and the gene expression data was obtained using Illumina Human GeneChip v4. Processing of the data was performed by collaborators in Leeds (Dr. Alistair Droop) (described in Material and Methods (section 2.16). Differential gene expression analysis of Y-27632 compared with vehicle (DMSO)-treated BTSCs highlighted 98 genes whose expression significantly differed, albeit with fold changes <2 (Figure 3.6 and Table A2). Against expectations, Y-27632 treatment (20 μM, 24 hours) did not elevate the expression of proneural/neural differentiation factors such as neurogenic differentiation 1 (NEUROD1) (262) and neurotrophic receptor tyrosine kinase 2 (NTRK2) (263) that have been previously implicated in differentiation (Figure 3.6).

Symbol	Gene	FC
LYPD1	LY6/PLAUR domain containing 1	1.83
MAP1B	microtubule-associated protein 1B	1.81
RPE65	retinal pigment epithelium-specific protein 65kDa	1.72
LOC728755	uncharacterized LOC728755	1.66
AIF1L	allograft inflammatory factor 1-like	1.60
GFAP	glial fibrillary acidic protein	1.53
WLS	wntless homolog (Drosophila)	1.50
TAGLN2	transgelin 2	1.49
FAM131B	family with sequence similarity 131, member B	1.49
SLC4A4	solute carrier family 4 (sodium bicarbonate cotransporter), member 4	1.48
CKAP2	cytoskeleton associated protein 2	-1.52
NPTX1	neuronal pentraxin I	-1.52
INTS7	integrator complex subunit 7	-1.53
SUFU	suppressor of fused homolog (Drosophila)	-1.55
CDH5	cadherin 5, type 2 (vascular endothelium)	-1.58
NUF2	NUF2, NDC80 kinetochore complex component	-1.63
PPIA	peptidylprolyl isomerase A (cyclophilin A)	-1.63
NEK2	NIMA-related kinase 2	-1.66
ID2	inhibitor of DNA binding 2, dominant negative helix-loop-helix protein	-1.76
TRAF4	TNF receptor-associated factor 4	-1.86

Figure 3.6 Microarray gene expression analysis (ArrayExpress) of Y-27632 (20 μM) vs vehicle (DMSO) treated GBM1 BTSCs cells. The table shows the expression of the top 10 upregulated (green) and downregulated (red) genes. From the 98 genes whose expression significantly differed (fold change <2), there was no elevated expression of neuronal differentiation markers.

Next, I performed several washout treatments. Y-27632 (20 μM) was added to GBM1 BTSCs for 24 hours; the media containing the inhibitor was removed and cells washed with PBS. Fresh media was subsequently added without the inhibitor. Time-lapse microscopy was performed for 24 hours before removal of Y-27632 / vehicle control and for 24 hours after. As can be seen in the still frames in Figure 3.7A, the BTSCs established the neurite-like outgrowth phenotype following the 24-hour incubation with Y-27632. However, it was remarkable to see that 2 hours after the removal of inhibitor the cells started to lose their neurite outgrowth phenotype; by 8 hours the neurite outgrowth was almost completely abolished (Figure 3.7A). Potentially an incubation time of 24 hours might not be enough to induce a permanent neuronal differentiation, I therefore treated the cells with the inhibitor for 3 and 5 days. Previous results suggested that Y-27632 might have a short lifetime in media (there was a reduction of neurite outgrowth after 48 hours, see Figure 3.3), so media was changed every other day adding fresh inhibitor each time. Following the 3 and 5 days incubation, the media containing the compound was removed and replaced with fresh media lacking Y-27632 for 8 hours (Figure 3.7B and C). Immunofluorescence was performed and it is possible to see from Figure 3.7B (3 days) and C (5 days) that removal of the compound, independent of the inhibitor incubation time, resulted in the loss of neurite-like outgrowth. Quantification of TuJ1 positive cells showed a significant decrease in neurite-like protrusion comparable to control cells following the 8-hour removal. Finally, in order to ascertain if this reversible phenotype was specific to Y-27632 or if other ROCK inhibitors had the same neurite-like protrusion reversibility, I also performed washout assays on BTSCs treated with H1152 and GSK 269962. Similar to the 5-day Y-27632 treatment, BTSCs were treated with H1152 (10 μM) and GSK 269962 (5 μM) for 5 days (media change every two days) and removed for 8 hours. Results show that, like the Y-27632 washout treated cells, the H1152 and GSK29962 induced a reversible neurite-like outgrowth phenotype and that an 8-hour

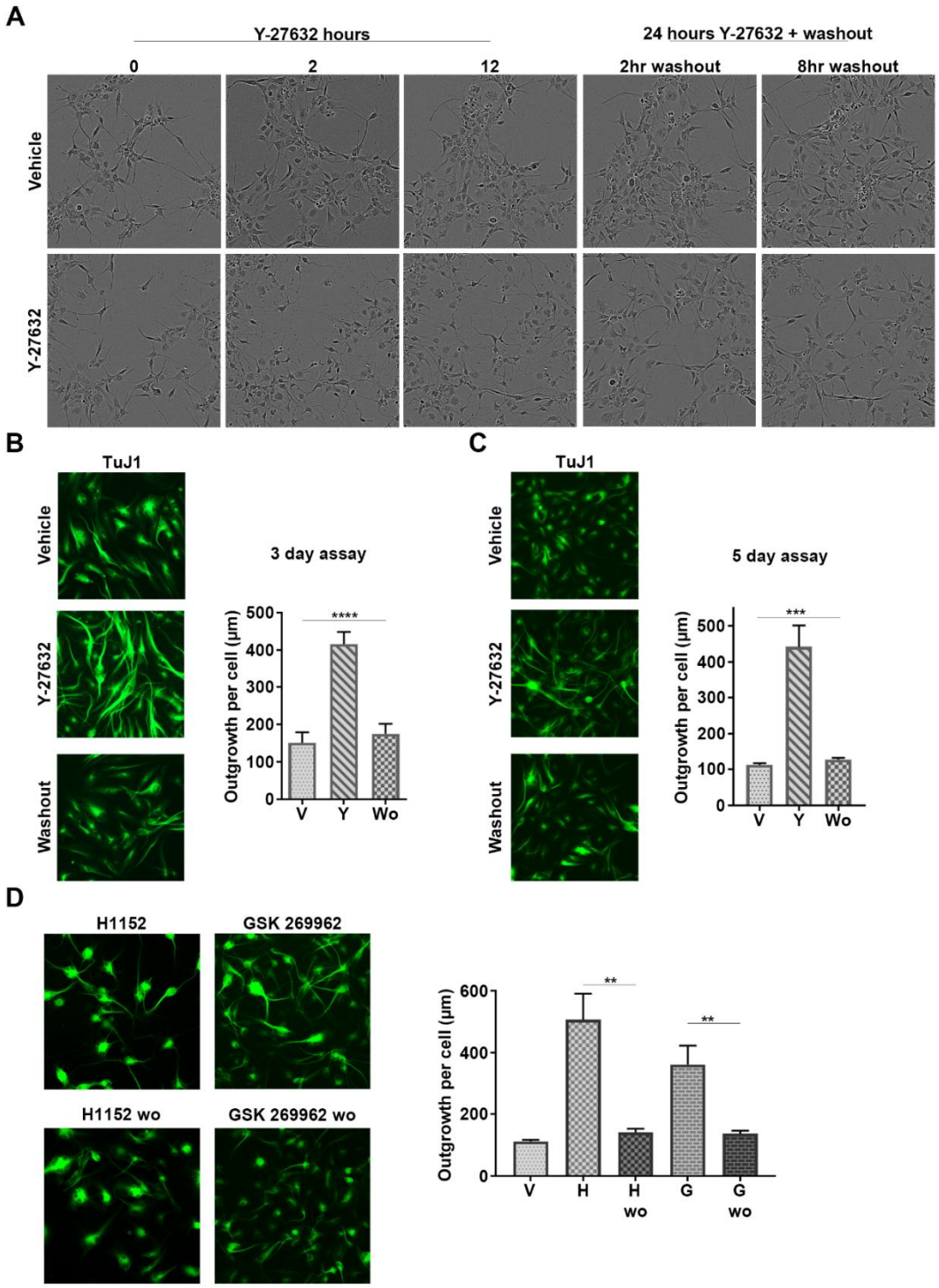

Figure 3.7 Chemical induction of the neurite-like phenotype through ROCK pathway inhibition is reversible. **A**- Still frames of time-lapse movies imaging GBM1 BTSCs after the addition of Y-27632 (20 µM) and washout of the compound. Two hours after the removal of Y-27632 (20 µM, 24 hours), GBM1 BTSCs visibly start retracting their TuJ1 positive projections (24hr Yi + 2hr washout). **B**- Left, representative images of vehicle control (top), Y-27632 (middle), and wash-out condition (bottom, wo). Right, quantification of average TuJ1 positive neurite-like outgrowth per cell (µm) after 3-day treatment with vehicle, Y-27632 (20 µM) in the presence and absence of inhibitor washout for 8 hours. **C**- GBM1 BTSCs were treated for 5 days with Y-27632 followed by an 8-hour wo period. Left, representative immunofluorescence images of vehicle (top), Y-27632 (middle), and wo condition (bottom). Right, quantification of immunofluorescence of TuJ1 positive neurite outgrowths. **D**- Neurite-like phenotype observed in GBM1 BTSCs with distinct ROCK pathway inhibitors (H1152, 10 µM, GSK 269962 5 µM; 5 days) is also reversible after washout. Left, immunofluorescent images of TuJ1 positive neurite outgrowth after a 5-day treatment with H1152 and GSK 269962 followed by the 8 hour wo. Right, quantification of TuJ1 positive neurite-like outgrowths in BTSCs post 5-day treatment with H1152 and GSK 269962 and respective 8-hour washout. Data are biological triplicates, mean ± SD, ** $p<0.01$, *** $p<0.001$, ****, $p<0.0001$ 2-way ANOVA)

wash out of the inhibitor was sufficient to revert the phenotype to a level that is comparable to control cells (Figure 3.7D).

It has been reported that ROCK inhibition results in the apoptosis and decreased proliferation of myeloid cancer cells and in patient-derived chronic myeloid leukaemia cells (264). To further explore if Y-27632 treated GBM1 BTSCs had any effect on cell proliferation, I determined clonal growth capacity of GBM1 BTSCs and their proliferation capacity following treatment. In order to assess the effect of Y-7632 on the clonal growth ability of BTSCs, the cells were seeded at clonal density (Figure 3.8A) and the single cells were counted the next day. Cells were allowed to form colonies for 7 days; the number of colonies was determined and the percentage of cells able to form colonies obtained. Moreover, in order to test whether Y-27632 had any effect on the cells, I included a washout condition (8-hour washout). In Figure 3.8A, it is possible to see that in all three conditions (vehicle, Y-27632 and Y-27632 washout) the cells had a similar ability to form colonies, indicating that Y-27632 does not affect the BTSCs clonal growth ability.

In parallel, I determined the percentage of proliferative cells in Y-27632 treated and washout cells compared with vehicle-treated BTSCs. In order to ascertain the effect Y-27632 had on proliferative BTSCs, I treated cells with 20 μM of Y-27632 (with and without 8-hour washout) and vehicle control and stained the cells for the proliferative marker Ki67 after 24-hour treatment (Figure 3.8B). Results from the Ki67 staining (Figure 3.8B, left) and quantification of Ki67 positive cells (Figure 3.8B, right) demonstrated that there was no significant difference in the proliferative potential of the three conditions. Additionally, I performed live cell analysis of GBM1 BTSCs treated under the same conditions and quantified cellular growth using the IncuCyte proliferation assay package (Figure 3.8C). Confluence curves were based on relative values (normalized to the t_0 time point). Results from the live cell analysis showed that once again that the addition of Y-27632 does not change the proliferation capacity of BTSCs (Figure 3.8C).

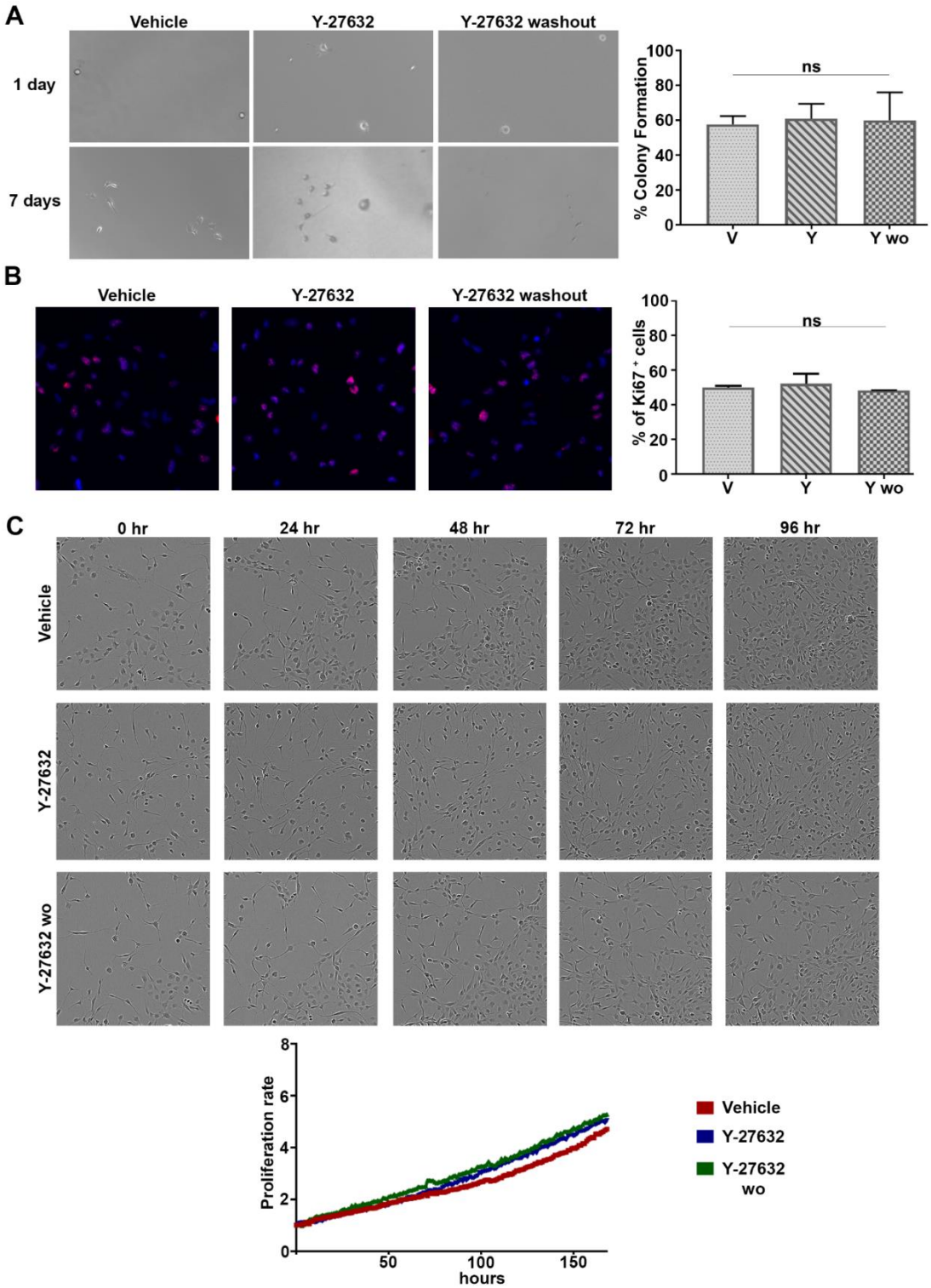

Figure 3.8 Brain tumour stem cells maintain their self-renewal characteristics, proliferation ability and clonal growth capacity following treatment with Y-27632. **A**- Left top panel, Phase contrast images depict cells 24 hours after seeding with vehicle, 24 hours after Y-27632 treatment (Y-27632) and 2 hours washout following a 24-hour Y-27632 treatment (Y-27632+washout). Left bottom panel shows colonies of cells originating from a single cell following a 5 day period. Right, quantification of clonal growth demonstrates there is no significant difference in colony formation amongst the distinct conditions. **B**- Left, immunofluorescence images of BTSCs for Ki67 (red); right, quantification of Ki-67 positive cells illustrating that Y-27632 (20 μM) treatment did not alter self-renewal capacity of BTSCs. **C**- Top panel, still frames of live cell imaging of BTSCs after the addition of vehicle control, Y-27632 (20 μM) and washout (after 2 hours) of the compound. The images were taken over a time-lapse microscopy period of 6 days. Bottom panel, graph quantifying the cellular proliferation of BTSCs under the different conditions. (Biological triplicates, mean ± SD, ns: non-significant, One-way ANOVA).

In summary, these results show that the presence of Y-27632 in BTSCs cells has no effect on the proliferative capacity of the cells under any of the conditions assayed. Consistent with qualitative and quantitative observations of unchanged cellular growth in live cell time-lapse microscopy experiments (Figure 3.8C, top panel), Y-27632 treatment did not reduce the number of proliferative BTSCs as assessed by Ki-67 staining. Together, these findings indicate that the neurite-like projections resulting from Y-27632 treatment in GBM1 BTSCs is a reversible phenotype that is not associated with cellular differentiation/gene expression changes nor reduction in proliferation. Instead, these changes in morphology are a likely result of cytoskeletal rearrangement.

3.1.5. Simultaneous addition of differentiating factor with Y-27632 increases neurite-like projections resistance to washout.

In vitro brain tumour stem cell differentiation can be induced by using BMP-4 (118). The most promising therapeutic avenue that focuses on forced differentiation of BTSCs comes from *in vitro* studies in which cells were forced to differentiate following the exposure to BMPs or serum (118, 119). Interestingly, Maldonado et al. (265) recently showed that the addition of ROCK pathway inhibitor to human induced pluripotent stem cells could selectively influence the differentiation of these cells in a lineage-specific fashion due to epithelial-to-mesenchymal transition (EMT) modulation. Therefore, to further investigate whether this outgrowth phenotype linked to ROCK pathway inhibitors was exclusively associated with the undifferentiated state of the BTSCs and whether Y-27632 could influence the differentiation of BMP-4 treated BTSCs in a lineage-specific manner, Y-27632 and BMP-4 were added to GBM1 BTSCs at different time-points.

Firstly, I differentiated the BTSCs with BMP-4 and serum and on the third day added Y-27632 (20 μM) (Figure 3.9A). The second approach was to add Y-27632 (20

μM) at the same time as BMP-4 and serum, that is, before the cells were differentiated (Figure 3.9B). New media was added to the cells every two days for a total of 5 days. On the fifth day, the cells were fixed and then stained for TuJ1 and GFAP markers in both conditions. As expected vehicle control and Y-27632 treated cells were mostly negative for GFAP whereas the addition of BMP-4 and serum lead to the differentiation of BTSCs into an astrocytic phenotype (Figure 3.9A and B, $GFAP^+$ outgrowth graph) (108). Removal of BMP-4 (washout, B4 Wo) did not alter the $GFAP^+$ nor the $TuJ1^+$ outgrowth per cell, neither in the same day addition, nor in the third-day addition of Y-27632 (Figure 3.9). Addition of Y-27632, at day 3, after BTSCs differentiation with BMP-4 and serum slightly increased $GFAP^+$ and $TuJ1^+$ outgrowths (Figure 3.9A). Nevertheless, washout of Y-27632 from the cells reverted the $GFAP^+$ and $TuJ1^+$ outgrowth to the same levels as the solo BMP-4 treated cells. In summary, when comparing BMP-4 treated cells with BMP-4 and Y-27632 treated BTSCS, the chemical inhibition of ROCK does not enhance the 2 fold increase in neurite outgrowth that accompanied BMP-4 induced differentiation.

Focusing on the same day addition scenario, from the immunofluorescence images in Figure 3.9B it is possible to see that the simultaneous addition of Y-27632, BMP-4 and serum lead to a significant increase in $TuJ1^+$ neurite-like projections. Quantification of $TuJ1^+$ outgrowths shows that the increase is ~5 fold when compared to vehicle control and ~2 fold when compared to Y-27632 (Figure 3.9B, $TuJ1^+$ outgrowth graph). Even though the washout of Y-27632 from this condition (BMP-4+Y Wo) led to a decrease of neurite-like projections, the $TuJ1^+$ neurite-like outgrowth is still higher when compared to the solo BMP-4 treated cells. More interestingly, by comparing Y-27632 treated cells and BMP-4+Y washout cells it is possible to see that the $TuJ1^+$ neurite outgrowth is similar in both the conditions. On the other hand, there is a significant decrease in $GFAP^+$ outgrowth per cell following washout of Y-27632 (Figure 3.9B, $GFAP^+$ outgrowth graph). However, even with the decrease of $GFAP^+$ outgrowths for BMP-4+Y washout, these cells continue to have a higher $GFAP^+$

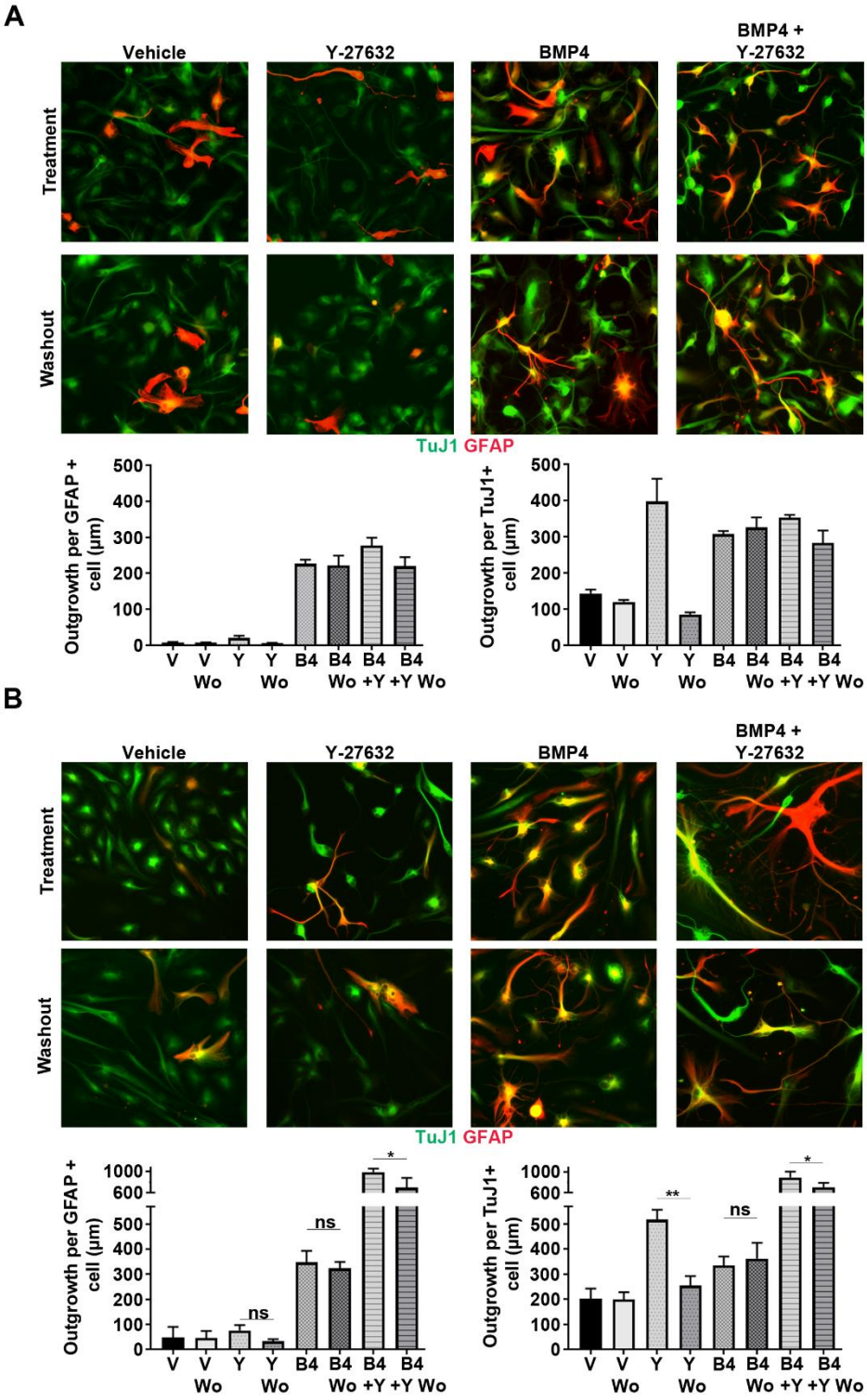

Figure 3.9 Simultaneous addition of BMP4 and Y-27632 to BTSCs leads to a significant increase in TuJ1 neurite-like outgrowth when compared to Y-27632 treated cells, which is maintained after washout treatment. **A**- BTSCs cells were initially differentiated using BMP4 and Y-27632 was added 3 days after BMP4. Top panel, representative immunofluorescence images of TuJ1 and GFAP positive cells following the addition of vehicle, Y-27632 and BMP4 after 5 days as mentioned on top. Addition of Y-27632 was done at day 3 following BMP4 differentiation. **B**- Simultaneous addition of BMP4 and Y-27632 to BTSCs. Top panel, immunofluorescence staining of TuJ1 and GFAP positive BTSCs cells following the treatment with vehicle (V), Y-27632 (20 uM, Y), BMP4 (B4, 100 ng/ml) and BMP4 with Y-27632 (Y,20 uM) for 5 days. (**A, B**) Middle panel shows the same conditions followed by an 8-hour "washout" treatment. Bottom panel, quantification of the average GFAP (left) and TuJ1 (right) positive neurite outgrowth per cell for all conditions. Biological triplicates, mean ± SD, *, $p<0.05$; **, $p<0.01$; Two-way ANOVA.

outgrowth when compared to solo BMP-4 treated cells. Results from both of these experiments suggest that addition of Y-27632 to differentiated cells induces no significant change in the neurite-like protrusions of these cells. Nevertheless, the addition of Y-27632 to cells that are still differentiating can alter the neurite-like protrusions in these cells in a more permanent manner when compared to the addition of Y-27632 following differentiation.

3.2. Chemical ROCK inhibition results in neurite-like outgrowths which cells utilize to form a functional and resistant network.

Previous results demonstrate that, with pan-ROCK inhibition, the GBM1 BTSCs remain in an undifferentiated and proliferative state. Nevertheless, it is possible that the phenotypic changes observed following Y-27632 treatment are due to the cells innate morphological plasticity. Osswald et al. (266) recently showed that brain tumour cells possess highly functional membrane protrusions which they use to connect with other brain tumour cells and form a functional network. Additionally, this phenomenon of communication amongst cells has been previously described in a number of different cancer and non-cancer cell types (267-272). Hence, I next investigated if GBM1 BTSCs treated with Y-27632 had the ability to use these neurite-like projections and establish a cellular network.

3.2.1. Neurite-like outgrowth induced by Y-27632 inhibition resembles an intricate network of connected cells.

Firstly, I used microscopy to analyse whether the neurite-like projections overlapped in a fashion that would represent an underlying network. For this purpose, I treated GBM1 BTSCs with Y-27632 (20 μM) and vehicle control for 24 hours, the cells were then stained for TuJ1. In order to obtain images in which the TuJ1 positive

outgrowths were sharp and devoid of background, a confocal microscope was used. Next, to see if these neurite-like projections would overlap and expose a network, a bar was manually placed over every neurite-like projection and a circle was placed over every nucleus in the image (Figure 3.10A). Maintaining the manually placed bars and circle but removing the background immunofluorescence image, uncovered a remarkable network-like arrangement in Y-27632 treated cells compared to the vehicle control counterparts. A closer look at the Y-27632 image in Figure 3.10A shows that there are a few small networks (under 5 participating cells), but the image is overtaken by one single network (cells participating in this network are coloured blue). Quantifications of the number of cells in a network showed that vehicle cells only had 2 to 3 cells participating in a network while Y-27632 treated cells had a much larger number of cells participating in a network ranging from 20 to over 40 cells. Finally, when the number of cells that were able to participate (cells which had overlapping projections) in the network were quantified, it showed that control cells only have 20% of their cells in the network while Y-27632 treated cells have an average of 90% in the network.

Next, with the help of collaborators, we used computational analysis (based on these confocal immunocytochemistry images) to predict if GBM1 BTSCs could form a network through these chemically-induced neurite-like protrusions. In Figure 3.10B, on the left side each of the graphs (Vehicle, Y-27632) it is possible to view the computational network resulting from the analysis. Each node corresponds to a single cell while the line between (named edge) corresponds to the connection between the cells. The computational network shows that the Y-27632 treated cells are in a compact network and that almost any cell is able to communicate with any other given cell – independent of their localization (Figure 3.10B, right). In contrast, in the vehicle-treated computational network, there only 3 cells are able to communicate with each other (Figure 3.10B, left).

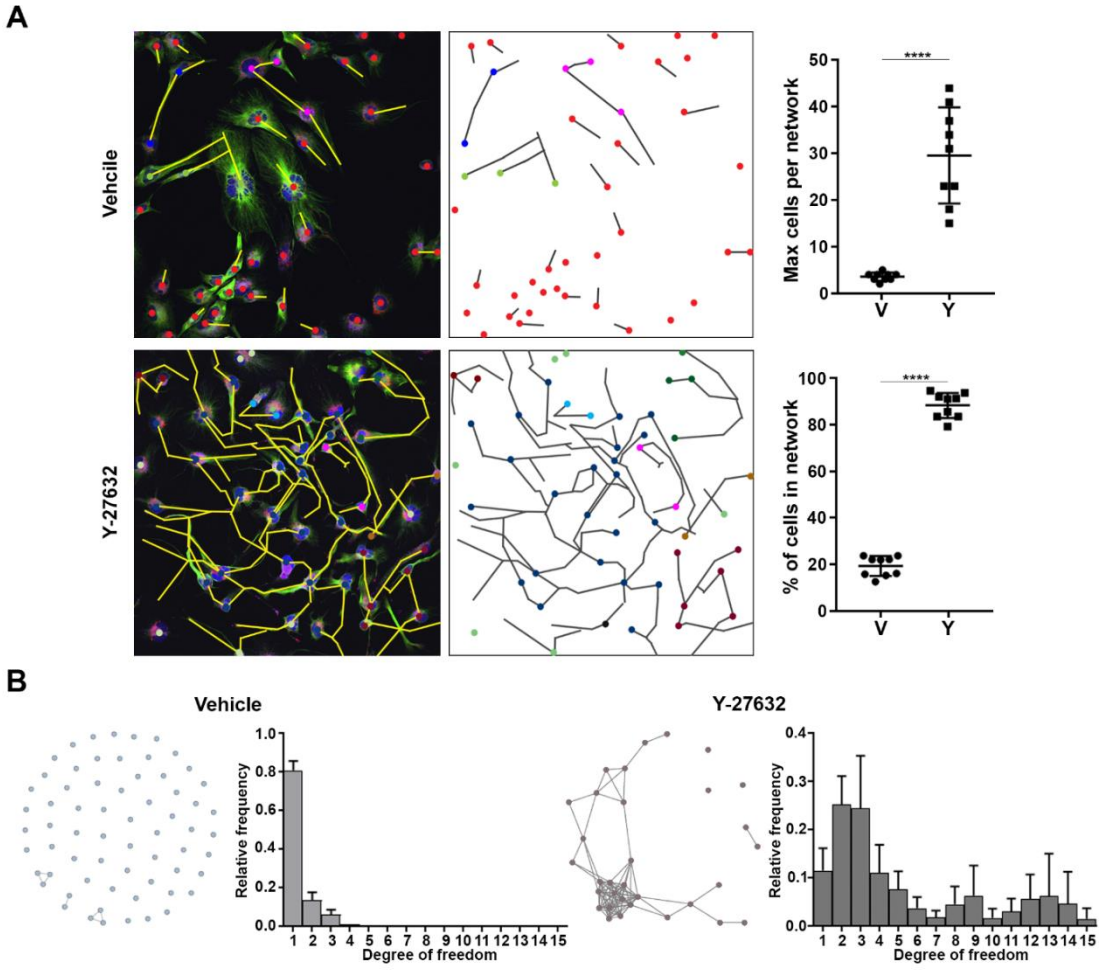

Figure 3.10 Neurite induced outgrowth following chemical ROCK inhibition resembles an intricate network of connected cells. **A**- Left, GBM1 BTSCs neurite-like protrusions were stained with TuJ1 and overlaid by bars revealing cells are in a complex network. Right, quantification of maximum cells per network (top) and the percentage of cells that are participating in a network (bottom) are displayed. **B**- Mathematical predictions of degrees of freedom for vehicle control and Y-27632 20 uM cells. Y-27632 treated cells have a higher degree of freedom which corresponds to the number of direct cellular contact per cell. In the vehicle condition, 80 % of the cells establish only one direct connection as compared with 90% of the Y-27632 cells which establish between 2-11 direct connections. (9 images per condition were analysed, mean ± SD, ****, P<0.0001, One-way ANOVA).

Graphs on the right represent the degree of freedom the cell has in the network. Degree represents the number of edges (direct connections) a specific node (cell) has with other nodes (Figure 3.10B, graphs). So, nodes that have a high degree of freedom means the node has more direct contact points with other nodes. The histogram shows that vehicle cells have fewer connections per cell on average when compared to the Y-27632 treated cells (Figure 3.10B, graphs). In the vehicle condition over 80% of the

connected cells do not establish a direct connection with any other cell. While for the Y-27632 treated cells, only 10% of the connecting cells establish a single direct connection while the remaining 90% establish between 2 and 15 direct connections (Figure 3.10B, graphs). These results show that the Y-27632 treated cells have the means and potential to form networks and the mathematical analysis predicts that they are able to work in a network.

3.2.2. BTSCs neurite-like protrusions resulting from ROCK inhibition establish networks at the expense of cellular mobility.

Cells are able to communicate directly with each other and even alter their own behaviour as a result of this interaction (273). With this in mind, I investigated if there was a change in cellular behaviour when the cells were treated with Y-27632 and whether neurite-like projections would allow cells to communicate with each other. To assess changes in cellular behaviour, I first performed time-lapse microscopy on GBM1 BTSCs cells in the presence and absence of 20 μM Y-27632 for 68 hours. Given that cell confluence can be a determinant factor in cell movement (273), I seeded the cells at two different confluencies (low density, 7.5 $x10^4$ cells per cm^2 and high density, $20x10^4$ cells per cm^2). Cells were then tracked using Image J and the Manual Tracking plugin. (Figure 3.11A).

As shown by the coloured lines (each cellular path is emphasized by an arrow) in Figure 3.11A, top panel, cells that were seeded at low density and treated with Y-27632 had no alteration in cellular movement when compared to the vehicle control cells. In tandem, an increase of cell density did not result in an alteration of movement of the vehicle treated cells. Interestingly, when cells are seeded at a high density and treated with Y-27632 it is possible to see that these cells have a reduction in their movement (Figure 3.11A). Measurements of the distance travelled per cell per minute shows that low-density vehicle or Y-27632 treated cells and high-density vehicle treated cells show

no significant change in cellular movement. However, when these conditions are compared with high-density Y-27632 treated cells there is a highly significant reduction in cellular movement (Figure 3.11B). These results indicate that Y-27632 alone does not alter cellular movement, but that another factor might be involved in this alteration.

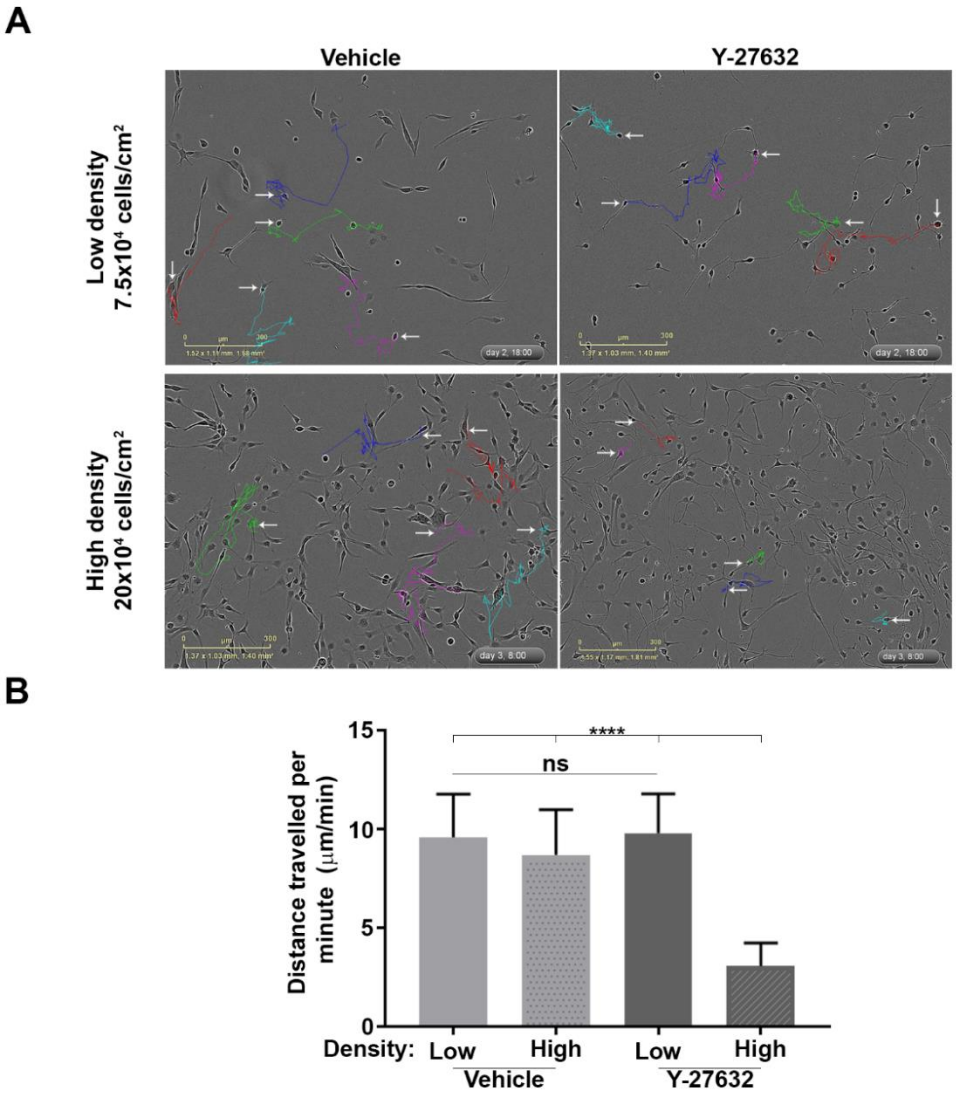

Figure 3.11 Establishment of a network in GBM1 BTSCs cells reduces the mobility of the stem cells. **A**- Cells seeded at a low confluency (7.5x104 cell/cm2, top panel) and at high confluency (20x104 cell/cm2, bottom panel) were treated with either vehicle control (left) or Y-27632 20 μM (right) and then tracked over 68 hours using the Manual tracking software in Fiji. Each cellular movement is depicted by the coloured line and highlighted with an arrow. **B**- Quantification of cellular distance travelled per minute in each given condition. Distance is measured in μm/min. (Biological triplicates, mean ± SD, ****, $p<0.0001$; Two-way ANOVA).

Manual tracking of the cells allowed us to observe the cellular behaviour and a remarkable phenotype was highlighted in this process. At low density, cells treated with Y-27632 showed the neurite-like phenotype, but the cells were sparse and these neurites were not long enough to reach other cells/neurites. However, at high density, the neurite-like projections were able to reach other protrusions/cells and this was associated with an interesting phenotype in which the cell body remained steady and the protrusions were interacting with other cells/neurites (Figure 3.11). In summary, the presence of the inhibitor alone does not affect cellular movement; cells seeded at low density and treated with Y-27632 do not establish connections and therefore move as much as their control counterparts. Cell density does not play a role because high-density vehicle cells move as much as low-density cells. These results suggest that Y-27632 induced neurites allow cells to establish networks at the cost of mobility reduction. Nevertheless, these results do not indicate whether this network is functional and if cells are in fact using these projections as a mean of long-distance communication.

3.2.3. Projections resulting from Y-27632 form a functional network in BTSCs

There is no better example for long-distance intercellular communication than neurons. These extremely well-organized cells interact using stable cellular extensions: axons and dendrites (267). Communication amongst these cells arises through changes in concentration of intracellular calcium and this leads to direct signalling between adjacent cells (267, 268). Neurite-like protrusions in BTSCs resulting from the addition of Y-27632 are reminiscent of neurons cellular extensions and the previous result suggested these cells have the means to form an intricate network of cells. To investigate whether Y-27632 treated cells are able to use this network of neurite-like protrusion to communicate, I next assessed gap junction communication between cells and calcium signalling-dependent cellular communication.

To study gap junction cellular communication, I used a scrape-loading dye transfer technique utilizing Lucifer yellow dye. This technique is based on the observation of transfer of low molecular weight fluorescent Lucifer yellow dye between cells. For this, I seeded GBM1 BTSCs and treated them with 20 μM of Y-27632 or vehicle control for 24 hours, after which I introduced a scratch wound (which allows the uptake of the dye) and Lucifer yellow (0.05%) was added for 2 mins. After the removal of the dye, two PBS washes and an eight-minute incubation period the cells were immediately visualized with confocal microscopy. Results in Figure 3.12A demonstrate that vehicle control BTSCs upload the dye but do not transmit the dye to non-contiguous cells; white arrows denote isolated BTSCs loaded with Lucifer yellow but lack of adjacent cells prevents dye transfer (Figure 3.12A, Vehicle). In contrast, Y-27632 treated BTSCs are not only able to upload the dye but also transmit it to non-contiguous cells (Figure 3.12A, Y-27632). The dye is not only visualized in the cell bodies, but also in the neurites, which is essential for transmission to non-adjacent cells (Figure 3.12A, Y-27632). Transmission of dye, in Y-27632 treated GBM1 BTSC through neurites to non-contiguous cells is denoted by the white arrow in Figure 3.12A. Quantifications of the dye transfer, assessed via the manual counting of Lucifer yellow labelled cells, as shown in Figure 3.12A (right) illustrates that, in the Y-27632 treated cells, over 60% of cells were stained positively for Lucifer yellow while only 15% of control cells were positive for the dye.

Next, calcium signalling-dependent communication in BTSCs was investigated using live cell imaging of real-time calcium flux. For this, BTSCs cells were seeded and treated with 20 μM of Y-27632 or vehicle control for 24 hours. On the day of the imaging, cells were stained with Fluoro 3, AM, which is a calcium indicator that exhibits an increase in fluorescence after binding to calcium, allowing, therefore, the visualization of the spatial dynamics of calcium signalling. In order to induce damage and provoke a calcium wave, a 2-photon laser was used and individual cells were targeted and ablated. Images were captured showing a clear difference between vehicle

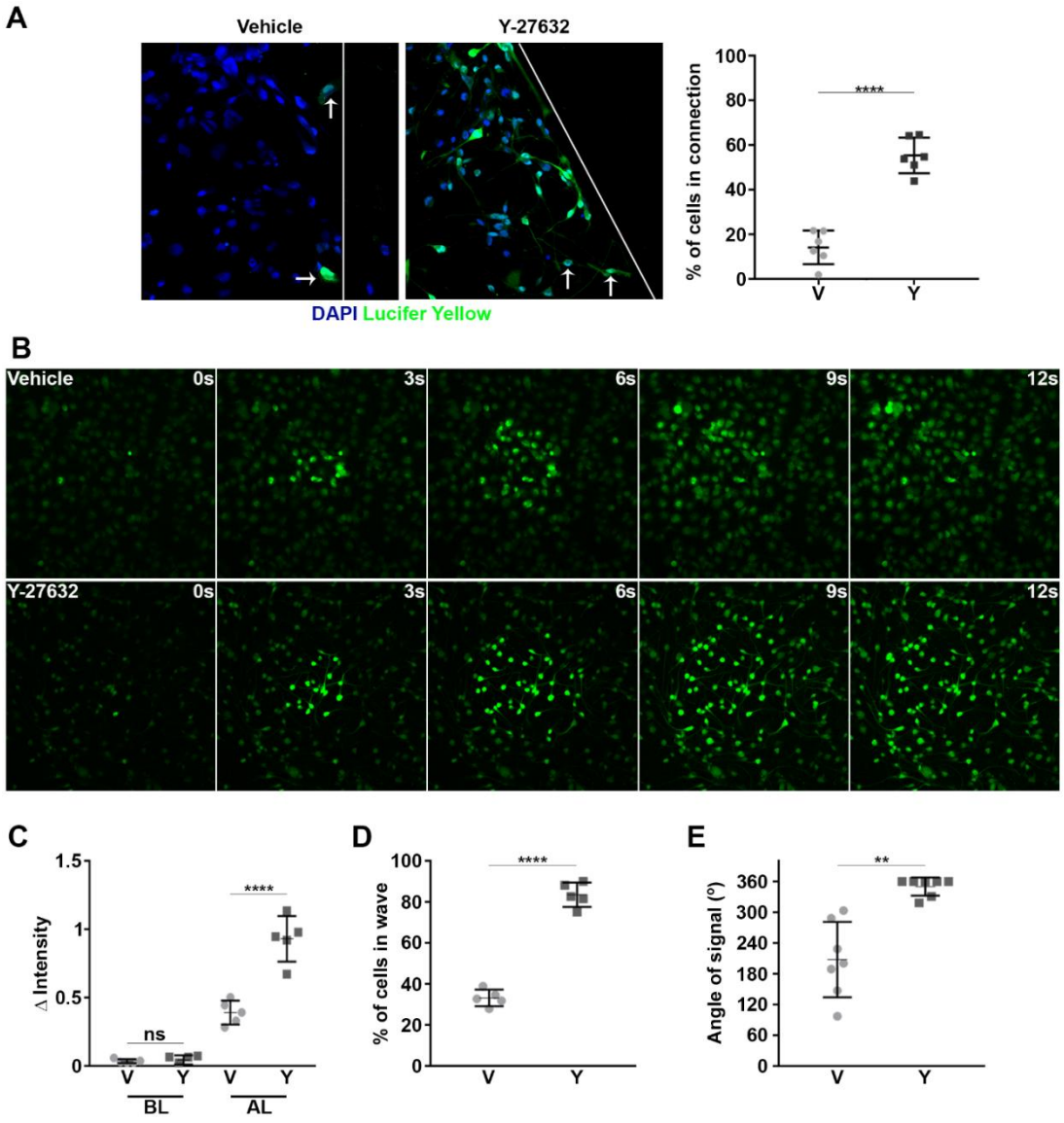

Figure 3.12 Projections resulting from treatment with Y-27632 form a functional network. **A**- Lucifer Yellow scrape-loading and dye transfer assay. In Y-27632 treated cells it is possible to see the transmission of Lucifer Yellow into non-contiguous cells which are connected by the neurites-like protrusions (white arrows on the right image). Vehicle control cells were not able to transmit Lucifer Yellow because cells are not connected (white arrows depict cells that were not able to transfer the dye). White line denotes the location of the scratch wound. **B**- Still frames of calcium signalling using live cell imaging. Cells treated with Y-27632 show the calcium wave moving through the projection and into cells which are non-adjacent to the injury site. In the vehicle condition, only cells that are adjacent to the injury site transmit the calcium signalling. Green staining – Fluoro 3, AM. **C**– Quantification of the difference in calcium intensity in vehicle (V) and Y-27632 (Y) treated cells before the laser damage (BL) and after the laser damage (AL). Y-27632 treated cells had a higher difference in intensity due to a higher number of cells being subjected to the increase in calcium after the laser damage. (10 cells per image and 5 images were analysed per condition, dots depicts average of each image; ns, non-significant; ****, $p<0.0001$; One-way ANOVA). **D** – Quantification of the number of cells participating in the calcium signalling following laser damager. (10 cells per image and 5 images were analysed per condition, dots depicts average of each image; ****, $p<0.0001$; Student's t-test). **E**- Quantification of the angle of dispersion of the calcium wave. (7 images were analysed per condition, dots depicts average of each image, **, $p<0.01$; Student's t-test).

and Y-27632 treated BTSCs cells with regards to the transmission of the calcium signalling (Figure 3.12B). In control cells, the calcium signalling wave was mainly transmitted amongst adjacent cells and faded away quickly while in the Y-27632 treated GBM1 BTSCs the calcium-induced signal moved through the neurite-like protrusions and continued into adjacent cells via the neurite outgrowths. Quantification of the signalling wave was performed via three approaches: measurement of changes in calcium intensity before and after the laser damage; percentage of cells that participated in the calcium signalling wave, and the angle of the signalling wave.

In order to measure the difference in fluorescence intensity, the intensity of 10 random cells was assessed per image, in each case the BL (before laser damage) was measured as the difference in intensity between the first image and the last image before the laser damage. While AL (after laser damage) was the intensity difference between the first image following laser damage and the following 7 images after which the intensity level returned to basal levels. Figure 3.12C shows that the selected cells in both control and Y-27632 treated conditions had the same intensity levels before the laser damage. However, after damage, the selected Y-27632 treated BTSCs showed a significantly higher increase in intensity, demonstrating that more cells participated in the signalling wave (compared to the vehicle control) and that the intensity of the calcium signalling wave was maintained throughout the cells (Figure 3.12C). This phenomenon is clearly observed in Figure 3.12D where the number of cells in the calcium wave per image was quantified and the comparison between the two conditions showed that approximately 80% of the Y-27632 treated BTSCs participated in the calcium wave against only 35% of the control BTSCs. Furthermore, measurements of the angle show that Y-27632 treated cells transmitted the wave to nearly the four corners of the image while vehicle cells were unidirectional most of the time (350° vs 207°). In summary, this data demonstrates that the neurite-like protrusions that arise from the treatment with Y-27632 are able to form a cellular

network that can be used by the cells to communicate via a calcium flux, therefore creating a long-distance communication system amongst the cells.

3.2.4. Projections resulting from ROCK inhibition are used by BTSCs to traffic whole cellular organelles

Cellular communication is a fundamental prerequisite for the development and maintenance of cancer cells (266). Studies have shown that a wide range of cell types, including T-cells, stem cells, epithelial cells and myocardial cells are able to form tunnelling nanotubes (269-272) and that sub-cellular organelles can be transferred between these connections (269, 271). Given that the neurite-like projections observed in Y-2732 treated GBM1 BTSCs are analogous to these tunnelling nanotubes, this led to the investigation of whether the transfer of cellular organelles can also occur between these BTSCs through the projections.

To study organelle movement, GBM1 BTSCs were treated with 20 μM of Y-27632 or vehicle control for 24 hours and lysosomes and mitochondria were stained using LysoTracker and MitoTracker respectively. Fluorescence images shown in Figure 3.13A demonstrate that in the control condition, lysosomes (purple) and mitochondria (red) are located mainly in the cell body of the GBM1 BTSCs. However, in the Y-27632 treated cells both lysosomes and mitochondria are not solely concentrated in the cell body but dispersed along the neurites (Figure 3.13A). Quantifications of the quantity of lysosomes and mitochondria localized outside the cell body shows a drastic variation of these between vehicle and Y-27632 GBM1 BTSCs; with <10% versus 30% of lysosomes localized outside the cell body in vehicle and Y-27632 treated BTSCs respectively. For mitochondria the percentage is <10% versus 40% (Figure 3.13A, right). To further study this organelle movement in the neurites-like projections, live cell imaging was performed on these cells. Figure 3.13B shows still frames from the live cell imaging for the Y-27632 treated GBM1 BTSCs where the white arrows accompany the movement of two distinct mitochondria along the neurites. Measurements of

mitochondrial movement in both control and Y-27632 treated BTSCs show that in the latter condition BTSCs mitochondrion move on average, per frame, three times further than in the control cells (Figure 3.13B, right). Therefore, these results demonstrate that Y-27632 treated cells are able to use the neurite-like formation to transport bulky cargoes such as mitochondria and lysosomes.

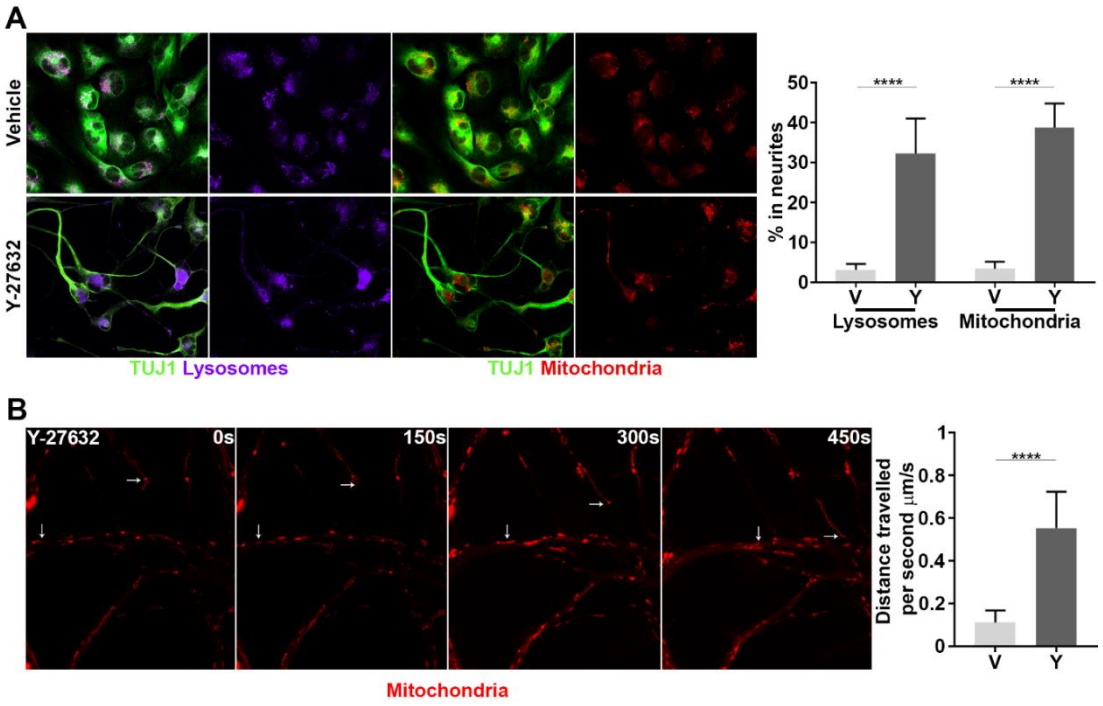

Figure 3.13 Neurite-like protrusions induced by Y-27632 are used to transfer organelles between cells. **A**- Left, Confocal images showing lysosomes stained using LysoTracker (left side, purple) and mitochondria stained with MitoTracker (right side, red). Lysosomes and mitochondria in the control cells are located compactly within the cell body whilst the lysosomes and mitochondria in the Y-27623 treated BTSCs are dispersed throughout the neurite-like protrusions. Right, quantification of the percentage of lysosomes and mitochondria that are found in the neurites of the cells for control and Y-27632 treated cells. (10 images were analysed per condition, mean ± SD, ****, $p<0.0001$; One- way ANOVA) **B**- Left, live cell imaging of mitochondria in Y-27632 treated cells demonstrates movement of mitochondria along the neurite-like protrusions (white arrow indicates the translocation of mitochondria). Right, quantification of mitochondria migration in cells either treated with vehicle control or Y-27632. 5 movies were analysed per condition, mean ± SD, ****, $p<0.0001$; Two-way ANOVA).

3.2.5. Presence of Y-27632 in BTSCs has no protective effect in DNA double-stranded breaks caused by radiation

Recent evidence indicated that brain tumour cells interconnect and form a multicellular network (266). During tumour recurrence, the interconnected cells may

use contractile and or/neurite-like extensions to communicate over long distances and it is thought that these complex cellular interactions promote therapy resistance (266). In order to investigate whether the presence of this network in these cells has the same survival advantage as demonstrated by Osswald et al. (266), the BTSCs were treated with Y-27632 (20 μM) and vehicle control and subjected to increasing doses of radiation; 2, 8, 20 Gy.

As shown in Figure 3.14A, in the 0 Gy condition both Y-27632 and vehicle treated GBM1 BTSCs show a residual amount of DNA double-stranded breaks (identified using an anti-γH2AX antibody) showing that neither treatment induced DNA damage. As expected irradiation resulted in DNA damage, demonstrating that the radiation treatment was effective (Figure 3.14 A). Moreover, as the dose of radiation increases there is an accompanying increase in the amount of DNA double-stranded breaks (Figure 3.14A). It is noteworthy that quantification of DNA damage (shown as the percentage of nuclei area stained positive for γH2AX) demonstrates that there is no significant difference in DNA damage between control and Y-27632 treated BTSCs at the same radiation dose (Figure 3.14B). Taken together, these results indicate that treatment of Y-27632 in BTSCs does not alter the sensitivity to radiation-induced DNA damage.

3.2.6. Chemical ROCK inhibition provides resistance to nuclei fragmentation after irradiation

Osswald et al (266). demonstrated that connected brain tumour cells were protected from cell death following radiotherapy. To examine whether Y-27632-induced interconnectivity in BTSCs would help protect these cells from radiation, I treated GBM1 BTSCs with vehicle control or Y-27632 for 24 hours and then irradiated the cells with 2, 8, and 20 Gy. Three (Figure 3.15A) and five days (Figure 3.15B) after radiation, the cells were stained with DAPI and nuclear damage was assessed. In order to determine if the effects resulted from the compound or from the neurite-like

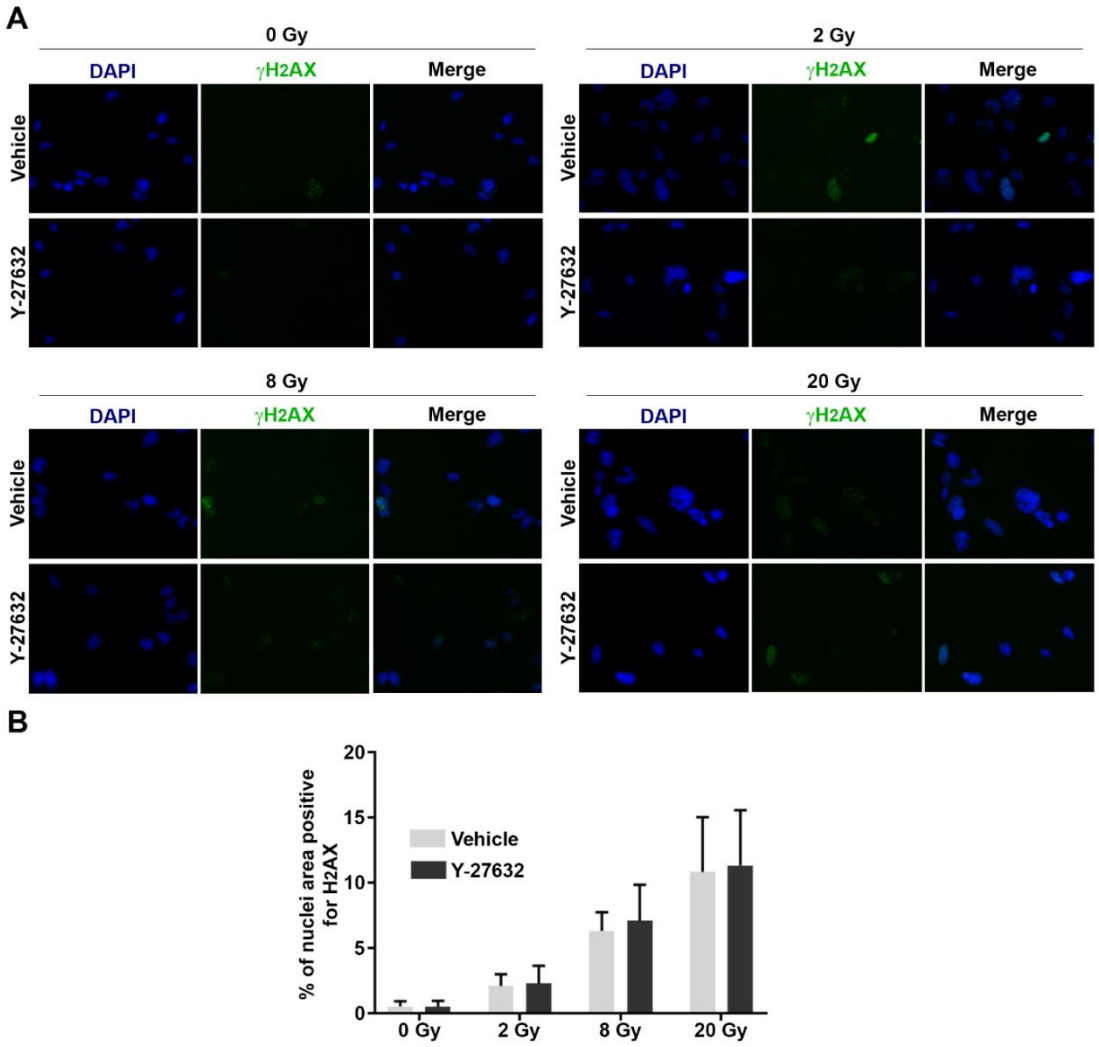

Figure 3.14 BTSCs treated with Y-27632 or vehicle suffer the same amount of DNA damage when subjected to increasing doses of radiation. **A**- Immunofluorescence images of BTSCs following irradiation with 2, 8 and 20 Gy for control (top panel) and Y-27632 treated cells (bottom panel). Two hours after irradiation cells were stained for double-stranded breaks using histone H2A variant γH2AX. Blue staining corresponds to DAPI staining while green staining is the positive γH2AX foci. **B**- Quantification of DNA damage presented as the percentage of nuclei area positive for γH2AX was obtained using colour threshold on ImageJ. Both conditions showed that cells possess the same amount of DNA double-stranded breaks following ionizing irradiation. (Biological triplicates, mean ±SD, statistical analysis in each irradiation group shows the difference in each condition is non-significant, One-way ANOVA).

protrusions induced by the compound, a treatment washout condition was also tested. For the washout treatment, BTSCs were treated with 20μM Y-27632 for 24 hours after which the media containing Y-27632 was removed, the cells were washed with PBS and fresh media (without the compound) was added. Eight hours after the washout of the compound the cells were assayed as outlined above.

Representative images of nuclei damage three days after irradiation show that non-irradiated cells do not present/have a low level of nuclei damage when compared to the other radiation doses. In the 20 Gy radiated cells the vehicle and Y-27632 washout condition display a higher degree of nuclei damage when compared to the Y-27632 treated BTSCs, such is highlighted by the white arrows in Figure 3.15A. Quantification of the percentage of nuclei damage (Figure 3.15A, right) demonstrates that in all of the radiation doses the Y-27632 treated cells have a significantly lower ($p<0.001$ for 2 Gy and $p<0.0001$ for 8 and 20 Gy) percentage of nuclei damage when compared to their control counterparts (vehicle and Y-27632 washout).

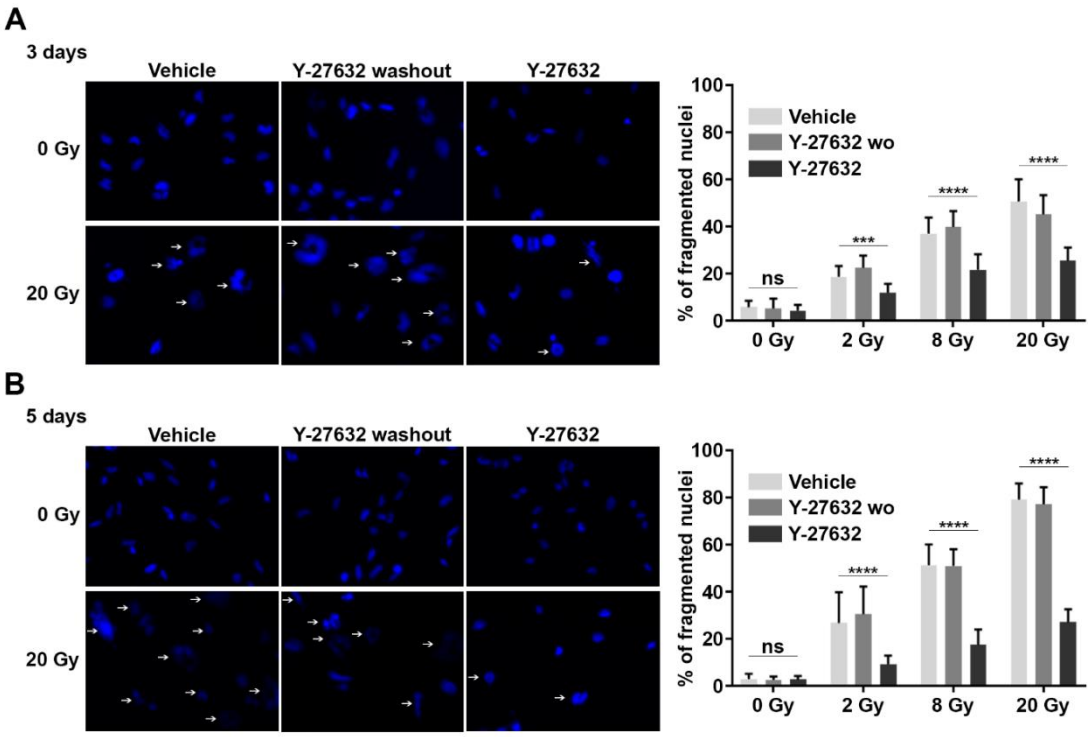

Figure 3.15 Y-27632 treated BTSCs are more resistant to nuclei fragmentation caused by irradiation. GBM1 BTSCs treated with vehicle (water), Y-27632 or Y-27632 washout were subjected to increasing doses of radiation (0-20 Gy). Three **(A)** and 5 days **(B)** after irradiation nuclei fragmentation was assessed. Left, representative images of nuclei from GBM1 BTSCs stained with DAPI, 3 days **(A)** and 5 days **(B)** following 0 and 20 Gy irradiation. Right, quantification of the percentage of fragmented nuclei in BTSCs three **(A)** and five **(B)** days after irradiation treatment. Arrows indicative of fragmented nuclei. (Biological triplicates, mean ± SD, **0, P<0.001; ****, P<0.0001, Two-way ANOVA)

Nevertheless, to exclude the possibility that Y-27632 treated cells might have a delayed response to radiation and three days is not sufficient to elicit nuclei damage in

the Y-27632 treated cells, the experimental conditions were repeated but the period following irradiation increased to five days (Figure 3.15B). Interestingly, five days following irradiation, vehicle and Y-27632 washout treated BTSCs possessed an even higher percentage of damaged nuclei for all of the radiation doses (white arrows in Figure 3.15B denotes nuclei damage). Specifically, for the 20 Gy radiation, there is an increase of nuclei damage from 55% on day 3 to 80% on day 5, as displayed in Figure 3.15. Contrary to the control conditions, the Y-27632 treated cells maintained the percentage of nuclei damage 5 days post-irradiation. For the 20 Gy radiation the marginal increase in nuclei damage went from 25% on day 3 to 27% at day 5 (Figure 3.15). In summary, these results show that the induction of a neurite-like network in GBM1 BTSCs via chemical ROCK inhibition had a significant protective effect against nuclei damage caused by radiation.

3.2.7. Resistance to nuclei fragmentation is linked to ROCK inhibition induced cellular connectivity

On average 20% of the cells in the Y-27632 treated GBM1 BTSCs are not part of a network (Figure 3.10), and this feature can be used as an internal control. This mixture of connected cells and non-connected cells allows for the in-depth investigation not only into the effect radiation has on the cells that are in the network but most importantly into the effect it has on the non-connected cells.

A more detailed appraisal of the nuclei in the 20 Gy Y-27632 treated GBM1 BTSCs experiment (Figure 3.16A) shows that the majority of the nuclei damage seen in this condition arose from cells that are not part of the network of connected cells, as can be seen in Figure 3.16A. Focusing on the connected portion of the cells, the pie charts displayed in Figure 3.16B show that the increase in radiation only elicits a small increase in damaged nuclei and in fact there is no difference when comparing day 3 to day 5. Whilst, in the non-connected population the increase in radiation is leading to

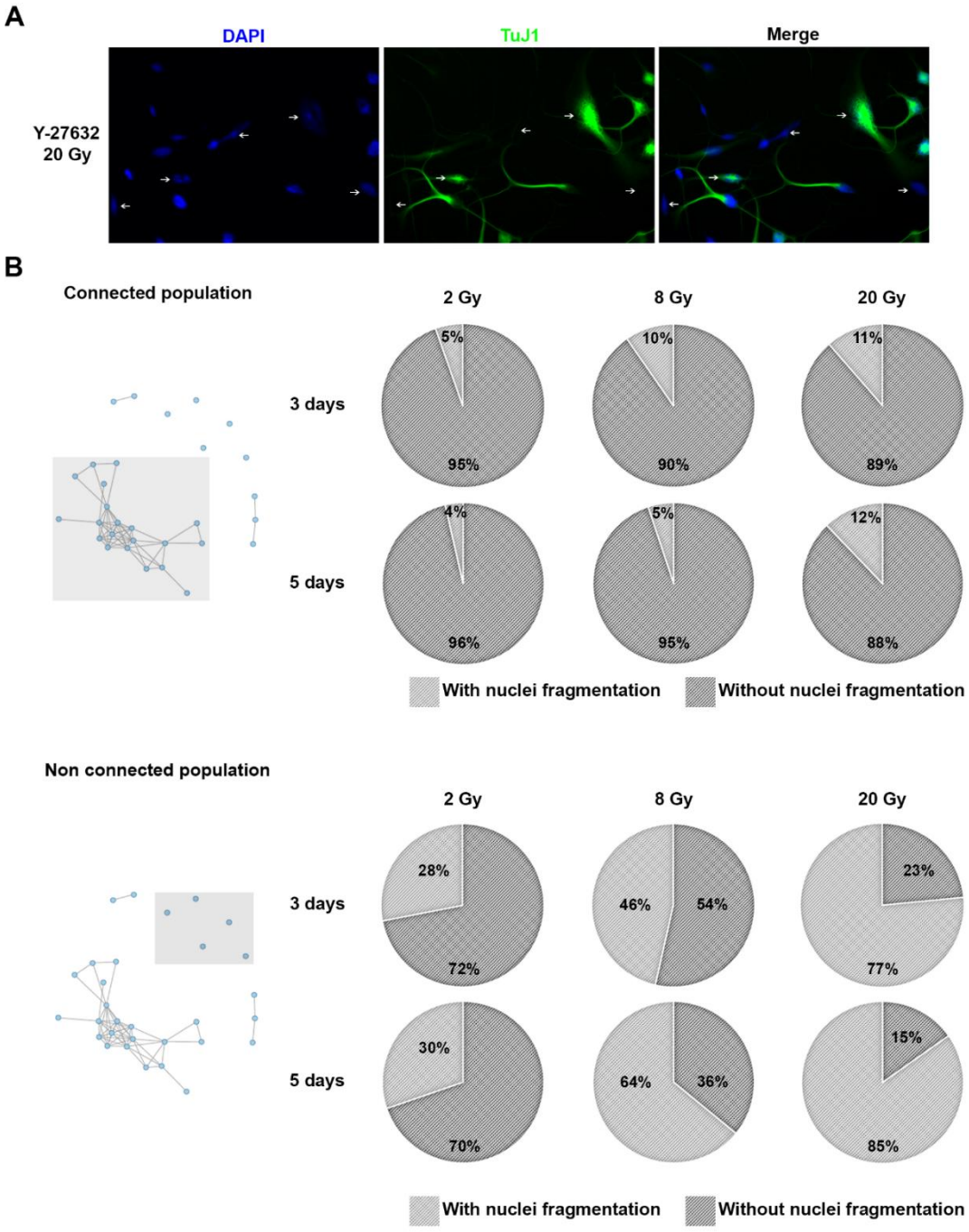

Figure 3.16 Nuclear damage in the Y-27632 treated BTSCs originates from the non-connected BTSCs population. BTSCs treated with vehicle, Y-27632 or Y-27632 washout were subjected to increasing doses of irradiation. **A**- Immunofluorescence images of DAPI and TuJ1 staining depicts Y-27632 treated BTSCs 5 days following 20 Gy radiation. White arrows highlight fragmented nuclei which belong to cells which are not part of the network of connected cells. **B**- Quantification of nuclei damage in the connected (top) and non-connected population (bottom) 3 days and 5 days after irradiation. Increase in the radiation dose leads to a drastic increase in nuclei fragmentation in the non-connected cells. For 3 days, at 20 Gy, 77% of the non-connected cells have nuclei fragmentation vs 11% of the connected cells whilst for 5 days that percentage increases to 85% for the non-connected cells versus 12% of the connected BTSCs.

a drastic increase in nuclei damage in this subpopulation of cells. In fact, comparison between connected and non-connected cells for the radiation dose of 20 Gy after 3 days, shows that 11% of the connected population display nuclei damage compared to 77% of the non-connected cells. This difference further increases 5 days post radiation, where 12% of connected cells show nuclei damaged compared to 85% of the non-connected cells. Taken together these results show that the radiotherapy resistance exhibited by Y-27632 treated GBM1 BTSCs is linked to cellular connectivity resulting from chemical ROCK inhibition.

3.2.8. Control BTSCs change their cellular behaviour following irradiation

The balance between cell survival and death after DNA damage is determined by factors involved in DNA damage recognition, DNA repair and the cells ability to tolerate the damage (274, 275). It is known that cell behaviour can change as a result of DNA damage (274). To further investigate the effect radiation has on vehicle, Y-27632 and Y-27632 washout treated BTSCs, cellular behaviour was assessed.

One way to study the behaviour of cells is to study their movement and this was performed using GBM1 BTSCs and time-lapse microscopy following irradiation. Cells were seeded and treated with vehicle control and 20 μM of Y-27632 for 24 hours. In order to discern if the effects resulted from the compound or from the neurite-like protrusions induced by the compound, a treatment washout condition was also tested. Cells were then irradiated with 0, 2, 8 and 20 Gy and analysed immediately using the IncuCyte imaging system for time-lapse microscopy over three days. Cellular tracing (coloured lines) can be seen in Figure 3.17A for all the tested conditions and shows that vehicle and treatment washout conditions increase their cellular movement with the increase of radiation. However, Y-27632 treated cells maintain a similar travel distance throughout the different irradiations. Figure 3.17B depicts the quantification of cellular movement and in fact, vehicle and treatment treated BTSCs

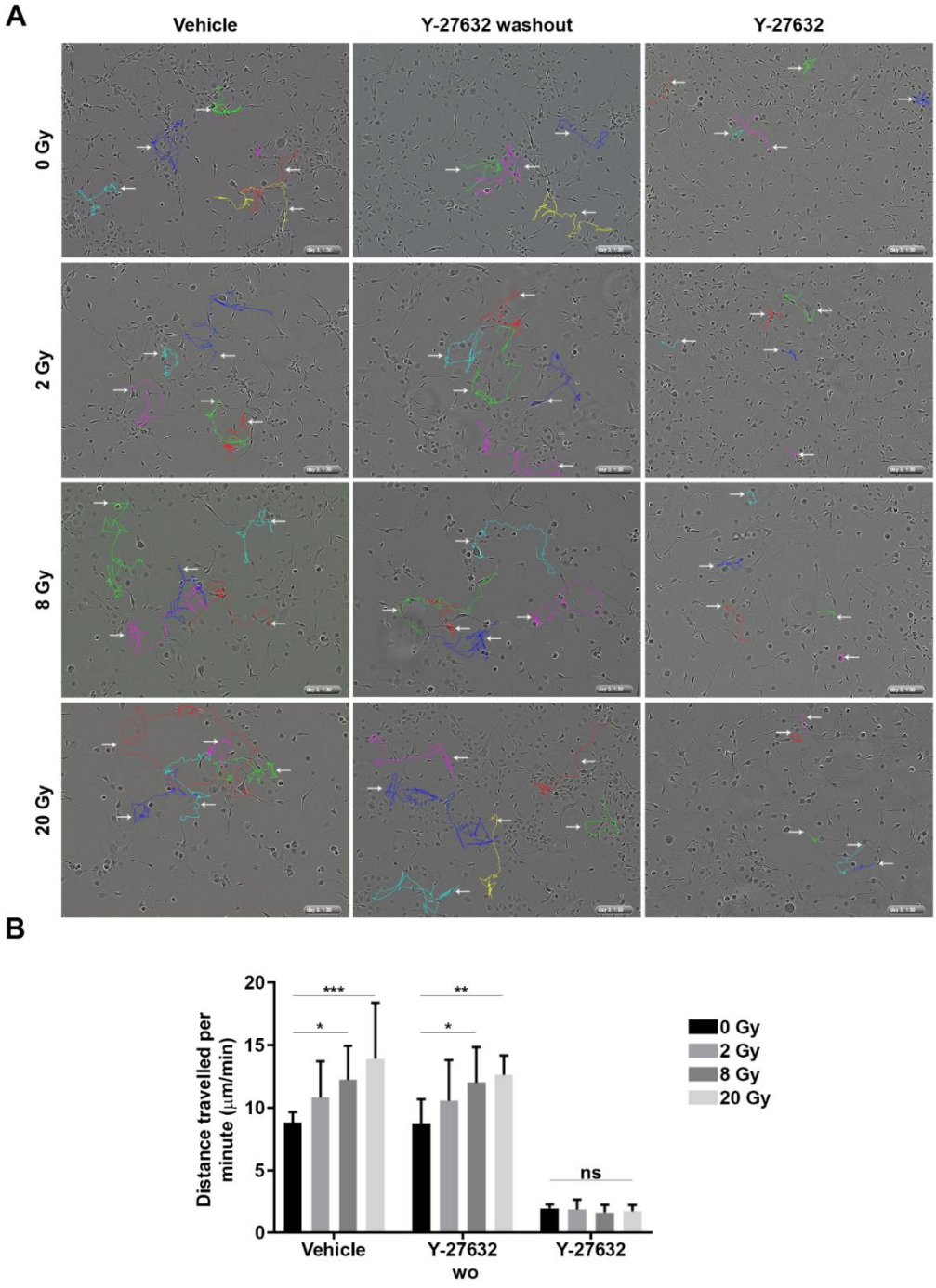

Figure 3.17 Increase in irradiation in control and Y-27632 washout BTSCs leads to an increase in cellular mobility of these cells. **A**- Live cell imaging of BTSCs treated either with vehicle control, Y-27632 or Y-27632 washout cells were irradiated with increasing radiation doses (2, 8, 20 Gy). Cells were then tracked for 3 days using the Manual Tracking software in Fiji. Each colour line illustrates the path each tracked cell undertook and white arrows highlight the path for easy visualization. **B**- Quantifications of the distance travelled for the cells in each given condition. Distance is measured in µm/min. (Biological triplicate, mean ±SD, *, p<0,05; **, p<0.01; ***, p<0.001; Two-way ANOVA)

significantly increased their cellular movement following irradiation with 8 and 20 Gy while BTSCs treated with Y-27632 showed no significant difference regarding cellular movement.

To study these radiation-induced changes in more depth the time-lapse movies were assessed for key features of cellular behaviour. A series of questions were posed for individual cells (see Figure 3.18 for details) eliciting Yes/No answers (with one exception) allowing the answers to be presented in a heat-map. This heat-map creates a general picture of cellular behaviour across treatment conditions and radiation doses. As expected, vehicle and Y-27632 washout treated cells (control conditions) exhibited similar cellular behaviour, which contrasted with the Y-27632 treated BTSCs. There is a divergence across all radiation conditions between control conditions and Y-27632 treated cells regarding neurite phenotype and network participation.

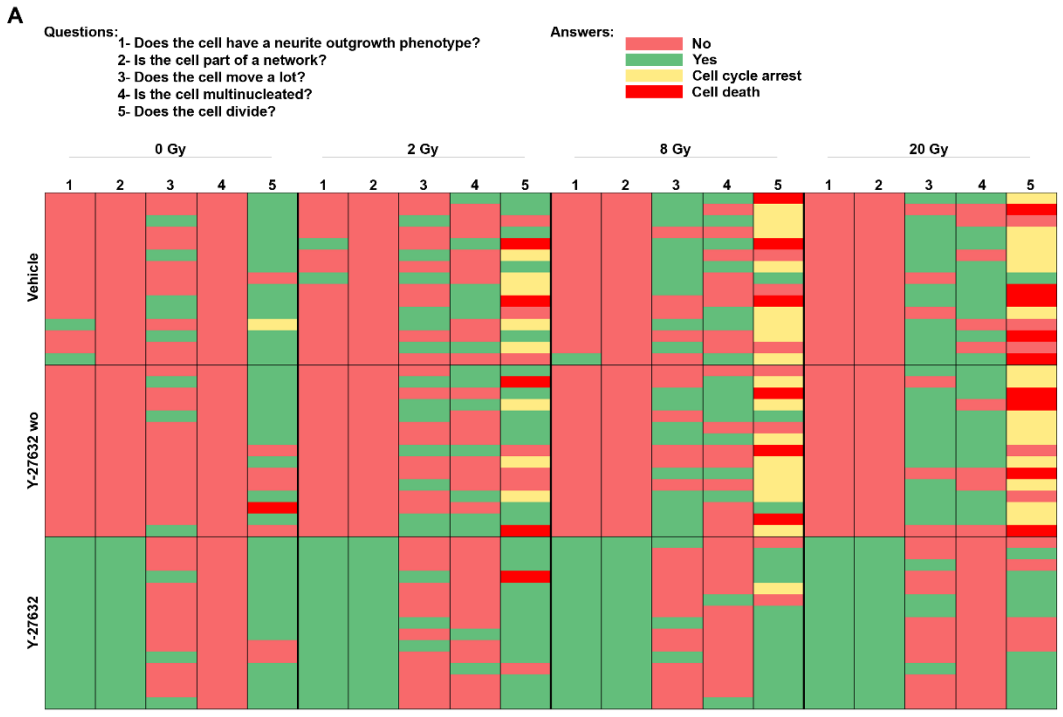

Figure 3.18 Heatmap illustrates changes in key features of cellular behaviour caused by radiation treatment. BTSCs were treated with vehicle control, Y-27632 (20μM) and Y-27632 washout (2-hour washout) and subjected to increasing doses of radiation (0, 2, 8, 20 Gy). Answers to the 5 questions (questions and answers shown in the figure) are displayed in the heat-map thus creating an overall picture of alterations in cellular behaviour across treatment conditions and radiation doses.

All Y-27632 treated cells had the neurite-like phenotype and were in a network, whereas very few control cells had the phenotype and none of them were in a network.

In order to determine changes in movement that resulted from radiation, the basal level of movement was set as the distance travelled per minute in non-irradiated cells; the average values used were obtained from experiments presented in Figure 3.11. For control conditions (vehicle and Y-27632 washout) this value was set at 10 μm/min, while for Y-27632 treated cells it was 2.5μm/min (values under these thresholds would be marked as No and over as Yes). For both control conditions, there was a trend showing that cells increase their movement with increasing radiation dose, for example, in the 20 Gy radiation dose nearly all cells have increased their movement from basal levels. In contrast, Y-27632 treated BTSCs did not change their movement with increasing doses of irradiation.

Next, I wanted to investigate the balance between cell survival and death. I asked whether cells were multinucleated and if they divided during the time-lapse movie. Very interestingly, control BTSCs at 0 Gy had zero multinucleated cells and almost all cells divided. However, with increasing radiation doses there was also an increase in the number of multinucleated cells as well as in the number of cells that were not able to divide and were in cell cycle arrest or died. This change is visible at 2 Gy and becomes more drastic at 8 and 20 Gy; in the 20 Gy dose, the majority of the cells were multinucleated and either in cell cycle arrest or dead. Remarkably, the Y-27632 treated cells were overall unaffected by increasing radiation doses. Even though, there was a slight increase in the number of cells that did not divide during the time lapse movie in the 20 Gy radiation dose, I did not observe any cells in cell cycle arrest or cell death. In summary, these results indicate that control cells did alter their cellular behaviour following irradiation whilst Y-27632 treated cells maintained their cellular behaviour whilst enduring increasing doses of radiation.

3.2.9. Radiation induces distinct morphological changes in BTSCs

To investigate alterations in cell morphology caused by radiation in GBM1 BTSCs I assessed the cytoplasmic area and neurite outgrowth in the irradiated cells and non-irradiated controls. BTSCs were treated in the same previous conditions (vehicle, Y-27632 and washout) and 5 days after irradiation they were stained with the cytoskeletal marker TuJ1. Images displayed in Figure 3.19A show that BTSCs treated with water or treatment washout and subjected to 20 Gy radiation display a morphology which is very distinct from that observed in the non-irradiated control (0 Gy) BTSCs (Figure 3.19A, top and middle panel). This alteration in cell morphology – increased cell size and cell flattening – is a characteristic morphology associated with cellular senescence (276). However, Y-27632 treated BTSCs maintain their cellular morphology after being submitted to 20 Gy radiation (Figure 3.19A, bottom panel). In order to quantify changes in the cytoplasmic area in these BTSCs, the ratio between cytoplasm and nuclei was quantified. As shown in Figure 3.19B, increasing doses of radiation in control (vehicle and Y-27632 washout) cells led to the increases in the ratio of cytoplasm to nuclei meaning there is an increase in the cellular body size which is associated with the increase of radiation. In contrast, Y-27632 treated cells show no significant change in their cell body morphology following irradiation (Figure 3.19B).

I also assessed neurite-like outgrowth 5 days following irradiation. Representative images of Y-27632 treated GBM1 BTSCs (Figure 3.20), demonstrate that cells maintain their neurite-like outgrowths with the increase of radiation. Comparison of TuJ1 staining for 0 Gy and 20 Gy show a clear distinction in neurite-like protrusions, with the latter possessing a higher number of protrusions, as seen in Figure 3.20A. Measurements of outgrowths per cell were done on BTSCs treated with water, Y-27632 and Y-27632 washout for the following radiation doses – 0, 2, 8 and 20 Gy. The graph shown in Figure 3.20B shows that control and treatment washout show no change in

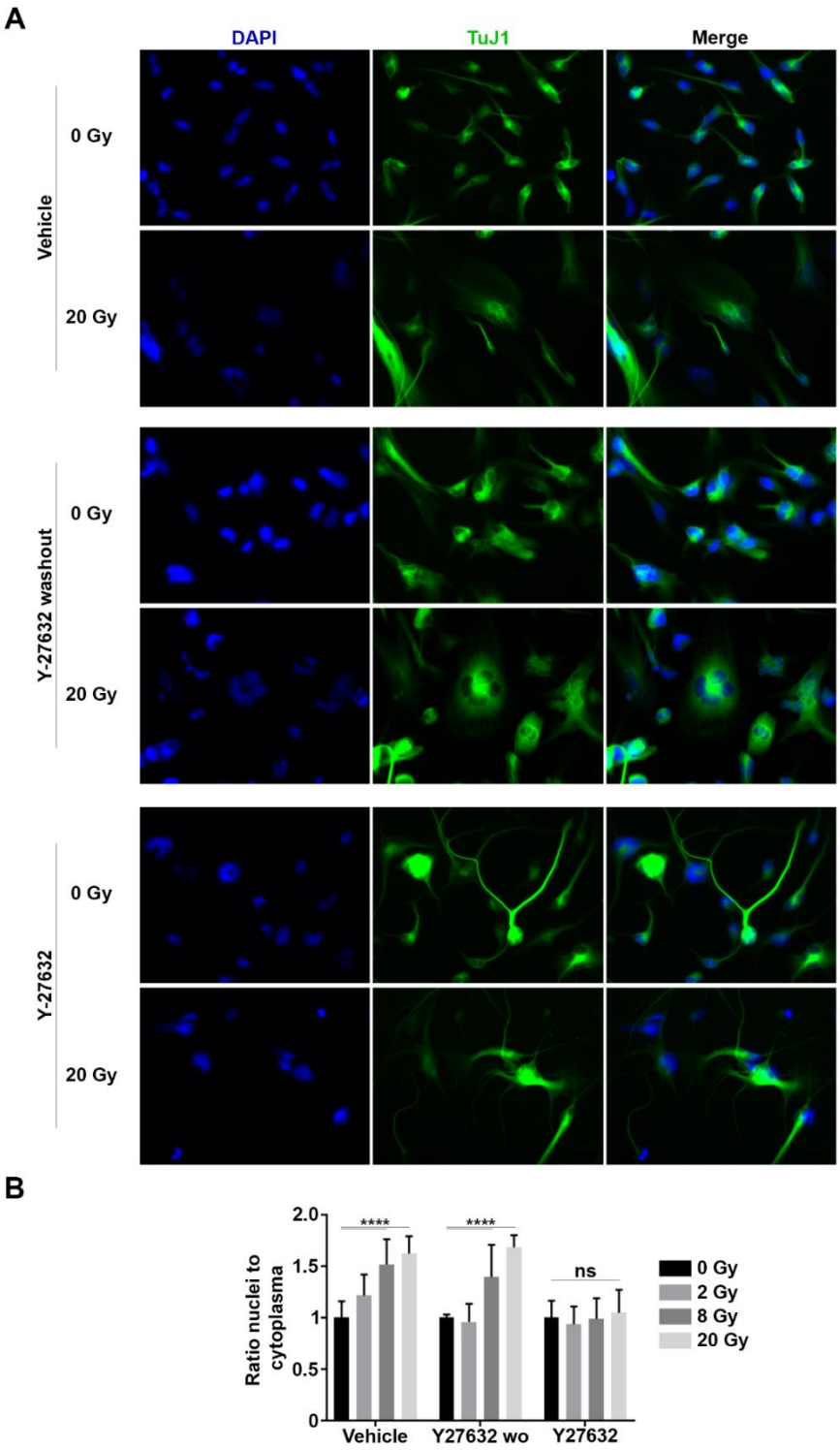

Figure 3.19 Increase in radiation dose leads to the expansion of cytoplasmic area in vehicle control and Y-27632 washout BTSCs five days following irradiation. Cytoplasmic area of Y-27632 treated BTSCs remain unaffected by irradiation. **A**- BTSCs treated either with water, Y-27632 and Y-27632 washout were subjected to increasing doses of irradiation. Immunofluorescence images of TuJ1 positive staining depict only 0 Gy (control) and 20 Gy conditions. 20 Gy irradiation results in an increase of cytoplasmic area in control and washout BTSCs while Y-27632 treated cell maintained their cytoplasmic to nuclei ratio. **B**- Quantification of cytoplasmic area in BTSCs for the treatments conditions above mentioned but containing as well the 2 and 8 Gy irradiation. Increasing doses of irradiation resulted in the expansion of the cell's cytoplasm in control and Y-2632 washout treated BTSCs. Areas of DAPI positive and TuJ1 positive staining were measured using colour threshold on ImageJ. (Biological triplicate, mean ±SD, ns: non-significant; ****; P<0.0001; Two-way ANOVA)

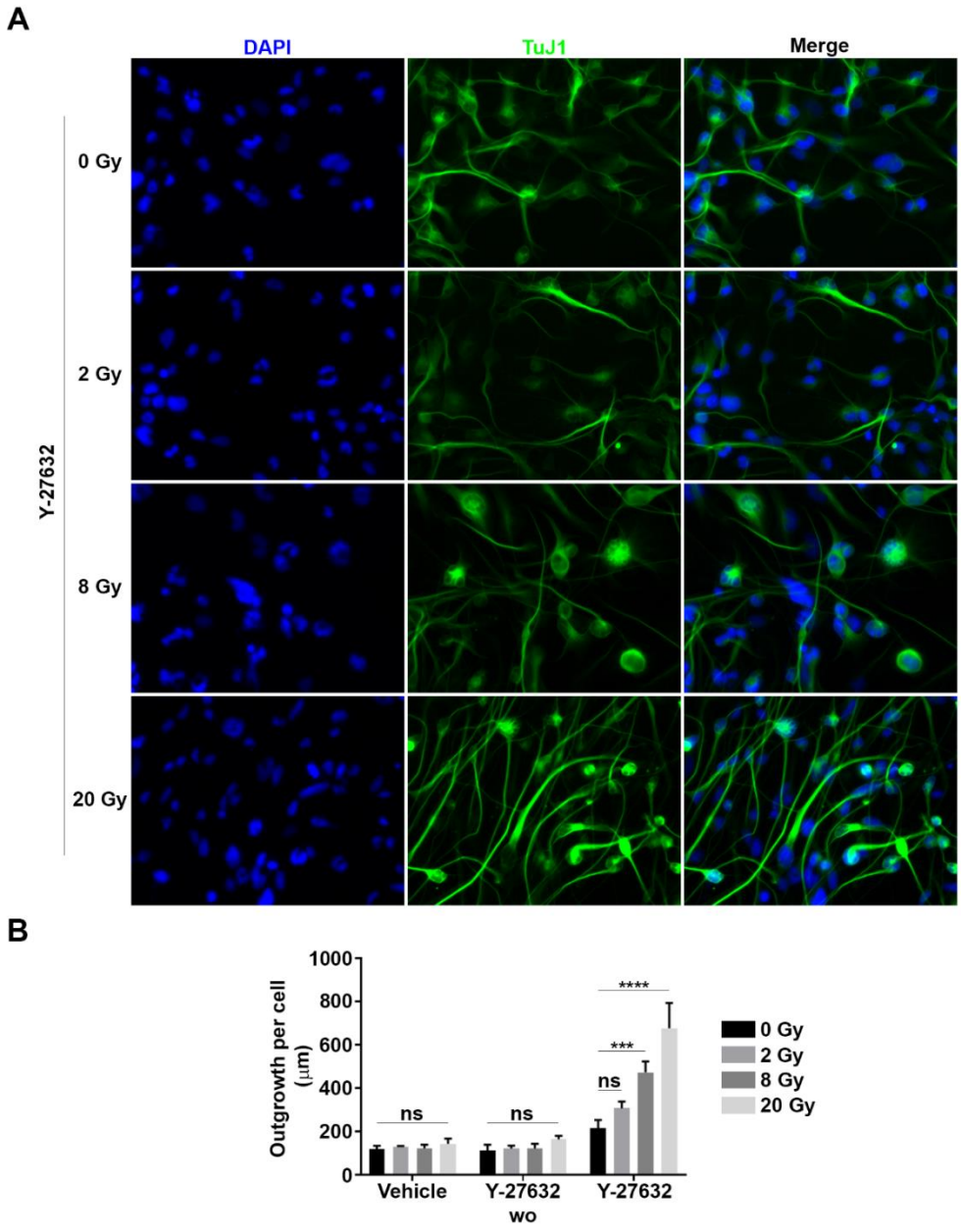

Figure 3.20 Increasing radiation doses result in the increase of neurite-like protrusions in the Y-27632 treated GBM1 BTSCs. Vehicle control and Y-27632 washout displayed no alteration in neurite-like protrusions in response to radiation. **A**- Representative immunofluorescence images of TuJ1 positive staining of Y-27632 treated cells subjected to increasing doses of radiation (0, 2, 8, 20 Gy). BTSCs subjected to higher radiation doses (8 and 20 Gy) show a more pronounced neurite-like phenotype. Nuclei are stained with DAPI. **B**- Quantification of the average TuJ1 positive neurite outgrowth per cell (µM) in GBM1 BTSCs treated with vehicle control, Y-27632 (20µM) and Y-27632 washout (Y-27632 wo, 2-hour washout) five days after radiation. (Biological triplicate mean ±SD, ns: non-significant; ***, P<0.001; ****, P<0.0001; Two-way ANOVA)

neurite-like outgrowth regardless of radiation dose. In contrast, Y-27632 treated BTSCs exhibit an increase in neurite outgrowths with increasing radiation. The increase is significantly higher in the 20 Gy dose where there is almost a ~4 fold increase when compared to the 0 Gy dose. Taken together, these results indicate that all treatment conditions change their morphology, albeit differently, after being subjected to radiation therapy. While control and Y-27632 washout treated cells increase the cytoplasmic area, Y-27632 treated cells displayed an increase in neurite-like protrusion following radiation.

3.2.10. Chemical ROCK inhibition leads to a survival advantage

Cells react to DNA damage by activating complex signalling pathways that decide cell fate by either promoting DNA repair or initiating cellular death (274). It is known that DNA damage is an inducer of cellular senescence which, in some cases can lead to apoptosis (276). Previous results (Figure 3.19) demonstrated that vehicle and Y-27632 washout BTSCs displayed a morphology that resembles cellular senescence. Therefore, I next sought to investigate the effect different radiation doses had on cellular proliferation and viability of BTSCs.

To assess cellular proliferation, live cell imaging was performed on BTSCs treated with vehicle, Y-27632 (20μM) and Y-27632 washout (8-hour washout) and then subjected to 0, 2, 8 and 20 Gy radiation doses. Using the IncuCyte proliferation assay package, growth rates were obtained and confluency curves were calculated based on relative values which were normalized to the t_0 time point. Results show that at 0 and 2 Gy there is no difference between the three tested conditions (Figure 3.21A). However, for the 8 Gy radiation dose the vehicle and Y-27632 washout proliferation curves start to diverge at day 3 and at day 5 Y-27632 treated BTSCs show a significant increase in proliferation when compared to the control cells (Figure 3.21A, vehicle and Y-27632 washout). For 20 Gy, as demonstrated in Figure 3.21A, the separation in proliferation rate between the control and Y-27632 treated BTSCs occurs earlier, at

day 2 the curves start to diverge and at day 3 and day 5 there is a highly significant difference in the proliferation rates between these conditions ($p<0.001$ for 3 and $p<0.0001$ for 5 days).

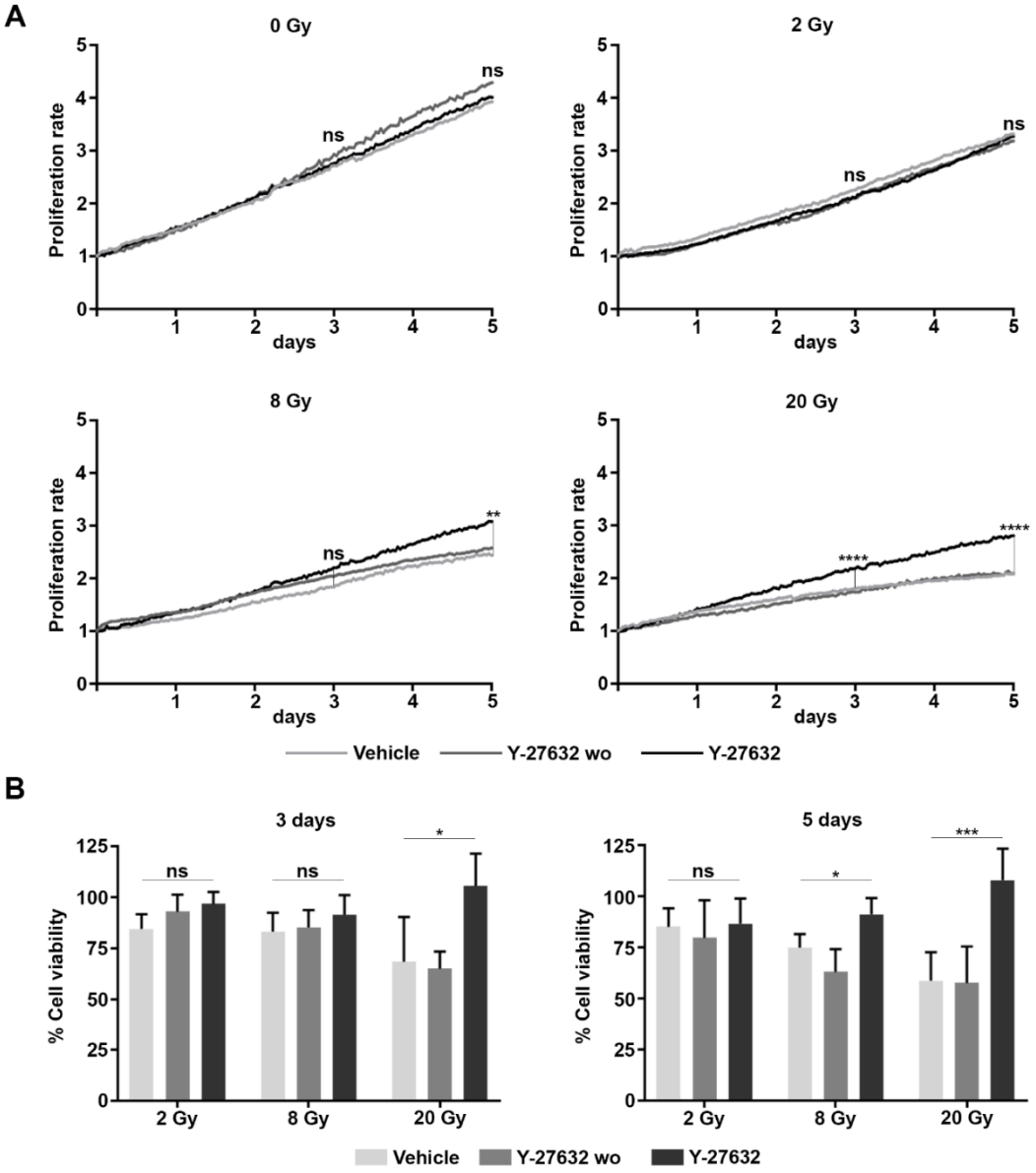

Figure 3.21 Chemical ROCK inhibition leads to a survival advantage after radiation. BTSCs treated with vehicle control, Y-27632 (20μM) and Y-27632 washout (8-hour compound washout) were subjected to 2, 8 and 20 Gy radiation doses. **A**- Proliferation rates for BTSCs were measured using the IncuCyte software for 5 days after irradiation. (Biological triplicates; ns, non-significant; *, $p<0.05$; **, $p<0.01$; ***, $p<0.001$; ****, $p<0.0001$, Two-way ANOVA). **B**- Three and five days after radiation cell viability was assessed using CellTiter-Glo®. Values shown in each condition are normalized to the respective 0 Gy control. (Biological triplicates; mean ± SD; ns, non-significant; *, $p<0.05$; **, $p<0.001$, Two-way ANOVA)

Next, to test the effect these conditions had on cellular viability, I used the luminescence-based cell viability assays, CellTiter-Glo®. The BTSCs were subjected to the same conditions as outlined above and cellular viability was measured 3 and 5 days after radiation. Results from day 3, as seen in Figure 3.21B, shows a tendency for Y-27632 treated cells to have higher viability. For the 20 Gy radiation dose there is a significant difference in Y-27632 cellular viability when compared to its control counterparts. This viability difference between Y-27632 treated and control BTSCs further increases 5 days after radiation treatment, where it is possible to see a significant difference ($p<0.05$) at 8 Gy and a highly significant difference at 20 Gy ($p<0.001$). In summary, these results show that the induction of a neurite-like network in BTSCs via chemical ROCK inhibition promoted survival of BTSCs upon radiation treatment.

Radiation has a multitude of induced effects on cells one of them being disruption of mitochondrial function. Previous results showed that mitochondria were being transported along the Y-27632 neurite-like protrusions leading to the hypothesis that this transfer of mitochondria via neurite-like protrusions could be compensating for the radiation damage. To assess this, I measured the oxygen consumption rate (OCR) to assay mitochondrial respiration in live cells. The consequence of 20 Gy radiation on mitochondrial function was determined by measurement of OCR rates in GBM1 BTSCs following treatment with Y-27632 or vehicle control five days post radiation treatment. Figure 3.22A shows that in control conditions (0 Gy) the addition of Y-27632 to the BTSCs did not alter the oxygen consumption rate when compared to control cells. However, five days post 20 Gy radiation treatment, OCR measurement shows that Y-27632 treated cells not only have a higher basal level of oxygen consumption but also have a higher maximum oxygen consumption. These results suggest that Y-27632 treated cells cope better with oxidative stress then the control counterparts.

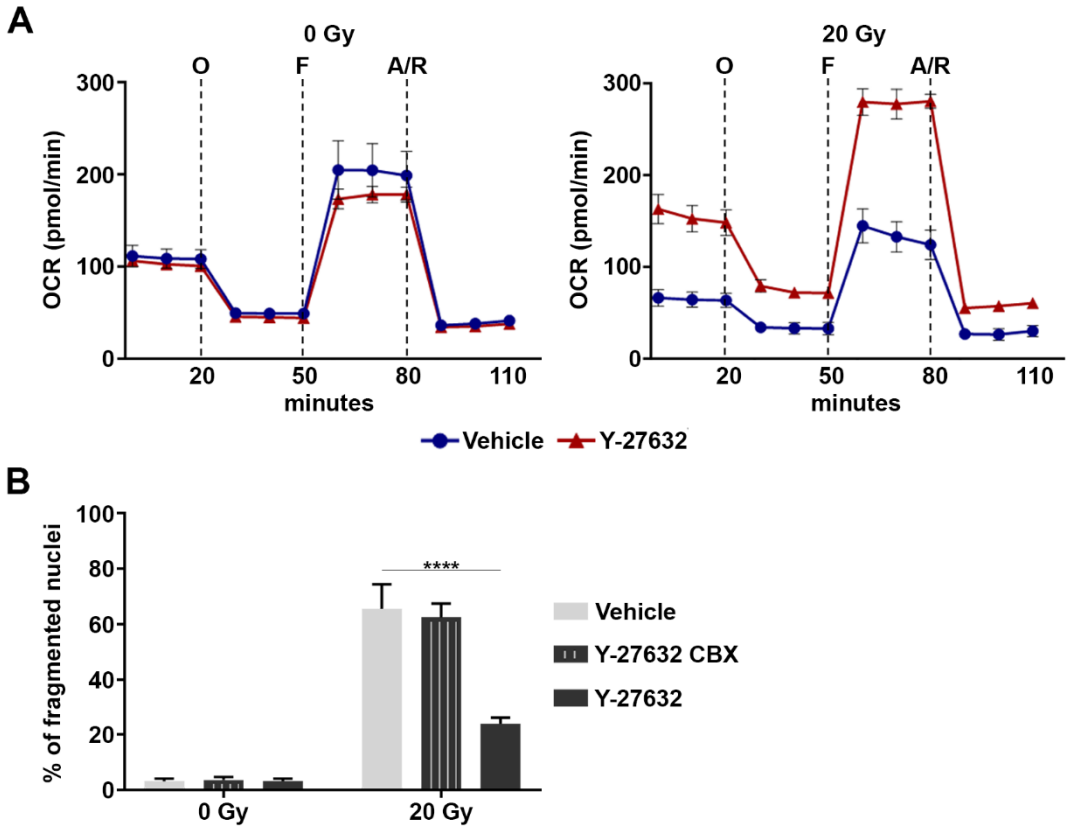

Figure 3.22 Survival advantage observed in Y-27632 connected cells is linked to metabolic activity and gap junctional communication. A- Mitochondrial bioenergetic (extracellular) analysis of GBM1 cells 5 days after 20 Gy radiation. (OCR: oxygen consumption rate; O: Oligomycin; F: FCCP; A/R: Antimycin/Rotenone). B- BTSCs treated with carbenoxolone (CBX) prior to 20 Gy radiation treatment. 5 days after irradiation nuclei fragmentation was assessed. Y-27632 CBX treated cells present the equal amount of fragmented nuclei as control cells.

Finally, in order to investigate what mechanisms were behind the survival advantage I treated the cells with gap junctional inhibitor, carbenoxolone (CBX), before radiation therapy. Cells were treated with Y-27632 or vehicle for 24 hours, and 30 minutes before radiotherapy the cells were additionally treated with carbenoxolone, which is a potent and effective gap junction blocker. Lack of nuclei fragmentation in 0 Gy condition demonstrates that carbenoxolone itself does not have a cytotoxic effect (Figure 3.22B). However, Y-27632 treated cells following the addition of carboxolene and subsequent 20 Gy radiation presented with the same amount of nuclei fragmentation when compared to the control cells (Figure 3.2B). Y-27632 treated cells

that were not additionally treated with carbenoxolone presented with significant reduction of nuclei fragmentation (in agreement with previous data). These results further confirm that this survival advantage in the face of radiation damage is related to the neurite-like network and is not a side effect of Y-27632 inhibition.

3.3. Discussion

GBM infiltration is a major hurdle towards more efficient GBM therapy due to the intricate mechanisms which underlie this process. The complex phenomenon of invasion involves the dynamic reorganization of the actin cytoskeleton, which is mediated by two isoforms of RHO-associated serine/threonine kinases, ROCK 1 and 2. ROCK, which plays a pivotal role in cancer, has been shown to be highly expressed in several tumour tissues, including lung, prostate and gastric cancers and glioma (185). In light of the absence of reliable tumour type-specific data, and coupled with the notion of using ROCK inhibition as a potential anti-cancer treatment strategy, my thesis aimed at providing insight into the effect chemical pan ROCK pathway inhibition had on crucial features for the malignancy of GBM cells – such as changes in morphology, motility and/or differentiation of patient-derived BTSCs.

Experimental design rationale. With the development of pan-ROCK small molecule inhibitors, it has been possible to study the role of the ROCK signalling pathway in cancer. In addition, ROCK loss-of-function mutations and RNAi-mediated ROCK1 and ROCK2 knockdowns have been studied in the cancer (cellular) context (256, 277). In my study, I chose small molecule inhibition over gene knockout/knockdown approaches due to their therapeutic potential (278) and their ability to regulate cell fate decisions (279). Small molecule inhibitors can provide several 'practical' advantages over genetic loss-of-function approaches. For example, the rapid diffusion of the small molecule inhibitors into the cells leads to protein

inhibition in a precise timely manner; whilst with RNAi, experiments have to be deferred until stable protein inhibition is achieved. They can also provide novel insight into biological processes, in particular when their mechanisms-of-action diverge from gene/protein knockdown-like loss-of-function kinetics (280). While RNAi and CRISPR techniques lead to the loss of important protein-protein interactions by slowly decreasing the amount of existing protein in the cells, small molecule inhibitors can rapidly inhibit the biological function of the protein, thus allowing the protein to act as a scaffold for other biological protein-protein interactions (280, 281).

The aptitude of small molecules to target enzymatic activity without targeting protein structure makes them powerful tools for the study of ROCK kinase function. In addition, the inhibition of proteins that possess a well-defined substrate – i.e. proteases, kinases (such as ROCK) and G protein-coupled receptors – have been successfully achieved by pharmacological approaches (280). Most importantly, the potential usage of chemical inhibitors in the clinic to target ROCK highlights the needs for studies that elucidate the mechanism through which the small molecule inhibitors affect cancer, ultimately leading to an approach that is translatable into clinical practice. It is known that Y-27632, H1152 and GSK 269962 inhibit ROCK 1 and 2 by competing with ATP for the kinase binding site. From all available pan-ROCK inhibitors, Y-27632 is the most established and widely-studied one, and I therefore used this compound to investigate the effect pan-ROCK inhibition had on morphology, differentiation, and migration of BTSCs.

Morphological effect in BTSCs. Studies addressing the effect of ROCK pathway inhibitors in glioma have focused on the use of human GBM cell lines. These cells have been shown to be genetically and biologically different from patient tumours, raising the question of clinical relevance and translational potential of these study results (119). The in vitro expansion of patient-derived BTSCs has been successfully used in phenotypic and genetic screening of chemical compounds and has proven to be a disease-relevant experimental model (125, 126, 258). The ability of long-term culturing

BTSCs as an adherent monolayer provides a suitable basis for the study of morphological changes caused by ROCK inhibition(126).

In the GBM1 BTSCs, Y-27632 led to morphological changes and the appearance of multiple long thin processes, which resembled the outgrowth of neurite-like projections. Positive immunofluorescence staining of these processes for neuronal microtubule proteins, β-tubulin III and microtubule-associated protein 2, enabled the quantification of the measurement of the overall neurite-like outgrowth per GBM cell (282). Moreover, the immunofluorescence results suggested cytoskeletal involvement and were consistent with data reported from distinct cell types, which showed that the chemical inhibition of Y-27632 leads to morphological changes (192, 283, 284). These morphological changes were further corroborated by the results obtained from the differential gene expression analysis of Y-27632 treated cells compared with vehicle cells. Despite, the low fold change (<2), there was a slight increase in the expression of genes related to microtubule dynamics and stabilization such as microtubule-associated protein 1B (MAP1B, (285, 286)) and microtubule-actin crosslinking factor 1 (MACF1, (287). Additionally, there was also an increase in the expression of allograft inflammatory factor 1-like (AIF1L), which is a gene involved in actomyosin contractility (288, 289). Studies have shown that this morphology alteration is a result of the abrogation of cells' actin stress fibres and of microtubule stabilization resulting from the polymerization of microtubules (192, 283, 284).

Exposure of GBM1 BTSCs to low concentrations (0.2 μM and 2 μM) of the inhibitor was sufficient to increase the neurite-like outgrowths by ~2-fold. The maximum increase was observed for the concentrations of 20 μM and 100 μM (resulting in a ~4-fold increase). However, concentrations over 20 μM did not produce a significant increase in protrusions length. The projection-like phenotype increased with longer exposure to the compound, reaching a plateau at 24 hours. This time dependent increase in neurite-like outgrowth can be explained by the mechanism of cellular uptake of Y-26532. Studies have shown that Y-27632 does not freely permeate

the cellular membrane, but possibly relies on carrier-dependent diffusion; thus, neurite-like outgrowths gradually increase with the uptake of Y-27632, until reaching a plateau when the carrier is saturated (283, 290). These results identified the Y-27632 treatment of 20 μM for 24 hours as well suited to robustly study the effect of chemical ROCK inhibition in undifferentiated GBM BTSCs.

Given the importance of molecular and phenotypic heterogeneity in GBM tumours, I next used a panel of distinct patient-derived BTSCs lines to investigate the Y-27632 effect on the morphology of distinct GBM subtypes (258). The GBM1 BTSC line shared features with the classical/proneural subtype; the GBM13 BTSC line belonged to the proneural subtype; and the GBM20 BTSC line shared features with the proneural/mesenchymal subtypes (74). In these distinct BTSC lines, treatment with the chemical ROCK inhibitor resulted in similar neurite-outgrowth phenotype throughout the panel of BTSCs, demonstrating that this morphological alteration is independent of subtype.

It has been shown that Y-27632 has the ability to inhibit other kinases – e.g. citron kinase, protein kinase N and protein kinase C – albeit with a much lower inhibitor constant (K_i value); Y-27632 affinity for ROCK kinase is 10 times higher than other kinases (283, 290). In order to clarify the link between the outgrowth phenotype and the ROCK signalling pathway, thus excluding off-target effects, different ROCK inhibitors and ROCK downstream effector inhibitors were used on GBM1 BTSCs. The activation of ROCK triggers two pathway arms (249, 291). On the one hand, ROCK phosphorylates the myosin binding subunit of myosin light chain (MLC) phosphatase, which ultimately results in the increase of myosin II activity (291). As a result of this increase, so is the contractility of actomyosin and stress fibres are formed (291). On the other hand, ROCK is also able to activate LIM-kinase through phosphorylation (249). Active LIM-kinase then phosphorylates cofilin, leading to the inhibition of its actin-depolymerizing activity (249). In my study, the use of distinct ROCK inhibitors, H1152 (256) and GSK 269962 (292), as well as an inhibitor of the downstream effector

protein non-muscle myosin II, Blebbistatin (261) resulted in the same neurite-outgrowth phenotype observed for Y-27632. However, with the addition of a LIM kinase inhibitor (261) the neurite-like outgrowths were absent. These observations suggest that the part ROCK pathways inhibition plays in the appearance of neurite-like outgrowths is mediated through its role in actomyosin contractility (as a result of the regulation of non-muscle myosin II).

Potential differentiation effect in BTSCs. Several studies have reported that ROCK pathway inhibition with Y-27632 can lead to differentiation of mouse embryonic stem cells into motor and sensory neurons (192, 293); of bone marrow stem cells into neurons and glial cells (mainly astrocytes) (294); and of mesenchymal stem cells into neurons (295). These studies raised the question of whether the outgrowth phenotype observed in undifferentiated GBM cells upon ROCK inhibition could be associated with cellular differentiation. Forced differentiation of BTSCs could constitute a promising therapeutic approach which prevents tumour progression and recurrence (115-118), thus providing a strong rationale for investigating whether the ROCK inhibition-induced BTSCs neurite-like outgrowth was associated with neuronal differentiation. Indeed, the observation of TuJ1 positive outgrowths raised the possibility of a Y-27632 differentiation effect GBM BTSCs. The analysis of the GBM1 BTSCs gene expression demonstrated that treatment with 20 μM of Y-27632 did not elevate the expression of proneural/neural differentiation factors such as NEURO D1 (262) or NTRK2(263), which have been previously implicated in differentiation. In addition, removal of Y-27632 from the media resulted in the retraction of neurite-like projections independently of the 3 or 5 days incubation time with the inhibitor. Moreover, neurite-like processes, induced over a 5-day treatment with H1152 and GSK 269962, were also reversible following the removal of the compound. These results suggest that the chemical ROCK inhibition is associated with cytoskeletal reorganization rather than cellular differentiation, also suggesting that

positive TuJ1 staining alone is not sufficient to characterize BTSC differentiation (293, 294).

Despite the absence of expression of proneural/neural differentiation factors, further analysis of the microarray data showed an increase in gene expression of GFAP in Y-27632 treated cell (fold change of 1.53). This slight increase suggests the potential shift in lineage commitment of the BTSCs into an astrocytic lineage. Furthermore, it has been reported that the addition of BMP-4 to BTSCs has shown to elicit the differentiation of BTSCs, with the cells being biased toward the acquisition of an astroglial fate (118). Interestingly, Maldonado et al. (265) recently showed that the addition of Y-27632 to human induced pluripotent stem cells could selectively influence the differentiation of these cells in a lineage-specific fashion due to EMT modulation. This finding is consistent with reports that EMT events plays an important role in human embryonic stem cell differentiation (296) and that these events occur due to ROCK mediated cytoskeleton reorganization (297). In my study, simultaneous addition of Y-27632 and BMP-4 resulted in ~2-fold increase of TuJ1 positive outgrowths and in a ~2.5-fold increase of GFAP positive outgrowths when compared to Y-27632 treated GBM1 BTSCs. These observations contrast sharply with the effects of adding Y-27632 to BMP-4 differentiated BTSCs, which did not increase the GFAP and TuJ1 positive outgrowth when compared to Y-27632 treatment. The different response to washout was also striking. In the Y-27632 treatment condition, washout led to the reversion of the phenotype, as expected; however, in the condition of simultaneous addition of Y-27632 and BMP-4, washout led only to a moderate fading of the phenotype. These results suggest that the neurite-outgrowth phenotype is associated with undifferentiated cells; the addition of the compound to previously differentiated cells did not significantly increase neurite-like outgrowth but simultaneous addition to undifferentiated cells did. Even though further studies are needed to confirm these results, there is an indication that the simultaneous addition of Y-27632 and BMP-4 to BTSCs produces a neurite-like outgrowth phenotype that is

more resistant to washout when compared to Y-27632 washout of cells alone; and that there might be a shift in phenotype from astrocytes to neurons, due to the high number of cells containing TuJ1 positive outgrowths.

Effect of BTSCs on stem-like features/migration. With regards to the *in vitro* effect that ROCK pathway inhibition has on cellular proliferation and migration, a plethora of conflicting results have been published in recent years. Zohrabian et al.(211) reported that the use of Y-27632 in the human malignant glioblastoma cell line LN-18 led to the suppression of cell migration and the reduction of cell proliferation. Tilson et al. (216) argued that the chemical inhibition actually increased proliferation of BTSCs, and Salhia et al. (187) showed that Y-27632 increased the migration and invasion of astrocytoma cells by 2-fold. In other cell types, there is a similar apparent dissonance , with Routhier et al. (214) showing that Y-27632 blocks tumour melanoma growth, although Watanabe et al. (215) described an increase in the survival of human embryonic stem cells upon Y-27632 treatment.

Results obtained from differential gene expression analysis of Y-27632 compared to vehicle-treated cells demonstrated a decrease (albeit with fold changes >-2) in expression of genes related to the regulation of mitosis and spindle formation such as NDC80 kinetochore complex component (NUF2,(298)), NIMA-related kinase 2 (NEK2, (299)), Cyclin dependent kinase 1 (CDK1, (300, 301)) and Polo kinase like 3 (PLK3, (302)). This finding suggests that the addition of Y-27632 to BTSCs might affect the cell's capacity to proliferate. Hence, in this study, the effect of Y-27632 on BTSCs proliferation and self-renewal capacity was further investigated using the following assays: clonal growth; KI67 staining and live cell imaging. Chemical ROCK inhibition did not alter the ability of the cells to self-renew, as indicated by the clonal growth experiment. Moreover, the proliferation capacity of the cells remained unchanged, as depicted by KI67 staining and proliferation rates obtained from live cell imaging. Considering the link between reduced proliferation and BTSCs differentiation that has

been described for BTSCs (303, 304), these results further corroborate the finding that Y-27632 is not inducing differentiation in BTSCs.

With regards to motility, reports which focus on cellular migration following the inhibition of ROCK with Y-27632 traditionally use radial monolayer migration assays, as described in Zohrabian et al. (211) and Routhier et al. (214). These analyse the ability of cells to move outside of an initial circle in which they were plated. Unfortunately, these studies neglect (potential) movement occurring within the confines of the circle. It is also difficult to differentiate migration from proliferation in these assays, so the analysis of such results is far from clear cut and can lead to misinterpretations. Interestingly, in my study, when random motility was analysed in BTSCs cells (low confluency), using ImageJ to track each individual cell, migration was not altered in Y-27632 treated cells when compared to the vehicle control cells.

Nevertheless, these results once again cast doubt regarding the implementation of ROCK pathway inhibitors in a clinical setting and further demonstrate that a better understanding of the multifaceted and complex roles employed by this signalling pathway are needed before treating this inhibitor as an anti-cancer agent.

Multicellular network in BTSCs. Studies have described that changes in morphology seen upon ROCK pathway inhibition in undifferentiated GBM are also consistent with the notion that ROCK inhibition can contribute to axonal elongation and regeneration (305-307). As the main function of axons is to transmit information to other cells, i.e. neurons, muscles and glands, it is plausible that BTSCs can also use these projections to communicate. The notion of intercellular communication is far from a new concept, with communication amongst cells being essential for the normal functioning of any organism (308-310). Furthermore, in recent years, thin membranous tubes (termed either tunnelling nanotubes or membrane nanotubes, MNs) that enable intercellular communications have been described for immune cells (269), human prostate cancer cells (270), endothelial progenitor cells (271), and astrocytes(272). In fact, it has been recently discovered that GBM cells are also able to

use these tubular cytoplasmic extensions (termed tumour microtubes, TMs) as a communication structure thus forming a functional network (266). It therefore comes as no surprise that these tubular extensions have been proposed to represent a new mode of cell-to-cell communication. These recent discoveries have raised the question of whether the cellular projections induced by Y-27632 allow BTSCs to establish a transient network of neurite-like protrusions that increase cell to cell communication. Hence, this next section will address the potential functional links between ROCK inhibition induced neurite outgrowths and their involvement in network formation.

Live cell imaging of the BTSCs treated with Y-27632 uncovered an unexpected cellular behaviour. BTSCs treated with the inhibitor and seeded at low density showed no alteration in cell motility when compared to the vehicle cells. On the other hand, BTSCs seeded at a higher density and similarly treated with Y-27632 showed a substantial reduction in motility. The cells exhibited the expected Y-27632 induced phenotype, with prominent neurite-like outgrowths, at both densities. The key difference was that, in the former case, the cells were too sparse and the processes were unable to overlap/connect. In the latter, however, the projections would actively search for/interact with other cells/projections while the cells bodies would remain steady, which is a similar phenotype seen in neuronal growth clones during development (311). Further investigation into these potential connections resulted in the creation of blueprints based on the tracing of the Y-27632 induced neurite-like projections in immunofluorescence images. Those schematic representations revealed that the cell processes overlapped in a manner that suggested the existence of an underlying network. The overall layout resembled a complex network of communication in which a BTSC could interact both with its direct neighbours and with distant cells within the multicellular BTSC network.

Interestingly, Potter et al. (312) demonstrated that cells which are in a multicellular network have an improved perception of sensorial stimuli and respond more efficiently to stimuli when compared to cells which are in close proximity to each

other. The study argued that even though long-range communication resulted in receiving weaker communication signals, this communication led to a significant improvement on the awareness of stimuli of the surroundings (312). My results suggest that this cellular behaviour could also be occurring in the GBM1 BTSCs, with cells using their neurite-like protrusions (induced by the ROCK pathway inhibition) to search for other neurite-like projections and establish a connection. In addition, these results are consistent with studies that report that increased gap junctional communication is correlated with decreased *in vitro* motility in glioma cells (313, 314). Specifically, a study by McDonough et al. (313) demonstrated that glioma cells that communicate have a reduced migration rate when they are cultured as multicellular spheroids, suggesting that there is a direct inverse relationship between the number of cells in gap junctional communication and the motility rate of those cells. This observation suggested a link between communication and reduction in motility which led to the examination of possible mechanisms of communication between cells in greater detail.

Intercellular calcium waves have already been shown to be responsible for the coordination of the activity of individual cells in a multicellular network (315) – a feature present in neurons and astrocytes in the normal brain (316, 317). In this study, long-range calcium waves were propagated along the Y-27632-induced projections following damage caused by a fatal laser dose, demonstrating that the BTSCs are able to relay information amongst each other using these induced projections. Through the previously described nanotubes, intercellular communication can be mediated by chemical synapses or by gap junctions, with the latter being key for calcium wave propagation. Gap junctions are membrane channels formed by connexions (Cx) which allow the passage of small molecules between cells (318). It has been shown by Charles et al. (319) that, following mechanical stimuli, glioma cells transmitted a calcium wave using gap junctions. In this study, the functional connection of BTSCs connected via the induced projections was verified by the transfer of the gap junction permeable dye

lucifer yellow along the projections to other connected cells; the results suggest that the calcium wave in the Y-27632 treated BTSCs is being transmitted via gap junctions (320).

However, reports by Charles et al. (319) and more recently Osswald et al. (266), showed that communication via gap junctions in glioma cells is dependent on the expression of connexin 43, (Cx43) which is not present in these Y-27632 treated BTSCs. However, there are contradictory reports regarding the subpopulations in which Cx43 plays a major role in gap junction communication (321). Some authors report that Cx43 exists mainly in the differentiated subpopulation of the brain tumour cells and is absent from the stem cell subpopulation (322); others contend that Cx43 expression is only found in astrocytes and is reduced in astrocytomas (323), and others yet defending that the expression of Cx43 decreases with the increase of malignancy (324). A large variety of Cx molecules are expressed in the central nervous system, with Cx26 and Cx43 being the predominant molecules expressed in neural progenitor cells (325, 326), while Cx30, Cx43, and Cx46 dominate in astrocytes (327). In addition, there is also studies stating that Cx46 is the major player in gap junction communication in BTSCs (322, 328). Therefore, it is feasible that Cx 43 does not play an important role in gap junction communication for the BTSCs in my study and that another Cx is mediating the gap junction communication in these cells. My results based on Lucifer yellow transfer show that gap junctions play an important role in intercellular communication between BTSCS. However, further studies are needed to pinpoint which Cx is the key player in this mechanism.

Furthermore, it has been proposed that these communicating systems might also enable the direct transport of not only molecules, but also of sub cellular organelles (269, 271, 329). In my study, the tracking of mitochondria and lysosomes with MitoTracker and Lyostracker demonstrated that lysosomes and mitochondria are present along the neurite-like protrusions (it is possible to visualize in more detail, in the live cell imaging, that the lysosomes and mitochondria are being transported along

these projections). Even though the movement of mitochondria in the Y-27632 induced neurites is not sufficient to absolutely guarantee the exchange of mitochondria from one cell to another, it does suggest that there is local ATP production and vesicle trafficking in these projections. Therefore, further studies are needed to characterize this behaviour in more detail. For example, visualization of membrane material exchange could be achieved by methods described in Vidulescu et al. (270), which would provide more insight into the exchange of organelles in the Y-27632 induced neurite-like projections.

Although these Y-27632 induced neurite-like networks share characteristics with the previously described MNs and TMs (266, 269-271, 308-310), differences do exist. Similarly to MNs and TMs, the Y-27632 induced neurite-like projections are able to propagate intercellular calcium waves; enable transport of mitochondria and other vesicles along the projections and communicate with other cells via gap junctional communication. In addition, MNs and TMs can be formed *de novo* – a process in which a protrusion explores the surroundings to establish a connection with a protrusion from another cell – yet, the majority of these membrane tubes result from cell division, in which the daughter cells maintain a long-distance contact with the parent cell. This latter feature was rarely observed in my study. The Y-27632 induced neurite-like protrusions mainly resulted from *de novo* connections. In addition, an important feature which exists in MNs but is completely absent in the Y-7632 induced neurite-like projections is that MNs are exclusively extended above the substrate (plasticware) and not attached to it, which is observed in the Y-27632 neurite-like processes. Regarding the life time of these tubules, TMs are long-lived and can be observed for up to 200 days after establishing connections. Additionally, in the Y-27632 neurite-like projections, the gap junctional communication is not mediated by Cx43.

However, similarly to the MNs, the Y-27632 induced neurite-like projections are more short-lived, lasting up to 60 mins. As previously mentioned, all projections

observed following pan ROCK inhibition were positive for β-Tubulin III and MAP-2. Whilst the presence of MAP-2 was observed in TMs and only in a subset of MNs, the presence of β-Tubulin III was not seen either in MNs or TMs. Moreover, TMs were GFAP positive, demonstrating that the cells had differentiated into an astrocytic lineage (266, 269).

Given the unique features (when compared to MNs and TMs) of the microtubes resulting from the Y-27632 induced neurite-like projections and the networks formed by them, I propose that they may be classified as a distinct form of microtubes and be termed neurite-like microtubes NLMs. However, given that TMs are observed in an *in vivo* environment and NLMs have been observed *in vitro*, one could argue that the features which are not shared between TMs and NLMs could be a result from the growth of TMs in a 3D environment and that culturing of NLMs *in vivo* could provide these microtubes with the stimuli to develop a similar phenotype to the TMs. Osswald et al. (266) acknowledge that, despite the stem-like conditions of their *in vitro* culture, they were unable to detect TMs in *in vitro* conditions and these were only observed *in vivo*. This fact, coupled with the knowledge that the Rho family GTPases is one of the many canonical pathways involved in neurite outgrowth and neurite-like protrusions, suggest that this study has potentially uncovered one of the core/crucial processes involved in creating a multicellular communicating network both *in vitro* and *in vivo*.

Treatment resistance in BTSCs linked to networks. Previous studies have linked the existence of tumour microtube networks in glioma to treatment resistance (266, 330). However, these studies focused on microtubes that were developed in vivo following implantation into a mouse brain. This resistance to therapeutic treatment has not been demonstrated in in vitro 2D models. Additionally, the positive staining for GFAP in the TMs indicates that even though BTSCs were implanted into the mouse brain, the network consisted of BTSCs that had differentiated into astrocytes (266). In my study the BTSCs maintained their stem-like features following Y-27632 treatment; therefore, the investigation of potential resistance to therapy provided by the

multicellular BTSC network is novel. Thus, given the importance of BTSCs for tumour progression and treatment resistance and the desirability of 2D models (insofar as they can provide preliminary information regarding drug screening in a fast, reliable and controlled manner (331)), I tested the ability of the Y-27632 induced NLM network to enable treatment resistance.

The standard care for GBM patients involves surgical removal of the tumour followed by adjuvant radiotherapy and chemotherapy. The standard dose of radiation received by GBM patients is 60 Gy, which is delivered in fractions of 1.8-2 Gy over ~8 months. This regime is very difficult to mimic in vitro because of the increase in variability caused by the fractionation of the radiation dose, which could lead to the misinterpretation of results. Therefore, in this study three different radiation doses were used in order to cover a wide range of radiation effects, ranging from a low radiation dose of 2 Gy, to an intermediate radiation dose of 8 Gy, and a high radiation dose of 20 Gy.

Both Y-27632 treated and control cells suffered the same amount of double stranded DNA breaks following radiation therapy, as demonstrated by the γH2Ax staining. However, my study shows that Y-27632 induced NLMs coped better with the cytotoxic effects of radiation therapy. In control cells, there was a steady increase of nuclear fragmentation over time. This phenotype was most evident five days after radiation in control cells, with over 80% presenting nuclear fragmentation, and was in stark contrast to Y-27632 induced NLM-connected cells, where the proportion of cells presenting such damage was seven times lower. The nuclear fragmentation pattern of the control cells was reminiscent of DNA micronucleation/multinucleation, which is a feature of mitotic catastrophe (332). Mitotic catastrophe – a mechanism of delayed mitotic-linked death caused by chemical or physical stress – has been described as the main form of cell death induced by radiation (333-335). It is well recognized that aberrant mitosis is linked to chromosomal breaks and improper chromosome segregation and that this will ultimately lead to micro/multinucleation. This is

consistent with the results observed in my study, in which control cells were unable to progress in the cell cycle following 20 Gy radiation, with the majority of the cells either dying or suffering from cell cycle arrest. Therefore, there is a good argument that control cells are going through mitotic catastrophe and that this will ultimately result in cell death.

In addition to the presence of multinucleation, morphological changes associated with mitotic catastrophe (332, 335) were also seen in live cell imaging and in immunofluorescence images of the control cells. One of the most prominent morphological changes caused by mitotic catastrophe was the formation of giant cells which appeared to be enlarged and flattened when compared to the non-irradiated control cells. Observation of the time lapse movies showed that these giant cells resulted from repeated unsuccessful attempts to divide, which finally caused fusion of the mitotic cells. This behaviour was rarely seen in the Y-27632 treated BTSCs, suggesting that these cells were able to divide successfully, even when exposed to increasing radiation doses. Indeed, a close look at nuclei fragmentation in the Y-27632 treated cells showed that few cells in NLM networks presented multinucleation. The presence of multinucleation was largely observed in cells which were not part of a network, thus suggesting connection to a network provided a protective effect.

The benefits of being part of an NLM network also appear to extend to viability and proliferation. Consistently with results reported by Osswald et al. (266) and Weil et al. (330) regarding TMs, the lower rates of multinucleated cells in the Y-27632 treated BTSCs when compared to vehicle correlate with increased survival. These results are also in agreement with the cell viability assays that show a twofold difference in viability between Y-27632 treated BTSCs and vehicle 5 days after a 20 Gy radiation dose. Proliferation experiments demonstrate that although Y-27632 treated cells suffer a reduction in proliferation when compared to the non-irradiated cells, they continue to proliferate more than control cells, with the difference in the rate of proliferation increasing with the radiation dose and the passage of time. Furthermore, the reduction

in proliferation observed for the Y-27632 induced cells can be (partially) attributed to the multinucleation/cell cycle arrest that was observed in the non-connected BTSC subpopulations.

Even though these results argue in favour of the network offering a survival advantage to the Y-27632 treated cells, there is nevertheless the possibility that the compound can offer (partial or full) protection. Literature regarding the effect of ROCK pathway inhibition following radio and chemotherapy remains ambiguous. While Ader et al (336) demonstrated that inhibition with Y-27632 induces radiosensitization in U87, Street et al. (337) showed that Y-27632 increased the resistance of neuroblastoma cells to cisplatin. In order to test whether the survival effect (seen after radiation) is due to the formation of NLMs networks and not the inhibitor *per se*, I removed Y-27632 by media washout prior to radiation treatment. This resulted in the loss of the neurite-like projections in the BTSCs. Hence, all radiation experiments contained two control conditions. The vehicle control which would demonstrate that the effects observed did not result from the solvent used to dissolve Y-27632 (in this case water). Additionally, a washout condition was also tested, in this condition cells were exposed to the ROCK pathway inhibitor for 24 hours and prior to the radiation Y-27632 was removed and the NLMs were abolished. This second control would thus demonstrate that the effect observed was due to the NLMs and not related to the ROCK inhibitor. Throughout the experiment the washout cells behaved identically to the control cells. These findings strengthen the hypothesis that Y-27632 itself is not promoting a significant protective effect, but it is in fact the network formed by the neurite-like projections (induced by Y-27632) that is granting a survival advantage to the connected BTSCs. Further studies are needed to confirm that this radio protective effect is the sole result of neurite formation and interaction and exclude the possibility of contribution of an unknown target/pathway that the Y-27632 inhibitor might be targeting – perhaps through the use of a compound that modulates neurite formation without the influence of the ROCK pathway.

Indeed, the exact mechanism through which the connected cells are protected from radiotherapy upon chemical network induction is not known. The cytotoxic effect mediated by radiotherapy has been established to involve an increase in intracellular calcium (338); and it has been shown that even small increases in calcium can result in apoptotic death in glioma cells (339). Therefore, I hypothesise that connected cells are able to maintain calcium homeostasis because they are able to distribute the calcium increase among the cells in the network. This sharing of calcium may result in overall non-lethal calcium levels in each individual cell, whilst in the non-connected cells the intracellular calcium levels ultimately trigger cell death. The capacity of cells to exchange calcium was evident in my study, as observed by a calcium 'wave' that was invoked in connected BTSCs following laser damage.

Further, my study demonstrates that inhibition of gap junctional communication, using carbenoxolone, was sufficient to revert the protective effect observed in the NLM-connected cells. Carbenoxolone was added to Y-27632 treated BTSCs before 20 Gy radiation and these cells presented with the same multinucleation seen in the control cells, even though the multicellular network was present. These results provide good indication that gap junctional communication is an important enabler of such a protective effect. While calcium exchange clearly contributes towards resilience, given that other macromolecules besides calcium can be transmitted along the gap junctions, it is also possible that many other molecules could be involved in network survival. For example, amino acids, microRNAs, ATP and even glutathione (a tripeptide with an antioxidant capacity that can directly protect cells from radiation), are molecules known to travel via gap junctions (340, 341) and which could, through direct action or via metabolic cascades, enable such survival. Furthermore, these results strengthen the notion of a protective effect that is based on NLM rather than the Y-27632 inhibitor itself.

Additionally, my study has raised the possibility that exchanges of ATP play a role in survival. The assessment of mitochondrial function 5 days after 20 Gy treatment

showed that NLM connected cells not only had a higher basal respiration level, but they also coped better with oxidative stress. As mentioned in the previous section, the neurite-like projections resulting from the ROCK pathway inhibition were enriched with mitochondria and live cell imaging showed that these organelles were being trafficked along the projections. These observations suggest that mitochondria may be playing a role in the survival advantage seen in the NLM-connected cells, either by being transferred to a neighbouring cell or by producing ATP, which can then be transferred to a neighbouring cell (via gap junctions).

Lastly, given that one of the most striking features of GBM is its inter tumour heterogeneity, this study presents the limitation of only focusing on GBM1 BTSCs and currently lacks the assessment of radioresistance in other patient-derived GBM cell lines. Despite initially demonstrating that several distinct patient-derived GBM cells are able to develop neurite-like projections following Y-27632 treatment, the study of functional network formation and radioresistance was solely performed on GBM1 BTSCs. Thus, further studies with distinct patient-derived GBM cell lines are required in order to confirm that this network-mediated survival capacity is a shared characteristic in GBM.

4. Modelling of cellular migration using cerebral organoids

4.1. Establishing an organoid model to study tumour invasion and growth

At the beginning of my study, there was a gap in knowledge regarding existent 3D models that could potentially be used to study GBM invasion into healthy brain tissue. In the literature, invasion into 3D matrices or organotypic brain slices were available for the study of cellular migration. However, these either lacked the 3D environment that is essential for tumour invasion (brain matrix) or were not appropriate for long term studies (222, 229). Then, in 2013, Lancaster et al. (233) published a ground-breaking paper which showed the development of a cerebral organoid.

Organoid technology has been used to generate *ex vivo* systems for several distinct organs (230-232, 234, 248, 342). This new methodology provides a promising alternative to model brain development and disease progression in a system mimicking *in vivo* conditions (343, 344). The advancement in cerebral organoid technology motivated me to use such an organoid approach to study the cellular and molecular mechanisms of GBM, which have been previously difficult to model *ex vivo*. So, in a pioneering effort, I began to develop a model that would allow the study of GBM progression and invasion using a cerebral organoid.

As is expected with method development, several distinct experimental approaches were tried, with varying degrees of success in producing a reproducible

model, as shown in Figure 4.1. However, the unsuccessful approaches presented should not be viewed as failures, but instead as the building blocks needed for the development of the novel invasion model described in my study.

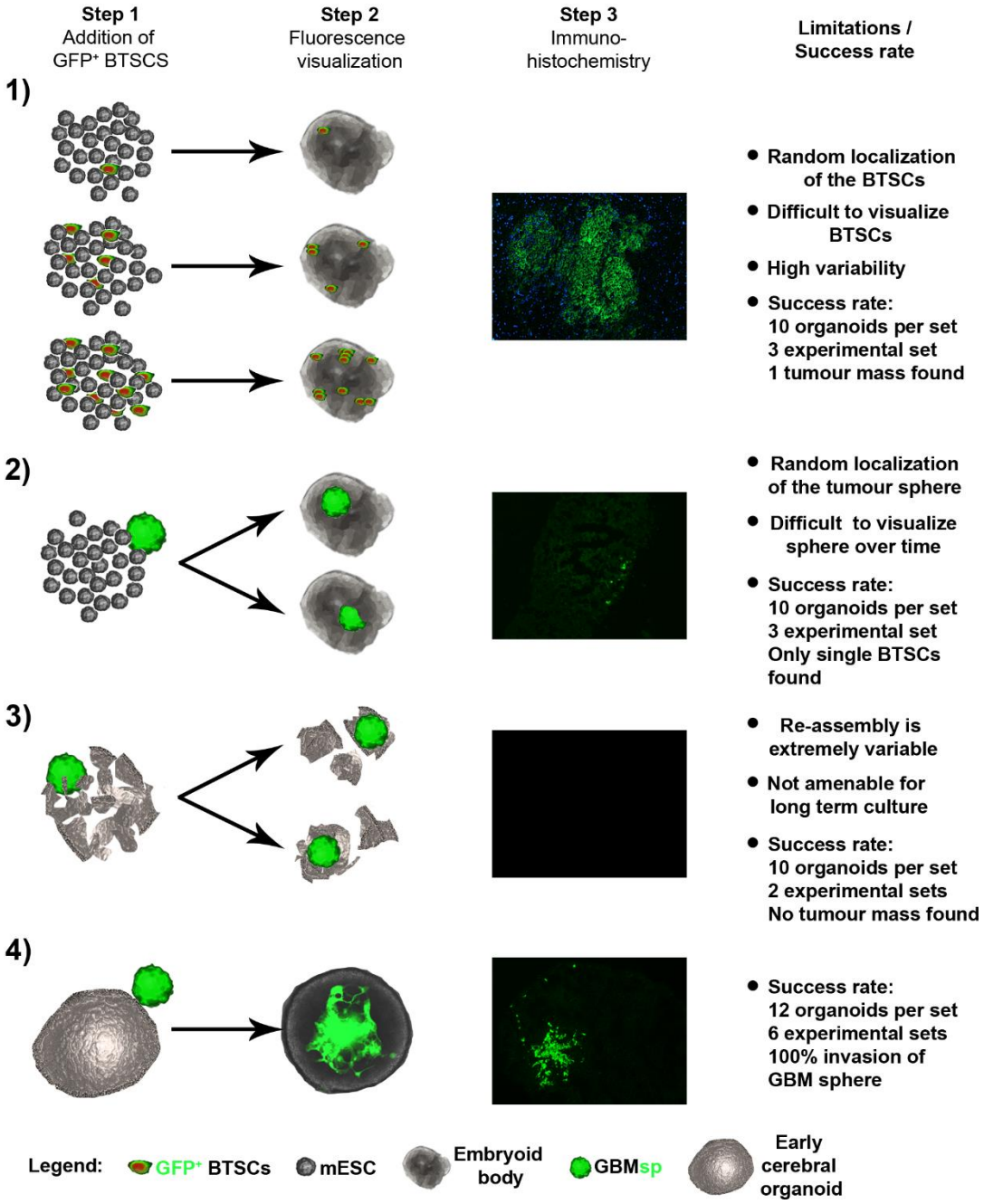

Figure 4.1 Range of experimental approaches used along this study to develop a 3D invasion model.

4.1.1. Experimental approach 1

To assess the suitability of this organoid system to study processes related to GBM progression, i.e. migration and invasion, it was necessary to verify that BTSCs could be incorporated into a cerebral organoid/BTSC hybrid structure without interfering with the growth of the organoid or of the BTSCs. This first approach was modelled on the early organoid work presented by Sato et al. (342), which showed that a single adult intestinal stem cell was sufficient to generate gut organoids; I attempted to develop hybrid tumour organoids through the addition of (different numbers of) single BTSCs to the mESCs necessary to develop the mouse organoid. Therefore, I studied the addition of 0, 5, and 50 individual GFP-BTSCs to the organoid system and, in parallel, the addition of 1 GFP-BTSC. To be able to visualize the BTSCs, these were transduced with GFP lentiviral particles.

Incorporation of 0, 5, 50 GFP-BTSCs. I introduced 0, 5, and 50 GFP-labelled BTSCS to the initial 2,000 mESCs necessary to initiate the organoid development and followed the experimental timeline (adapted from Lancaster et al. (233)) outlined in Figure 4.2A. Images of the organoid growth were obtained on day 4,6 and 9, as shown in Figure 4.2B.

Observation of the organoids on day 4 demonstrated that the GFP-BTSCs cells were incorporated into the organoid. However, the placement of the GFP-BTSCs cells within the organoid was random. In addition, such placement demonstrated that the real-time visualization of these cells could be hindered, given the possibility of GFP-BTSCs being located deep within the organoid (Figure 4. 2B, day 4). Furthermore, images from day 6 show that the addition of BTSCs did not disturb the formation of the ectodermal outer layers; this is suggested by the brightened surface tissue, in contrast to the darker inner non-ectodermal tissues (Figure 4. 2B, day 6). On day 9,

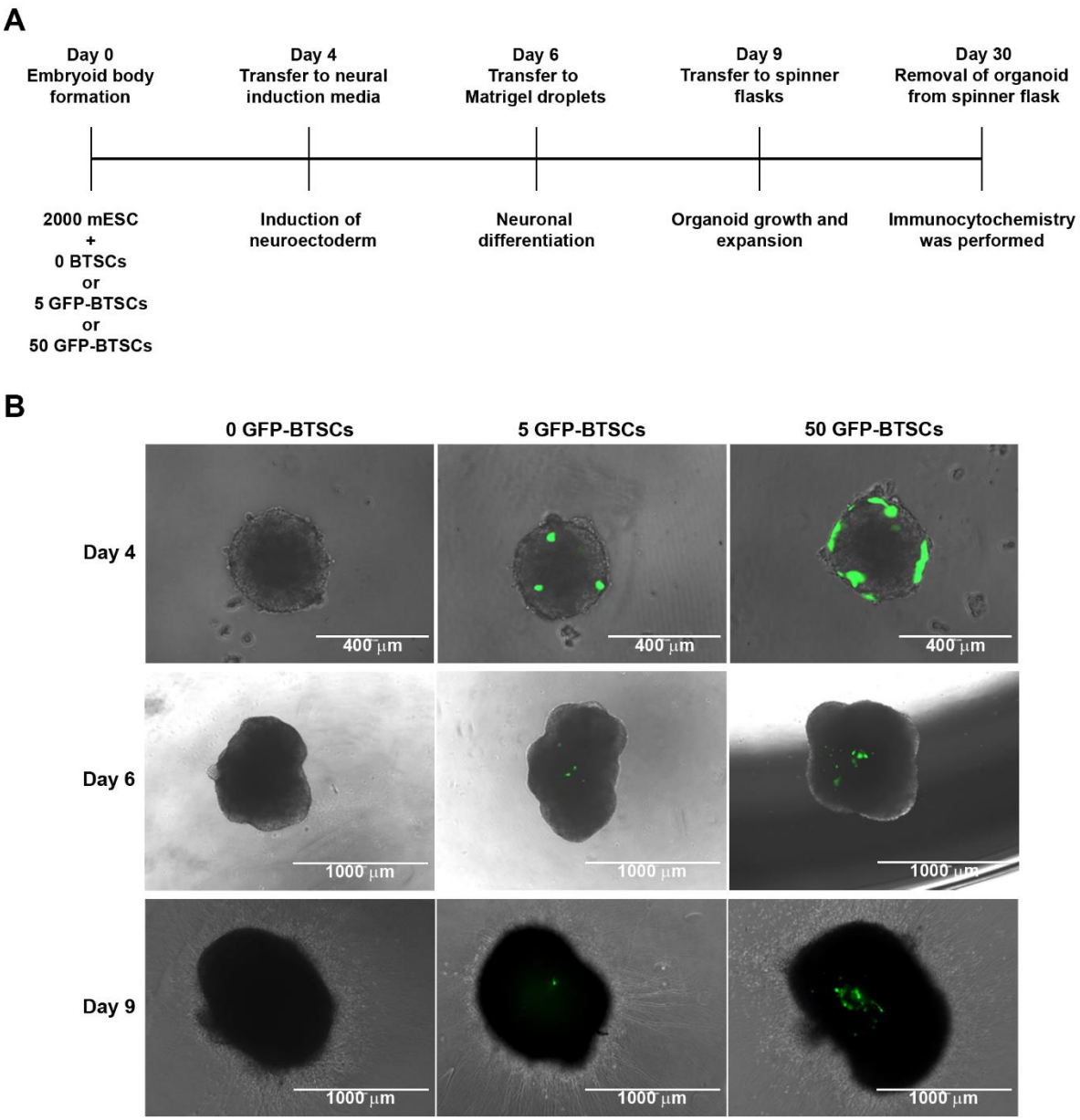

Figure 4.2 Addition of GFP-BTSCs to the developing organoid allows the formation of a tumour-organoid hybrid. **A**- Schematic overview of organoid development with the simultaneous addition of 0, 5 or 50 GFP-BTSCs to 2000 single mESCs during the embryoid body format.

following neuronal differentiation, the BTSC containing organoids did not present any morphologic changes when compared to the non-tumour cell containing organoids (Figure 4. 2B, day 9).

The rate at which the organoid grew made it difficult to provide nutrients to the cells in its core. Thus, after 9 days, they were transferred to a spinner flask (233). In this experimental approach, 30 organoids per condition (0, 5, 50 GFP-BTSCs) were

developed. From all the developed BTSC containing organoids (60 total) a tumour cell mass was visible in only one of these organoids, resulting in a success rate of 1.6%. Characterization of this organoid showed that it stained for SOX2, as shown in Figure 4.3A, which depicts a specific Sox2 positive region in which cells are organized into layers. This is suggestive of cortical identity (higher magnification of the inset on the right)(233). Further staining for human specific VIMENTIN revealed a tumour cell mass in this organoid which initially had the addition of 5 GFP-BTSCs (Figure 4.3B). In summary, this data shows that even though this specific approach lacks reproducibility, it demonstrates that the organoid can withstand the addition of BTSCs without apparent changes to its morphology. Despite the initial promising results, which suggested that this hybrid organoid had the potential to be used to study GBM

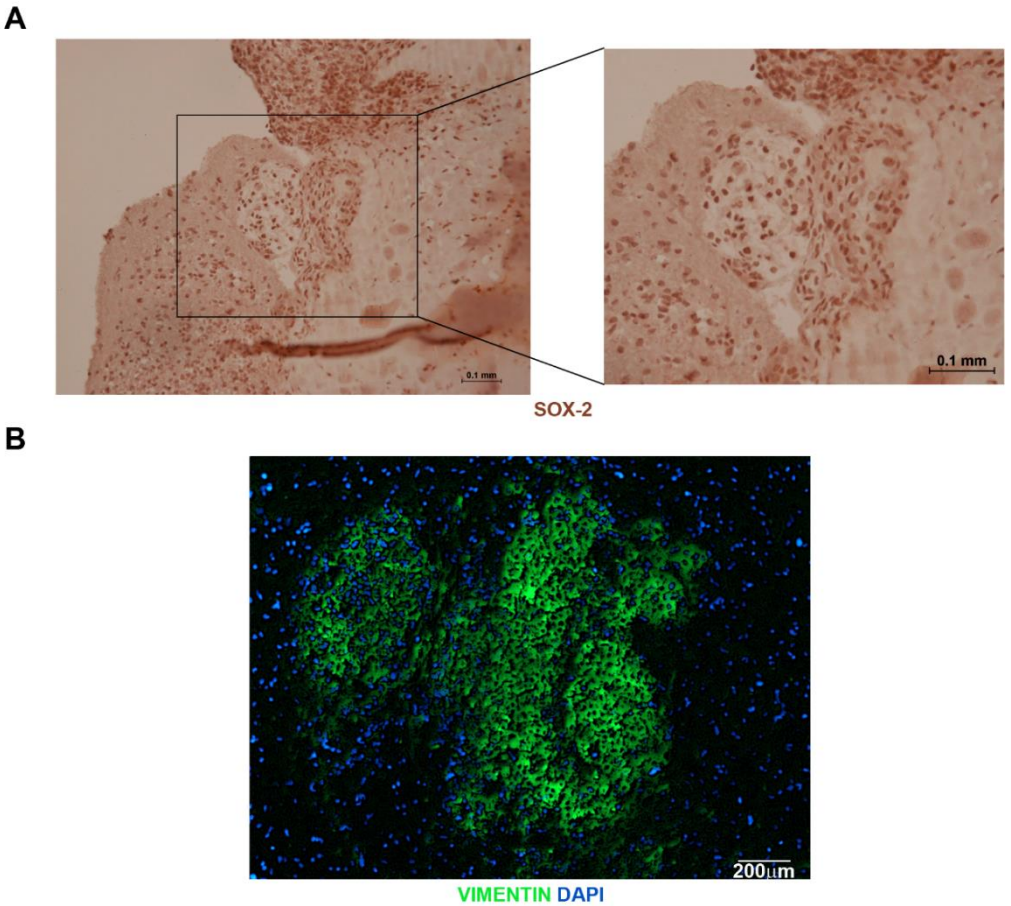

Figure 4.3 Organoid system features Sox-2 positive cells and human BTSCs following 30 days of development and growth. **A**- Left, SOX2 positive staining in organoid denotes the presence of neural stem cells. Right, higher magnification of inset demonstrates organization of these SOX2 positive cells into layers. **B**- Human-specific VIMENTIN staining of BTSCs depicts a tumour mass along a large continuous tissue within the organoid. This tumour originated from 5 BTSCs. Nuclei stained with DAPI.

invasion, the cell mass was only discovered in one hybrid organoid and this experimental approach was abandoned.

Incorporation of 1 GFP-BTSC. Heterogeneity in cancer is generated during tumour evolution; stem-like cells drive tumour growth and give rise to more differentiated cell progenies of neuronal, astroglial and oligodendroglial phenotypes (18). Recent studies have shown that the innate growth dynamics of a homogeneous population of stem cells is sufficient to develop an ample range of clonal growth behaviour (25, 74). The idea of developing a model system that could study this characteristic heterogeneous GBM phenotype, coupled with the single cell work presented by Sato et al. (342) led me to investigate the potential of establishing a model amenable to study GBM self-renewal and progression.

To study this feature, organoids containing a single GFP-BTSCs were formed. To select for a single cell for each organoid, I seeded out single GFP-BTSCs into a 96 well-plate and on the following day, using light-emitting diode (LED) microscopy, the plate was viewed; only wells containing single cells were selected (Figure 4.4A). As shown in the experimental timeline in Figure 4.4A, 2000 mESCs were added to the single cell well and development of the organoid system continued as described. It is noteworthy that the success rate of creating single BTSCs organoids varied. From a full 96 well plate, roughly 49% of the wells contained a single cell which could be used; the rest of the plate either had zero or multiple BTSCs. Following the addition of the mESCs, single BTSC-harbouring embryoid bodies were only formed in 20% of cases. Hence, a full 96 well plate would result in roughly 10 single BTSC embryoid bodies (Figure 4.4A). Once again, given the random placement of the GFP-BTSCs in the organoid, it is possible that organoids containing single cells within its interior were discarded, given that the visualization of the GFP-BTSCs was not possible. The development of a single cell-containing organoid was monitored with microscopy imaging, with images being taken as soon as the embryoid body (EB) was visible. As demonstrated in Figure

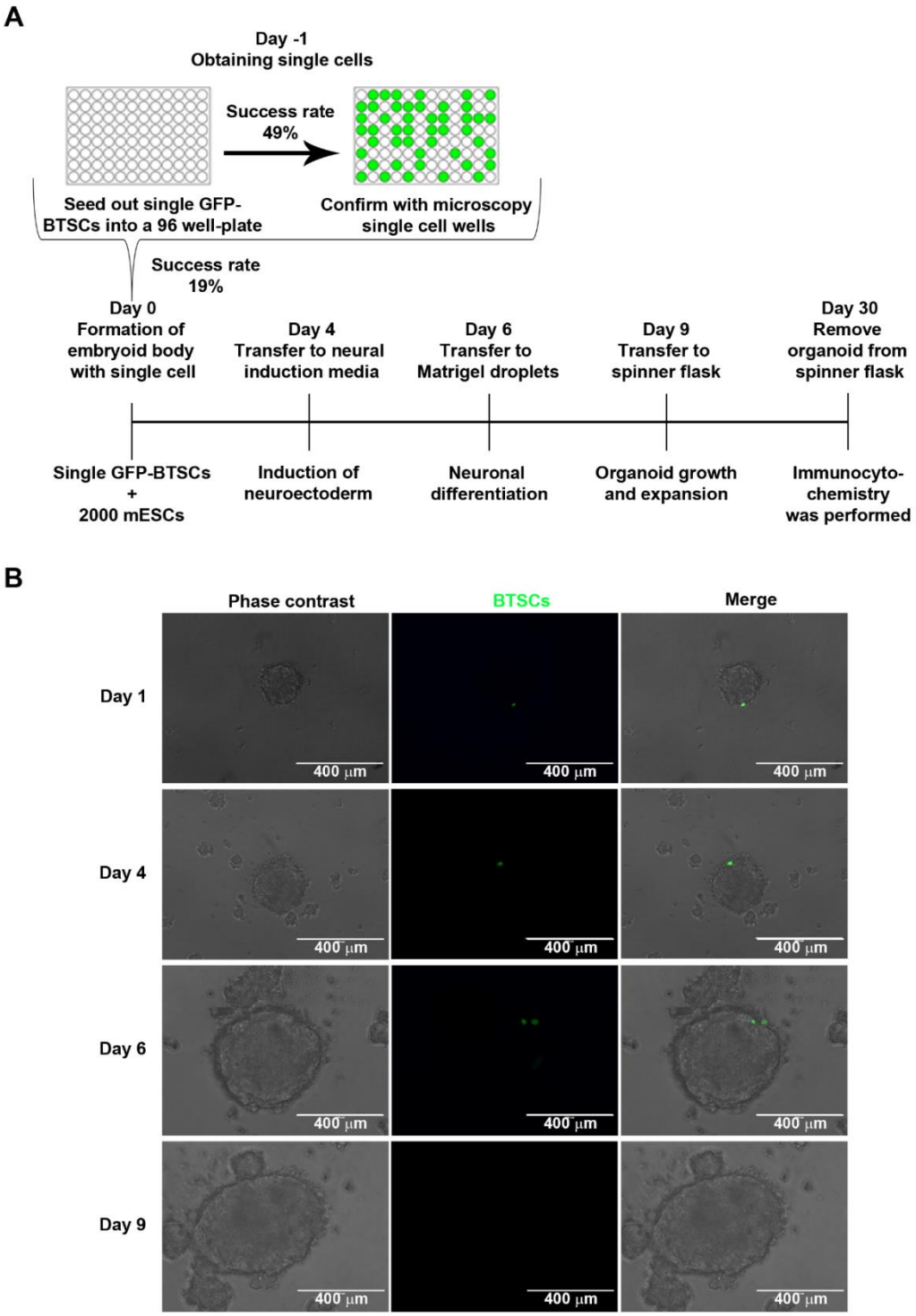

Figure 4.4 Development of single brain tumour stem cell organoid. **A**-A single cells were plated into a 96-well prior to embryoid body formation. Single BTSCs were confirmed after microscope visualization of each well and 2000 mESCs was added to single cell wells. Organoid development continued as described in the timeline. Seeding of full 96-well plate resulted in 49% of the wells containing single cells of which 20% were successfully incorporated into the organoid. **B**- Representative images of single BTSCs organoid development. Day 1 and 4 demonstrates organoid with single cell while day 6 shows potential proliferation. However, at day 9 GFP-BTSCs are not visible.

4.4 B, at day 1 and 3, it is possible to discern a single BTSC in the embryoid body. Images from day 6 show a potential division of the single cell, given that two GFP dots are visible. However, on day 9 there is no visible GFP staining. In this experimental approach, despite the development of 30 organoids in total, a tumour cell mass was not found in any organoid.

In sum, the results from this first experimental approach demonstrated that although it is possible to incorporate GFP-BTSCs into the organoid system the placement of the cells in the organoid is stochastic and can lead to difficulty regarding the observation of the GFP-BTSCs within the organoid.

4.1.2. Experimental approach 2

To improve visualization and placement of the BTSCs, instead of adding single BTSCs to the 2000 mESCs, which proved hard to track and measure, I created GFP-BTSC spheroids. Tumour compartment progression was measured using colour thresholding on Image J. Homogeneous GBM spheroids generated by aggregation of 500 GBM1 BTSCs stably expressing GFP during a 24-hour incubation period were added to the 2000 mESC necessary for organoid development. As shown in the timeline in Figure 4.5A, embryoid bodies containing the GFP-BTSC spheres were subjected to neuroectoderm induction, neuronal differentiation and then spinner flask expansion and growth. Images of the growing organoids with the GFP-BTSCs were taken on days 1, 3, 5 and 7, as shown in Figure 4.5B. On day 1, the GFP-BTSC spheroids were successfully integrated into the embryoid body. However, by day 3, a portion of the GFP-BTSCs sphere started to separate from the original sphere and migrate to a distant region of the organoid. Images from days 5 and 7 illustrate there is cellular movement, as depicted by the "breakage" of the original tumour sphere. Additionally, there is no observable sign of changes to the size of the tumour compartment. To quantify tumour compartment progression, the percentage of GFP-BTSC area in the

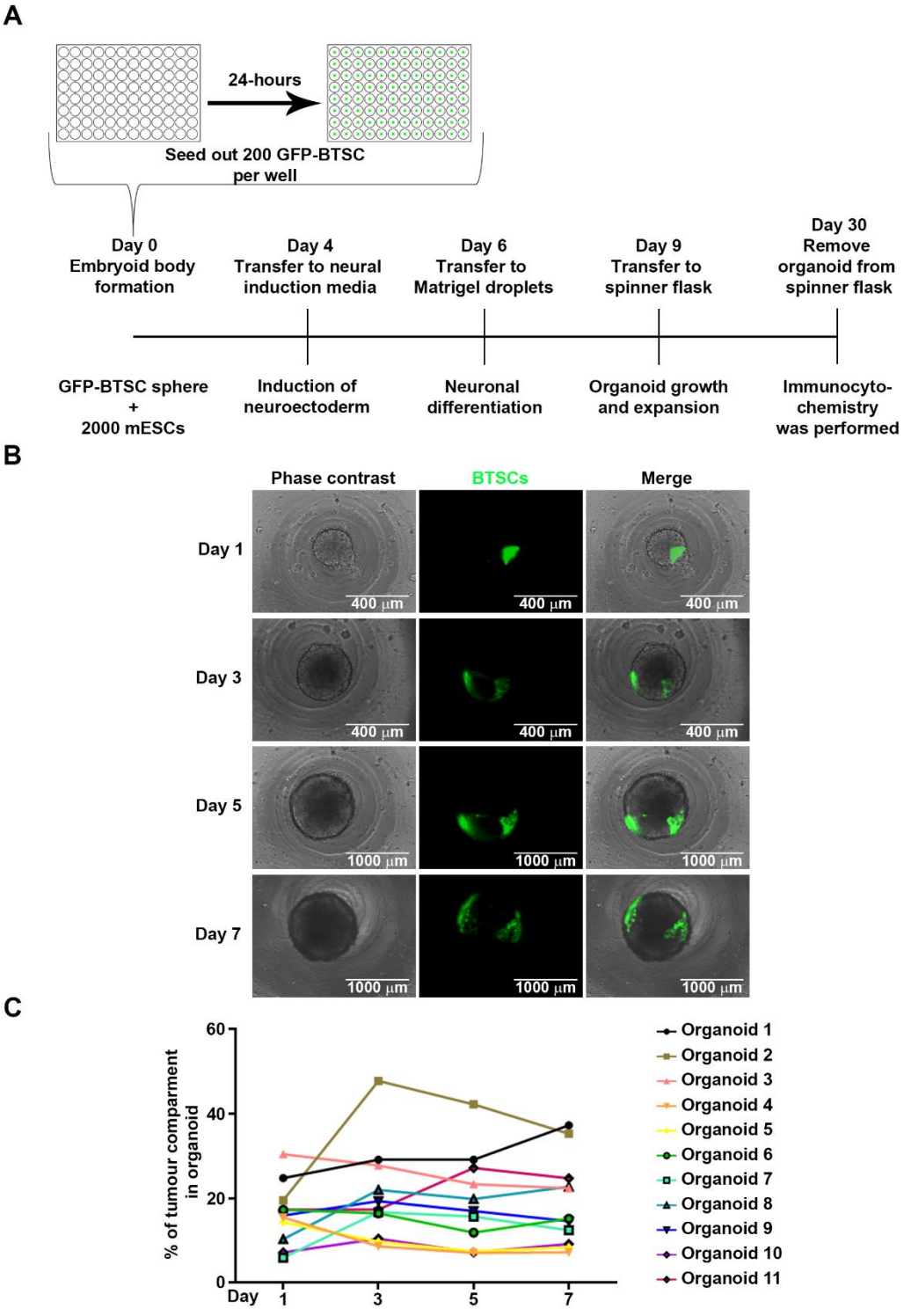

Figure 4.5 Development of organoid system with tumour compartment. **A**- GFP-BTSCs spheres were made the day prior to embryoid body formation. On day 0 2000 mESCs were added to the BTSCs sphere and organoid development progressed as shown in the experimental approach. **B**- Illustrative images of a single organoid during seven days of development. Images show that BTSCs break off from the sphere and start to migrate/invade within the organoid. **C**- Quantifications of the percentage of tumour compartment in the organoid in 11 independent organoids during seven days of development.

growing cerebral organoid was assessed, using Image J colour thresholding. As shown in Figure 4.5C, in most of the organoids (72%) there was an overall decrease in the area of the tumour compartment when compared to day 1. Furthermore, sections of the organoid following expansion in the spinner flask for 20 days showed no sign of a tumour compartment.

These results demonstrate that the addition of GFP-BTSC spheres, instead of single cells, improved the visualization of the tumour compartment within the hybrid organoid. However, this experimental approach was repeated using 30 organoids and no tumour cell mass was encountered in these organoids. Thus, this experimental approach was abandoned and a new approach was devised in order to bypass the first stages of EB differentiation.

4.1.3. Experimental approach 3

The development of mESCs into cerebral organoids includes an initial EB stage, in which a differentiating environment is present (233, 345). Given that the brain tumour stem cells were added to the mESCs at the embryoid body stage, it is plausible that this randomly differentiating environment was affecting the ability of BTSCs to maintain stem-like features. To mitigate the effect micro-environmental cues might have on the BTSCs, the Lancaster et al. (250) protocol was adapted to produce an early stage cerebral organoid (eCO) (Figure 4.6A) . With this approach, the mouse eCOs were differentiated prior to adding the GFP-BTSCs spheroids. Thus, the BTSCs avoided the randomly-occurring cell interactions within the developing EB (345). Development of the eCOs diverges from that of cerebral organoid from day 6. The eCOs were not transferred into Matrigel droplets, as the cerebral organoids were, but instead remained in the ULA-24 well plate and had neuronal differentiation media added to them.

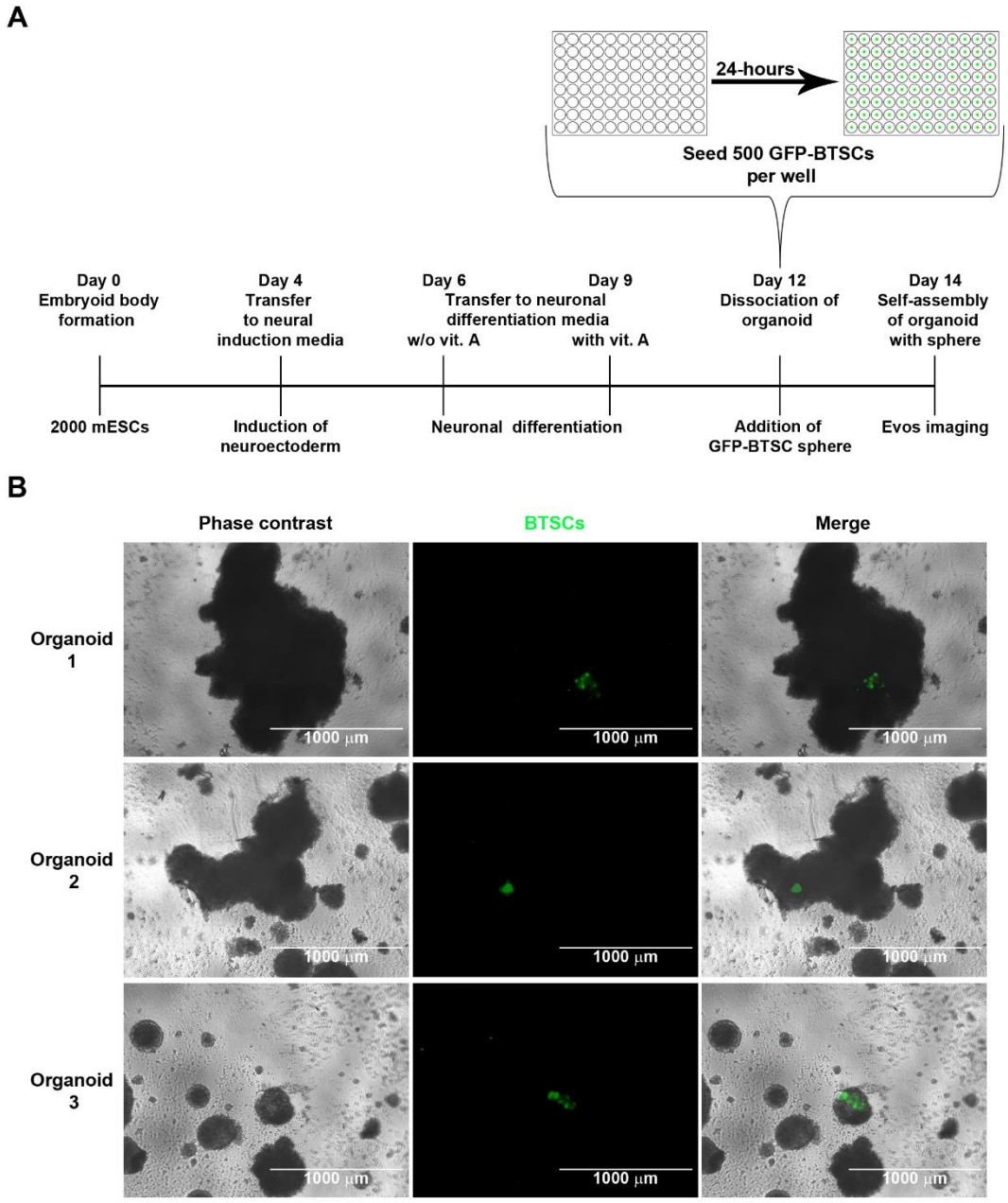

Figure 4.6 Self-assembly of dissociated eCOs with GFP-BTSCs sphere. **A**- Mouse eCOs were developed following the experimental approach presented. At day 6 organoids were not added to Matrigel to facilitate its dissociation on day 9. 24-hours prior to organoid dissociation GFP-BTSCs spheres were formed and added to the dissociated organoid. At day 12 the re-assembled organoid was imaged. **B**- Representative images of 3 distinct self-assembled organoids at day 12. Images show heterogeneity in the re-assembly process.

Taking advantage of the inherent cellular capacity to self-assemble and self-organize (which is the autonomous organization of components into structures without external intervention), I next attempted to introduce the BTSC-spheroid by dissociating the eCOs. At day 12, following neuronal differentiation of the cerebral

organoid, I manually dissociated the eCOs and added GFP-BTSC spheroids (made the previous day from 500 GFP-BTSCs) and allowed the organoid to re-assemble with the BTSC spheroid (Figure 4. 6A). At day 14, images were taken of the self-assembled eCOs with the BTSCs spheres. Figure 4.6B depicts three distinct re-assembled eCOs and images show that the self-assembly of the eCOs with the BTSC-spheroids generated phenotypic variability. Whilst organoid 1 managed to re-self-assemble with the BTSC sphere inside it, specimens 2 and 3 showed cellular debris which did not re-assemble into the organoids.

This experimental approach was repeated using 20 organoids and only 5% of these reassembled correctly. Therefore, the attempt to re-assemble dissociated eCOs with pre-formed GFP-BTSC spheroids did not result in a reproducible method to form a tumour compartment in eCOs. However, the interesting cellular behaviour observed in Figure 4.5B, allied with the ability to develop eCOs, led me to devise a new experimental approach that could conceivably model aspects of GBM behaviour – more specifically tumour migration/invasion.

4.1.4. Experimental approach 4

A characteristic feature of GBM behaviour, which is linked to its dismal prognosis, is the ability of the tumour cells to extensively infiltrate into healthy brain tissue. Experimental modelling of this process is challenging, as it requires both tumour and neural tissue compartments. Results from Figure 4.5 show BTSCs migrating/invading within the mouse organoid. Thus, I decided to further investigate this phenotype by using mouse early-stage cerebral organoids to develop an *ex vivo* 3D model of GBM invasion. eCOs were used in this approach because they allowed the BTSCs to be incorporated following the development of the cerebral organoid. In addition, as demonstrated by Lancaster et al. (250), the appearance of neural identity in mouse organoids occurred after the neural induction stage of development.

Following the experimental approach depicted in Figure 4.7, eCOs and GFP-BTSC spheroids were separately generated. They were co-cultured for 8 days after introduction on day 12 of the eCOs development. Imaging of the invasion assay shows the BTSC spheroid was incorporated into the eCO on day 2 (Figure 4. 8A). On day 4, cells had already detached from the BTSC-spheroid and were invading the eCOs. By day 8, the BTSCs were extensively invading the eCOs (Figure 4. 8A). Higher

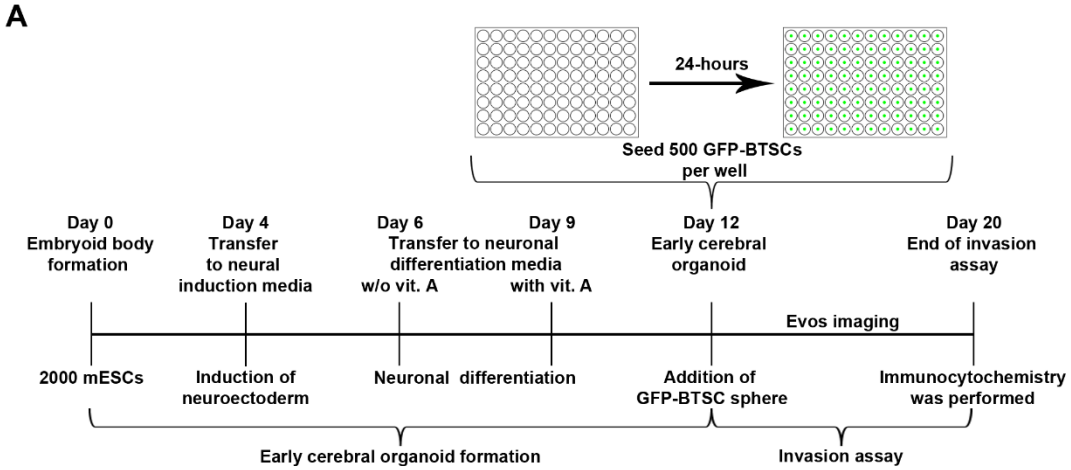

Figure 4.7 Overview of the experimental approach. The eCOs were formed from 2000 single mESCs and were subject to embryoid body formation and neural differentiation. BTSCs spheroid aggregates consisting of 500 cells were formed 24 hours prior co-culture with eCOs from day 12.

magnification images taken at early time points illustrate that, following 6 hours, the BTSC spheroid had already fused with the eCO. After 18 hours, it was possible to visualize cells detaching from the BTSC-spheroid and migrating into the eCOs (Figure 4. 8B; invading cells denoted by arrows).

Qualitative immunohistological analysis was used to confirm that neuronal identity was induced in the eCOs 12 days after formation (Figure 4.9). The presence of positive staining for the neuron-specific microtubule-associated proteins TuJ-1 and Doublecortin (DCX) confirms the neural tissue identity in the eCOs (Figure 4. 9 A and B). Moreover, the presence of GFAP-positive cells with astroglial morphologies further exemplifies the similarities that eCOs have with brain-like structures.

Following the invasion assay, hybrid organoids (eCO/BTSCs organoids) were fixed and sectioned so further characterization of the inner layers of the hybrid organoid

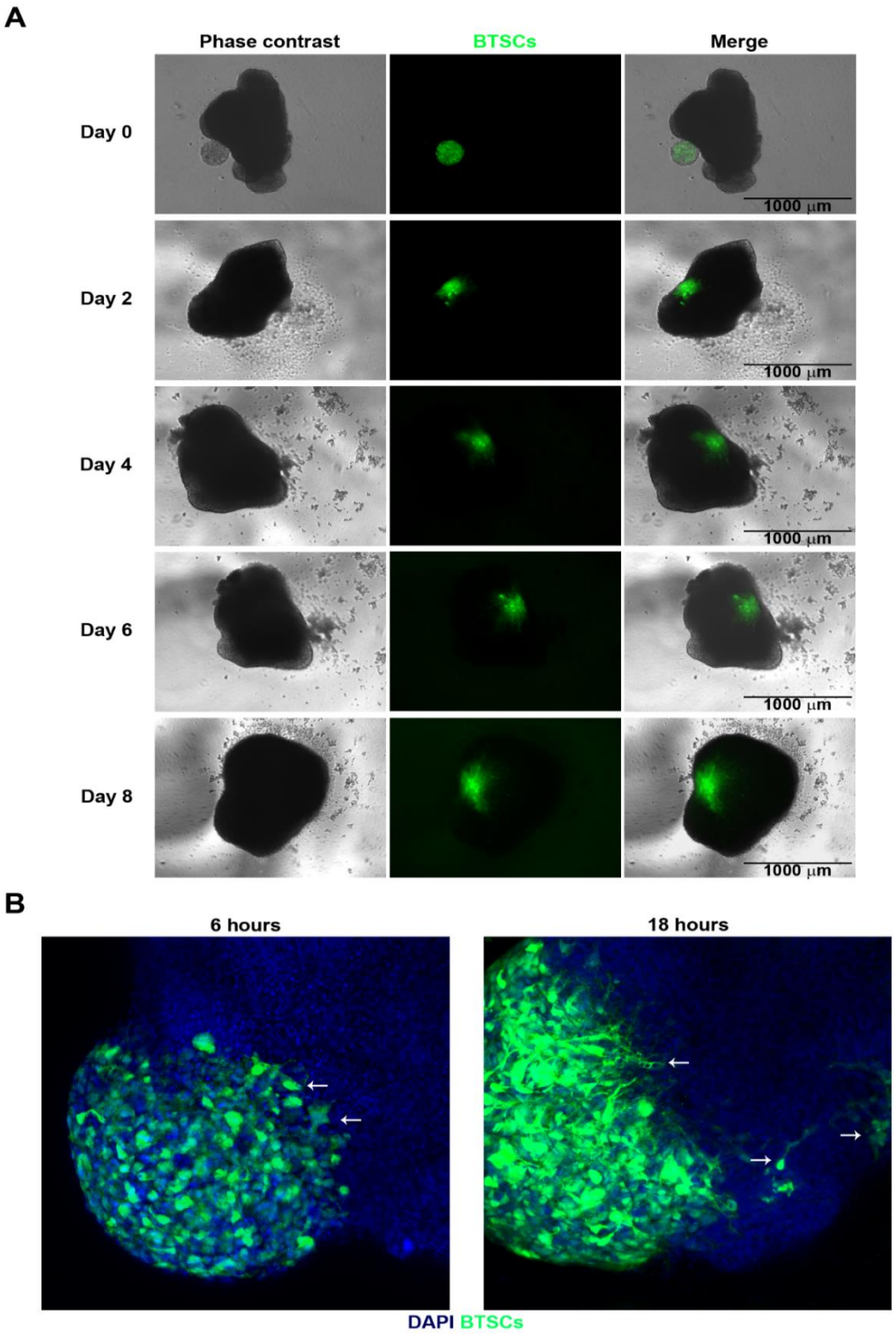

Figure 4.8 Brain tumour stem cells start detaching from tumour sphere and invading the eCO 6 hours after co-culture. A- Illustrative images of BTSCs invasion into eCOs during 8 days. At day 2, it is possible to see the BTSC sphere has been incorporated into the mouse eCO, by day 4 BTSCs have started to invade and by day 8 the BTSCs have extensively invaded the mouse eCO. B- Representative confocal microscopy image showing fusion of GFP-BTSC sphere with eCO at 6 hours and 18 hours following co-culture with eCO. Images demonstrates that at 6 hours the BTSCs start to migrate and that at 18 hours some BTSCs have detached from the sphere resulting in a migratory BTSC phenotype (arrow denote migratory/invading BTSCs). Green indicates a positive signal for GFP and nuclei (blue) were stained with DAPI.

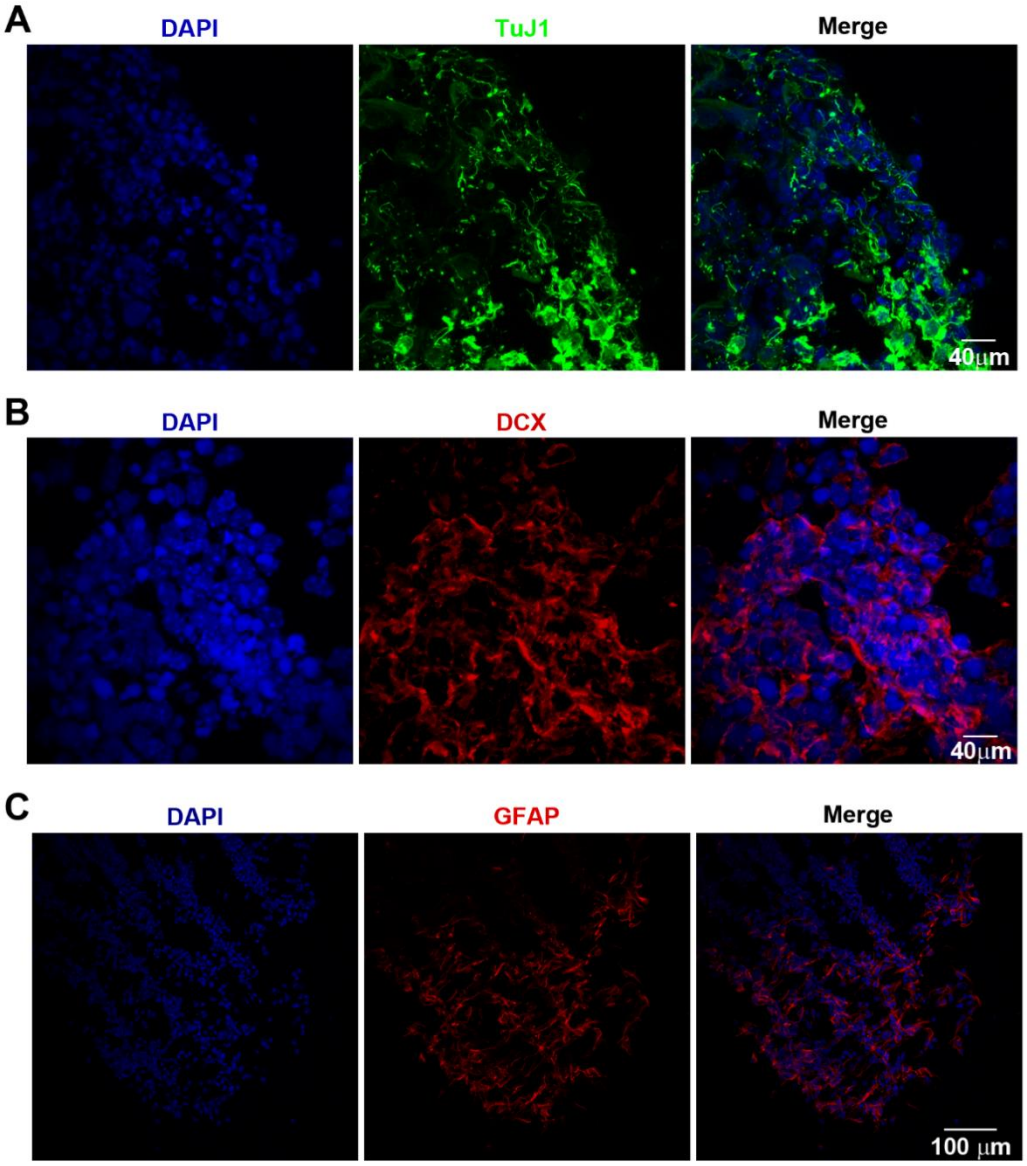

Figure 4.9 Illustrative confocal microscopy immunofluorescence images of the cerebral/neural identity of mouse eCOs at day 12 of the neural induction protocol **A**- The false colours depicts the expression of the neuronal cytoskeletal marker TuJ1. **B**- The false colours indicate doublecortin expression in eCO cells. **C**- The false colours illustrates positive staining for the astrocytic marker GFAP in eCO cells. Nuclei were stained with DAPI.

could be assessed. The inner layers possessed large tumour compartments, as exemplified in Figure 4.10A. In this figure, it is possible to see individual tumour cells (positively stained by VIMENTIN) separating from the spheroid and migrating into the eCO (denoted by white arrows). Furthermore, these BTSCs continued to express stemness markers, like NESTIN and SOX2, illustrating that the BTSCs maintained their characteristic stem cell-like nature during the invasion assay (Figure 4.10B).

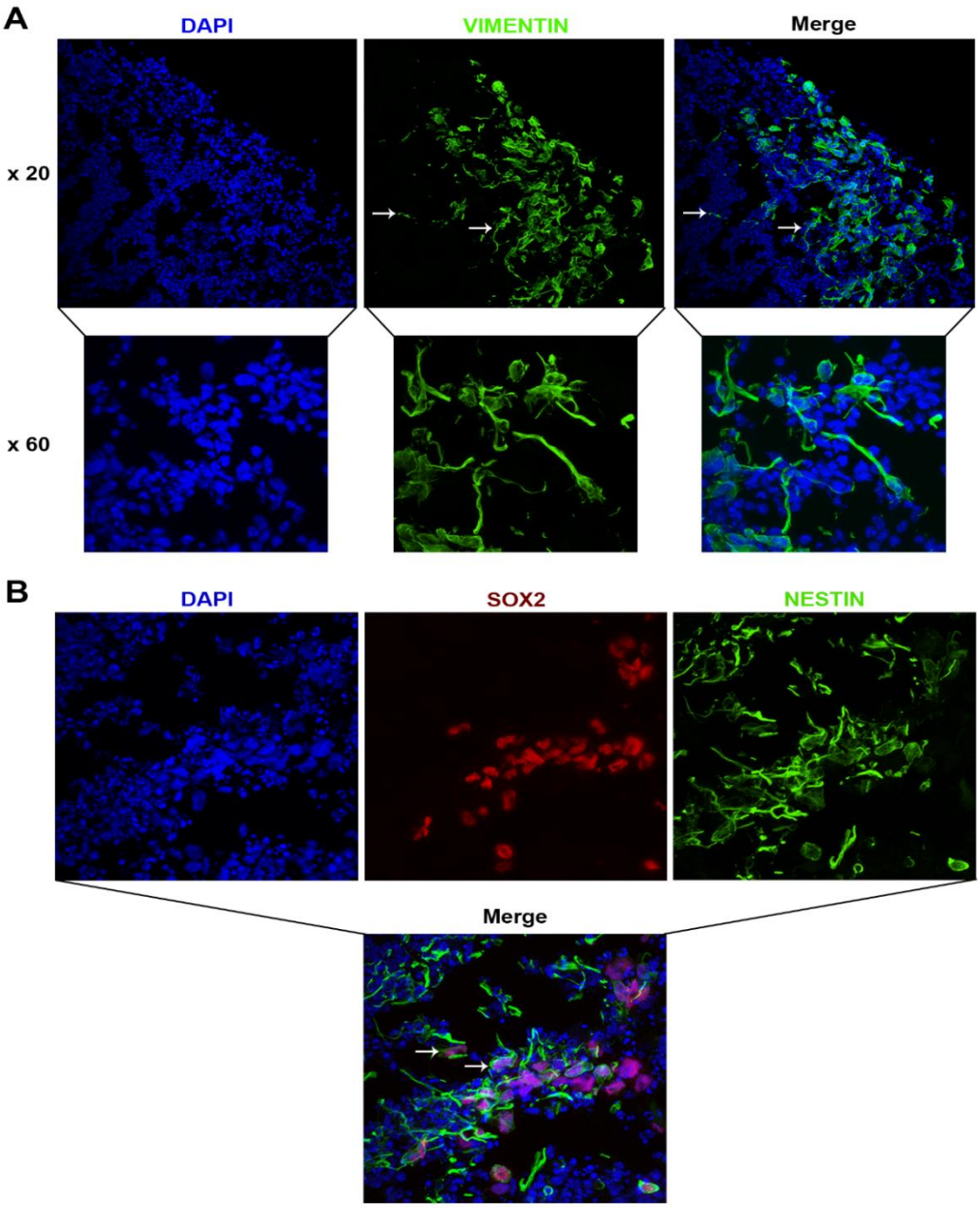

Figure 4.10 Representative confocal microscopy images of stemness markers of the BTSCs cellular compartment in histological sections of the eCO/BTSC organoids. **A**- The false colours indicate the positive expression for human VIMENTIN, illustrating the incorporation of the BTSC sphere into the eCO. 60x inset images shows BTSC cells dispersed amongst eCO cells. The arrowhead highlights the migratory edge of GBM cells within the tissue. **B**- The false colours indicate positive staining for SOX2 and NESTIN in GBM cells (marker co-localization is highlighted with white arrows). Nuclei were stained with DAPI.

The infiltrative/migratory cellular phenotype of these BTSCs was corroborated by the co-expression of VIMENTIN and MMP2 proteins, which has been previously linked to glioma invasion (Figure 4. 11A)(77, 151). However, positive staining for

MMP9 protein was rarely detected (Figure 4. 11B). Moreover, the expression of the cell cycle marker Ki-67 was low or absent in the invasive cell population, indicating a migratory, rather than a proliferative BTSCs population (Figure 4. 11C).

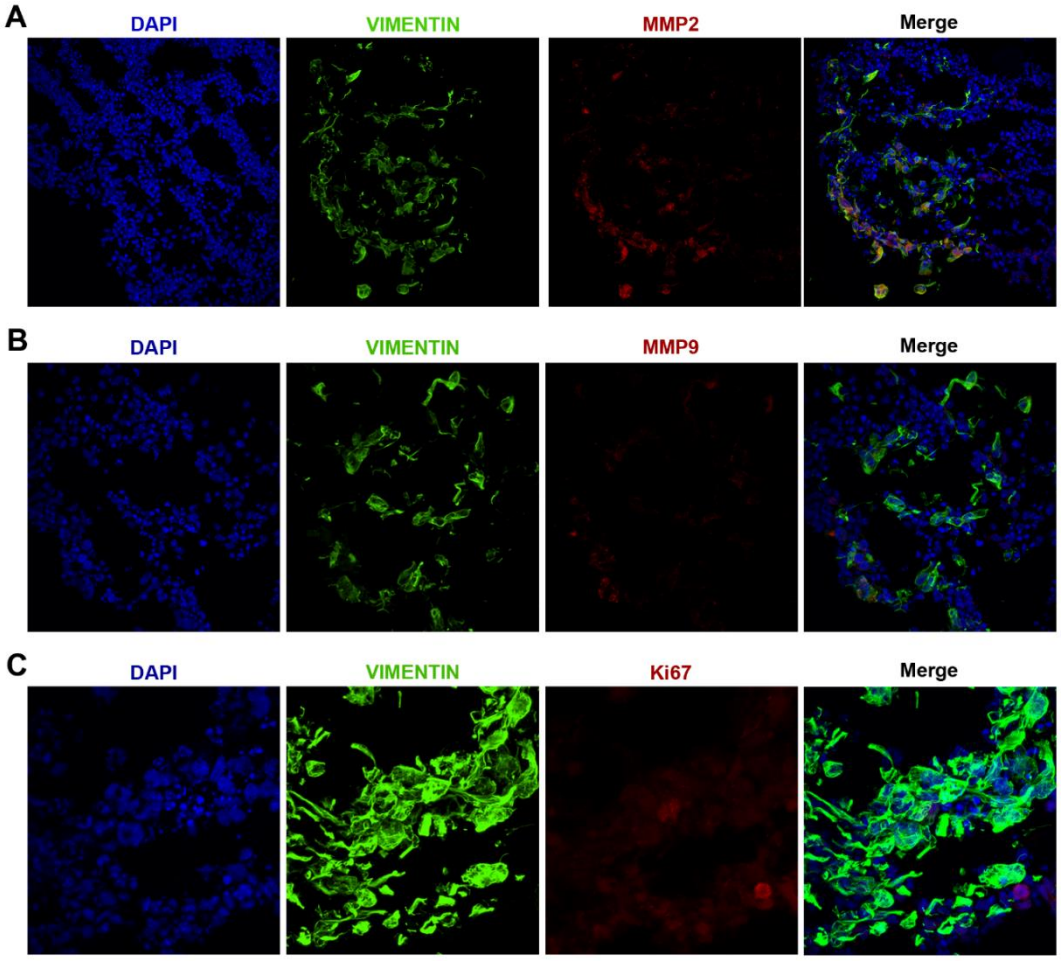

Figure 4.11 Representative confocal microscopy immunofluorescence images of the invasive GBM cellular compartment in histological sections of self-aggregated hybrid organoids (eCO/BTSC). **A**- The false colours indicate VIMENTIN and MMP2 immunopositivity and co-localization in GBM cells. **B**- False colours indicate positive signal for VIMENTIN (green) and rare signal for MMP9 (red) in BTSCS cells. **C**- False colours indicate positive signal for VIMENTIN (green) and negative signal for Ki67 (red). Nuclei (blue) were stained with DAPI.

.

4.2. Studying the cellular dynamics of eCO self-assembly

Based on the unprompted fusion and invasion of BTSC spheroids into eCOs, I next assessed the dynamics of this process and whether this spontaneous hybrid-organoid phenotype was dependent on cellular context. For this, I used neural progenitor cells 1 (NP), which were derived from excess tissues from epilepsy surgery as described in (126). NP1 cells share some similarities with brain tumour stem cells, in that they have the ability to proliferate (albeit limited) and differentiate into distinct cell types but unlike BTSCs they are not able to self-renew. As described for BTSC spheroid formation, NP1 spheroids were generated from aggregation of 500 GFP expressing cells during a 24-hour incubation period. Time-lapse microscopy (still frames shown in Figure 4.12A) demonstrated that both BTSC and NP1 spheroids were able to attach to, then fuse with, and subsequently incorporate into the eCO structures.

Comparison of the incorporation rates between these two conditions showed that BTSC spheroids demonstrated a more rapid fusion into eCOs than NP1 spheroids (note: incorporated BTSC and NP spheroids are referred to as BTSC and NP compartments). While the BTSC spheroids incorporated the eCO within 18 hours of co-culture (100%, n=76), NP1 spheroids required a co-culture period of at least 24 hours before fusion (96%±3.7, n=70). Histological analysis, shown in Figure 4.12B, illustrates a prominent phenotypic difference between eCO/BTSC and eCO/NP hybrid organoids. Comparison of the histological sections of eCO/BTSC with those of eCO/NP demonstrates that the BTSCs have invaded the eCO more extensively whilst the NP cells only managed to invade the superficial layers of the eCO. Moreover, quantification of the distance of BTSCs and NP migration following a 24 hour co-culture period showed that BTSCs exhibited a significantly increased ability to

infiltrate the eCO when compared to their NP counterparts (Figure 4. 12C). Consistently, after a 52-hour co-culture period, the BTSC compartments were more invasive and significantly larger (≥5-fold) compared to the NP compartments (Figure 4. 12D). Accordingly, the BTSCs constantly infiltrated the inner layers and core of the

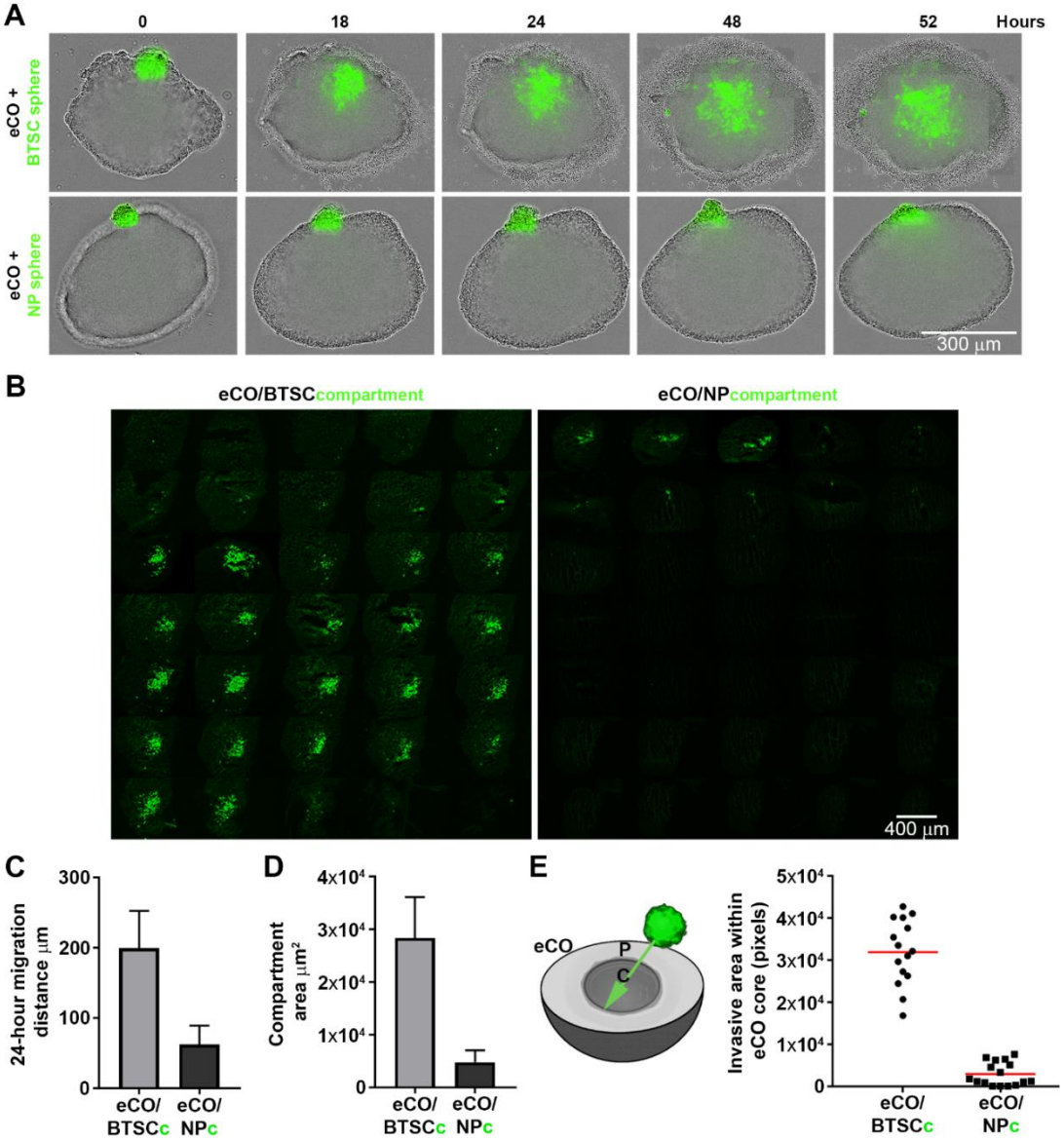

Figure 4.12 Infiltration of cells into the eCO is specific to brain tumour stem cells. **A**- Still frames of live cell imaging of GFP- BTSCs and GFP-NP spheroids invading mouse eCO. The images were taken over a time-lapse microscopy period of 52 hours and the fusion resulted in the formation of BTSC and NP cellular compartments within the hybrid organoid structures. **B**- Histological sections of an entire self-aggregated hybrid organoid – left, eCO/BTSC; right, eCO/NP. BTSCs and NP cells are GFP+ and it is possible to see in the left image that the BTSCs cells have invading the eCO more extensively when compared to the NP cells. Note the overt difference in GBM versus NP compartment spread. **C**- 24 hours migration distance of BTSCs and NP cells within the eCOs. (24 hybrid organoid was measured for each condition; **, P<0,01). **D**- Quantification of BTSCs and NP cell compartment area (μm^2) within the eCOs. (24 hybrid organoids were measured for each condition; ****, P<0.0001) **E**- Comparisons of BTSCs and NP cells cellular compartments invading the mouse eCO core. Red bars represent the median. (Each dot represents a single hybrid organoid; ****, P<0.0001).

eCOs more effectively than NP cells (Figure 4.12E). In summary, this data demonstrates that the fusion of BTSCs/NP spheroids with mESC-derived eCOs resulted in the robust formation of hybrid organoids, revealing a significant difference in the infiltration capacity of BTSCs versus NP cells.

4.3. Discussion

The invasive nature of GBM is a significant therapeutic challenge. To understand the invasive characteristics of GBM cells, it is necessary to study the interactions that the tumour cells have with the healthy brain. However, modelling this process in real time is challenging and there is a lack of models that recapitulate the human brain environment. The generation of both neural and a GBM tissue compartment within the same modelling approach is crucial for the study of GBM infiltration into the brain parenchyma.

Different aspects of GBM cell migration have been studied using 2D/ 3D *in vitro* culture and *in vivo* models (222, 229). The 2D *in vitro* investigation of cell migration has the benefit of encompassing techniques that are simple and fast to employ; the most commonly used are scratch assay and tracking of cells. With these techniques, cellular migration is based either on the ability of cells to repopulate a scratch (former) or on the tracking of individual cells on a 2D substrate (latter). Nevertheless, these techniques are not without caveats. In the scratch assay the results are easily misinterpreted, due to difficulties in distinguishing cellular proliferation from migration; in the tracking assay, due to the random directionality of cellular movement, the tracking is not straightforward. Most importantly, these 2D *in vitro* models fail to recapitulate the 3D microenvironment that the tumour cells need in which to thrive (218). Additionally, it has been shown that the invasive phenotype of glioblastoma cells in these 2D model is not similar to the invasive behaviour observed in 3D model systems (229).

More recently, the use of intravital imaging to study fluorescent tumour cells in mouse models has provided insight into cancer cell migration *in vivo* (225). However, this technique is resource-intense and not suitable for high-throughput imaging applications (266). Of particular interest is the parallel drive to use three-dimensional *ex vivo* modelling of tumour invasion. The study of GBM invasion in 3D matrices (i.e. collagen and Matrigel) has shed light onto the mechanisms behind the invasive phenotype of GBMs (346, 347). However, the recent progress in organoid technology has started to provide a methodological platform for disease modelling in 3D (226, 230-234). Cerebral organoids can have a striking resemblance to *in vivo* tissue of the developing human brain with regards to the presence neuronal and glial cell types. My study uses a modified version of the Lancaster et al. (233) protocol as a basis for developing a hybrid tumour and cerebral organoid fusion approach.

The initial attempts in my study were based on placing tumour cells into the forming embryoid body derived from mouse ESCs. The use of GFP-expressing BTSCs permitted the detection of individual cells, and further staining of the hybrid tumour-organoid with human specific VIMENTIN revealed a tumour mass in one of the organoids. This cell mass resembled an orthotopic brain tumour xenograft observed in animal models following the injection of tumour cells (119). Despite the successful discovery of a tumour mass in one of the hybrid organoid, this technique had a very low success rate – 1 in 60 – and did not represent a robust methodology. Furthermore, given the random positioning of the GFP-BTSCs within the EB it was very difficult to localize the cells. For example, in the case of the addition of 1 GFP-BTSCs there are $3.3x10^{5735}$ possible locations for that specific cell within one EB. This variability and the difficulty to locate/visualize the tumour cell in the growing EB and organoid resulted in the testing of different approaches.

Accordingly, the next attempt focused on the use of a tumour sphere composed of GFP-BTSCs, followed by 'placement' of the sphere into the aggregating mouse ESCs during the EB formation step of the Lancaster at al. protocol. This technique improved

the visualization of the tumour cells. However, the spheroid tumour compartment did not resemble GBM infiltration over 30 days. Qualitative assessment of these GBM spheroid containing organoids, using tumour specific VIMENTIN immunostaining, suggested that few (or even scattered individual cells) were present in sectioned organoids. The lack of tumour cells can be a result of the random sequence of events/signalling cues that occur within the EB, which argues that this environment might result in the loss of BTSC expansion and migration ability (345).

The ideal matrix for the study of GBM invasion *in vitro* requires the presence of viable brain cells and tumour cells. To establish an experimental approach that would recapitulate *in vivo* GBM invasion in real time, brain-like structures and GFP-BTSCs spheres were developed independently and then co-cultured. The development of early-stage cerebral organoids, using a protocol adapted from Lancaster et al. (250), resulted in the creation of brain-like structures that possessed neural identity. This neural identity was inferred by the presence of neuron-specific microtubule-associated proteins TuJ-1 and DCX (348). Further, the presence of GFAP positive cells which possessed astroglial morphologies further confirmed the similarities these eCOs has with parenchymal tissue (348). Using this model of co-culturing eCO and GFP-BTSC spheroids, a spontaneous incorporation of GFP-BTSCs into mouse eCOs was observed. In addition, this fusion resulting from the co-culture of these two viable tissues is in agreement with previous reports describing spontaneous fusion of cerebral organoids (238, 239).

This model further allowed for the study of the dynamics and specificity of the GBM invasion process. Real time microscopy identified that the invasion occurred in three different stages, in which the sphere first attached to the eCO, fused and then infiltrated the eCOs. In addition, the use of GFP-BTSCs spheres and GFP-NP spheres showed that both spheres had the ability to attach and fuse with the eCOs. For the BTSCs spheres that was a rapid process (<18 hours), while for the NP spheres the fusion required a longer co-culture period (>24 hours). Interestingly, only the GFP-

BTSC spheres had the ability to extensively invade the eCOs; this is demonstrated by the invasive pattern of BTSCs in the eCOs shown in the immunofluorescent images of the eCO/ BTSCs hybrid organoids. These BTSCs did not express the cell cycle marker Ki67, and low Ki67 expression has been linked to active cell migration (349, 350). The combination of these observations suggests these cells have a migratory phenotype (instead of a proliferative one). Additional characterisation of the tumour compartment revealed that BTSCs stained positive for SOX2 and NESTIN, thus further suggesting this model represents a viable platform to study BTSCs while conserving their stem-like features. In GBM, matrix metalloproteinase (MMP) 2 and 9 have been implicated in GBM migration and invasion. MMP-9 expression was rarely detected in the invading cells of the BTSC/eCO model, but MMP-2 was present and co-localized with VIMENTIN staining, indicating the invasive phenotype of these cells (151, 351). These results are consistent with the published observation that heterogeneous MMP-2 and MMP-9 expression patterns in GBM cells depend on the cellular and experimental context (151). In addition, real time imaging of the migrating BTSCs demonstrated that these cells had a more elongated morphology; and immunopositivity of BTSCs for MMP-2 and VIMENTIN indicate a mesenchymal 'mode' of migration within the eCOs (142, 153). However, it has been shown that GBM cells can switch between these two forms of motility as an adaption mechanism in response to enzyme blockade (152). Therefore, it may be feasible to use this model to study amoeboid migration in BTSCs by using an MMP inhibitor (152).

There are limitations to these self-assembling GBM organoids. These include the inherent variability of clinical tumour specimens, which poses a significant challenge for *ex vivo* modelling of a heterogeneous cancer such as GBM; as well as the documented variability of cerebral organoids (233, 352) To address the issue of GBM variability, the experiments were carried out using a comprehensively-characterized *in vitro*/*in vivo* model of GBM BTSCs (126). It has been suggested that the endogenous variability of a growing organoid, which is currently poorly understood, may only be

adequately elucidated through a resource-intense single cell sequencing technique, in order to 'map' the cellular diversity (353). While my study does not address cerebral organoid composition, it nevertheless provides insight into the management of the innate variability. In particular, it indicates that early-stage cerebral organoids (eCO) are well suited for generating self-assembling hybrid organoids with an infiltrative tumour compartment. As long-term culture of cerebral organoids shows an increase in cellular diversity and complexity of architectures (233, 353), my study sought to reduce organoid variability by using short a 12-day mESCs differentiation periods. Accordingly, the spontaneous infiltration of an individual cerebral organoid by a BTSCs sphere has now been observed 114 times across 6 different experimental sets, hence representing a phenotypic reproducibility of 100% which is indicative of the robustness of the self-assembly process despite the cerebral organoid variability. The self-assembling GBM organoids cannot currently be used to examine GBM cells migration along blood vessels and into the corpus callosum which are important features of GBM invasion in the human brain. However, taken together with the recent study by Mansour et al. (246) in which they demonstrate the ability to vascularize brain organoids by transplanting these into an adult mouse brain, it opens up the possibility of using this invasion model in an *in vivo* context to study how the presence of blood vessels might affect the invasion behaviour of the BTSCs.

Although, the cerebral organoids developed in my study possess several distinct brain cells and a 3D structure, they currently are not exact replicas of the adult human brain. In fact, it has been shown that cerebral organoids are more representative of a developing fetal brain than that of an adult brain. This limitation, thus, raises the question of the clinical relevance of the cerebral organoid for the study of adult GBM. Despite, the absence of adult brain structures, the cerebral organoids developed in my study possess brain cells which are known to involved in GBM invasion, such as astrocytes and neurons. Thus, the model here developed whilst not identical to an adult brain can be used to discern the mechanism by which GBM utilizes the patient's own

brain cells to aide in its invasion. However, further improvements of this invasion model could be achieved thanks to the recent development of brain organoids of different brain regions (i.e. forebrain and midbrain). These distinct brain organoids hold the potential of increasing the clinical relevance of this model given that they possess a higher resemblance to the adult brain. Given that 61% of GBM tumours occurs in the forebrain, the use of forebrain organoids to develop an invasion model has the potential to further increase the clinical relevance of this model.

This self-assembling organoid has the potential to be adapted into a human context by replacing R1 mESCs with human ESCs; however, further adaptions to the protocol are necessary to develop human eCOs. Additionally, there has been a recent demonstration (354) that patient-derived gut organoids were able to reliably predict the response to targeted therapy. Taking into account the specificity of GBM BTSCs infiltration into the eCOs, this argues favourably for the potential of using this hybrid organoid model with a similar purpose.

In summary, in this chapter I have described the approaches to development of a 3D invasion model. My study demonstrated that the co-culture of BTSC spheres with mESC-derived eCOs resulted in the robust development of a hybrid tumour-organoid model. It did so in a GBM-specific fashion, while enabling the BTSCs to maintain stem-like characteristics. Furthermore, this model allowed the detailed study of the invasion mode of BTSCs cells into brain-like structures, emulating the tight extracellular spaces the tumour cells may encounter while migrating through a human brain.

5. Conclusion

At present, GBM remains a disease that is associated with very poor clinical outcomes (16). Recent and substantial advances in treatment (surgery, chemotherapy and radiotherapy) have yielded some benefit in extending overall survival, however this is measured in months rather than years (18). For most GBMs, recurrence is unavoidable, and most deaths occur within 2 years of diagnosis (18). Thus, GBM is considered an unmet clinical need. Despite the heterogeneity present in all GBM cells, one crucial feature typifies the malignancy — invasiveness (16). Migration of GBM cells into healthy brain tissue reduces the effectiveness of surgical resection and radio/chemotherapy. Therefore, the understanding to GBM invasion is fundamental for the efficient treatment of this dire disease (17). One of the key biological processes behind GBM invasion involves the reorganization of the actin cytoskeleton, which in turn is critically regulated by kinases (194). The role of ROCK kinases in cancer has been extensively studied, in particular in regards to motility and invasion. Nevertheless, there is still no consensus regarding the effect that ROCK kinases have on cellular tumourigensis; i.e., cell proliferation, survival and differentiation. With the ongoing efforts to use ROCK pathway inhibitors in a clinical setting as an anti-tumour agent, it is important to discern the effect chemical ROCK pathway inhibition has on cellular functions.

To this end, this study firstly aimed to investigate, in depth, the effect of pan chemical ROCK inhibition, using Y-27632. The data indicates that chemical inhibition of the ROCK signalling pathway induced a dose and time dependent neurite-like outgrowth phenotype in BTSCs. This phenotype was also induced in a panel of

phenotypically distinct human derived glioblastoma cell lines, demonstrating that different GBM subtypes were also susceptible to pan chemical ROCK inhibition. These results are consistent with the notion that ROCK inhibition can contribute to axonal elongation and regeneration (305, 307, 355). In contrast to studies that describe a reduction in cellular proliferation upon chemical ROCK inhibition, time-lapse microscopy, clonal growth and Ki-67 immunocytochemistry results illustrated that cell proliferation and self-renewal capacity of BTSCs remains unaltered after ROCK inhibitor treatment. In addition, and despite the existence of reports which link cellular differentiation with the treatment of Y-27632, in my study there was no evidence of differentiation in the BTSCs. These results, based on the minimal gene expression changes, also indicate that chemical obstruction of the ROCK pathway did not significantly alter cell fate. Accordingly, the phenotype induced by several ROCK pathway inhibitors in the BTSCs stem-like cells was reversible following compound removal.

Interestingly, my study demonstrated that cells which were able to establish a transient network of neurite-like protrusions had a reduction in motility, when compared to vehicle and Y-27632 treatment on sparsely seeded BTSCs (the latter presented no alteration in motility). These results show that BTSCs abdicate their ability to move in favour of network establishment. The resulting functional multicellular network is capable of communication via gap junctions through calcium waves. Even though the discovery of cell-to-cell communication via tunnelling membranes is not entirely novel, in this study I have identified a type of networking system, composed of neurite-like microtubes, which has not been previously described. These neurite-like microtubes, here termed NLMs, may merit their own classification, for despite sharing some characteristics with TMs and NMs, they display unique features (i.e. absence of Cx43 in gap junctions; projections were positive for MAP-2 and TuJ-1, amongst others).

In this study, it was shown that Y-27632 induced NLMs networks were able to resist radiotherapy, a feature that has been previously described for astrocytoma cells (266). Although the exact mechanism behind this resistance is as yet unknown, this study does shed some light on this process. My results suggest that the resistance is linked to gap junctional communication. A possible explanation for this resistance is the establishment of calcium homeostasis. This homeostasis is granted by the dispersion of intracellular calcium throughout all the cells in the network, instead of the accumulation of this calcium intracellularly, which could cause cell death. In addition, it has been shown that radiotherapy causes particular damage to the cells 'powerhouses'— the mitochondria. In this study, it was demonstrated that the Y-27632 induced NLMs were enriched with mitochondria; therefore, it is possible that the ATP, produced by functional mitochondria, is being transported to other cells which suffer mitochondrial damage upon high-dose radiation.

Future work will focus on the study of network dynamics and radioresistance in additional GBM cell lines. Despite demonstrating, in this study, that distinct GBM cell lines were able to develop neurite-like projections following ROCK pathway inhibition, functional analysis of the established network and analysis of cell survival after radiation were solely performed on the GBM1 cell line. Thus, further studies are necessary to ascertain whether the survival advantage observed is a common GBM feature and if there is any form of predisposition, i.e. related to GBM subtypes, for cells to establish the multicellular network. This knowledge could pave the way for the implementation of this network phenotype as a method to discover and validate GBM radiosensitizing agents. Additionally, further *in vitro* and *in vivo* investigations are also needed to elucidate the exact mechanisms behind this survival benefit of radiation-treated BTSC networks, and to better understand how these connected cells are using gap junctional communication to survive. The combination of mRNA sequencing with spatial transcriptomics may provide valuable insight into the mechanistic link between cellular networks and cell survival. Whilst the mRNA sequencing data could determine

what genes are differentially expressed between control cells and Y-27632 treated cells, the spatial transcriptomics can provide spatial information regarding the location of these genes, thus allowing the in depth study of factors that can potentially travel though gap junctions.

In summary, the BTSCs remain undifferentiated despite chemical inhibition of the ROCK-NM II axis. In addition, this Y-27632 induced NLM network model can be used to study network dynamics in a system that is reversible in undifferentiated BTSCs. Furthermore, it allows the investigation of the effect of multicellular networking in regards to GBM resistance, progression and invasion in a 2D context, which has not been available before. Thus, these studies have the potential to lead to novel therapeutic approaches that focus on the specific targeting of these chemically-induced BTSCs networks.

The second part of my thesis focused on the development of a 3D hybrid tumour-cerebral organoid model, which aimed at the study of GBM progression and invasion in real-time. In the absence of models that allowed real-time imaging of GBM invasion into healthy brain tissue, my study pioneered a method that is based on the self-assembly of BTSC-spheroids with early-stage cerebral organoids. Several distinct experimental approaches were tested via qualitative assessments, subsequently leading to the quantification of the spontaneous infiltration of individual eCOs by BTSCs spheroids, which was observed in 100% of the cases, indicating the robustness of the hybrid organoid model presented in this study. The eCO/GBM hybrid organoids were characterized by a migratory and invasive tumour phenotype resulting from a significantly increased migration and tissue infiltration capacity of the GBM tumour compartment, as compared with its control (NP) counterpart. Furthermore, this study demonstrated that the GFP-BTSC spheroids used a mesenchymal mode to invade the eCOs and opens the possibility of using this model to study the different modes of migration in real-time. The technique described demonstrated that organoids can be used to develop an *ex vivo* experimental model system that aims, in real-time, to

recapitulate the infiltrative characteristic of GBM that makes current therapy so ineffective. Furthermore, the eCO/GBM hybrid organoids (and their non-cancerous controls) provide the foundation for the future development of assays to investigate the underlying mechanisms of invasion and screen for drugs that abrogate this phenotype. Thus, this is a model which can yield critical information about anti-migratory GBM strategies in a timely fashion using *ex vivo* real time observation.

For the advancement of this model, it would be essential to continue to build upon the developed cerebral organoid in a direction that more closely mimics the tumour microenvironment. At the moment, the cerebral organoid model lacks key features of the tumour microenvironment, such as an immune system and blood vessels. The ability to grow cerebral organoids using induced pluripotent stem cells (iPSCs) derived from the patient's own cells opens the possibility of developing a patient specific organoid which could be amenable to the incorporation of the patient's own immune cells. By using the patient derived iPSCs to grow the cerebral organoid and the patient's own immune cells, there is no risk of the immune system considering the organoid as foreign and attacking it. Thus, the development of an immune competent tumour organoid model would be valuable for the study of immunotherapies. In addition, studies which further elucidate the role ROCK signalling pathway plays in GBM cell migration and in the development of microtubes in a 3D environment are required. In this context, the development of the 3D *ex vivo* BTSCs invasion model provides a suitable experimental tool to study the involvement of NLM networks in GBM invasion and survival in a 3D context.

In summary, my thesis demonstrated that Y-27632 treated BTSCs are able to form a functional cellular communication network, composed of NLMs, which promoted an increase in BTSCs resistance to radiotherapy as compared with non-connected Y-27632 treated BTSCs and vehicle.

6. Appendix

Antibody	Species	Reactivity	Dilution	Method	Fixation	Source	Catalogue number
Anti-TuJ-1	Mouse	Human, Mouse, Rat	1:500	IF	PFA	Convance	801213
Anti-MAP-2	Chicken	Mouse, Rat, Sheep, Cow, Dog, Human, Cynomolgus monkey, Common marmoset, Aplysia	1:10000	IF	PFA	Abcam	ab5392
Anti-phospho-H_2AX	Mouse	Vertabrates	1:800	IF	PFA	Merck	JBW301
Anti-Ki67	Rabbit	Mouse, Rat, Human, Common marmoset	1:200	IF	PFA	Abcam	ab16667
Anti-SOX2	Rabbit	Mouse, Rat, Horse, Chicken, Human, Pig, Xenopus laevis, Zebrafish, Quail, Rainbow trout, Spotted catshark, Thornback ray	1:100	IHC	Paraffin	Abcam	ab97959
Anti-VIMENTIN	Mouse	Rat, Horse, Chicken, Cow, Cat, Dog, Human, Pig	1:100	IHC	Paraffin	Abcam	ab8069
Anti-SOX2	Rabbit	Human, Mouse	1:150	IHC	PFA	Cell signalling	35795
Anti-VIMENTIN	Mouse	Human, Dog, Rat, Rabbit	1:200	IHC	PFA	DAKO	M0725
Anti-GFAP	Rabbit	Mouse, Human, Rat, Rabbit	1:200	IHC	PFA	DAKO	Z0334
Anti-DCX	Goat	Chicken, Cow, Dog, Horse, Human, Mouse, Pig, Rat	1:300	IHC	PFA	Santa Cruz Antibodies	sc-8066
Anti-Nestin	Mouse	Human	1:200	IHC	PFA	Millipore	MAB5326

Table A1- Antibody table

Symbol	Gene	Fold change
LYPD1	LY6/PLAUR domain containing 1	1.83
MAP1B	microtubule-associated protein 1B	1.81
RPE65	retinal pigment epithelium-specific protein 65kDa	1.72
LOC728755	uncharacterized LOC728755	1.66
AIF1L	allograft inflammatory factor 1-like	1.60
GFAP	glial fibrillary acidic protein	1.53
WLS	wntless homolog (Drosophila)	1.50
TAGLN2	transgelin 2	1.49
FAM131B	family with sequence similarity 131, member B	1.49
SLC4A4	solute carrier family 4 (sodium bicarbonate cotransporter), member 4	1.48
NF1	neurofibromin 1	1.48
STMN4	stathmin-like 4	1.45
FADS2	fatty acid desaturase 2	1.45
RBM4|RBM14 -RBM4	RNA binding motif protein 4|RBM14-RBM4 readthrough	1.45
EEF1A1	eukaryotic translation elongation factor 1 alpha 1	1.43
TRAPPC6A	trafficking protein particle complex 6A	1.43
CLDN1	claudin 1	1.43
DHCR7	7-dehydrocholesterol reductase	1.43
ANKRD20A1| ANKRD20A3| ANKRD20A2| ANKRD20A4	ankyrin repeat domain 20 family, member A1|ankyrin repeat domain 20 family, member A3|ankyrin repeat domain 20 family, member A2|ankyrin repeat domain 20 family, member A4	1.43

SCD	stearoyl-CoA desaturase (delta-9-desaturase)	1.43
CSPG5	chondroitin sulfate proteoglycan 5 (neuroglycan C)	1.42
MACF1	microtubule-actin crosslinking factor 1	1.42
PYCR1	pyrroline-5-carboxylate reductase 1	1.40
SCARB1	scavenger receptor class B, member 1	1.39
LRP4	low density lipoprotein receptor-related protein 4	1.39
BATF3	basic leucine zipper transcription factor, ATF-like 3	1.38
PDGFA	platelet-derived growth factor alpha polypeptide	1.38
RNF212	ring finger protein 212	1.38
HM13	histocompatibility (minor) 13	1.38
MATN2	matrilin 2	1.38
NUP98	nucleoporin 98kDa	1.37
FOXK1	forkhead box K1	1.37
PMP22	peripheral myelin protein 22	1.37
TMC7	transmembrane channel-like 7	1.37
PDIA6	protein disulfide isomerase family A, member 6	1.37
SH3BGR	SH3 domain binding glutamic acid-rich protein	1.36
RPS25	ribosomal protein S25	-1.36
SRSF3	serine/arginine-rich splicing factor 3	-1.36
USP8	ubiquitin specific peptidase 8	-1.36
MAD2L1	MAD2 mitotic arrest deficient-like 1 (yeast)	-1.37
RPL10	ribosomal protein L10	-1.37
SLC41A3	solute carrier family 41, member 3	-1.37
RPL23	ribosomal protein L23	-1.37

NUDCD2	NudC domain containing 2	-1.37
NDUFB9	NADH dehydrogenase (ubiquinone) 1 beta subcomplex, 9, 22kDa	-1.38
LGALS3	lectin, galactoside-binding, soluble, 3	-1.38
ECT2	epithelial cell transforming sequence 2 oncogene	-1.38
PUS3	pseudouridylate synthase 3	-1.38
FAM183CP	family with sequence similarity 183, member C, pseudogene	-1.38
PCNA	proliferating cell nuclear antigen	-1.38
SLC12A2	solute carrier family 12 (sodium/potassium/chloride transporter), member 2	-1.39
FTH1	ferritin, heavy polypeptide 1	-1.39
BORA	bora, aurora kinase A activator	-1.40
CENPW	centromere protein W	-1.40
GALNT1	UDP-N-acetyl-alpha-D-galactosamine:polypeptide N-acetylgalactosaminyltransferase 1 (GalNAc-T1)	-1.40
UQCRH	ubiquinol-cytochrome c reductase hinge protein	-1.41
FAM72D	family with sequence similarity 72, member D	-1.41
RANBP3L	RAN binding protein 3-like	-1.42
PORCN	porcupine homolog (Drosophila)	-1.42
HIST1H1C	histone cluster 1, H1c	-1.42
MCTS1	malignant T cell amplified sequence 1	-1.42
PHYH	phytanoyl-CoA 2-hydroxylase	-1.43
FAM133B	family with sequence similarity 133, member B	-1.43

ABCB9	ATP-binding cassette, sub-family B (MDR/TAP), member 9	-1.43
LINC00152|MIR4435-1HG	long intergenic non-protein coding RNA 152|MIR4435-1 host gene (non-protein coding)	-1.43
CCNG2	cyclin G2	-1.44
PLK3	polo-like kinase 3	-1.45
BBS9	Bardet-Biedl syndrome 9	-1.45
CDK1	cyclin-dependent kinase 1	-1.45
PPIA|PPIAP30	peptidylprolyl isomerase A (cyclophilin A)|peptidylprolyl isomerase A (cyclophilin A) pseudogene 30	-1.46
VAMP1	vesicle-associated membrane protein 1 (synaptobrevin 1)	-1.47
TMEM132C	transmembrane protein 132C	-1.47
MRPL19	mitochondrial ribosomal protein L19	-1.48
HMGB2	high mobility group box 2	-1.49
CKAP2	cytoskeleton associated protein 2	-1.52
NPTX1	neuronal pentraxin I	-1.52
INTS7	integrator complex subunit 7	-1.53
SUFU	suppressor of fused homolog (Drosophila)	-1.55
CDH5	cadherin 5, type 2 (vascular endothelium)	-1.58
NUF2	NUF2, NDC80 kinetochore complex component	-1.63
PPIA|PPIAL4G	peptidylprolyl isomerase A (cyclophilin A)|peptidylprolyl isomerase A (cyclophilin A)-like 4G	-1.63
NEK2	NIMA-related kinase 2	-1.66

ID2	inhibitor of DNA binding 2, dominant negative helix-loop-helix protein	-1.76
TRAF4	TNF receptor-associated factor 4	-1.86

Table A2- List of genes differentially expressed from microarray gene anlyasis.

7. Bibliography

1. Agnihotri, S., Burrell, K.E., Wolf, A., Jalali, S., Hawkins, C., Rutka, J.T. and Zadeh, G. Glioblastoma, a Brief Review of History, Molecular Genetics, Animal Models and Novel Therapeutic Strategies. *Archivum Immunologiae et Therapiae Experimentalis.* 2013, **61**(1), pp.25-41.
2. Messali, A., Villacorta, R. and Hay, J.W. A review of the economic burden of glioblastoma and the cost effectiveness of pharmacologic treatments. *Pharmacoeconomics.* 2014, **32**(12), pp.1201-1212.
3. Schwartzbaum, J.A., Fisher, J.L., Aldape, K.D. and Wrensch, M. Epidemiology and molecular pathology of glioma. *Nature Reviews Neurology.* 2006, **2**(9), p.494.
4. Davis, M.E. Glioblastoma: Overview of Disease and Treatment. *Clin J Oncol Nurs.* 2016, **20**(5 Suppl), pp.S2-8.
5. Wilson, T., Karajannis, M. and Harter, D. Glioblastoma multiforme: State of the art and future therapeutics. *Surgical Neurology International.* 2014, **5**(1), pp.64-64.
6. Ohgaki, H. and Kleihues, P. Population-Based Studies on Incidence, Survival Rates, and Genetic Alterations in Astrocytic and Oligodendroglial Gliomas. *Journal of Neuropathology & Experimental Neurology.* 2005, **64**(6), pp.479-489.
7. Dolecek, T.A., Propp, J.M., Stroup, N.E. and Kruchko, C. CBTRUS Statistical Report: Primary Brain and Central Nervous System Tumors Diagnosed in the United States in 2005-2009. *Neuro-Oncology.* 2012, **14**(suppl 5), pp.v1-v49.
8. Brodbelt, A., Greenberg, D., Winters, T., Williams, M., Vernon, S. and Collins, V.P. Glioblastoma in England: 2007–2011. *European Journal of Cancer.* 2015, **51**(4), pp.533-542.
9. Hanif, F., Muzaffar, K., Perveen, K., Malhi, S.M. and Simjee, S.U. Glioblastoma Multiforme: A Review of its Epidemiology and Pathogenesis through Clinical Presentation and Treatment. *Asian Pac J Cancer Prev.* 2017, **18**(1), pp.3-9.
10. Preusser, M., de Ribaupierre, S., Wöhrer, A., Erridge, S.C., Hegi, M., Weller, M. and Stupp, R. Current concepts and management of glioblastoma. *Ann Neurol.* 2011, **70**(1), pp.9-21.
11. Iacob, G. and Dinca, E.B. Current data and strategy in glioblastoma multiforme. *Journal of medicine and life.* **2**(4), pp.386-393.

12. Salcman, M. Epidemiology and factors affecting survival. In: Apuzzo, M.L.J. ed. Park Ridge, IL: American Association of Neurological Surgeons, pp.95-105.
13. Stupp, R., Mason, W.P., van den Bent, M.J., Weller, M., Fisher, B., Taphoorn, M.J.B., Belanger, K., Brandes, A.A., Marosi, C., Bogdahn, U., Curschmann, J., Janzer, R.C., Ludwin, S.K., Gorlia, T., Allgeier, A., Lacombe, D., Cairncross, J.G., Eisenhauer, E. and Mirimanoff, R.O. Radiotherapy plus Concomitant and Adjuvant Temozolomide for Glioblastoma. *New England Journal of Medicine.* 2005, **352**(10), pp.987-996.
14. Thakkar, J.P., Dolecek, T.A., Horbinski, C., Ostrom, Q.T., Lightner, D.D., Barnholtz-Sloan, J.S. and Villano, J.L. Epidemiologic and Molecular Prognostic Review of Glioblastoma. *Cancer Epidemiology Biomarkers & Prevention.* 2014, **23**(10), pp.1985-1996.
15. Ohka, F., Natsume, A. and Wakabayashi, T. Current Trends in Targeted Therapies for Glioblastoma Multiforme. *Neurology Research International.* 2012, **2012**, pp.1-13.
16. Ostrom, Q.T., Bauchet, L., Davis, F.G., Deltour, I., Fisher, J.L., Langer, C.E., Pekmezci, M., Schwartzbaum, J.A., Turner, M.C., Walsh, K.M., Wrensch, M.R. and Barnholtz-Sloan, J.S. The epidemiology of glioma in adults: a "state of the science" review. *Neuro-Oncology.* 2014, **16**(7), pp.896-913.
17. Kesari, S. Understanding Glioblastoma Tumor Biology: The Potential to Improve Current Diagnosis and Treatments. *Seminars in Oncology.* 2011, **38**, pp.S2-S10.
18. Grossman, S.A. and Batara, J.F. Current management of glioblastoma multiforme. *Seminars in Oncology.* 2004, **31**(5), pp.635-644.
19. Hide, T., Makino, K., Nakamura, H., Yano, S., Anai, S., Takezaki, T., Kuroda, J.-i., Shinojima, N., Ueda, Y. and Kuratsu, J.-i. New treatment strategies to eradicate cancer stem cells and niches in glioblastoma. *Neurologia medico-chirurgica.* 2013, **53**(11), pp.764-772.
20. Singh, S.K., Hawkins, C., Clarke, I.D., Squire, J.A., Bayani, J., Hide, T., Henkelman, R.M., Cusimano, M.D. and Dirks, P.B. Identification of human brain tumour initiating cells. *Nature.* 2004, **432**(7015), pp.396-401.
21. Sottoriva, A., Spiteri, I., Piccirillo, S.G., Touloumis, A., Collins, V.P., Marioni, J.C., Curtis, C., Watts, C. and Tavaré, S. Intratumor heterogeneity in human glioblastoma reflects cancer evolutionary dynamics. *Proceedings of the National Academy of Sciences.* 2013, **110**(10), pp.4009-4014.
22. Wechsler-Reya, R. and Scott, M.P. The Developmental Biology of Brain Tumors. *Annual Review of Neuroscience.* 2001, **24**(1), pp.385-428.
23. Zhu, Y. and Parada, L.F. The Molecular and Genetic Basis of Neurological Tumours. *Nature Reviews Cancer.* 2002, **2**(8), pp.616-626.

24. Huse, J.T. and Holland, E.C. Targeting brain cancer: advances in the molecular pathology of malignant glioma and medulloblastoma. *Nature Reviews Cancer.* 2010, **10**(5), pp.319-331.
25. Patel, A.P., Tirosh, I., Trombetta, J.J., Shalek, A.K., Gillespie, S.M., Wakimoto, H., Cahill, D.P., Nahed, B.V., Curry, W.T., Martuza, R.L., Louis, D.N., Rozenblatt-Rosen, O., Suva, M.L., Regev, A. and Bernstein, B.E. Single-cell RNA-seq highlights intratumoral heterogeneity in primary glioblastoma. *Science.* 2014, **344**(6190), pp.1396-1401.
26. Louis, D.N., Perry, A., Reifenberger, G., von Deimling, A., Figarella-Branger, D., Cavenee, W.K., Ohgaki, H., Wiestler, O.D., Kleihues, P. and Ellison, D.W. The 2016 World Health Organization Classification of Tumors of the Central Nervous System: a summary. *Acta Neuropathol.* 2016, **131**(6), pp.803-820.
27. Ohgaki, H. and Kleihues, P. The Definition of Primary and Secondary Glioblastoma. *Clinical Cancer Research.* 2013, **19**(4), pp.764-772.
28. Smith, C. and Ironside, J.W. Diagnosis and pathogenesis of gliomas. *Current Diagnostic Pathology.* 2007, **13**(3), pp.180-192.
29. Bush, N.A.O., Chang, S.M. and Berger, M.S. Current and future strategies for treatment of glioma. *Neurosurgical Review.* 2017, **40**(1), pp.1-14.
30. Lacroix, M., Abi-Said, D., Fourney, D.R., Gokaslan, Z.L., Shi, W., DeMonte, F., Lang, F.F., McCutcheon, I.E., Hassenbusch, S.J., Holland, E., Hess, K., Michael, C., Miller, D. and Sawaya, R. A multivariate analysis of 416 patients with glioblastoma multiforme: prognosis, extent of resection, and survival. *Journal of Neurosurgery.* 2001, **95**(2), pp.190-198.
31. McGirt, M.J., Chaichana, K.L., Gathinji, M., Attenello, F.J., Than, K., Olivi, A., Weingart, J.D., Brem, H. and Quiñones-Hinojosa, A.r. Independent association of extent of resection with survival in patients with malignant brain astrocytoma. *Journal of Neurosurgery.* 2009, **110**(1), pp.156-162.
32. Wrensch, M., Jenkins, R.B., Chang, J.S., Yeh, R.-F., Xiao, Y., Decker, P.A., Ballman, K.V., Berger, M., Buckner, J.C. and Chang, S. Variants in the CDKN2B and RTEL1 regions are associated with high-grade glioma susceptibility. *Nature genetics.* 2009, **41**(8), p.905.
33. Kuhnt, D., Becker, A., Ganslandt, O., Bauer, M., Buchfelder, M. and Nimsky, C. Correlation of the extent of tumor volume resection and patient survival in surgery of glioblastoma multiforme with high-field intraoperative MRI guidance. *Neuro-Oncology.* 2011, **13**(12), pp.1339-1348.
34. Roder, C., Bisdas, S., Ebner, F.H., Honegger, J., Naegele, T., Ernemann, U. and Tatagiba, M. Maximizing the extent of resection and survival benefit of patients in glioblastoma surgery: High-field iMRI versus conventional and 5-ALA-assisted surgery. *European Journal of Surgical Oncology (EJSO).* 2014, **40**(3), pp.297-304.

35. Hadjipanayis, C.G., Widhalm, G. and Stummer, W. What is the Surgical Benefit of Utilizing 5-Aminolevulinic Acid for Fluorescence-Guided Surgery of Malignant Gliomas? *Neurosurgery.* 2015, **77**(5), pp.663-673.
36. Zhao, S., Wu, J., Wang, C., Liu, H., Dong, X., Shi, C., Shi, C., Liu, Y., Teng, L., Han, D., Chen, X., Yang, G., Wang, L., Shen, C. and Li, H. Intraoperative Fluorescence-Guided Resection of High-Grade Malignant Gliomas Using 5-Aminolevulinic Acid–Induced Porphyrins: A Systematic Review and Meta-Analysis of Prospective Studies. *PLoS ONE.* 2013, **8**(5), pp.e63682-e63682.
37. Walker, M.D., Green, S.B., Byar, D.P., Alexander, E., Batzdorf, U., Brooks, W.H., Hunt, W.E., MacCarty, C.S., Mahaley, M.S., Mealey, J., Owens, G., Ransohoff, J., Robertson, J.T., Shapiro, W.R., Smith, K.R., Wilson, C.B. and Strike, T.A. Randomized Comparisons of Radiotherapy and Nitrosoureas for the Treatment of Malignant Glioma after Surgery. *New England Journal of Medicine.* 1980, **303**(23), pp.1323-1329.
38. Walker, M.D., Alexander, E., Hunt, W.E., MacCarty, C.S., Mahaley, M.S., Mealey, J., Norrell, H.A., Owens, G., Ransohoff, J., Wilson, C.B., Gehan, E.A. and Strike, T.A. Evaluation of BCNU and/or radiotherapy in the treatment of anaplastic gliomas. *Journal of Neurosurgery.* 1978, **49**(3), pp.333-343.
39. Andersen, A. Postoperative irradiation of glioblastomas: results in a randomized series. *Acta radiologica: oncology, radiation, physics, biology.* 1978, **17**(6), pp.475-484.
40. Kristiansen, K., Hagen, S., Kollevold, T., Torvik, A., Holme, I., Stat, M., Nesbakken, R., Hatlevoll, R., Lindgren, M., Brun, A., Lindgren, S., Notter, G., Andersen, A.P. and Elgen, K. Combined modality therapy of operated astrocytomas grade III and IV. Confirmation of the value of postoperative irradiation and lack of potentiation of bleomycin on survival time: A prospective multicenter trial of the scandinavian glioblastoma study grou. *Cancer.* 1981, **47**(4), pp.649-652.
41. Sandberg-Wollheim, M., Malmström, P., Strömblad, L.G., Anderson, H., Borgström, S., Brun, A., Cronqvist, S., Hougaard, K. and Salford, L.G. A randomized study of chemotherapy with procarbazine, vincristine, and lomustine with and without radiation therapy for astrocytoma grades 3 and/or 4. *Cancer.* 1991, **68**(1), pp.22-29.
42. Shapiro, W.R. and Young, D.F. Treatment of malignant glioma: A controlled study of chemotherapy and irradiation. *Archives of neurology.* 1976, **33**(7), pp.494-500.
43. Walker, M.D., Strike, T.A. and Sheline, G.E. An analysis of dose-effect relationship in the radiotherapy of malignant gliomas. *International journal of radiation oncology, biology, physics.* 1979, **5**(10), pp.1725-1731.
44. Chang, C.H., Horton, J., Schoenfeld, D., Salazer, O., Perez-Tamayo, R., Kramer, S., Weinstein, A., Nelson, J.S. and Tsukada, Y. Comparison of

postoperative radiotherapy and combined postoperative radiotherapy and chemotherapy in the multidisciplinary management of malignant gliomas. A joint radiation therapy oncology group and eastern cooperative oncology group study. *Cancer.* 1983, **52**(6), pp.997-1007.

45. Bleehen, N.M. and Stenning, S.P. A Medical Research Council trial of two radiotherapy doses in the treatment of grades 3 and 4 astrocytoma. The Medical Research Council Brain Tumour Working Party. *British journal of cancer.* 1991, **64**(4), pp.769-774.
46. Barani, I.J. and Larson, D.A. Radiation therapy of glioblastoma. *Cancer treatment and research.* 2015, **163**, pp.49-73.
47. Network, N.C.C. *Clinical Practice Guidelines in Oncology: Central nervous system cancers [v.1.2015].* Unpublished, 2015.
48. Carlsson, S.K., Brothers, S.P. and Wahlestedt, C. Emerging treatment strategies for glioblastoma multiforme. *EMBO Molecular Medicine.* 2014, **6**(11), pp.1359-1370.
49. Stupp, R., Hegi, M.E., Mason, W.P., van den Bent, M.J., Taphoorn, M.J.B., Janzer, R.C., Ludwin, S.K., Allgeier, A., Fisher, B., Belanger, K., Hau, P., Brandes, A.A., Gijtenbeek, J., Marosi, C., Vecht, C.J., Mokhtari, K., Wesseling, P., Villa, S., Eisenhauer, E., Gorlia, T., Weller, M., Lacombe, D., Cairncross, J.G. and Mirimanoff, R.-O. Effects of radiotherapy with concomitant and adjuvant temozolomide versus radiotherapy alone on survival in glioblastoma in a randomised phase III study: 5-year analysis of the EORTC-NCIC trial. *The Lancet Oncology.* 2009, **10**(5), pp.459-466.
50. Tobias, A., Ahmed, A., Moon, K.-S. and Lesniak, M.S. The art of gene therapy for glioma: a review of the challenging road to the bedside. *Journal of Neurology, Neurosurgery & Psychiatry.* 2013, **84**(2), pp.213-222.
51. Rainov, N.G. A Phase III Clinical Evaluation of Herpes Simplex Virus Type 1 Thymidine Kinase and Ganciclovir Gene Therapy as an Adjuvant to Surgical Resection and Radiation in Adults with Previously Untreated Glioblastoma Multiforme. *Human Gene Therapy.* 2000, **11**(17), pp.2389-2401.
52. Colombo, F., Barzon, L., Franchin, E., Pacenti, M., Pinna, V., Danieli, D., Zanusso, M. and Palù, G. Combined HSV-TK/IL-2 gene therapy in patients with recurrent glioblastoma multiforme: biological and clinical results. *Cancer Gene Therapy.* 2005, **12**(10), pp.835-848.
53. Freeman, G.J., Long, A.J., Iwai, Y., Bourque, K., Chernova, T., Nishimura, H., Fitz, L.J., Malenkovich, N., Okazaki, T., Byrne, M.C., Horton, H.F., Fouser, L., Carter, L., Ling, V., Bowman, M.R., Carreno, B.M., Collins, M., Wood, C.R. and Honjo, T. Engagement of the Pd-1 Immunoinhibitory Receptor by a Novel B7 Family Member Leads to Negative Regulation of Lymphocyte Activation. *The Journal of Experimental Medicine.* 2000, **192**(7), pp.1027-1034.

54. Reardon, D.A., Kaley, T.J., Dietrich, J., Lim, M., Dunn, G.P., Gan, H.K., Cloughesy, T.F., Clarke, J.L., Park, A.J. and Macri, M.J. *Phase 2 study to evaluate the clinical efficacy and safety of MEDI4736 (durvalumab) in patients with glioblastoma (GBM).* American Society of Clinical Oncology. 2016.
55. Polyzoidis, S. and Ashkan, K. DCVax®-L—Developed by Northwest Biotherapeutics. *Human Vaccines & Immunotherapeutics.* 2014, **10**(11), pp.3139-3145.
56. Liau, L.M., Ashkan, K., Tran, D.D., Campian, J.L., Trusheim, J.E., Cobbs, C.S., Heth, J.A., Salacz, M., Taylor, S. and D'Andre, S.D. First results on survival from a large Phase 3 clinical trial of an autologous dendritic cell vaccine in newly diagnosed glioblastoma. *Journal of translational medicine.* 2018, **16**(1), p.142.
57. Khasraw, M., Ameratunga, M. and Grommes, C. Bevacizumab for the treatment of high-grade glioma: an update after Phase III trials. *Expert Opinion on Biological Therapy.* 2014, **14**(5), pp.729-740.
58. Khasraw, M., Ameratunga, M.S., Grant, R., Wheeler, H. and Pavlakis, N. Antiangiogenic therapy for high-grade glioma. *Cochrane Database of Systematic Reviews.* 2014.
59. Gilbert, M.R., Dignam, J.J., Armstrong, T.S., Wefel, J.S., Blumenthal, D.T., Vogelbaum, M.A., Colman, H., Chakravarti, A., Pugh, S., Won, M., Jeraj, R., Brown, P.D., Jaeckle, K.A., Schiff, D., Stieber, V.W., Brachman, D.G., Werner-Wasik, M., Tremont-Lukats, I.W., Sulman, E.P., Aldape, K.D., Curran, W.J. and Mehta, M.P. A Randomized Trial of Bevacizumab for Newly Diagnosed Glioblastoma. *New England Journal of Medicine.* 2014, **370**(8), pp.699-708.
60. Perez-Soler, R. HER1/EGFR targeting: refining the strategy. *The Oncologist.* 2004, **9**(1), pp.58-67.
61. Heimberger, A.B., Crotty, L.E., Archer, G.E., Hess, K.R., Wikstrand, C.J., Friedman, A.H., Friedman, H.S., Bigner, D.D. and Sampson, J.H. Epidermal growth factor receptor VIII peptide vaccination is efficacious against established intracerebral tumors. *Clinical cancer research : an official journal of the American Association for Cancer Research.* 2003, **9**(11), pp.4247-4254.
62. Zussman, B.M. and Engh, J.A. Outcomes of the ACT III study: Rindopepimut (CDX-110) therapy for glioblastoma. *Neurosurgery.* 2015, **76**(6), p.N17.
63. Weller, M., Butowski, N., Tran, D., Recht, L., Lim, M., Hirte, H., Ashby, L., Mechtler, L., Goldlust, S., Iwamoto, F., Drappatz, J., O'Rourke, D., Wong, M., Finocchiaro, G., Perry, J., Wick, W., He, Y., Davis, T., Stupp, R. and Sampson, J. ATIM-03. ACT IV: An international, double-blind, phase 3 trial of rindopepimut in newly diagnosed, EGFRvIII-expressing glioblastoma. *Neuro-Oncology.* 2016, **18**(suppl_6), pp.vi17-vi18.

64. Marusyk, A. and Polyak, K. Tumor heterogeneity: causes and consequences. *Biochimica et Biophysica Acta (BBA)-Reviews on Cancer.* 2010, **1805**(1), pp.105-117.
65. Soeda, A., Hara, A., Kunisada, T., Yoshimura, S.-i., Iwama, T. and Park, D.M. The Evidence of Glioblastoma Heterogeneity. *Scientific Reports.* 2015, **5**(1), pp.7979-7979.
66. Nickel, G.C., Barnholtz-Sloan, J., Gould, M.P., McMahon, S., Cohen, A., Adams, M.D., Guda, K., Cohen, M., Sloan, A.E. and LaFramboise, T. Characterizing Mutational Heterogeneity in a Glioblastoma Patient with Double Recurrence. *PLoS ONE.* 2012, **7**(4), pp.e35262-e35262.
67. McLendon, R., Friedman, A., Bigner, D., Van Meir, E.G., Brat, D.J., M. Mastrogianakis, G., Olson, J.J., Mikkelsen, T., Lehman, N., Aldape, K., Alfred Yung, W.K., Bogler, O., VandenBerg, S., Berger, M., Prados, M., Muzny, D., Morgan, M., Scherer, S., Sabo, A., Nazareth, L., Lewis, L., Hall, O., Zhu, Y., Ren, Y., Alvi, O., Yao, J., Hawes, A., Jhangiani, S., Fowler, G., San Lucas, A., Kovar, C., Cree, A., Dinh, H., Santibanez, J., Joshi, V., Gonzalez-Garay, M.L., Miller, C.A., Milosavljevic, A., Donehower, L., Wheeler, D.A., Gibbs, R.A., Cibulskis, K., Sougnez, C., Fennell, T., Mahan, S., Wilkinson, J., Ziaugra, L., Onofrio, R., Bloom, T., Nicol, R., Ardlie, K., Baldwin, J., Gabriel, S., Lander, E.S., Ding, L., Fulton, R.S., McLellan, M.D., Wallis, J., Larson, D.E., Shi, X., Abbott, R., Fulton, L., Chen, K., Koboldt, D.C., Wendl, M.C., Meyer, R., Tang, Y., Lin, L., Osborne, J.R., Dunford-Shore, B.H., Miner, T.L., Delehaunty, K., Markovic, C., Swift, G., Courtney, W., Pohl, C., Abbott, S., Hawkins, A., Leong, S., Haipek, C., Schmidt, H., Wiechert, M., Vickery, T., Scott, S., Dooling, D.J., Chinwalla, A., Weinstock, G.M., Mardis, E.R., Wilson, R.K., Getz, G., Winckler, W., Verhaak, R.G.W., Lawrence, M.S., O'Kelly, M., Robinson, J., Alexe, G., Beroukhim, R., Carter, S., Chiang, D., Gould, J., Gupta, S., Korn, J., Mermel, C., Mesirov, J., Monti, S., Nguyen, H., Parkin, M., Reich, M., Stransky, N., Weir, B.A., Garraway, L., Golub, T., Meyerson, M., Chin, L., Protopopov, A., Zhang, J., Perna, I., Aronson, S., Sathiamoorthy, N., Ren, G., Yao, J., Wiedemeyer, W.R., Kim, H., Won Kong, S., Xiao, Y., Kohane, I.S., Seidman, J., Park, P.J., Kucherlapati, R., Laird, P.W., Cope, L., Herman, J.G., Weisenberger, D.J., Pan, F., Van Den Berg, D., Van Neste, L., Mi Yi, J., Schuebel, K.E., Baylin, S.B., Absher, D.M., Li, J.Z., Southwick, A., Brady, S., Aggarwal, A., Chung, T., Sherlock, G., Brooks, J.D., Myers, R.M., Spellman, P.T., Purdom, E., Jakkula, L.R., Lapuk, A.V., Marr, H., Dorton, S., Gi Choi, Y., Han, J., Ray, A., Wang, V., Durinck, S., Robinson, M., Wang, N.J., Vranizan, K., Peng, V., Van Name, E., Fontenay, G.V., Ngai, J., Conboy, J.G., Parvin, B., Feiler, H.S., Speed, T.P., Gray, J.W., Brennan, C., Socci, N.D., Olshen, A., Taylor, B.S., Lash, A., Schultz, N., Reva, B., Antipin, Y., Stukalov, A., Gross, B., Cerami, E., Qing Wang, W., Qin, L.-X., Seshan, V.E., Villafania, L., Cavatore, M., Borsu, L., Viale, A., Gerald, W.,

Sander, C., Ladanyi, M., Perou, C.M., Neil Hayes, D., Topal, M.D., Hoadley, K.A., Qi, Y., Balu, S., Shi, Y., Wu, J., Penny, R., Bittner, M., Shelton, T., Lenkiewicz, E., Morris, S., Beasley, D., Sanders, S., Kahn, A., Sfeir, R., Chen, J., Nassau, D., Feng, L., Hickey, E., Zhang, J., Weinstein, J.N., Barker, A., Gerhard, D.S., Vockley, J., Compton, C., Vaught, J., Fielding, P., Ferguson, M.L., Schaefer, C., Madhavan, S., Buetow, K.H., Collins, F., Good, P., Guyer, M., Ozenberger, B., Peterson, J. and Thomson, E. Comprehensive genomic characterization defines human glioblastoma genes and core pathways. *Nature.* 2008, **455**(7216), pp.1061-1068.

68. Brennan, C., Momota, H., Hambardzumyan, D., Ozawa, T., Tandon, A., Pedraza, A. and Holland, E. Glioblastoma Subclasses Can Be Defined by Activity among Signal Transduction Pathways and Associated Genomic Alterations. *PLoS ONE.* 2009, **4**(11), pp.e7752-e7752.
69. Mischel, P.S., Shai, R., Shi, T., Horvath, S., Lu, K.V., Choe, G., Seligson, D., Kremen, T.J., Palotie, A., Liau, L.M., Cloughesy, T.F. and Nelson, S.F. Identification of molecular subtypes of glioblastoma by gene expression profiling. *Oncogene.* 2003, **22**(15), pp.2361-2373.
70. Kitange, G.J., Templeton, K.L. and Jenkins, R.B. Recent advances in the molecular genetics of primary gliomas. *Current Opinion in Oncology.* 2003, **15**(3), pp.197-203.
71. Parsons, D.W., Jones, S., Zhang, X., Lin, J.C.H., Leary, R.J., Angenendt, P., Mankoo, P., Carter, H., Siu, I.M., Gallia, G.L., Olivi, A., McLendon, R., Rasheed, B.A., Keir, S., Nikolskaya, T., Nikolsky, Y., Busam, D.A., Tekleab, H., Diaz, L.A., Hartigan, J., Smith, D.R., Strausberg, R.L., Marie, S.K.N., Shinjo, S.M.O., Yan, H., Riggins, G.J., Bigner, D.D., Karchin, R., Papadopoulos, N., Parmigiani, G., Vogelstein, B., Velculescu, V.E. and Kinzler, K.W. An Integrated Genomic Analysis of Human Glioblastoma Multiforme. *Science.* 2008, **321**(5897), pp.1807-1812.
72. Young, R.M., Jamshidi, A., Davis, G. and Sherman, J.H. Current trends in the surgical management and treatment of adult glioblastoma. *Annals of translational medicine.* 2015, **3**(9), pp.121-121.
73. Alifieris, C. and Trafalis, D.T. Glioblastoma multiforme: Pathogenesis and treatment. *Pharmacology & Therapeutics.* 2015, **152**, pp.63-82.
74. Verhaak, R.G.W., Hoadley, K.A., Purdom, E., Wang, V., Qi, Y., Wilkerson, M.D., Miller, C.R., Ding, L., Golub, T., Mesirov, J.P., Alexe, G., Lawrence, M., O'Kelly, M., Tamayo, P., Weir, B.A., Gabriel, S., Winckler, W., Gupta, S., Jakkula, L., Feiler, H.S., Hodgson, J.G., James, C.D., Sarkaria, J.N., Brennan, C., Kahn, A., Spellman, P.T., Wilson, R.K., Speed, T.P., Gray, J.W., Meyerson, M., Getz, G., Perou, C.M. and Hayes, D.N. Integrated Genomic Analysis Identifies Clinically Relevant Subtypes of Glioblastoma Characterized by Abnormalities in PDGFRA, IDH1, EGFR, and NF1. *Cancer Cell.* 2010, **17**(1), pp.98-110.

75. Phillips, H.S., Kharbanda, S., Chen, R., Forrest, W.F., Soriano, R.H., Wu, T.D., Misra, A., Nigro, J.M., Colman, H., Soroceanu, L., Williams, P.M., Modrusan, Z., Feuerstein, B.G. and Aldape, K. Molecular subclasses of high-grade glioma predict prognosis, delineate a pattern of disease progression, and resemble stages in neurogenesis. *Cancer Cell.* 2006, **9**(3), pp.157-173.
76. Jung, V., Romeike, B.F.M., Henn, W., Feiden, W., Moringlane, J.R., Zang, K.D. and Urbschat, S. Evidence of Focal Genetic Microheterogeneity in Glioblastoma Multiforme by Area-Specific CGH on Microdissected Tumor Cells. *Journal of Neuropathology & Experimental Neurology.* 1999, **58**(9), pp.993-999.
77. Brell, M., Ibáñez, J., Felpete, A., Burguera, B., Frontera, M. and Couce, M.E. Quantitative analysis of matrix metalloproteinase-2 mRNA expression in central and peripheral regions of gliomas. *Brain Tumor Pathology.* 2011, **28**(2), pp.137-144.
78. Bello, L., Francolini, M., Marthyn, P., Zhang, J., Carroll, R.S., Nikas, D.C., Strasser, J.F., Villani, R., Cheresh, D.A. and Black, P.M. αvβ3 and αvβ5 Integrin Expression in Glioma Periphery. *Neurosurgery.* 2001, **49**(2), pp.380-390.
79. Pistollato, F., Abbadi, S., Rampazzo, E., Persano, L., Puppa, A.D., Frasson, C., Sarto, E., Scienza, R., D'Avella, D. and Basso, G. Intratumoral Hypoxic Gradient Drives Stem Cells Distribution and MGMT Expression in Glioblastoma. *STEM CELLS.* 2010, pp.N/A-N/A.
80. Hegi, M.E., Diserens, A.-C., Gorlia, T., Hamou, M.-F., de Tribolet, N., Weller, M., Kros, J.M., Hainfellner, J.A., Mason, W., Mariani, L., Bromberg, J.E.C., Hau, P., Mirimanoff, R.O., Cairncross, J.G., Janzer, R.C. and Stupp, R. MGMT Gene Silencing and Benefit from Temozolomide in Glioblastoma. *New England Journal of Medicine.* 2005, **352**(10), pp.997-1003.
81. Gilbert, M.R., Wang, M., Aldape, K.D., Stupp, R., Hegi, M., Jaeckle, K.A., Armstrong, T.S., Wefel, J.S., Won, M., Blumenthal, D.T., Mahajan, A., Schultz, C.J., Erridge, S.C., Brown, P.D., Chakravarti, A., Curran, W.J. and Mehta, M.P. RTOG 0525: A randomized phase III trial comparing standard adjuvant temozolomide (TMZ) with a dose-dense (dd) schedule in newly diagnosed glioblastoma (GBM). *Journal of Clinical Oncology.* 2011, **29**(15_suppl), pp.2006-2006.
82. Pegg, A.E. Repair of O6-alkylguanine by alkyltransferases. *Mutation Research/Reviews in Mutation Research.* 2000, **462**(2-3), pp.83-100.
83. Thon, N., Eigenbrod, S., Grasbon-Frodl, E.M., Lutz, J., Kreth, S., Popperl, G., Belka, C., Kretzschmar, H.A., Tonn, J.C. and Kreth, F.W. Predominant influence of MGMT methylation in non-resectable glioblastoma after radiotherapy plus temozolomide. *Journal of Neurology, Neurosurgery & Psychiatry.* 2011, **82**(4), pp.441-446.

84. Baur, M., Preusser, M., Piribauer, M., Elandt, K., Hassler, M., Hudec, M., Dittrich, C. and Marosi, C. Frequent MGMT (06-methylguanine-DNA methyltransferase) hypermethylation in long-term survivors of glioblastoma: a single institution experience. *Radiology and Oncology*. 2010, **44**(2).
85. Hegi, M.E., Liu, L., Herman, J.G., Stupp, R., Wick, W., Weller, M., Mehta, M.P. and Gilbert, M.R. Correlation of O 6 -Methylguanine Methyltransferase (MGMT) Promoter Methylation With Clinical Outcomes in Glioblastoma and Clinical Strategies to Modulate MGMT Activity. *Journal of Clinical Oncology*. 2008, **26**(25), pp.4189-4199.
86. Juillerat-Jeanneret, L., Bernasconi, C.C., Bricod, C., Gros, S., Trepey, S., Benhattar, J. and Janzer, R.C. Heterogeneity of Human Glioblastoma: Glutathione-S-Transferase and Methylguanine-Methyltransferase. *Cancer Investigation*. 2008, **26**(6), pp.597-609.
87. Szerlip, N.J., Pedraza, A., Chakravarty, D., Azim, M., McGuire, J., Fang, Y., Ozawa, T., Holland, E.C., Huse, J.T., Jhanwar, S., Leversha, M.A., Mikkelsen, T. and Brennan, C.W. Intratumoral heterogeneity of receptor tyrosine kinases EGFR and PDGFRA amplification in glioblastoma defines subpopulations with distinct growth factor response. *Proceedings of the National Academy of Sciences*. 2012, **109**(8), pp.3041-3046.
88. Huang, H.J.S., Nagane, M., Klingbeil, C.K., Lin, H., Nishikawa, R., Ji, X.-D., Huang, C.-M., Gill, G.N., Wiley, H.S. and Cavenee, W.K. The Enhanced Tumorigenic Activity of a Mutant Epidermal Growth Factor Receptor Common in Human Cancers Is Mediated by Threshold Levels of Constitutive Tyrosine Phosphorylation and Unattenuated Signaling. *Journal of Biological Chemistry*. 1997, **272**(5), pp.2927-2935.
89. Snuderl, M., Fazlollahi, L., Le, L.P., Nitta, M., Zhelyazkova, B.H., Davidson, C.J., Akhavanfard, S., Cahill, D.P., Aldape, K.D., Betensky, R.A., Louis, D.N. and Iafrate, A.J. Mosaic Amplification of Multiple Receptor Tyrosine Kinase Genes in Glioblastoma. *Cancer Cell*. 2011, **20**(6), pp.810-817.
90. Little, S.E., Popov, S., Jury, A., Bax, D.A., Doey, L., Al-Sarraj, S., Jurgensmeier, J.M. and Jones, C. Receptor Tyrosine Kinase Genes Amplified in Glioblastoma Exhibit a Mutual Exclusivity in Variable Proportions Reflective of Individual Tumor Heterogeneity. *Cancer Research*. 2012, **72**(7), pp.1614-1620.
91. Vital, A.L., Tabernero, M.D., Crespo, I., Rebelo, O., Tão, H., Gomes, F., Lopes, M.C. and Orfao, A. Intratumoral patterns of clonal evolution in gliomas. *neurogenetics*. 2010, **11**(2), pp.227-239.
92. Vartanian, A., Singh, S.K., Agnihotri, S., Jalali, S., Burrell, K., Aldape, K.D. and Zadeh, G. GBM's multifaceted landscape: highlighting regional and microenvironmental heterogeneity. *Neuro-oncology*. 2014, **16**(9), pp.1167-1175.

93. Singh, S.K., Clarke, I.D., Hide, T. and Dirks, P.B. Cancer stem cells in nervous system tumors. *Oncogene.* 2004, **23**(43), pp.7267-7273.
94. Bonnet, D. and Dick, J.E. Human acute myeloid leukemia is organized as a hierarchy that originates from a primitive hematopoietic cell. *Nature Medicine.* 1997, **3**(7), pp.730-737.
95. Al-Hajj, M., Wicha, M.S., Benito-Hernandez, A., Morrison, S.J. and Clarke, M.F. Prospective identification of tumorigenic breast cancer cells. *Proceedings of the National Academy of Sciences.* 2003, **100**(7), pp.3983-3988.
96. Emmenegger, B.A. and Wechsler-Reya, R.J. Stem cells and the origin and propagation of brain tumors. *J Child Neurol.* 2008, **23**(10), pp.1172-1178.
97. Kong, D.S. Cancer stem cells in brain tumors and their lineage hierarchy. *Int J Stem Cells.* 2012, **5**(1), pp.12-15.
98. Modrek, A.S., Bayin, N.S. and Placantonakis, D.G. Brain stem cells as the cell of origin in glioma. *World J Stem Cells.* 2014, **6**(1), pp.43-52.
99. Friedmann-Morvinski, D., Bushong, E.A., Ke, E., Soda, Y., Marumoto, T., Singer, O., Ellisman, M.H. and Verma, I.M. Dedifferentiation of Neurons and Astrocytes by Oncogenes Can Induce Gliomas in Mice. *Science.* 2012, **338**(6110), pp.1080-1084.
100. Sanai, N., Alvarez-Buylla, A. and Berger, M.S. Neural stem cells and the origin of gliomas. *The New England journal of medicine.* 2005, **353**(8), pp.811-822.
101. Sanai, N., Tramontin, A.D., Quiñones-Hinojosa, A., Barbaro, N.M., Gupta, N., Kunwar, S., Lawton, M.T., McDermott, M.W., Parsa, A.T., Manuel-García Verdugo, J., Berger, M.S. and Alvarez-Buylla, A. Unique astrocyte ribbon in adult human brain contains neural stem cells but lacks chain migration. *Nature.* 2004, **427**(6976), pp.740-744.
102. Quiñones-Hinojosa, A., Sanai, N., Soriano-Navarro, M., Gonzalez-Perez, O., Mirzadeh, Z., Gil-Perotin, S., Romero-Rodriguez, R., Berger, M.S., Garcia-Verdugo, J.M. and Alvarez-Buylla, A. Cellular composition and cytoarchitecture of the adult human subventricular zone: a niche of neural stem cells. *J Comp Neurol.* 2006, **494**(3), pp.415-434.
103. Galli, R., Binda, E., Orfanelli, U., Cipelletti, B., Gritti, A., De Vitis, S., Fiocco, R., Foroni, C., Dimeco, F. and Vescovi, A. Isolation and Characterization of Tumorigenic, Stem-like Neural Precursors from Human Glioblastoma. *Cancer Research.* 2004, **64**(19), pp.7011-7021.
104. Lee, J.H., Lee, J.E., Kahng, J.Y., Kim, S.H., Park, J.S., Yoon, S.J., Um, J.Y., Kim, W.K., Lee, J.K., Park, J., Kim, E.H., Chung, W.S., Ju, Y.S., Park, S.H., Chang, J.H. and Kang, S.G. Human glioblastoma arises from subventricular zone cells with low-level driver mutations. *Nature.* 2018, **560**(7717), pp.243-247.
105. Murat, A., Migliavacca, E., Gorlia, T., Lambiv, W.L., Shay, T., Hamou, M.-F., de Tribolet, N., Regli, L., Wick, W., Kouwenhoven, M.C.M., Hainfellner, J.A., Heppner, F.L., Dietrich, P.-Y., Zimmer, Y., Cairncross, J.G., Janzer, R.-C.,

Domany, E., Delorenzi, M., Stupp, R. and Hegi, M.E. Stem Cell–Related "Self-Renewal" Signature and High Epidermal Growth Factor Receptor Expression Associated With Resistance to Concomitant Chemoradiotherapy in Glioblastoma. *Journal of Clinical Oncology*. 2008, **26**(18), pp.3015-3024.

106. Bao, S., Wu, Q., McLendon, R.E., Hao, Y., Shi, Q., Hjelmeland, A.B., Dewhirst, M.W., Bigner, D.D. and Rich, J.N. Glioma stem cells promote radioresistance by preferential activation of the DNA damage response. *Nature*. 2006, **444**(7120), pp.756-760.
107. Liu, G., Yuan, X., Zeng, Z., Tunici, P., Ng, H., Abdulkadir, I.R., Lu, L., Irvin, D., Black, K.L. and Yu, J.S. Analysis of gene expression and chemoresistance of CD133+ cancer stem cells in glioblastoma. *Molecular cancer*. 2006, **5**, pp.67-67.
108. Reya, T., Morrison, S.J., Clarke, M.F. and Weissman, I.L. Stem cells, cancer, and cancer stem cells. *Nature*. 2001, **414**(6859), pp.105-111.
109. Lan, X., Jörg, D.J., Cavalli, F.M.G., Richards, L.M., Nguyen, L.V., Vanner, R.J., Guilhamon, P., Lee, L., Kushida, M.M., Pellacani, D., Park, N.I., Coutinho, F.J., Whetstone, H., Selvadurai, H.J., Che, C., Luu, B., Carles, A., Moksa, M., Rastegar, N., Head, R., Dolma, S., Prinos, P., Cusimano, M.D., Das, S., Bernstein, M., Arrowsmith, C.H., Mungall, A.J., Moore, R.A., Ma, Y., Gallo, M., Lupien, M., Pugh, T.J., Taylor, M.D., Hirst, M., Eaves, C.J., Simons, B.D. and Dirks, P.B. Fate mapping of human glioblastoma reveals an invariant stem cell hierarchy. *Nature*. 2017, **549**(7671), pp.227-232.
110. Spiegl-Kreinecker, S., Buchroithner, J., Elbling, L., Steiner, E., Wurm, G., Bodenteich, A., Fischer, J., Micksche, M. and Berger, W. Expression and functional activity of the ABC-transporter proteins P-glycoprotein and multidrug-resistance protein 1 in human brain tumor cells and astrocytes. *Journal of neuro-oncology*. 2002, **57**(1), pp.27-36.
111. Dean, M., Fojo, T. and Bates, S. Tumour stem cells and drug resistance. *Nature Reviews Cancer*. 2005, **5**(4), pp.275-284.
112. Chen, J., McKay, R.M. and Parada, L.F. Malignant Glioma: Lessons from Genomics, Mouse Models, and Stem Cells. *Cell*. 2012, **149**(1), pp.36-47.
113. Li, F., Tiede, B., Massagué, J. and Kang, Y. Beyond tumorigenesis: cancer stem cells in metastasis. *Cell Research*. 2007, **17**(1), pp.3-14.
114. Persano, L., Pistollato, F., Rampazzo, E., Della Puppa, A., Abbadi, S., Frasson, C., Volpin, F., Indraccolo, S., Scienza, R. and Basso, G. BMP2 sensitizes glioblastoma stem-like cells to Temozolomide by affecting HIF-1α stability and MGMT expression. *Cell Death & Disease*. 2012, **3**(10), pp.e412-e412.
115. Niu, C., Li, M., Ni, Y., Chen, J., Mei, J., Li, J. and Fu, X. Effect of all-trans retinoic acid on the proliferation and differentiation of brain tumor stem cells. *Journal of Experimental & Clinical Cancer Research*. 2010, **29**(1), pp.113-113.

116. Zhuang, W., Long, L., Zheng, B., Ji, W., Yang, N., Zhang, Q. and Liang, Z. Curcumin promotes differentiation of glioma-initiating cells by inducing autophagy. *Cancer Science.* 2012, **103**(4), pp.684-690.
117. Teres, S., Llado, V., Higuera, M., Barcelo-Coblijn, G., Martin, M.L., Noguera-Salva, M.A., Marcilla-Etxenike, A., Garcia-Verdugo, J.M., Soriano-Navarro, M., Saus, C., Gomez-Pinedo, U., Busquets, X. and Escriba, P.V. 2-Hydroxyoleate, a nontoxic membrane binding anticancer drug, induces glioma cell differentiation and autophagy. *Proceedings of the National Academy of Sciences.* 2012, **109**(22), pp.8489-8494.
118. Piccirillo, S.G.M., Reynolds, B.A., Zanetti, N., Lamorte, G., Binda, E., Broggi, G., Brem, H., Olivi, A., Dimeco, F. and Vescovi, A.L. Bone morphogenetic proteins inhibit the tumorigenic potential of human brain tumour-initiating cells. *Nature.* 2006, **444**(7120), pp.761-765.
119. Lee, J., Kotliarova, S., Kotliarov, Y., Li, A., Su, Q., Donin, N.M., Pastorino, S., Purow, B.W., Christopher, N., Zhang, W., Park, J.K. and Fine, H.A. Tumor stem cells derived from glioblastomas cultured in bFGF and EGF more closely mirror the phenotype and genotype of primary tumors than do serum-cultured cell lines. *Cancer Cell.* 2006, **9**(5), pp.391-403.
120. Joo, K.M., Kim, S.Y., Jin, X., Song, S.Y., Kong, D.-S., Lee, J., II, Jeon, J.W., Kim, M.H., Kang, B.G., Jung, Y., Jin, J., Hong, S.-C., Park, W.-Y., Lee, D.-S., Kim, H. and Nam, D.-H. Clinical and biological implications of CD133-positive and CD133-negative cells in glioblastomas. *Laboratory Investigation.* 2008, **88**(8), pp.808-815.
121. Beier, D., Hau, P., Proescholdt, M., Lohmeier, A., Wischhusen, J., Oefner, P.J., Aigner, L., Brawanski, A., Bogdahn, U. and Beier, C.P. CD133+ and CD133-Glioblastoma-Derived Cancer Stem Cells Show Differential Growth Characteristics and Molecular Profiles. *Cancer Research.* 2007, **67**(9), pp.4010-4015.
122. Wang, J., Sakariassen, P.Ø., Tsinkalovsky, O., Immervoll, H., Bøe, S.O., Svendsen, A., Prestegarden, L., Røsland, G., Thorsen, F., Stuhr, L., Molven, A., Bjerkvig, R. and Enger, P.Ø. CD133 negative glioma cells form tumors in nude rats and give rise to CD133 positive cells. *International Journal of Cancer.* 2008, **122**(4), pp.761-768.
123. Son, M.J., Woolard, K., Nam, D.-H., Lee, J. and Fine, H.A. SSEA-1 Is an Enrichment Marker for Tumor-Initiating Cells in Human Glioblastoma. *Cell Stem Cell.* 2009, **4**(5), pp.440-452.
124. Lathia, J.D., Mack, S.C., Mulkearns-Hubert, E.E., Valentim, C.L.L. and Rich, J.N. Cancer stem cells in glioblastoma. *Genes & Development.* 2015, **29**(12), pp.1203-1217.
125. Pollard, S.M., Yoshikawa, K., Clarke, I.D., Danovi, D., Stricker, S., Russell, R., Bayani, J., Head, R., Lee, M., Bernstein, M., Squire, J.A., Smith, A. and Dirks, P.

Glioma Stem Cell Lines Expanded in Adherent Culture Have Tumor-Specific Phenotypes and Are Suitable for Chemical and Genetic Screens. *Cell Stem Cell.* 2009, **4**(6), pp.568-580.

126. Wurdak, H., Zhu, S., Romero, A., Lorger, M., Watson, J., Chiang, C.-y., Zhang, J., Natu, V.S., Lairson, L.L., Walker, J.R., Trussell, C.M., Harsh, G.R., Vogel, H., Felding-Habermann, B., Orth, A.P., Miraglia, L.J., Rines, D.R., Skirboll, S.L. and Schultz, P.G. An RNAi Screen Identifies TRRAP as a Regulator of Brain Tumor-Initiating Cell Differentiation. *Cell Stem Cell.* 2010, **6**(1), pp.37-47.
127. Paulus, W., Baur, I., Beutler, A.S. and Reeves, S.A. Diffuse brain invasion of glioma cells requires beta 1 integrins. *Laboratory investigation.* 1996, **75**(6), pp.819-826.
128. Dandy, W.E. Removal of right cerebral hemisphere for certain tumors with hemiplegia. *Journal of the American Medical Association.* 1928, **90**(11), pp.823-823.
129. Burger, P.C., Dubois, P.J., Schold, S.C., Smith, K.R., Odom, G.L., Crafts, D.C. and Giangaspero, F. Computerized tomographic and pathologic studies of the untreated, quiescent, and recurrent glioblastoma multiforme. *Journal of Neurosurgery.* 1983, **58**(2), pp.159-169.
130. Gaspar, L.E., Fisher, B.J., Macdonald, D.R., Leber, D.V., Halperin, E.C., Schold, S.C. and Cairncross, J.G. Supratentorial malignant glioma: Patterns of recurrence and implications for external beam local treatment. *International Journal of Radiation Oncology*Biology*Physics.* 1992, **24**(1), pp.55-57.
131. Rao, Y. and Wu, J.Y. Neuronal migration and the evolution of the human brain. *Nature Neuroscience.* 2001, **4**(9), pp.860-862.
132. Cuddapah, V.A., Robel, S., Watkins, S. and Sontheimer, H. A neurocentric perspective on glioma invasion. *Nature Reviews Neuroscience.* 2014, **15**(7), pp.455-465.
133. Demuth, T. and Berens, M.E. Molecular Mechanisms of Glioma Cell Migration and Invasion. *Journal of Neuro-Oncology.* 2004, **70**(2), pp.217-228.
134. Paw, I., Carpenter, R.C., Watabe, K., Debinski, W. and Lo, H.-W. Mechanisms regulating glioma invasion. *Cancer Letters.* 2015, **362**(1), pp.1-7.
135. Beauchesne, P. Extra-Neural Metastases of Malignant Gliomas: Myth or Reality? *Cancers.* 2011, **3**(1), pp.461-477.
136. Hamilton, J.D., Rapp, M., Schneiderhan, T.M., Sabel, M., Hayman, A., Scherer, A., Kröpil, P., Budach, W., Kretschmar, U., Arne Gerber, P., Prabhu, S., Ginsberg, L.E., Bölke, E. and Matuschek, C. Glioblastoma Multiforme Metastasis Outside the CNS: Three Case Reports and Possible Mechanisms of Escape. *Journal of Clinical Oncology.* 2014, **32**(22), pp.e80-e84.
137. Lun, M., Lok, E., Gautam, S., Wu, E. and Wong, E.T. The natural history of extracranial metastasis from glioblastoma multiforme. *Journal of Neuro-Oncology.* 2011, **105**(2), pp.261-273.

138. Scherer, H.J. Structural development in gliomas. *American Journal of Cancer.* 1938, **34**(3), pp.333-351.
139. G. Gritsenko, P., Ilina, O. and Friedl, P. Interstitial guidance of cancer invasion. *The Journal of Pathology.* 2012, **226**(2), pp.185-199.
140. Montana, V. and Sontheimer, H. Bradykinin promotes the chemotactic invasion of primary brain tumors. *Journal of Neuroscience.* 2011, **31**(13), pp.4858-4867.
141. Ridley, A.J. Cell Migration: Integrating Signals from Front to Back. *Science.* 2003, **302**(5651), pp.1704-1709.
142. Friedl, P. and Alexander, S. Cancer Invasion and the Microenvironment: Plasticity and Reciprocity. *Cell.* 2011, **147**(5), pp.992-1009.
143. Friedl, P. Prespecification and plasticity: shifting mechanisms of cell migration. *Current Opinion in Cell Biology.* 2004, **16**(1), pp.14-23.
144. Cha, J., Kang, S.-G. and Kim, P. Strategies of Mesenchymal Invasion of Patient-derived Brain Tumors: Microenvironmental Adaptation. *Scientific Reports.* 2016, **6**(1), pp.24912-24912.
145. Zhong, J., Paul, A., Kellie, S.J. and O'Neill, G.M. Mesenchymal Migration as a Therapeutic Target in Glioblastoma. *Journal of Oncology.* 2010, **2010**, pp.1-17.
146. Sahai, E. and Marshall, C.J. Differing modes of tumour cell invasion have distinct requirements for Rho/ROCK signalling and extracellular proteolysis. *Nature Cell Biology.* 2003, **5**(8), pp.711-719.
147. Tamariz, E. and Grinnell, F. Modulation of Fibroblast Morphology and Adhesion during Collagen Matrix Remodeling. *Molecular Biology of the Cell.* 2002, **13**(11), pp.3915-3929.
148. Ballestrem, C., Hinz, B., Imhof, B.A. and Wehrle-Haller, B. Marching at the front and dragging behind. *The Journal of Cell Biology.* 2001, **155**(7), pp.1319-1332.
149. Friedl, P. and Wolf, K. Proteolytic interstitial cell migration: a five-step process. *Cancer and Metastasis Reviews.* 2009, **28**(1-2), pp.129-135.
150. Wolf, K., Wu, Y.I., Liu, Y., Geiger, J., Tam, E., Overall, C., Stack, M.S. and Friedl, P. Multi-step pericellular proteolysis controls the transition from individual to collective cancer cell invasion. *Nature Cell Biology.* 2007, **9**(8), pp.893-904.
151. Hagemann, C. A complete compilation of matrix metalloproteinase expression in human malignant gliomas. *World Journal of Clinical Oncology.* 2012, **3**(5), pp.67-67.
152. Koh, I., Cha, J., Park, J., Choi, J., Kang, S.-G. and Kim, P. The mode and dynamics of glioblastoma cell invasion into a decellularized tissue-derived extracellular matrix-based three-dimensional tumor model. *Scientific Reports.* 2018, **8**(1), pp.4608-4608.

153. Wolf, K. Amoeboid shape change and contact guidance: T-lymphocyte crawling through fibrillar collagen is independent of matrix remodeling by MMPs and other proteases. *Blood.* 2003, **102**(9), pp.3262-3269.
154. Lämmermann, T. and Sixt, M. Mechanical modes of 'amoeboid' cell migration. *Current Opinion in Cell Biology.* 2009, **21**(5), pp.636-644.
155. Lorentzen, A., Bamber, J., Sadok, A., Elson-Schwab, I. and Marshall, C.J. An ezrin-rich, rigid uropod-like structure directs movement of amoeboid blebbing cells. *Journal of Cell Science.* 2011, **124**(8), pp.1256-1267.
156. Paluch, E., Sykes, C., Prost, J. and Bornens, M. Dynamic modes of the cortical actomyosin gel during cell locomotion and division. *Trends in Cell Biology.* 2006, **16**(1), pp.5-10.
157. Lauffenburger, D.A. and Horwitz, A.F. Cell Migration: A Physically Integrated Molecular Process. *Cell.* 1996, **84**(3), pp.359-369.
158. Friedl, P. and Wolf, K. Tumour-cell invasion and migration: diversity and escape mechanisms. *Nature Reviews Cancer.* 2003, **3**(5), pp.362-374.
159. Pollard, T.D. and Borisy, G.G. Cellular Motility Driven by Assembly and Disassembly of Actin Filaments. *Cell.* 2003, **112**(4), pp.453-465.
160. Yamaguchi, H. and Condeelis, J. Regulation of the actin cytoskeleton in cancer cell migration and invasion. *Biochimica et Biophysica Acta (BBA) - Molecular Cell Research.* 2007, **1773**(5), pp.642-652.
161. Sahai, E. Mechanisms of cancer cell invasion. *Current Opinion in Genetics & Development.* 2005, **15**(1), pp.87-96.
162. Xue, C., Wyckoff, J., Liang, F., Sidani, M., Violini, S., Tsai, K.-L., Zhang, Z.-Y., Sahai, E., Condeelis, J. and Segall, J.E. Epidermal Growth Factor Receptor Overexpression Results in Increased Tumor Cell Motility In vivo Coordinately with Enhanced Intravasation and Metastasis. *Cancer Research.* 2006, **66**(1), pp.192-197.
163. Wang, L., Zhao, K.A.I., Ren, B., Zhu, M., Zhang, C., Zhao, P., Zhou, H.U.A., Chen, L.E.I., Yu, S. and Yang, X. Expression of cortactin in human gliomas and its effect on migration and invasion of glioma cells. *Oncology Reports.* 2015, **34**(4), pp.1815-1824.
164. Zhang, S. and Qi, Q. MTSS1 suppresses cell migration and invasion by targeting CTTN in glioblastoma. *Journal of Neuro-Oncology.* 2015, **121**(3), pp.425-431.
165. Jensen, R.L. Hypoxia in the tumorigenesis of gliomas and as a potential target for therapeutic measures. *Neurosurgical Focus.* 2006, **20**(4), pp.E24-E24.
166. Zhou, J., Schmid, T., Schnitzer, S. and Brüne, B. Tumor hypoxia and cancer progression. *Cancer Letters.* 2006, **237**(1), pp.10-21.
167. Evans, S.M. Hypoxia Is Important in the Biology and Aggression of Human Glial Brain Tumors. *Clinical Cancer Research.* 2004, **10**(24), pp.8177-8184.

168. Fortin Ensign, S.P., Mathews, I.T., Symons, M.H., Berens, M.E. and Tran, N.L. Implications of Rho GTPase Signaling in Glioma Cell Invasion and Tumor Progression. *Frontiers in Oncology.* 2013, **3**.
169. Katsetos, C.D., Dráberová, E., Šmejkalová, B., Reddy, G., Bertrand, L., de Chadarévian, J.-P., Legido, A., Nissanov, J., Baas, P.W. and Dráber, P. Class III β-Tubulin and γ-Tubulin are Co-expressed and Form Complexes in Human Glioblastoma Cells. *Neurochemical Research.* 2007, **32**(8), pp.1387-1398.
170. Madaule, P. and Axel, R. A novel ras-related gene family. *Cell.* 1985, **41**(1), pp.31-40.
171. Boureux, A., Vignal, E., Faure, S. and Fort, P. Evolution of the Rho Family of Ras-Like GTPases in Eukaryotes. *Molecular Biology and Evolution.* 2007, **24**(1), pp.203-216.
172. Jaffe, A.B. and Hall, A. RHO GTPASES: Biochemistry and Biology. *Annual Review of Cell and Developmental Biology.* 2005, **21**(1), pp.247-269.
173. Vega, F.M. and Ridley, A.J. Rho GTPases in cancer cell biology. *FEBS Letters.* 2008, **582**(14), pp.2093-2101.
174. Aspenström, P., Ruusala, A. and Pacholsky, D. Taking Rho GTPases to the next level: The cellular functions of atypical Rho GTPases. *Experimental Cell Research.* 2007, **313**(17), pp.3673-3679.
175. Karlsson, R., Pedersen, E.D., Wang, Z. and Brakebusch, C. Rho GTPase function in tumorigenesis. *Biochimica et Biophysica Acta (BBA) - Reviews on Cancer.* 2009, **1796**(2), pp.91-98.
176. Manser, E., Leung, T., Salihuddin, H., Zhao, Z.-s. and Lim, L. A brain serine/threonine protein kinase activated by Cdc42 and Rac1. *Nature.* 1994, **367**(6458), pp.40-46.
177. Adam, L., Vadlamudi, R., Mandal, M., Chernoff, J. and Kumar, R. Regulation of microfilament reorganization and invasiveness of breast cancer cells by kinase dead p21-activated kinase-1. *The Journal of biological chemistry.* 2000, **275**(16), pp.12041-12050.
178. Eitaki, M., Yamamori, T., Meike, S., Yasui, H. and Inanami, O. Vincristine enhances amoeboid-like motility via GEF-H1/RhoA/ROCK/Myosin light chain signaling in MKN45 cells. *BMC Cancer.* 2012, **12**(1), pp.469-469.
179. Salhia, B., Tran, N.L., Chan, A., Wolf, A., Nakada, M., Rutka, F., Ennis, M., McDonough, W.S., Berens, M.E., Symons, M. and Rutka, J.T. The Guanine Nucleotide Exchange Factors Trio, Ect2, and Vav3 Mediate the Invasive Behavior of Glioblastoma. *The American Journal of Pathology.* 2008, **173**(6), pp.1828-1838.
180. Tran, N.L., McDonough, W.S., Savitch, B.A., Fortin, S.P., Winkles, J.A., Symons, M., Nakada, M., Cunliffe, H.E., Hostetter, G., Hoelzinger, D.B., Rennert, J.L., Michaelson, J.S., Burkly, L.C., Lipinski, C.A., Loftus, J.C., Mariani, L. and Berens, M.E. Increased Fibroblast Growth Factor-Inducible 14

Expression Levels Promote Glioma Cell Invasion via Rac1 and Nuclear Factor-κB and Correlate with Poor Patient Outcome. *Cancer Research.* 2006, **66**(19), pp.9535-9542.

181. Wennerberg, K., Ellerbroek, S.M., Liu, R.-Y., Karnoub, A.E., Burridge, K. and Der, C.J. RhoG Signals in Parallel with Rac1 and Cdc42. *Journal of Biological Chemistry.* 2002, **277**(49), pp.47810-47817.
182. Iden, S. and Collard, J.G. Crosstalk between small GTPases and polarity proteins in cell polarization. *Nature Reviews Molecular Cell Biology.* 2008, **9**(11), pp.846-859.
183. Berzat, A. and Hall, A. Cellular responses to extracellular guidance cues. *The EMBO Journal.* 2010, **29**(16), pp.2734-2745.
184. Bigarella, C.L., Borges, L., Costa, F.F. and Saad, S.T.O. ARHGAP21 modulates FAK activity and impairs glioblastoma cell migration. *Biochimica et Biophysica Acta (BBA) - Molecular Cell Research.* 2009, **1793**(5), pp.806-816.
185. Yan, B., Chour, H.H., Peh, B.K., Lim, C. and Salto-Tellez, M. RhoA protein expression correlates positively with degree of malignancy in astrocytomas. *Neuroscience Letters.* 2006, **407**(2), pp.124-126.
186. Malchinkhuu, E., Sato, K., Maehama, T., Mogi, C., Tomura, H., Ishiuchi, S., Yoshimoto, Y., Kurose, H. and Okajima, F. S1P2 receptors mediate inhibition of glioma cell migration through Rho signaling pathways independent of PTEN. *Biochemical and Biophysical Research Communications.* 2008, **366**(4), pp.963-968.
187. Salhia, B., Rutten, F., Nakada, M., Beaudry, C., Berens, M., Kwan, A. and Rutka, J.T. Inhibition of Rho-Kinase Affects Astrocytoma Morphology, Motility, and Invasion through Activation of Rac1. *Cancer Research.* 2005, **65**(19), pp.8792-8800.
188. Riento, K. and Ridley, A.J. ROCKs: multifunctional kinases in cell behaviour. *Nature Reviews Molecular Cell Biology.* 2003, **4**(6), pp.446-456.
189. Chrzanowska-Wodnicka, M. Rho-stimulated contractility drives the formation of stress fibers and focal adhesions. *The Journal of Cell Biology.* 1996, **133**(6), pp.1403-1415.
190. Ito, M., Nakano, T., Erdödi, F. and Hartshorne, D.J. Myosin phosphatase: Structure, regulation and function. *Molecular and Cellular Biochemistry.* 2004, **259**(1/2), pp.197-209.
191. Mierke, C., Rosel, D., Fabry, B. and Brabek, J. Contractile forces in tumor cell migration. *European Journal of Cell Biology.* 2008, **87**(8-9), pp.669-676.
192. Kamishibahara, Y., Kawaguchi, H. and Shimizu, N. Promotion of mouse embryonic stem cell differentiation by Rho kinase inhibitor Y-27632. *Neuroscience Letters.* 2014, **579**, pp.58-63.
193. Harper, J.M., Krishnan, C., Darman, J.S., Deshpande, D.M., Peck, S., Shats, I., Backovic, S., Rothstein, J.D. and Kerr, D.A. Axonal growth of embryonic stem

cell-derived motoneurons in vitro and in motoneuron-injured adult rats. *Proceedings of the National Academy of Sciences.* 2004, **101**(18), pp.7123-7128.
194. Hall, A. The cytoskeleton and cancer. *Cancer and Metastasis Reviews.* 2009, **28**(1-2), pp.5-14.
195. Wyckoff, J.B., Pinner, S.E., Gschmeissner, S., Condeelis, J.S. and Sahai, E. ROCK- and Myosin-Dependent Matrix Deformation Enables Protease-Independent Tumor-Cell Invasion In Vivo. *Current Biology.* 2006, **16**(15), pp.1515-1523.
196. Yee, H.F., Melton, A.C. and Tran, B.N. RhoA/Rho-Associated Kinase Mediates Fibroblast Contractile Force Generation. *Biochemical and Biophysical Research Communications.* 2001, **280**(5), pp.1340-1345.
197. Nakagawa, O., Fujisawa, K., Ishizaki, T., Saito, Y., Nakao, K. and Narumiya, S. ROCK-I and ROCK-II, two isoforms of Rho-associated coiled-coil forming protein serine/threonine kinase in mice. *FEBS letters.* 1996, **392**(2), pp.189-193.
198. Inaba, N., Ishizawa, S., Kimura, M., Fujioka, K., Watanabe, M., Shibasaki, T. and Manome, Y. Effect of inhibition of the ROCK isoform on RT2 malignant glioma cells. *Anticancer research.* 2010, **30**(9), pp.3509-3514.
199. Leong, S.Y., Faux, C.H., Turbic, A., Dixon, K.J. and Turnley, A.M. The Rho Kinase Pathway Regulates Mouse Adult Neural Precursor Cell Migration. *STEM CELLS.* 2011, **29**(2), pp.332-343.
200. Amano, M., Nakayama, M. and Kaibuchi, K. Rho-kinase/ROCK: A key regulator of the cytoskeleton and cell polarity. *Cytoskeleton.* 2010, **67**(9), pp.545-554.
201. Shin, J.-Y., Kim, Y.-I.Y.-W., Cho, S.-J., Lee, M.K., Kook, M.-C., Lee, J.H., Lee, S.S., Ashktorab, H., Smoot, D.T., Ryu, K.W. and Choi, I.J. MicroRNA 135a Suppresses Lymph Node Metastasis through Down-Regulation of ROCK1 in Early Gastric Cancer. *PLoS ONE.* 2014, **9**(1), pp.e85205-e85205.
202. Kamai, T., Arai, K., Sumi, S., Tsujii, T., Honda, M., Yamanishi, T. and Yoshida, K.I. The rho/rho-kinase pathway is involved in the progression of testicular germ cell tumour. *BJU international.* 2002, **89**(4), pp.449-453.
203. Cui, G., Cui, M., Li, Y., Liang, Y., Li, W., Guo, H. and Zhao, S. MiR-186 targets ROCK1 to suppress the growth and metastasis of NSCLC cells. *Tumor Biology.* 2014, **35**(9), pp.8933-8937.
204. Kamai, T., Tsujii, T., Arai, K., Takagi, K., Asami, H., Ito, Y. and Oshima, H. Significant association of Rho/ROCK pathway with invasion and metastasis of bladder cancer. *Clinical cancer research : an official journal of the American Association for Cancer Research.* 2003, **9**(7), pp.2632-2641.
205. Morgan-Fisher, M., Wewer, U.M. and Yoneda, A. Regulation of ROCK Activity in Cancer. *Journal of Histochemistry & Cytochemistry.* 2013, **61**(3), pp.185-198.

206. Itoh, K., Yoshioka, K., Akedo, H., Uehata, M., Ishizaki, T. and Narumiya, S. An essential part for Rho–associated kinase in the transcellular invasion of tumor cells. *Nature Medicine.* 1999, **5**(2), pp.221-225.
207. Murata, T., Arii, S., Nakamura, T., Mori, A., Kaido, T., Furuyama, H., Furumoto, K., Nakao, T., Isobe, N. and Imamura, M. Inhibitory effect of Y-27632, a ROCK inhibitor, on progression of rat liver fibrosis in association with inactivation of hepatic stellate cells. *Journal of Hepatology.* 2001, **35**(4), pp.474-481.
208. Uehata, M., Ishizaki, T., Satoh, H., Ono, T., Kawahara, T., Morishita, T., Tamakawa, H., Yamagami, K., Inui, J., Maekawa, M. and Narumiya, S. Calcium sensitization of smooth muscle mediated by a Rho-associated protein kinase in hypertension. *Nature.* 1997, **389**(6654), pp.990-994.
209. Zheng, B., Liang, L., Wang, C., Huang, S., Cao, X., Zha, R., Liu, L., Jia, D., Tian, Q., Wu, J., Ye, Y., Wang, Q., Long, Z., Zhou, Y., Du, C., He, X. and Shi, Y. MicroRNA-148a Suppresses Tumor Cell Invasion and Metastasis by Downregulating ROCK1 in Gastric Cancer. *Clinical Cancer Research.* 2011, **17**(24), pp.7574-7583.
210. Chau, Z., Gulati, N., Nandu, H., Nagpal, J., Zohrabian, V., Murali, R. and Jhanwar-Uniyal, M. RhoA/Rho kinase influences glioblastoma multiforme cell migration and proliferation via interaction with TGF-β and ERK signaling pathways. *Cancer Research.* 2007, **67**(9), pp.5408-5408.
211. Zohrabian, V.M., Forzani, B., Chau, Z., Murali, R. and Jhanwar-Uniyal, M. Rho/ROCK and MAPK signaling pathways are involved in glioblastoma cell migration and proliferation. *Anticancer research.* 2009, **29**(1), pp.119-123.
212. Wan, X., Cheng, Q., Peng, R., Ma, Z., Chen, Z., Cao, Y. and Jiang, B. ROCK1, a novel target of miR-145, promotes glioma cell invasion. *Molecular medicine reports.* 2014, **9**(5), pp.1877-1882.
213. Davies, S.P., Reddy, H., Caivano, M. and Cohen, P. Specificity and mechanism of action of some commonly used protein kinase inhibitors. *The Biochemical journal.* 2000, **351**(Pt 1), pp.95-105.
214. Routhier, A., Astuccio, M., Lahey, D., Monfredo, N., Johnson, A., Callahan, W., Partington, A., Fellows, K., Ouellette, L., Zhidro, S., Goodrow, C., Smith, A., Sullivan, K., Simone, P., Le, L., Vezuli, B., Zohni, M., West, E., Gleason, D. and Bryan, B. Pharmacological inhibition of Rho-kinase signaling with Y-27632 blocks melanoma tumor growth. *Oncology reports.* 2010, **23**(3), pp.861-867.
215. Watanabe, K., Ueno, M., Kamiya, D., Nishiyama, A., Matsumura, M., Wataya, T., Takahashi, J.B., Nishikawa, S.-i.S., Muguruma, K. and Sasai, Y. A ROCK inhibitor permits survival of dissociated human embryonic stem cells. *Nature Biotechnology.* 2007, **25**(6), pp.681-686.
216. Tilson, S.G., Haley, E.M., Triantafillu, U.L., Dozier, D.A., Langford, C.P., Gillespie, G.Y. and Kim, Y. ROCK Inhibition Facilitates In Vitro Expansion of

Glioblastoma Stem-Like Cells. *PLOS ONE.* 2015, **10**(7), pp.e0132823-e0132823.

217. Rath, N. and Olson, M.F. Rho-associated kinases in tumorigenesis: re-considering ROCK inhibition for cancer therapy. *EMBO reports.* 2012, **13**(10), pp.900-908.
218. Justus, C.R., Leffler, N., Ruiz-Echevarria, M. and Yang, L.V. In vitro Cell Migration and Invasion Assays. *Journal of Visualized Experiments.* 2014, (88).
219. Decaestecker, C., Debeir, O., Van Ham, P. and Kiss, R. Can anti-migratory drugs be screened in vitro? A review of 2D and 3D assays for the quantitative analysis of cell migration. *Medicinal Research Reviews.* 2007, **27**(2), pp.149-176.
220. Környei, Z., Czirók, A., Vicsek, T.s. and Madarász, E. Proliferative and migratory responses of astrocytes to in vitro injury. *Journal of neuroscience research.* 2000, **61**(4), pp.421-429.
221. Coomber, B.L. and Gotlieb, A.I. In vitro endothelial wound repair. Interaction of cell migration and proliferation. *Arteriosclerosis (Dallas, Tex.).* **10**(2), pp.215-222.
222. Ananthanarayanan, B., Kim, Y. and Kumar, S. Elucidating the mechanobiology of malignant brain tumors using a brain matrix-mimetic hyaluronic acid hydrogel platform. *Biomaterials.* 2011, **32**(31), pp.7913-7923.
223. Wolf, K., Alexander, S., Schacht, V., Coussens, L.M., von Andrian, U.H., van Rheenen, J., Deryugina, E. and Friedl, P. Collagen-based cell migration models in vitro and in vivo. *Seminars in Cell & Developmental Biology.* 2009, **20**(8), pp.931-941.
224. Charles, N.A., Holland, E.C., Gilbertson, R., Glass, R. and Kettenmann, H. The brain tumor microenvironment. *Glia.* 2011, **59**(8), pp.1169-1180.
225. Condeelis, J. and Segall, J.E. Intravital imaging of cell movement in tumours. *Nature Reviews Cancer.* 2003, **3**(12), pp.921-930.
226. Shamir, E.R. and Ewald, A.J. Three-dimensional organotypic culture: experimental models of mammalian biology and disease. *Nature Reviews Molecular Cell Biology.* 2014, **15**(10), pp.647-664.
227. Parker, J.J., Lizarraga, M., Waziri, A. and Foshay, K.M. A Human Glioblastoma Organotypic Slice Culture Model for Study of Tumor Cell Migration and Patient-specific Effects of Anti-Invasive Drugs. *Journal of Visualized Experiments.* 2017, (125).
228. Merz, F., Gaunitz, F., Dehghani, F., Renner, C., Meixensberger, J., Gutenberg, A., Giese, A., Schopow, K., Hellwig, C., Schäfer, M., Bauer, M., Stöcker, H., Taucher-Scholz, G., Durante, M. and Bechmann, I. Organotypic slice cultures of human glioblastoma reveal different susceptibilities to treatments. *Neuro-Oncology.* 2013, **15**(6), pp.670-681.
229. Jung, S., Kim, H.-W., Lee, J.-H., Kang, S.-S., Rhu, H.-H., Jeong, Y.-I., Yang, S.-Y., Chung, H.-Y., Bae, C.-S., Choi, C., Shin, B.-A., Kim, K.-K. and Ahn, K.-Y.

Brain tumor invasion model system using organotypic brain-slice culture as an alternative to in vivo model. *Journal of Cancer Research and Clinical Oncology.* 2002, **128**(9), pp.469-476.

230. Boj, S.F., Hwang, C.-I., Baker, L.A., Chio, I.I.C., Engle, D.D., Corbo, V., Jager, M., Ponz-Sarvise, M., Tiriac, H., Spector, M.S., Gracanin, A., Oni, T., Yu, K.H., van Boxtel, R., Huch, M., Rivera, K.D., Wilson, J.P., Feigin, M.E., Öhlund, D., Handly-Santana, A., Ardito-Abraham, C.M., Ludwig, M., Elyada, E., Alagesan, B., Biffi, G., Yordanov, G.N., Delcuze, B., Creighton, B., Wright, K., Park, Y., Morsink, F.H.M., Molenaar, I.Q., Borel Rinkes, I.H., Cuppen, E., Hao, Y., Jin, Y., Nijman, I.J., Iacobuzio-Donahue, C., Leach, S.D., Pappin, D.J., Hammell, M., Klimstra, D.S., Basturk, O., Hruban, R.H., Offerhaus, G.J., Vries, R.G.J., Clevers, H. and Tuveson, D.A. Organoid Models of Human and Mouse Ductal Pancreatic Cancer. *Cell.* 2015, **160**(1-2), pp.324-338.
231. McCracken, K.W., Catá, E.M., Crawford, C.M., Sinagoga, K.L., Schumacher, M., Rockich, B.E., Tsai, Y.-H., Mayhew, C.N., Spence, J.R., Zavros, Y. and Wells, J.M. Modelling human development and disease in pluripotent stem-cell-derived gastric organoids. *Nature.* 2014, **516**(7531), pp.400-404.
232. Smith, S.J., Wilson, M., Ward, J.H., Rahman, C.V., Peet, A.C., Macarthur, D.C., Rose, F.R.A.J., Grundy, R.G. and Rahman, R. Recapitulation of Tumor Heterogeneity and Molecular Signatures in a 3D Brain Cancer Model with Decreased Sensitivity to Histone Deacetylase Inhibition. *PLoS ONE.* 2012, **7**(12), pp.e52335-e52335.
233. Lancaster, M.A., Renner, M., Martin, C.-A., Wenzel, D., Bicknell, L.S., Hurles, M.E., Homfray, T., Penninger, J.M., Jackson, A.P. and Knoblich, J.A. Cerebral organoids model human brain development and microcephaly. *Nature.* 2013, **501**(7467), pp.373-379.
234. Gao, D., Vela, I., Sboner, A., Iaquinta, P.J., Karthaus, W.R., Gopalan, A., Dowling, C., Wanjala, J.N., Undvall, E.A., Arora, V.K., Wongvipat, J., Kossai, M., Ramazanoglu, S., Barboza, L.P., Di, W., Cao, Z., Zhang, Q.F., Sirota, I., Ran, L., MacDonald, T.Y., Beltran, H., Mosquera, J.-M., Touijer, K.A., Scardino, P.T., Laudone, V.P., Curtis, K.R., Rathkopf, D.E., Morris, M.J., Danila, D.C., Slovin, S.F., Solomon, S.B., Eastham, J.A., Chi, P., Carver, B., Rubin, M.A., Scher, H.I., Clevers, H., Sawyers, C.L. and Chen, Y. Organoid Cultures Derived from Patients with Advanced Prostate Cancer. *Cell.* 2014, **159**(1), pp.176-187.
235. Simian, M. and Bissell, M.J. Organoids: A historical perspective of thinking in three dimensions. *The Journal of Cell Biology.* 2017, **216**(1), pp.31-40.
236. Clevers, H. Modeling development and disease with organoids. *Cell.* 2016, **165**(7), pp.1586-1597.
237. Fatehullah, A., Tan, S.H. and Barker, N. Organoids as an in vitro model of human development and disease. *Nature Cell Biology.* 2016, **18**(3), pp.246-254.

238. Bagley, J.A., Reumann, D., Bian, S., Lévi-Strauss, J. and Knoblich, J.A. Fused cerebral organoids model interactions between brain regions. *Nature methods.* 2017, **14**(7), p.743.
239. Xiang, Y., Tanaka, Y., Patterson, B., Kang, Y.-J., Govindaiah, G., Roselaar, N., Cakir, B., Kim, K.-Y., Lombroso, A.P. and Hwang, S.-M. Fusion of regionally specified hPSC-derived organoids models human brain development and interneuron migration. *Cell stem cell.* 2017, **21**(3), pp.383-398. e387.
240. Jo, J., Xiao, Y., Sun, A.X., Cukuroglu, E., Tran, H.-D., Göke, J., Tan, Z.Y., Saw, T.Y., Tan, C.-P. and Lokman, H. Midbrain-like organoids from human pluripotent stem cells contain functional dopaminergic and neuromelanin-producing neurons. *Cell Stem Cell.* 2016, **19**(2), pp.248-257.
241. Birey, F., Andersen, J., Makinson, C.D., Islam, S., Wei, W., Huber, N., Fan, H.C., Metzler, K.R.C., Panagiotakos, G. and Thom, N. Assembly of functionally integrated human forebrain spheroids. *Nature.* 2017, **545**(7652), p.54.
242. Qian, X., Nguyen, H.N., Song, M.M., Hadiono, C., Ogden, S.C., Hammack, C., Yao, B., Hamersky, G.R., Jacob, F., Zhong, C., Yoon, K.-j., Jeang, W., Lin, L., Li, Y., Thakor, J., Berg, D.A., Zhang, C., Kang, E., Chickering, M., Nauen, D., Ho, C.-Y., Wen, Z., Christian, K.M., Shi, P.-Y., Maher, B.J., Wu, H., Jin, P., Tang, H., Song, H. and Ming, G.-l. Brain-Region-Specific Organoids Using Mini-bioreactors for Modeling ZIKV Exposure. *Cell.* 2016, **165**(5), pp.1238-1254.
243. Mariani, J., Coppola, G., Zhang, P., Abyzov, A., Provini, L., Tomasini, L., Amenduni, M., Szekely, A., Palejev, D., Wilson, M., Gerstein, M., Grigorenko, E.L., Chawarska, K., Pelphrey, K.A., Howe, J.R. and Vaccarino, F.M. FOXG1-Dependent Dysregulation of GABA/Glutamate Neuron Differentiation in Autism Spectrum Disorders. *Cell.* 2015, **162**(2), pp.375-390.
244. Garcez, P.P., Loiola, E.C., Madeiro da Costa, R., Higa, L.M., Trindade, P., Delvecchio, R., Nascimento, J.M., Brindeiro, R., Tanuri, A. and Rehen, S.K. Zika virus impairs growth in human neurospheres and brain organoids. *Science.* 2016, **352**(6287), pp.816-818.
245. Miner, J.J. and Diamond, M.S. Understanding How Zika Virus Enters and Infects Neural Target Cells. *Cell Stem Cell.* 2016, **18**(5), pp.559-560.
246. Mansour, A.A., Gonçalves, J.T., Bloyd, C.W., Li, H., Fernandes, S., Quang, D., Johnston, S., Parylak, S.L., Jin, X. and Gage, F.H. An in vivo model of functional and vascularized human brain organoids. *Nature biotechnology.* 2018, **36**(5), p.432.
247. Ogawa, J., Pao, G.M., Shokhirev, M.N. and Verma, I.M. Glioblastoma Model Using Human Cerebral Organoids. *Cell Reports.* 2018, **23**(4), pp.1220-1229.
248. Hubert, C.G., Rivera, M., Spangler, L.C., Wu, Q., Mack, S.C., Prager, B.C., Couce, M., McLendon, R.E., Sloan, A.E. and Rich, J.N. A Three-Dimensional Organoid Culture System Derived from Human Glioblastomas Recapitulates

the Hypoxic Gradients and Cancer Stem Cell Heterogeneity of Tumors Found In Vivo. *Cancer Research.* 2016, **76**(8), pp.2465-2477.

249. Ross-Macdonald, P., de Silva, H., Guo, Q., Xiao, H., Hung, C.Y., Penhallow, B., Markwalder, J., He, L., Attar, R.M., Lin, T.a., Seitz, S., Tilford, C., Wardwell-Swanson, J. and Jackson, D. Identification of a nonkinase target mediating cytotoxicity of novel kinase inhibitors. *Molecular Cancer Therapeutics.* 2008, **7**(11), pp.3490-3498.
250. Lancaster, M.A. and Knoblich, J.A. Generation of cerebral organoids from human pluripotent stem cells. *Nature Protocols.* 2014, **9**(10), pp.2329-2340.
251. Team, R.C. *R: A language and environment for statistical computing. R Foundation for Statistical Computing, Vienna, Austria. 2014.* 2016.
252. Gentleman, R.C., Carey, V.J., Bates, D.M., Bolstad, B., Dettling, M., Dudoit, S., Ellis, B., Gautier, L., Ge, Y., Gentry, J., Hornik, K., Hothorn, T., Huber, W., Iacus, S., Irizarry, R., Leisch, F., Li, C., Maechler, M., Rossini, A.J., Sawitzki, G., Smith, C., Smyth, G., Tierney, L., Yang, J.Y.H. and Zhang, J. Bioconductor: open software development for computational biology and bioinformatics. *Genome biology.* 2004, **5**(10), pp.R80-R80.
253. Huber, W., Carey, V.J., Gentleman, R., Anders, S., Carlson, M., Carvalho, B.S., Bravo, H.C., Davis, S., Gatto, L., Girke, T., Gottardo, R., Hahne, F., Hansen, K.D., Irizarry, R.A., Lawrence, M., Love, M.I., MacDonald, J., Obenchain, V., Oleś, A.K., Pagès, H., Reyes, A., Shannon, P., Smyth, G.K., Tenenbaum, D., Waldron, L. and Morgan, M. Orchestrating high-throughput genomic analysis with Bioconductor. *Nature Methods.* 2015, **12**(2), pp.115-121.
254. Dunning, M.J., Smith, M.L., Ritchie, M.E. and Tavare, S. beadarray: R classes and methods for Illumina bead-based data. *Bioinformatics.* 2007, **23**(16), pp.2183-2184.
255. Smyth, G.K. Linear Models and Empirical Bayes Methods for Assessing Differential Expression in Microarray Experiments. *Statistical Applications in Genetics and Molecular Biology.* 2004, **3**(1), pp.1-25.
256. Kümper, S., Mardakheh, F.K., McCarthy, A., Yeo, M., Stamp, G.W., Paul, A., Worboys, J., Sadok, A., Jørgensen, C., Guichard, S. and Marshall, C.J. Rho-associated kinase (ROCK) function is essential for cell cycle progression, senescence and tumorigenesis. *eLife.* 2016, **5**.
257. Sadok, A., McCarthy, A., Caldwell, J., Collins, I., Garrett, M.D., Yeo, M., Hooper, S., Sahai, E., Kuemper, S. and Mardakheh, F.K. Rho kinase inhibitors block melanoma cell migration and inhibit metastasis. *Cancer research.* 2015, **75**(11), pp.2272-2284.
258. Polson, E.S., Kuchler, V.B., Abbosh, C., Ross, E.M., Mathew, R.K., Beard, H.A., Chuntharpursat-Bon, E., Williams, J., Da Silva, B. and Shao, H. The small molecule KHS101 induces bioenergetic dysfunction in glioblastoma cells through inhibition of mitochondrial HSPD1. *bioRxiv.* 2017, p.205203.

259. Fuentes, E.O., Leemhuis, J., Stark, G.B. and Lang, E.M. Rho kinase inhibitors Y27632 and H1152 augment neurite extension in the presence of cultured Schwann cells. *Journal of brachial plexus and peripheral nerve injury.* 2008, **3**(1), p.19.
260. Doe, C., Bentley, R., Behm, D.J., Lafferty, R., Stavenger, R., Jung, D., Bamford, M., Panchal, T., Grygielko, E. and Wright, L.L. Novel Rho kinase inhibitors with anti-inflammatory and vasodilatory activities. *Journal of Pharmacology and Experimental Therapeutics.* 2007, **320**(1), pp.89-98.
261. Vicente-Manzanares, M., Ma, X., Adelstein, R.S. and Horwitz, A.R. Non-muscle myosin II takes centre stage in cell adhesion and migration. *Nature Reviews Molecular Cell Biology.* 2009, **10**(11), pp.778-790.
262. Pataskar, A., Jung, J., Smialowski, P., Noack, F., Calegari, F., Straub, T. and Tiwari, V.K. NeuroD1 reprograms chromatin and transcription factor landscapes to induce the neuronal program. *The EMBO Journal.* 2016, **35**(1), pp.24-45.
263. Schäck, L., Budde, S., Lenarz, T., Krettek, C., Gross, G., Windhagen, H., Hoffmann, A. and Warnecke, A. Induction of neuronal-like phenotype in human mesenchymal stem cells by overexpression of Neurogenin1 and treatment with neurotrophins. *Tissue and Cell.* 2016, **48**(5), pp.524-532.
264. Burthem, J., Rees-Unwin, K., Mottram, R., Adams, J., Lucas, G., Spooncer, E. and Whetton, A. The ρ-kinase inhibitors Y-27632 and fasudil act synergistically with imatinib to inhibit the expansion of ex vivo CD34+ CML progenitor cells. *Leukemia.* 2007, **21**(8), p.1708.
265. Maldonado, M., Luu, R.J., Ramos, M.E.P. and Nam, J. ROCK inhibitor primes human induced pluripotent stem cells to selectively differentiate towards mesendodermal lineage via epithelial-mesenchymal transition-like modulation. *Stem Cell Research.* 2016, **17**(2), pp.222-227.
266. Osswald, M., Jung, E., Sahm, F., Solecki, G., Venkataramani, V., Blaes, J., Weil, S., Horstmann, H., Wiestler, B., Syed, M., Huang, L., Ratliff, M., Karimian Jazi, K., Kurz, F.T., Schmenger, T., Lemke, D., Gömmel, M., Pauli, M., Liao, Y., Häring, P., Pusch, S., Herl, V., Steinhäuser, C., Krunic, D., Jarahian, M., Miletic, H., Berghoff, A.S., Griesbeck, O., Kalamakis, G., Garaschuk, O., Preusser, M., Weiss, S., Liu, H., Heiland, S., Platten, M., Huber, P.E., Kuner, T., von Deimling, A., Wick, W. and Winkler, F. Brain tumour cells interconnect to a functional and resistant network. *Nature.* 2015, **528**(7580), pp.93-98.
267. Balduzzi, D. and Tononi, G. What can neurons do for their brain? Communicate selectivity with bursts. *Theory in Biosciences.* 2013, **132**(1), pp.27-39.
268. Rørth, P. Communication by touch: role of cellular extensions in complex animals. *Cell.* 2003, **112**(5), pp.595-598.

269. Rustom, A., Saffrich, R., Markovic, I., Walther, P. and Gerdes, H.-H. Nanotubular highways for intercellular organelle transport. *Science.* 2004, **303**(5660), pp.1007-1010.
270. Vidulescu, C., Clejan, S. and O'Connor, K.C. Vesicle traffic through intercellular bridges in DU 145 human prostate cancer cells. *Journal of Cellular and Molecular Medicine.* 2004, **8**(3), pp.388-396.
271. Koyanagi, M., Brandes, R.P., Haendeler, J., Zeiher, A.M. and Dimmeler, S. Cell-to-cell connection of endothelial progenitor cells with cardiac myocytes by nanotubes: a novel mechanism for cell fate changes? *Circulation research.* 2005, **96**(10), pp.1039-1041.
272. Gimsa, U., Iglič, A., Fiedler, S., Zwanzig, M., Kralj-Iglič, V., Jonas, L. and Gimsa, J. Actin is not required for nanotubular protrusions of primary astrocytes grown on metal nano-lawn. *Molecular Membrane Biology.* 2007, **24**(3), pp.243-255.
273. Fancher, S. and Mugler, A. Fundamental Limits to Collective Concentration Sensing in Cell Populations. *Physical Review Letters.* 2017, **118**(7), pp.078101-078101.
274. Roos, W.P., Thomas, A.D. and Kaina, B. DNA damage and the balance between survival and death in cancer biology. *Nature Reviews Cancer.* 2016, **16**(1), p.20.
275. Knizhnik, A.V., Roos, W.P., Nikolova, T., Quiros, S., Tomaszowski, K.-H., Christmann, M. and Kaina, B. Survival and death strategies in glioma cells: autophagy, senescence and apoptosis triggered by a single type of temozolomide-induced DNA damage. *PloS one.* 2013, **8**(1), p.e55665.
276. Sikora, E., Mosieniak, G. and Alicja Sliwinska, M. Morphological and functional characteristic of senescent cancer cells. *Current drug targets.* 2016, **17**(4), pp.377-387.
277. Lochhead, P.A., Wickman, G., Mezna, M. and Olson, M.F. Activating ROCK1 somatic mutations in human cancer. *Oncogene.* 2010, **29**(17), pp.2591-2598.
278. Khera, N. and Rajput, S. Therapeutic Potential of Small Molecule Inhibitors. *Journal of cellular biochemistry.* 2017, **118**(5), pp.959-961.
279. Efe, J.A. and Ding, S. The evolving biology of small molecules: controlling cell fate and identity. *Philosophical Transactions of the Royal Society B: Biological Sciences.* 2011, **366**(1575), pp.2208-2221.
280. Weiss, W.A., Taylor, S.S. and Shokat, K.M. Recognizing and exploiting differences between RNAi and small-molecule inhibitors. *Nature Chemical Biology.* 2007, **3**(12), pp.739-744.
281. Kaelin, W.G. Common pitfalls in preclinical cancer target validation. *Nature Reviews Cancer.* 2017, **17**(7), pp.425-440.
282. Pool, M., Thiemann, J., Bar-Or, A. and Fournier, A.E. NeuriteTracer: A novel ImageJ plugin for automated quantification of neurite outgrowth. *Journal of Neuroscience Methods.* 2008, **168**(1), pp.134-139.

283. Ishizaki, T., Uehata, M., Tamechika, I., Keel, J., Nonomura, K., Maekawa, M. and Narumiya, S. Pharmacological properties of Y-27632, a specific inhibitor of rho-associated kinases. *Molecular pharmacology.* 2000, **57**(5), pp.976-983.
284. Coleman, M.L. and Olson, M.F. Rho GTPase signalling pathways in the morphological changes associated with apoptosis. *Cell death and differentiation.* 2002, **9**(5), pp.493-504.
285. Tögel, M., Wiche, G. and Propst, F. Novel features of the light chain of microtubule-associated protein MAP1B: microtubule stabilization, self interaction, actin filament binding, and regulation by the heavy chain. *J Cell Biol.* 1998, **143**(3), pp.695-707.
286. Mack, T.G.A., Koester, M.P. and Pollerberg, G.E. The Microtubule-Associated Protein MAP1B Is Involved in Local Stabilization of Turning Growth Cones. *Molecular and Cellular Neuroscience.* 2000, **15**(1), pp.51-65.
287. Ka, M., Jung, E.M., Mueller, U. and Kim, W.Y. MACF1 regulates the migration of pyramidal neurons via microtubule dynamics and GSK-3 signaling. *Dev Biol.* 2014, **395**(1), pp.4-18.
288. Yasuda-Yamahara, M., Rogg, M., Yamahara, K., Maier, J.I., Huber, T.B. and Schell, C. AIF1L regulates actomyosin contractility and filopodial extensions in human podocytes. *PLoS One.* 2018, **13**(7), p.e0200487.
289. Liu, P., Li, W., Hu, Y. and Jiang, Y. Absence of AIF1L contributes to cell migration and a poor prognosis of breast cancer. *Onco Targets Ther.* 2018, **11**, pp.5485-5498.
290. Narumiya, S., Ishizaki, T. and Ufhata, M. Use and properties of ROCK-specific inhibitor Y-27632. In, 2000, pp.273-284.
291. Maekawa, M. Signaling from Rho to the Actin Cytoskeleton Through Protein Kinases ROCK and LIM-kinase. *Science.* 1999, **285**(5429), pp.895-898.
292. Lotz-Jenne, C., Lüthi, U., Ackerknecht, S., Lehembre, F., Fink, T., Stritt, M., Wirth, M., Pavan, S., Bill, R. and Regenass, U. A high-content EMT screen identifies multiple receptor tyrosine kinase inhibitors with activity on TGFβ receptor. *Oncotarget.* 2016, **7**(18), p.25983.
293. Kamishibahara, Y., Kawaguchi, H. and Shimizu, N. Rho kinase inhibitor Y-27632 promotes neuronal differentiation in mouse embryonic stem cells via phosphatidylinositol 3-kinase. *Neuroscience Letters.* 2016, **615**, pp.44-49.
294. Liu, X., Zhang, Z., Yan, X., Liu, H., Zhang, L., Yao, A., Guo, C., Liu, X. and Xu, T. The Rho kinase inhibitor Y-27632 facilitates the differentiation of bone marrow mesenchymal stem cells. *Journal of Molecular Histology.* 2014, **45**(6), pp.707-714.
295. Pacary, E., Tixier, E., Coulet, F., Roussel, S., Petit, E. and Bernaudin, M. Crosstalk between HIF-1 and ROCK pathways in neuronal differentiation of mesenchymal stem cells, neurospheres and in PC12 neurite outgrowth. *Molecular and Cellular Neuroscience.* 2007, **35**(3), pp.409-423.

296. Eastham, A.M., Spencer, H., Soncin, F., Ritson, S., Merry, C.L.R., Stern, P.L. and Ward, C.M. Epithelial-Mesenchymal Transition Events during Human Embryonic Stem Cell Differentiation. *Cancer Research.* 2007, **67**(23), pp.11254-11262.
297. Yilmaz, M. and Christofori, G. EMT, the cytoskeleton, and cancer cell invasion. *Cancer and Metastasis Reviews.* 2009, **28**(1-2), pp.15-33.
298. Ciferri, C., Musacchio, A. and Petrovic, A. The Ndc80 complex: hub of kinetochore activity. *FEBS Lett.* 2007, **581**(15), pp.2862-2869.
299. Fang, Y. and Zhang, X. Targeting NEK2 as a promising therapeutic approach for cancer treatment. *Cell Cycle.* 2016, **15**(7), pp.895-907.
300. Enserink, J.M. and Kolodner, R.D. An overview of Cdk1-controlled targets and processes. *Cell Div.* 2010, **5**, p.11.
301. Qian, J., Beullens, M., Huang, J., De Munter, S., Lesage, B. and Bollen, M. Cdk1 orders mitotic events through coordination of a chromosome-associated phosphatase switch. *Nat Commun.* 2015, **6**, p.10215.
302. Jiang, N., Wang, X., Jhanwar-Uniyal, M., Darzynkiewicz, Z. and Dai, W. Polo box domain of Plk3 functions as a centrosome localization signal, overexpression of which causes mitotic arrest, cytokinesis defects, and apoptosis. *J Biol Chem.* 2006, **281**(15), pp.10577-10582.
303. Silber, J., Lim, D.A., Petritsch, C., Persson, A.I., Maunakea, A.K., Yu, M., Vandenberg, S.R., Ginzinger, D.G., James, C.D., Costello, J.F., Bergers, G., Weiss, W.A., Alvarez-Buylla, A. and Hodgson, J.G. miR-124 and miR-137 inhibit proliferation of glioblastoma multiforme cells and induce differentiation of brain tumor stem cells. *BMC Medicine.* 2008, **6**(1), pp.14-14.
304. Korur, S., Huber, R.M., Sivasankaran, B., Petrich, M., Morin, P., Hemmings, B.A., Merlo, A. and Lino, M.M. GSK3β Regulates Differentiation and Growth Arrest in Glioblastoma. *PLoS ONE.* 2009, **4**(10), pp.e7443-e7443.
305. Joshi, A.R., Bobylev, I., Zhang, G., Sheikh, K.A. and Lehmann, H.C. Inhibition of Rho-kinase differentially affects axon regeneration of peripheral motor and sensory nerves. *Experimental Neurology.* 2015, **263**, pp.28-38.
306. Kozma, R., Sarner, S., Ahmed, S. and Lim, L. Rho family GTPases and neuronal growth cone remodelling: relationship between increased complexity induced by Cdc42Hs, Rac1, and acetylcholine and collapse induced by RhoA and lysophosphatidic acid. *Molecular and Cellular Biology.* 1997, **17**(3), pp.1201-1211.
307. Roloff, F., Scheiblich, H., Dewitz, C., Dempewolf, S., Stern, M. and Bicker, G. Enhanced Neurite Outgrowth of Human Model (NT2) Neurons by Small-Molecule Inhibitors of Rho/ROCK Signaling. *PLOS ONE.* 2015, **10**(2), pp.e0118536-e0118536.
308. Veranič, P., Lokar, M., Schütz, G.J., Weghuber, J., Wieser, S., Hägerstrand, H., Kralj-Iglič, V. and Iglič, A. Different Types of Cell-to-Cell Connections

Mediated by Nanotubular Structures. *Biophysical Journal.* 2008, **95**(9), pp.4416-4425.
309. Kumar, N.M. and Gilula, N.B. The Gap Junction Communication Channel. *Cell.* 1996, **84**(3), pp.381-388.
310. Karlsson, A., Karlsson, R., Karlsson, M., Cans, A.S., Strömberg, A., Ryttsén, F. and Orwar, O. Molecular engineering: Networks of nanotubes and containers. *Nature.* 2001, **409**(6817), pp.150-152.
311. Lowery, L.A. and Vactor, D.V. The trip of the tip: understanding the growth cone machinery. *Nature Reviews Molecular Cell Biology.* 2009, **10**(5), pp.332-343.
312. Potter, G.D., Byrd, T.A., Mugler, A. and Sun, B. Communication shapes sensory response in multicellular networks. *Proceedings of the National Academy of Sciences.* 2016, **113**(37), pp.10334-10339.
313. McDonough, W.S., Johansson, A., Joffee, H., Giese, A. and Berens, M.E. Gap junction intercellular communication in gliomas is inversely related to cell motility. *International Journal of Developmental Neuroscience.* 1999, **17**(5-6), pp.601-611.
314. Soroceanu, L., Manning, T.J. and Sontheimer, H. Reduced expression of connexin-43 and functional gap junction coupling in human gliomas. *Glia.* 2001, **33**(2), pp.107-117.
315. Leybaert, L. and Sanderson, M.J. Intercellular Ca 2+ Waves: Mechanisms and Function. *Physiological Reviews.* 2012, **92**(3), pp.1359-1392.
316. Charles, A.C., Merrill, J.E., Dirksen, E.R. and Sandersont, M.J. Intercellular signaling in glial cells: Calcium waves and oscillations in response to mechanical stimulation and glutamate. *Neuron.* 1991, **6**(6), pp.983-992.
317. Cornell-Bell, A., Finkbeiner, S., Cooper, M. and Smith, S. Glutamate induces calcium waves in cultured astrocytes: long-range glial signaling. *Science.* 1990, **247**(4941), pp.470-473.
318. Gleisner, M.A., Navarrete, M., Hofmann, F., Salazar-Onfray, F. and Tittarelli, A. Mind the Gaps in Tumor Immunity: Impact of Connexin-Mediated Intercellular Connections. *Frontiers in Immunology.* 2017, **8**.
319. Charles, A.C., Naus, C.C., Zhu, D., Kidder, G.M., Dirksen, E.R. and Sanderson, M.J. Intercellular calcium signaling via gap junctions in glioma cells. *The Journal of cell biology.* 1992, **118**(1), pp.195-201.
320. El-Fouly, M.H., Trosko, J.E. and Chang, C.-C. Scrape-loading and dye transfer. *Experimental Cell Research.* 1987, **168**(2), pp.422-430.
321. Uzu, M., Sin, W., Shimizu, A. and Sato, H. Conflicting Roles of Connexin43 in Tumor Invasion and Growth in the Central Nervous System. *International Journal of Molecular Sciences.* 2018, **19**(4), pp.1159-1159.
322. Hitomi, M., Deleyrolle, L.P., Mulkearns-Hubert, E.E., Jarrar, A., Li, M., Sinyuk, M., Otvos, B., Brunet, S., Flavahan, W.A., Hubert, C.G., Goan, W., Hale, J.S.,

Alvarado, A.G., Zhang, A., Rohaus, M., Oli, M., Vedam-Mai, V., Fortin, J.M., Futch, H.S., Griffith, B., Wu, Q., Xia, C.-h., Gong, X., Ahluwalia, M.S., Rich, J.N., Reynolds, B.A. and Lathia, J.D. Differential Connexin Function Enhances Self-Renewal in Glioblastoma. *Cell Reports.* 2015, **11**(7), pp.1031-1042.

323. Nagy, J.I. and Rash, J.E. Connexins and gap junctions of astrocytes and oligodendrocytes in the CNS. *Brain Research Reviews.* 2000, **32**(1), pp.29-44.
324. Naus, C.C. and Laird, D.W. Implications and challenges of connexin connections to cancer. *Nature Reviews Cancer.* 2010, **10**(6), pp.435-441.
325. Nakase, T. and Naus, C.C.G. Gap junctions and neurological disorders of the central nervous system. *Biochimica et Biophysica Acta.* 2004, **1662**(1-2), pp.149-158.
326. Buniello, A., Montanaro, D., Volinia, S., Gasparini, P. and Marigo, V. An expression atlas of connexin genes in the mouse. *Genomics.* 2004, **83**(5), pp.812-820.
327. Giaume, C., Leybaert, L., Naus, C.C. and Sáez, J.C. Connexin and pannexin hemichannels in brain glial cells: properties, pharmacology, and roles. *Frontiers in pharmacology.* 2013, **4**, pp.88-88.
328. Sin, W.-C., Crespin, S. and Mesnil, M. Opposing roles of connexin43 in glioma progression. *Biochimica et Biophysica Acta (BBA) - Biomembranes.* 2012, **1818**(8), pp.2058-2067.
329. Onfelt, B., Nedvetzki, S., Yanagi, K. and Davis, D.M. Cutting Edge: Membrane Nanotubes Connect Immune Cells. *The Journal of Immunology.* 2004, **173**(3), pp.1511-1513.
330. Weil, S., Osswald, M., Solecki, G., Grosch, J., Jung, E., Lemke, D., Ratliff, M., Hänggi, D., Wick, W. and Winkler, F. Tumor microtubes convey resistance to surgical lesions and chemotherapy in gliomas. *Neuro-Oncology.* 2017, **19**(10), pp.1316-1326.
331. Doke, S.K. and Dhawale, S.C. Alternatives to animal testing: A review. *Saudi Pharmaceutical Journal.* 2015, **23**(3), pp.223-229.
332. Roninson, I.B., Broude, E.V. and Chang, B.-D. If not apoptosis, then what? Treatment-induced senescence and mitotic catastrophe in tumor cells. *Drug Resistance Updates.* 2001, **4**(5), pp.303-313.
333. Glücksmann, A. and Spear, F.G. The Effect of Gamma Radiation on Cells in Vivo Part II. *The British Journal of Radiology.* 1939, **12**(140), pp.486-498.
334. Spear, F.G. and Glücksmann, A. The Effect of Gamma Radiation on Cells in Vivo . (Part III: Spaced Radiation). *The British Journal of Radiology.* 1941, **14**(158), pp.65-76.
335. Vakifahmetoglu, H., Olsson, M. and Zhivotovsky, B. Death through a tragedy: mitotic catastrophe. *Cell Death & Differentiation.* 2008, **15**(7), pp.1153-1162.
336. Ader, I., Delmas, C., Bonnet, J., Rochaix, P., Favre, G., Toulas, C. and Cohen-Jonathan-Moyal, E. Inhibition of Rho pathways induces radiosensitization and

oxygenation in human glioblastoma xenografts. *Oncogene.* 2003, **22**(55), pp.8861-8869.

337. Street, C.A., Routhier, A.A., Spencer, C., Perkins, A.L., Masterjohn, K., Hackathorn, A., Montalvo, J., Dennstedt, E.A. and Bryan, B.A. Pharmacological inhibition of Rho-kinase (ROCK) signaling enhances cisplatin resistance in neuroblastoma cells. *International journal of oncology.* 2010, **37**(5), pp.1297-1305.
338. McFerrin, M.B., Turner, K.L., Cuddapah, V.A. and Sontheimer, H. Differential role of IK and BK potassium channels as mediators of intrinsic and extrinsic apoptotic cell death. *American Journal of Physiology-Cell Physiology.* 2012, **303**(10), pp.C1070-C1078.
339. Hanahan, D. and Weinberg, R.A. Hallmarks of Cancer: The Next Generation. *Cell.* 2011, **144**(5), pp.646-674.
340. Smith, S. Neuronal cytomechanics: the actin-based motility of growth cones. *Science.* 1988, **242**(4879), pp.708-715.
341. Alexander, D. and Goldberg, G. Transfer of Biologically Important Molecules Between Cells Through Gap Junction Channels. *Current Medicinal Chemistry.* 2003, **10**(19), pp.2045-2058.
342. Sato, T., Vries, R.G., Snippert, H.J., Van De Wetering, M., Barker, N., Stange, D.E., Van Es, J.H., Abo, A., Kujala, P. and Peters, P.J. Single Lgr5 stem cells build crypt–villus structures in vitro without a mesenchymal niche. *Nature.* 2009, **459**(7244), p.262.
343. Sato, T., Stange, D.E., Ferrante, M., Vries, R.G., Van Es, J.H., Van Den Brink, S., Van Houdt, W.J., Pronk, A., Van Gorp, J. and Siersema, P.D. Long-term expansion of epithelial organoids from human colon, adenoma, adenocarcinoma, and Barrett's epithelium. *Gastroenterology.* 2011, **141**(5), pp.1762-1772.
344. Xia, Y., Sancho-Martinez, I., Nivet, E., Esteban, C.R., Campistol, J.M. and Belmonte, J.C.I. The generation of kidney organoids by differentiation of human pluripotent cells to ureteric bud progenitor–like cells. *Nature protocols.* 2014, **9**(11), p.2693.
345. Eiraku, M., Watanabe, K., Matsuo-Takasaki, M., Kawada, M., Yonemura, S., Matsumura, M., Wataya, T., Nishiyama, A., Muguruma, K. and Sasai, Y. Self-organized formation of polarized cortical tissues from ESCs and its active manipulation by extrinsic signals. *Cell stem cell.* 2008, **3**(5), pp.519-532.
346. Kaufman, L.J., Brangwynne, C.P., Kasza, K.E., Filippidi, E., Gordon, V.D., Deisboeck, T.S. and Weitz, D.A. Glioma Expansion in Collagen I Matrices: Analyzing Collagen Concentration-Dependent Growth and Motility Patterns. *Biophysical Journal.* 2005, **89**(1), pp.635-650.
347. Gordon, V.D., Valentine, M.T., Gardel, M.L., Andor-Ardó, D., Dennison, S., Bogdanov, A.A., Weitz, D.A. and Deisboeck, T.S. Measuring the mechanical

stress induced by an expanding multicellular tumor system: a case study. *Experimental cell research.* 2003, **289**(1), pp.58-66.

348. Royds, J., Ironside, J., Taylor, C., Graham, D. and Timperley, W. An immunohistochemical study of glial and neuronal markers in primary neoplasms of the central nervous system. *Acta neuropathologica.* 1986, **70**(3-4), pp.320-326.
349. Vescovi, A.L., Galli, R. and Reynolds, B.A. Brain tumour stem cells. *Nature Reviews Cancer.* 2006, **6**(6), p.425.
350. Brat, D.J., Castellano-Sanchez, A.A., Hunter, S.B., Pecot, M., Cohen, C., Hammond, E.H., Devi, S.N., Kaur, B. and Van Meir, E.G. Pseudopalisades in glioblastoma are hypoxic, express extracellular matrix proteases, and are formed by an actively migrating cell population. *Cancer research.* 2004, **64**(3), pp.920-927.
351. Zhao, J., Zhang, L., Dong, X., Liu, L., Huo, L. and Chen, H. High Expression of Vimentin is Associated With Progression and a Poor Outcome in Glioblastoma. *Applied immunohistochemistry & molecular morphology: AIMM.* 2016.
352. Jorfi, M., D'avanzo, C., Kim, D.Y. and Irimia, D. Three-Dimensional Models of the Human Brain Development and Diseases. *Advanced healthcare materials.* 2018, **7**(1), p.1700723.
353. Quadrato, G., Nguyen, T., Macosko, E.Z., Sherwood, J.L., Yang, S.M., Berger, D.R., Maria, N., Scholvin, J., Goldman, M. and Kinney, J.P. Cell diversity and network dynamics in photosensitive human brain organoids. *Nature.* 2017, **545**(7652), p.48.
354. Vlachogiannis, G., Hedayat, S., Vatsiou, A., Jamin, Y., Fernández-Mateos, J., Khan, K., Lampis, A., Eason, K., Huntingford, I. and Burke, R. Patient-derived organoids model treatment response of metastatic gastrointestinal cancers. *Science.* 2018, **359**(6378), pp.920-926.
355. Wood, M.D. and Mackinnon, S.E. Pathways regulating modality-specific axonal regeneration in peripheral nerve. *Experimental Neurology.* 2015, **265**, pp.171-175.